Electrochemistry as a Tool for Study, Delvelopment and Promotion of Catalytic Reactions

Petrushina, Irina

Publication date:
2015

Document Version
Publisher's PDF, also known as Version of record

Author: Irina Petrushina (Copiright © 2015 by Irina Petrushina)

Title: Electrochemistry as a Tool for Study, Development and Promotion of Catalytic Reactions

ISBN: 978-87-92986-37-5

Technical University of Denmark
Department of Energy Conversion
and Storage
Building 207
Kemitorvet
DK-2800 Lyngby
Denmark
Telephone: +45 45 25 23 02
E-mail: irpe@dtu.dk

Technical University of Denmark

Electrochemistry as a Tool for Study, Development and Promotion of Catalytic Reactions

Dissertation for the Doctor of Technices Degree

Irina M. Petrushina

Department of Energy Conversion and Storage
Technical University of Denmark
2015

Denne afhandling er af Danmarks Tekniske Universitet antaget til forsvar for den tekniske doktorgrad. Antagelsen er sket efter bedømmelse af den foreliggende afhandling.

Kgs. Lyngby, den 22. september 2015

Anders O. Bjarklev
Rektor

/Henrik C. Wegener
Prorektor

This thesis has been accepted by the Technical University of Denmark for public defence in fulfilment of the requirements for the degree of Doctor Technices. The acceptance is based on an evaluation of the present dissertation.

Kgs. Lyngby, 22 September 2015

Anders O. Bjarklev
President

/Henrik C. Wegener
Provost

"I have been so electrically occupied of late that I feel as if hungry for a little chemistry: but then the conviction crosses my mind that these things hang together under one law…"

(From the Letter to Eihard Mitschelich, 24 January 1838, In Frank A.J.L. James (ed.), The Correspondence of *Michael Faraday* (1993), Vol. 2, 488).

To my son Igor

PREFACE

Last decade electrochemistry is used more and more in other scientific fields, e.g. chemistry, physics, materials science, especially in connection with the development of batteries, fuel cells, and water electrolysis. As an electrochemist, I have many years of collaboration experience with researchers from these areas. As a rule, it was very important to find common features and differences in electrochemistry and e.g. inorganic heterogeneous redox reactions.This lead to much more effective collaboration and more impressive results.

In order to make this dissertation understandable for non-electrochemists, I start it with basics of electrochemistry, clarifying the common features and differences between chemical and electrochemical reactions.

This work is a result of my research in the field electrochemistry and catalysis at Technical University of Denmark. This research has shown that electrochemistry can be used not only as a tool in the study on mechanism and kinetics of catalytic and electrocatalytic reactions reactions, but can also be a tool for modification (tailoring) of catalyst activity and selectivity.

I have worked at DTU from 1993, first at the Department of Chemistry and since 2012 at the Department of Energy Conversion and Storage, but always in the same group created by Professor Niels J. Bjerrum. I want to express my gratitude to Professor N.J. Bjerrum, Assoc. Professors R.W. Berg and J. von Barner, Senior Researcher E. Christensen for their help and support in my research and teaching. I was lucky to supervise talented PhD students in the area related to the dissertation: Frederic Cappeln, Lars N. Cleeman, Aleksey Nikiforov, Antonio L. Tomas-Garcia, Carsten Prag.

I am grateful to the head of the Department of Energy Conversion and Storage, Søren Linderoth for helping me to finish this dissertation by imposing a rigid timeframe on my dissertation activities.

A lot of my experiments would be impossible without help of our technicians Claus B. Mortensen and Steen Blichfeldt. I am greateful to the secretary of our group Kirsten M. Thomsen for her kindness and help in my daily office activities.

Hellerup, February, 2015 Irina Petrushina

ABSTRACT

The first two chapters of the dissertation are dedicated to definition of the peculiarities of electrochemical processes and also common features and differences between heterogeneous redox and catalytic reactions and electrochemical reactions.
The main common characteristic of heterogeneous catalytic reactions and electrochemical reactions is defined. It is the Fermi level of the catalyst, which is also the electrochemical potential of the electrode. According to the Newns-Anderson theory,
Fermi level of catalysts affects (or even define) their activity. The electrochemical potential can be measured and changed by polarization in electrochemical experiment.
In Chapter 3 the nature of the electrochemical heterogeneous catalytic reactions is dicussed, including the new theory of electrochemical promotion. This theory is based on electrochemical change of the Fermi level of the catalyst. It also states that that there are two types of electrochemical promotion:
First type is based on change of the Fermi level through the charge of the electric double layer (EDL) between catalyst and its support without electrochemical reaction. This effect was abbreviated as EDLE.
Second type is based on change of Fermi level by electrochemical production of promoters, reducing or oxidizing current carriers of the catalyst support (O^{2-}, H^{+}, Na^{+}). This type was abbreviated as EEPP.
In Capters 4-7, the results of my research are given as examples of use of electrochemistry as a tool for study, promotion and development of catalysts.
This study can be devided into four parts:

(I) *Use of electrochemical technique (cyclic voltammetry) in study of the mechanism of chemical catalytic reactions (catalytic SO_2 oxidation to SO_3 on vanadia catalyst, the Contact process), nature of the cationic promotion of this process, the effect of water on the catalytic activity of vanadia (Chapter 4).*
It has been shown that the Contact process can be simulated by a solution of V_2O_5 in molten $M_2S_2O_7$ (M is an alkali metal) and the electrochemical reduction of the V(V) particles ideally reflects catalytic activity of the vanadia catalyst.
If the electrochemical reduction V(V) is reversible, then vanadia catalyst is highly active. By using cyclic voltammetry it has been shown that the reaction is reversible (fast) up to a fraction of 5 m/o of V_2O_5 and is a one-electron reaction at all studied

concentrations (i.e., up to 20 m/o of V_2O_5). This is in agreement with the published data on the vanadia catalyst and also in agreement with the publications concluding that V(V) complexes are monomeric (one-electrone redox reaction).

The presence of Li^+, Na^+ and Cs^+ ions cause a noticeable acceleration of V(V) $\leftrightarrow$ V(IV) reaction (the V(V)/V(IV) electrochemical couple kinetics changed from irreversible to reversible). Therefore voltammetry can be used as a reliable tool for the study of a mechanism of the cationic promotion of the SO_2 catalytic oxidation and for an optimization of the amount of the promoter.

We concluded that the alkali-ion promotion effect can be qualitatively devided into two types: *"large amount promoter"*, when the promoter changes physic-chemical properties of the bulk melt (i.e. Cs^+); and *"small amount additive"*, when the bulk properties are not significantly changed, but the thermodynamics and kinetics of catalytic reaction is changed (Na^+, Li^+).

The effect of water on the electrochemical behavior of V_2O_5 was studied in $K_2S_2O_7$-$KHSO_4$ -V_2O_5 and $K_2S_2O_7$-$KHSO_4$ -V_2O_4 melts in argon and SO_2/air atmospheres with a gold electrode at 440°C.

It was shown that the water has a promoting effect on the V(IV) $\rightarrow$ V(III) reduction increasing the concentration of V(III) species in the studied melts.

Both reactions, the V(V) $\rightarrow$ V(IV) reduction and the V(IV) oxidation, remain one-electron electrochemical reactions with increasing concentration of $KHSO_4$ in the molten $K_2S_2O_7$-$KHSO_4$ -V_2O_5 system.

Water had no noticeable effect on the kinetics of the V(V) $\rightarrow$ V(IV) reduction, but caused higher polarizations (i.e. inhibition) of the V(IV) $\rightarrow$ V(V) oxidation reaction both in the Ar and SO_2/air atmospheres.

(II) Study of electrochemical promotion of heterogeneous catalytic reactions on Pt/C/Polybenzimidazol-H_3PO_4 catalyst at 135-170℃ (Chapter 5).

In this study, for the first time polymeric proton-conducting electrolyte, i.e. polybenzimidazole/H_3PO_4 was used as a catalyst support for promotion of heterogeneous catalytic reactions. The following catalytic reactions were studied: Oxidative coupling of methane (OCM), NO reduction with hydrogen and methane and Fischer-Tropsh synthesis (FTS).

In Chapter 5.1, the possibility of creation of a new OCM route for catalytic CH_4 oxidation by the electrochemical production of Pt-H centers at the Pt-PBI(H_3PO_4)-gas boundary has been demonstrated.

It has been shown that Pt catalyst activity and selectivity toward the CH_4 *!* C_2H_2 reaction can be electrochemically promoted with the maximum promotion effect (3.8% C_2H_2 yield, 135°C) at -0.15 V. The promotion effect had an EEPP nature.

In Chapter 5.2, possibility of the electrochemical promotion of the catalytic NO reduction by hydrogen at the Pt-PBI(H_3PO_4)-gas boundary has been demonstrated. It has also been shown that the nature of this promotion effect can vary depending on the flow rate of the NO/H_2 /Ar gas mixture. At high NO/ H_2/ Ar flow rate (17 mL/min; 17 and 354 mL/min, respectively, at atmospheric pressure), it has been found that NO reduction can be electrochemically promoted at negative polarization with maximum (9.3% of NO conversion to N_2 at 135°C) at approximately -0.15 V, *i.e.*, close to the potential found for the maximum promotion of CH_4 oxidation at the same catalyst. The maximum rate enhancement ratio was 4.65. The value of Λ calculated for maximum promotion effect conditions was 1.26×10^3, *i.e.*, $\Lambda >> 1$. This means that this effect has an EEPP nature, the catalytic reaction was promoted by the electrochemically produced adsorbed hydrogen species.

At low NO/ H_2/ Ar flow rate (17 mL/min; 17 and 140 mL/min, respectively, at atmospheric pressure), NO reduction increased 20 times even without polarization. Moreover, under these conditions negative polarization decreased the rate of NO reduction ~*i.e.*, an opposite effect to what was found at high gas flow rates. However, the electrochemical promotion effect did occur at positive polarization with maximum increase (close to 60% NO conversion at 135°C) at approximately 0.08 V and with 1.5 times the zero polarization value. In the potential range of the promotion effect faradaic current is absent. It means that the promotion effect has a EDLE nature.

In Chapter 5.3, the reduction of NO by methane was studied in (NO,CH_4, Ar), Pt|PBI–H_3PO_4|Pt, (H_2,Ar) fuel cell at 135 and 165°C. It has been shown that in this system NO can be reduced chemically by methane to N_2. Maximum promotion effect on NO conversion reached 46.5% methane conversion at 135°C . The NO reduction was affected by negative polarization of the catalyst and was at maximum at the potentials of the electrochemical reduction of protons. Therefore, the promotion effect had EEPP nature. There was no significant effect of temperature increase (from 135 to 165°C) on the catalyst activity in the NO reduction by methane.

In Chapter 5.4., electrochemical promotion (EP) of FTS studied in the *CO, H_2, Ar // Pt/Ru/ C/Polybenzimidazol-H_3PO_4/Pt/H_2,Ar* cell at 170°C. The Pt/Ru catalyst was chosen because Ru was known to be an active FTS catalyst. The FTS product was methane. The maximum promotion was found between -0.050 V and 0 V and showed 11.1% or a CO conversion rateof 1.38×10^{-6} mol/s.

This case of electrochemical promotion had EDLE, because it took place during a positive polarization of the catalyst, i.e. there was no electrochemical production of promoter (H atoms) and probably in this way the oxidation of gaseous hydrogen was accelerated and conditions of CO adsorption were improved.

(III) Development of catalysts for the high temperature proton exchange membrane (PEM) water electrolysis (Chapter 6).

In Chapter 6.1, the catalysts composed of IrO_2 on a SiC/Si support have been studied in hot phosphoric acid (simulation of high temperature PEM electrolyte).

The electrochemical activity of IrO_2 was found to be improved in the presence of the support. The activity of 80 wt.% and 90 wt.% samples was found to be higher than that of unsupported catalyst. This was attributed to the improved surface properties of IrO_2 in the presence of the support, rather than to a better conductivity or surface area of the support itself, which possesses rather poor properties compared to IrO_2.

Based on the above results, the SiC/Si compound has been recommended as a potential candidate as a support of an anode electrocatalyst for phosphoric acid doped membrane steam electrolysers.

In Chapter 6.2, it has been shown that TaC represents a promising candidate for application as an IrO_2 electrocatalyst support for the anodic oxygen evolution reaction in the high-temperature PEM water electrolysis. The negative aspect represented by the formation of a surface film of $NaTaO_3$, characterised by low conductivity, may be overcome by applying a sufficient amount of IrO_2, in this particular case 50 wt.% or more. Such a supported electrocatalyst has shown properties similar to those of pure IrO_2, including electrocatalytic activity and the rate-determining step of the oxygen evolution reaction.

In Chapter 6.3, the data on electrochemical behaviour of WC as a hydrogen reduction electrocatalyst for high temperature PEM water electrolysis have been presented. That behaviour has been compared with platinum and it was shown that the relative increase of the electrochemical activity of WC towards the HER as a function of temperature is more pronounced, than for Pt and this has been especially observed in

the temperature range from 120°C to 150°C. Therefore there is a probability that at higher temperatures WC can substitute platinum for the hydrogen reduction reaction in high temperature PEM water electrolysers. This assumption was proved during the study of catalytic activity of WC, Mo_2C, TaC, NbC and Pt at 260°C in molten KH_2PO_4.

(IV) Transition metal carbides (WC, Mo_2C, TaC, NbC) as potential electrocatalysts for the hydrogen evolution reaction (HER) at medium temperatures (Chapter 7).

In Chapter 7, the results of the investigation of catalytic activity of WC, Mo_2C, TaC, NbC and Pt at 260°C in molten KH_2PO_4 were presented and discussed. Molten KH_2PO_4 proved to be a good model system for simulation of solid acid-based electrolyzer cells at medium temperatures. Optimised two-step oxidationcarburization reactions on transition metal wire surfaces lead to transition metal carbide coated electrodes, suitable for measurement of the intrinsic electrocatalytic properties. Problems due to contact and varying morphology can thus be avoided.

Under the conditions chosen (260 °C, 1 atm), WC is more active towards the HER than platinum. The catalytic activity increase in the row: TaC < NbC < Mo_2C = Pt < WC.

In Chapter 8, conclusions were made.

In Chapter 9 the outlook of future research was laid out.

RESUME (ABSTRACT IN DANISH)

De to første kapitler i afhandlingen er dedikeret til at definere specielle forhold ved elektrokemiske processer samt fælles træk og forskelle mellem heterogen (redox) katalytiske reaktioner og elektrokemiske reaktioner.
De vigtigste fælles kendetegn for heterogene katalytiske reaktioner og elektrokemiske reaktioner bliver defineret. Det er Fermi-niveauet af katalysatoren, som er det elektrokemiske potentiale på elektroden. Ifølge Newns-Andersons teori er det Fermi-niveauet af katalysatorer, som påvirker (eller endda definere) deres aktivitet. Det elektrokemisk potentiale kan måles og ændres ved polarisering i elektrokemiske forsøg.
I kapitel 3 bliver egenskaberne af den elektrokemiske del af den heterogene katalytiske reaktion diskuteret, herunder den nye teori for elektrokemisk promovering. Denne teori er baseret på en elektrokemisk ændring af Fermi-niveauet for katalysatoren. Det er også anført, at der er to typer af elektrokemiske promovering: Den første type er baseret på ændring af Fermi-niveauet gennem opladningen af det elektriske dobbeltlag (EDL) mellem katalysator og bæreren uden en elektrokemisk reaktion. Denne effekt blevet forkortet EDLE.
Den anden type er baseret på ændring af Fermi-niveauet ved elektrokemisk produktion af promotorer, reducerende eller oxiderende strømbærere fra katalysatorbæreren (O^{2-}, H^{+}, Na^{+}). Denne type blev forkortet EEPP.
I kapitlerne 4-7 er resultaterne af min forskning givet i form af eksempler på anvendelse af elektrokemi som et redskab til undersøgelse, promovering og udvikling af katalysatorer.
Denne undersøgelse kan opdeles i fire dele:

(I) Anvendelse af elektrokemisk teknik (cyklisk voltammetri) i undersøgelse af mekanismen for kemiske katalytiske reaktioner (katalytisk SO_2 oxidation til SO_3 på vanadiumpentoxid katalysator- Kontaktprocessen), beskaffenheden af den kationiske promovering af denne proces, og virkningen af vand på den katalytiske aktivitet (kapitel 4).
Det er blevet vist, at Kontaktprocessen kan simuleres på baggrund af en opløsning af V_2O_5 i smeltet $M_2S_2O_7$ (hvor M er et alkalimetal), og hvor den elektrokemiske reduktion af V(V) partikler ideelt afspejler den katalytiske aktivitet af en

vanadiumpentoxid- katalysatoren. Hvis den elektrokemiske reduktion af V(V) er reversibel, så er vanadiumpentoxid-katalysatoren yderst aktiv. Ved hjælp cyklisk voltammetri er det blevet vist, at reaktionen er reversibel (hurtigt) op til 5 m / o af V_2O_5 og er en én-elektron reaktionen ved alle undersøgte koncentrationer (dvs. op til 20 m / o af V_2O_5). Dette er i overensstemmelse med de offentliggjorte data på vanadiumpentoxid-katalysatoren og også i overensstemmelse med de publikationer som konkluderer, at V(V) komplekserne er monomere (en en-electron redox reaktion).

Tilstedeværelsen af Li^+, Na^+ og Cs^+ ioner forårsager en mærkbar fremskyndelse af V(V) $\leftrightarrow$ V(IV) reaktion (det V(V)/V(IV) elektrokemiske par ændrer kinetik fra irreversibel til reversibel). Derfor kan voltammetri anvendes som et pålideligt værktøj til undersøgelse af mekanismen for den kationiske promovering af SO_2's katalytiske oxidation og til en optimering af mængden af promotoren.

Det er konklusionen, at alkali-ion promoverings-effekten kvalitativt kan opdeles i to typer: *"large amount promotor"*, når promotoren ændrer de fysik-kemiske egenskaber for hovedparten af smelten (dvs. Cs^+); og *"small amount additive"*, når bulk-egenskaber ikke er ændret væsentligt, mens termodynamik og kinetik for reaktionen er ændret (Na^+, Li^+).

Virkningen af vand på den elektrokemiske opførsel af V_2O_5 blev undersøgt i $K_2S_2O_7$-$KHSO_4$ -V_2O_5 og $K_2S_2O_7$-$KHSO_4$ -$V2O_4$ smelter i argon og SO_2 / luft atmosfære med en guldelektrode ved 440 ° C.

Det blev vist, at vand har en promoverende virkning på V(IV) → V(III) reduktionen med forøgelse af koncentrationen af V(III) i de undersøgte smelter til følge.

Begge reaktioner, V(V) / V(IV) reduktionen og V(IV) oxidationen, forbliver en-elektron elektrokemiske reaktioner ved stigende koncentration af $KHSO_4$ i det smeltede $K_2S_2O_7$-$KHSO_4$ -V_2O_5 system.

Vand har ingen mærkbar effekt på kinetikken af V(V) / V(IV) reduktionen, men forårsagede højere polariseringer (dvs. inhibering) af V(IV) / V(V) oxidationsreaktionen både i Ar og SO_2 / luft atmosfære.

(II) Undersøgelse af den elektrokemiske promovering af heterogene katalytiske reaktioner på Pt / C / Polybenzimidazol-H_3PO_4 katalysatoren ved 135-170 ℃ (kapitel 5).

I denne undersøgelse blev for første gang en polymer protonledende elektrolyt, dvs. polybenzimidazol / H_3PO_4, anvendt som en katalysatorbærer til fremme af heterogene

katalytiske reaktioner. Følgende katalytiske reaktioner blev undersøgt: Den oxidatidative kobling af methan (OCM), NO reduktion med hydrogen og methan og Fischer-Tropsh syntese (FTS).

I kapitel 5.1 blev muligheden for oprettelse af en ny OCM rute til katalytisk CH_4 oxidation ved hjælp af den elektrokemiske produktion af Pt-H centre på Pt-PBI (H_3PO_4) -gasgrænse påvist.

Det blev også vist, at Pt katalysator-aktivitet og selektivitet mod $CH_4 \rightarrow C_2H_2$ reaktion kan elektrokemisk promoveres med den maksimale promoverings-effekt (3,8% C_2H_2 udbytte, 135°C) ved -0,15 V, og at den promoverende effekt havde en EEPP natur.

I kapitel 5.2 blev muligheden for en elektrokemiske promovering af den katalytiske NO reduktion med hydrogen ved Pt-PBI (H_3PO_4) -gas grænsen påvist. Det har også vist sig, at arten af denne promovering, kan variere afhængigt af strømningshastigheden af gasblandingen NO / H_2 / Ar. Ved høj NO / H_2 / Ar strømningshastighed (17 ml / min; 17 og 354 ml / min, ved atmosfærisk tryk), er det blevet konstateret, at NO reduktionen kan elektrokemisk promoveres ved negativ polarisering med maksimum (9,3% af NO konvertering til N_2 ved 135°C) ved ca. -0,15 V, dvs. tæt på det potentiale fundet for den maksimale promovering af CH_4 oxidationen med den samme katalysator. Den maksimale "rate enhancement ratio" var 4,65. Værdien af Λ beregnet for den maksimal promoverings- effekt var 1,26 × 103, dvs. $\Lambda >> 1$. Det betyder, at denne effekt har en EEPP karakter og at den katalytiske reaktion fremmes af elektrokemisk fremstillede adsorberet hydrogen .

Ved lav NO / H_2 / Ar strømningshastighed (17 ml / min; 17 og 140 ml / min, ved atmosfærisk tryk), steg NO reduktionen 20 gange selv uden polarisering. I henhold til disse betingelser faldt hastigheden af NO reduktion ved negativ polarisering ~ dvs. en modsat effekt til det, der blev fundet ved høj gas flow. Imidlertid fandt der en elektrokemiske promovering sted ved positiv polarisering med en maksimal effekt (tæt på 60% NO omdannelse ved 135°C) ved ca. 0,08 V og med 1,5 gange den ikke polariserede værdi. I dette potentiale område er faradaic strøm fraværende. Det betyder, at promoverings- effekten har en EDLE karakter.

I kapitel 5.3, blev reduktionen af NO med metan undersøgt i en (NO, CH_4, Ar), Pt | PBI-H_3PO_4 | Pt, (H_2, Ar) brændselscelle ved 135 og 165°C. Det er blevet vist, at i dette system kan NO kemisk reduceres med methan til N_2. Den maksimale promoverings-effekt kom op på 46,5% methan omdannelse ved 135°C. NO reduktionen blev påvirket af negativ polarisering af katalysatoren og nåede et

maksimum ved potentialet for den elektrokemisk reduktion af protoner. Derfor var promoverings-effekten af EEPP natur. Der var ingen signifikant effekt af en temperaturstigning (135-165°C) på katalysatorens aktivitet i NO reduktion ved hjælp af methan.

I kapitel 5.4 ses der på elektrokemisk promovering (EP) af FTS undersøgt i en *CO, H_2, Ar // Pt / Ru / C / Polybenzimidazol-H_3PO_4 / Pt / H_2, Ar*-celle ved 170°C. Pt / Ru-katalysatoren blev valgt, fordi Ru var kendt for at være en aktiv FTS katalysator. FTS produktet var methan. Den maksimale promovering blev fundet mellem -0,050 V og 0 V og viste 11,1% eller en CO-omdannelse-hastighed på $1{,}38 \times 10^{-6}$ mol / s.

Denne elektrokemiske promovering havde EDLE, fordi den fandt sted under en positiv polarisering af katalysatoren, dvs. der var ingen elektrokemiske fremstilling af protoner (H-atomer) og sandsynligvis blev oxidationen af gasformigt hydrogen på denne måde fremskyndet og betingelserne for CO adsorption således forbedret.

(III) Udvikling af katalysatorer til høj temperatur proton exchange membrane (PEM) vandelektrolyse (kapitel 6).

I kapitel 6.1 diskuteres katalysatorer sammensat af IrO_2 på en SiC / Si bærer i varm phosphorsyre (simulering af høj temperatur PEM elektrolyt).

Den elektrokemiske aktivitet af IrO_2 fandtes at blive forbedret i forbindelse med tilstedeværelse af en bærer. Aktiviteten af 80 vægt.% og 90 vægt.-% prøver viste sig at være højere end for en ikke-understøttet katalysator. Dette blev tilskrevet forbedrede overfladeegenskaber af IrO_2 i nærværelse af bæreren, i stedet for bidrag af en bedre ledningsevne eller overfladeareal af bæreren selv (som besidder temmelig dårlige egenskaber sammenlignet med IrO_2).

På baggrund af ovenstående resultater er SiC / Si forbindelse blevet anbefalet som en potentiel kandidat som bærer for anode elektrokatalysatoren til phosphorsyre- dopede membran- damp- elektrolyseanlæg.

I kapitel 6.2 er det blevet vist, at TaC repræsenterer en lovende kandidat til anvendelse som en IrO_2 elektrokatalysator-bærer til den anodiske oxygenudvikling i høj temperatur PEM vandelektrolyseceller. Det negative aspekt ved dannelsen af en overfladefilm af $NaTaO_3$ (kendetegnet ved lav ledningsevne) kan overvindes ved at anvende en tilstrækkelig mængde IrO_2, i dette særlige tilfælde 50 vægt.% eller mere. En sådan understøttet elektrokatalysator har vist egenskaber svarende til dem for ren IrO_2, herunder elektrokatalytisk aktivitet og det samme hastighedsbestemmende trin for oxygenudvikling.

I kapitel 6.3 fremlægges data for elektrokemisk adfærd af WC som en hydrogen elektrokatalysator for højtemperatur PEM vandelektrolyse . Egenskaberne er blevet sammenlignet med dem for platin, og det er blevet vist, at den relative forøgelse af den elektrokemiske aktivitet af WC mod HER som en funktion af temperaturen er mere udtalt end for Pt og dette er især observeret i temperaturområdet fra 120°C til 150°C. Derfor er der en sandsynlighed for, at WC ved højere temperaturer kan erstatte platin i højtemperatur PEM vandelektrolyseanlæg. Denne antagelse blev bevist i forbindelse med undersøgelsen af katalytisk aktivitet af WC, Mo_2C TaC, NbC og Pt ved 260°C i smeltet KH_2PO_4.

(IV) Transition metalcarbider (WC, Mo_2C, TaC, NbC) som potentielle elektrokatalysatorer for hydrogenudviklings-reaktionen (HER) i medium temperaturområdet (kapitel 7).

I kapitel 7 blev resultaterne af undersøgelsen af katalytisk aktivitet af WC, Mo_2C TaC, NbC og Pt på 260°C i smeltet KH_2PO_4 præsenteret og diskuteret. Smeltet KH_2PO_4 viste sig at være en god model for simulering af faste syre-baserede elektrolysatorceller ved medium temperaturer. Optimerede totrins oxidation-carburiserings- reaktioner på metaltråds- overflader førte til elektroder, der var egnede til at måle på en veldefineret måde de elektrokatalytiske egenskaber af stofferne. Problemer som følge af kontakt og varierende morfologi kan således undgås.

Under de valgte betingelser (260°C, 1 atm), er WC mere aktivt i forhold til HER end platin. Den katalytiske aktivitet stigning i rækken: TaC <NbC <Mo2C = Pt <WC.
I kapitel 8 er konklusionerne i forbindelse med afhandlingen fremlagt.
I kapitel 9 er udsigterne for en fremtidige forskning skitseret.

List of relevant publications by the author

A15. Transition metal carbides (WC, Mo_2C, TaC, NbC) as potential electrocatalysts for the hydrogen evolution reaction (HER) at medium temperatures.
S. Meyer, A.V. Nikiforov, I.M. Petrushina*, K. Köhler, E. Christensen, J.O. Jensen, N.J. Bjerrum, *Int. J. Hydr. Energy*, **40**, 2905 (2015).

A14. Corrosion behavior of construction materials for intermediate temperature steam electrolysers
A.V. Nikiforov, I.M. Petrushina*, J.O. Jensen and N. J. Bjerrum
Advanced Materials Research, **699**, p. 596, (2013).

A13. WC as a non-platinum hydrogen evolution electrocatalyst for high temperature water electrolysers
A.V.Nikiforov, I.M.Petrushina*, E.Christensen, N.V. Alexeev, V.A. Samokhin N.J.Bjerrum, *Inter. J. Hydr. Energy*, **37**, p.18591, (2012).

A12. Tantalum carbide as a novel support material for anode electrocatalysts in polymer electrolyte membrane water electrolyzers
J. Polonsky, I.M.Petrushina*, E. Christensen, K. Bouzek, C.B. Prag, J.E.T. Andersen, N.J. Bjerrum, *Inter. J. Hydr. Energy*, **37**, p.2173, (2012).

A11. Preparation and study of IrO_2/SiC-Si supported anode catalyst for high temperature PEM steam electrolysers.
A. V. Nikiforov, A. L. Tomas Garcia; I. M. Petrushina*, E. Christensen, N. J. Bjerrum *Inter. J. Hydr. Energy*, **36**, p.5797, (2011).

A10. Corrosion behaviour of construction materials for high temperature steam electrolysers.
A.V. Nikiforov, I.M.Petrushina*, E.Christensen, A.L. Tomas-Garcia, N.J.Bjerrum, *Inter. J. Hydr. Energy*, **36**, p.111, (2011).

A9. NO and CO electrochemical reduction in the NO(CO)/(Pt/Ru)/PBI(H_3PO_4)/Pt/H_2 membrane cell at 150°C.

I.M.Petrushina*, K. Wonsyld, L.N.Cleemann, N.J. Bjerrum, *Proceedings. 2nd International Conference on the Electrochemical Promotion of Catalysis (EPOCAP), Oleron Island, France (29 September – 3 October, 2008),* 183 (2009).

A8. Electrochemical promotion of catalytic reactions at Pt/C (or Pt/Ru/C)//PBI Catalyst.
I.M. Petrushina*, N.J. Bjerrum, V.A. Bandur, L.N. Cleemann, *Topics in Catalysis*, **44**, 427, (2007).

A7. Catalytic reduction of NO by methane using a Pt/C/polybenzimidazole/Pt/C fuel cell.
I.M. Petrushina*, L.N. Cleemann, R. Refshauge, N.J. Bjerrum, V.A. Bandur, *J. Electrochem. Soc.*, **154**, E84, **(**2007**).**

A6. Electrochemical Promotion of NO Reduction by Hydrogen on a Platinum/Polybenzimidazole Catalyst.

I. M. Petrushina*, V. A. Bandur, F. Cappeln, N. J. Bjerrum, R. Z. Sørensen, R. H. Refshauge, and Qingfeng Li, *J. Electrochem. Soc*., **150**, D87, (2003).

A5. Electrochemical promotion of oxidative coupling of methane on platinum/polybenimidazole catalyst.
I.M. Petrushina*, V.A. Bandur, N.J. Bjerrum, F. Cappeln, L. Qingfeng, *J. Electrochem. Soc*., **149**, D143, (2002).

A 4. Electrochemical promotion of sulfure dioxide catalytic oxidation,
I.M. Petrushina, V.A. Bandur, N.J. Bjerrum, *J. Electrochem. Soc.*, **147**, 3010, (2000).

A3. Electrochemical study on the cationic promotion of the catalytic SO_2 oxidation.
I.Petrushina*, N.J. Bjerrum and F. Cappeln, *J. Electrochem. Soc.*, **145**, 3721, (1998).

A 2. Electrochemical behavior of molten V_2O_5 –$K_2S_2O_7$-$KHSO_7$ systems.
I.M.Petrushina*, N.J.Bjerrum, R.W.Berg, and F.Cappeln, *J. Electrochem. Soc*., **144**, 532, (1997).

A1. Electrochemical Investigation of the Catalytical Processes in Sulfuric Acid Production.
N.J.Bjerrum, I.M.Petrushina*, and R.W.Berg, *J.Electrochem.Soc*, **142**, 1806, (1995).

Monography

B1. ***Electrolysis,*** Chapter 4 "Construction materials for PEM water electrolysers and their assessment"
A.V. Nikiforov, E.Christensen, I.M.Petrushina*, J.O.Jensen, N.J.Bjerrum
ISBN 980-953-307-273-4, **2012**, pp.61-86

Patent

Corrosion protection of steel in carbonate melts.
N.J.Bjerrum, F.Borup, I.M.Petrushina, Li Qingfeng. **Danish Patent nr. DK173118 B1, 2000**.

Table of Contents

1. DEFINITIONS AND CONCIDERATIONS

Electrochemistry is a science about an interexchange between chemical and electrical energy.

Electrochemical reaction is a hetergeneous redox reaction, i.e. the redox reaction which takes place at the interface between two phases.

There are three fundamental differences between chemical and electrochemical redox reactions

1) Electrochemical reaction always takes place at the interface between ***electronic (electrode)*** and ***ionic conductor (electrolyte)***.
2) In electrochemical reaction reduction and oxidation half-reactions should be ***physically separated***, i.e. take place at different electrodes.
3) Because of this physical separation, electrons are the participants of electrochemical reaction and cross the interface during the reaction (***electron transfer***). Moreover, the electron transfer is the most important step of electrochemical reaction.

The structure of the electrochemical interface (electric double layer, EDL), the type and the concentration of particles participating in its construcion have a dramatic effect on the mechanism and kinetics of the electrochemical reaction.

In chemical kinetics the ***reaction rate*** (or the ***rate constant***) and the **activation energy** define the mechanism and kinetics of the reaction.

In electrochemistry, the reaction rate is characterized by ***current***, I, in A (or ***i***, current density in A/cm^2). Faraday's law relates the reaction rate and current linearly:

$$v = nFI \qquad (1.1)$$

where v is the reaction rate, n is the number of electrons, participating in the reaction, and F is the Faraday's constant.

The *driving force* which makes the electrons to move from anode to cathode is a difference between the *potentials* of these electrodes.

Potential (E in Vor mV ***)*** *is a work of the electron transport from the electrode to infinity in the electrolyte, or in the opposite direction.*

$$\overline{\mu}_i$$

Electrochemical potential, is the other important characteristic of the electrochemical reaction. The electrochemical potential is equal to the Fermi level of electrons in an electrode (i.e. the highest occupied energy level).
The electrochemical potential can be expressed through chemical and electric potentials in the following equation

$$\overline{\mu}_i = \mu_i + z_i F\phi \qquad (1.2)$$

or

$$\Delta\overline{\mu}_i = \Delta\mu_i + z_i F\Delta\phi \qquad (1.3.)$$

where $\overline{\mu}_i$ is the ***electrochemical potential*** of the species ***i,*** μ_I is the chemical potential of the species ***i,*** ϕ is the electric potential of a phase, $\Delta\phi$ ***(or E)*** is the potential difference across the interface and z_iF is the electric charge of the particle per mole. If the particles are neutral, the electrochemical potential is equal to the chemical potential.
Fermi level of an electrode can be changed by polarization of the electrode, i.e. change of ***E***. When electrons are pumped to the electrode, i.e. it is charged negatively, the Fermi level increases, and when electrons are pumped from the electrode, i.e. it is charged positively, the Fermi level decreases.
Polarization of the electrode affects Fermi level and therefore changes the activation energy of the electrochemical reaction.
Consider the following electrochemical reaction, when oxidized particles get ***n*** electrons (i.e. get reduced) and become reduced particles:

$$O + ne \xleftrightarrow{k_b, k_f} R \qquad (1.4)$$

where k_f is the rate constant of the forward reaction, which is reduction, i.e. cathodic reaction, and k_b is the rate constant of the backward reaction, which is oxidation, i.e. anodic reaction.
For electrochemical reactions, the relation between the rate constant k and the activation energy ΔG^a will have the Arrenius form, i.e. for the cathodic and the anodic reactions,

$$k_c = A_c e^{-\Delta G_c^a / RT} \qquad (1.5)$$

$$k_a = A_a e^{-\Delta G_a^a / RT} \tag{1.6}$$

where ΔG_c^a and ΔG_a^a are activation free energies for cathodic and anodic reactions respectively, and A_c and A_a are constants. At equilibrium,

$$k_c = k_a = k^0 \tag{1.7}$$

where k^0 is the standard rate constant, and

$$\Delta G_c^{\,a} = \Delta G_a^{\,a} = \Delta G^{0a} \tag{1.8}$$

$$\Delta G^{0a} = \mathrm{nFE}^0 \tag{1.9}$$

where E^0 is the equilibrium potential of the electrochemical reaction.

When the electrode polarized positively to the potential E and the Fermi level decreases, the activation anodic free energy also decreases, i.e.

$$\Delta G_a^a = \Delta G^{0a} - (1-\alpha) nF(E - E^0) \tag{1.10}$$

and the activation cathodic free energy increases

$$\Delta G_c^a = \Delta G^{0a} + \alpha nF(E - E^0) \tag{1.11}$$

where α is the transfer coefficient ($0 < \alpha < 1$) and expresses a symmetry of the activation energy barrier (when it is symmetric $\alpha = 0.5$) and $E - E^0$ is polarization. Finally, current – potential relations for a steady state conditions can be expressed by the ***Butler-Volmer equation***

$$i = nFAk^0[C_O(0,t)e^{-\alpha nF/RT(E-E^0)} - C_R(0,t)e^{(1-\alpha)nF/RT(E-E^0)}] \tag{1.12}$$

where $C_O(0,t)$ and $C_R(0,t)$ are the interface concentrations of the oxidized and reduced particles, and A is the surface area of the electrode. Two exponential part of this equation are the cathodic and the anodic currents (i_c and i_a) and i is the net current.

If we introduce the exchange current, i_0 (at equilibrium $i_c = i_a = i_0$ and the net current is zero) and assume that the surface concentrations are equal the balk concentrations, than

$$i = i_0\left[e^{-(\alpha nF/RT)\eta} - e^{(1-\alpha)(nF/RT)\eta}\right] \tag{1.13}$$

$$\eta = E - E^0 \tag{1.14}$$

The exchange current is very important characteristic of kinetics of the electrochemical reaction, therefore in corrosion science it is often used as expression of the corrosion rate and in electrocatalysis as an expression of an activity of catalysts.

Commonly, the shorter version of (1.13) is used for the definition of the exchange current. At high anodic or cathodic polarization one of the parts of (1.13) is negleagable, e.g.

$$i = i_0 e^{-(\alpha nF/RT)\eta} \tag{1.15}$$

If we will take logarithm of the both sides of (1.15), we will obtain the Tafel equation

$$\eta = \frac{RT}{\alpha nF}\ln i_0 - \frac{RT}{\alpha nF}\ln i \tag{1.16}$$

2. HETEROGENEOUS CATALYSIS AND ELECTROCATALYSIS: DEFINITION OF COMMON FEATURES

Heterogeneous catalysts provide a surface for the chemical reaction to take place on. In order for the reaction to occur one or more reactants must reach the catalyst surface and adsorb onto it. After reaction, the products must desorb from the surface and diffuse away from the solid surface. Chemisorption of the reactants at the surface of the catalyst is the most important step of the whole reaction, because it decreases the activation energy barrier.

The most important features of chemisorption as a step of catalytic reaction are summarized in the Newns-Anderson model.1,2 Most of the catalysts are d-metals and therefore adsorption on a metal with the d states is of particular interst. Broading and shifting of the adsorbate's energy levels is a result of

chemisorptions. Moreover there is a strong interaction of these levels with the d band of the catalyst, creating a pair of bonding and antibonding chemisorptions orbitals (Fig.2.1 from Ref. [3]). The part of the adsorbate levels which are below the Fermi level will be occupied by the d electrons. Both bonding and antibonding levels affect the chemisoption bond, however filling of the antibonding orbital will strengthen the chemisorption bond and weaken the intramolecular bond, which will lead to dissociation of the adsorbed molecule. This is the essence of the nature of heterogeneous catalysis.

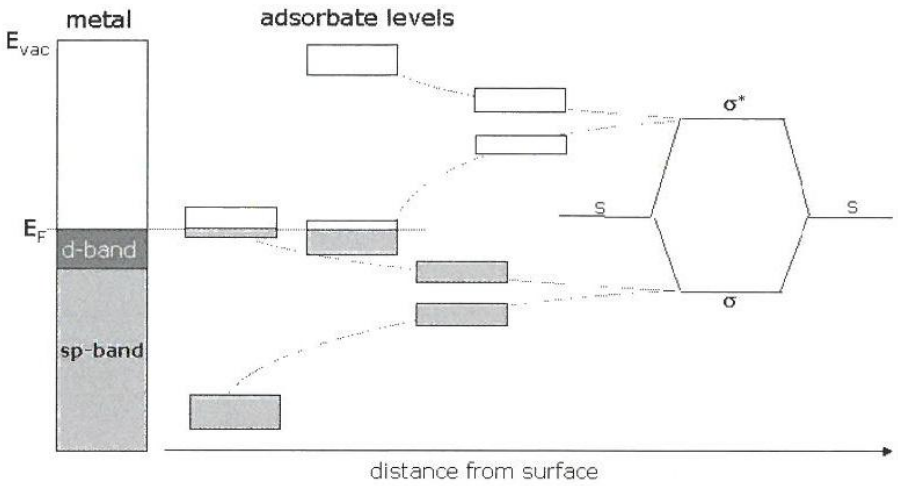

Fig. 2.1. Newns-Anderson approximation[3]

The Newns-Anderson theory helps to understand why there are two tools instead of one, i.e. besides a nature of the catalyst, control electrocatalysis.

Let us start with the definition of electrocatalysis.

If the electrode acts as a heterogeneous catalyst, i.e. accelerates the electrochemical reaction, the phenomemon is called ***electrocatalysis***. In this case reactants, products or intermediates are adsorbed on the electrode.

Heterogeneous catalysis and electrocatalysis are close phenomena, except that during the electrocatalysis the charge transfer across the interface takes place.It means that the ***rate of electrocatalytic reaction depends on the potential,*** i.e. in this case we have a reliable tool of control of the rate and selectivity of the reaction. The Newns-Anderson theory helps to understand the effect of potential on the catalytic activity, because polarization of the electrode changes the Fermi level of this electrode.

It is evident that in order to use electrochemistry as a tool in study or promotion of catalytic reactions, electrochemical interface (electronic/ionic conductors) should already exist in the catalytic system (e.g. Pt catalyst/Y_2O_3 stabilized ZrO_2 (YSZ) support) or can be created. For example, V_2O_5 in a molten alkali metal pyrosulphate is an ionic conductor, and therefore a noncatalyst electrode (e.g. gold) can be used in the study of V(V) $\leftrightarrow$ V(IV) equilibrium, which is the most important step in the catalytic oxidation of SO_2 to SO_3. All these cases will be dicussed in the thesis.
Historically, application of galvanic cells with solid electrolytes for the study of catalytic phenomena was suggested by Wagner[4]. He, for example, proposed to define a steady-state oxygen activity in metal or metal oxide catalysts by measuring the electromotive force (EMF) between these catalysts and and the reference electrode in the following system:
Ni/NiO (reference electrode)/ ZrO_2 (+ CaO)/ metal or metal oxide/ reacting mixture.
Later, similar systems were used in the study of electrochemical promotion.

3. ELECTROCHEMICAL PROMOTION. NEW DEVELOPMENT OF THE THEORY OF ELECTROCHEMICAL PROMOTION

It was found, that the rate and selectivity of a catalytic reaction can be remarkably and reversibly changed by electrochemical polarization of the electronic conductive catalyst on the ionic conductive support. This phenomenon was discovered by Vayenas *et al.* and named the "NEMCA effect" (non-faradaic electrochemical modification of catalytic activity).[5] Term "electrochemical promotion" was first proposed by Pritchard[6] in his response to Vayenas's paper.

The NEMCA effect has been demonstrated for more than 50 heterogeneous and one homogeneous catalytic reactions.[7] According to Vayenas *et al.*,[7-9] the NEMCA effect can be described by the following parameters:
The rate ***enhancement ratio***

$$\rho = r/r_o \qquad (3.1)$$

and the ***enhancement factor***

$$\Lambda = (r - r_o)/(I/2F) \qquad (3.2)$$

where r is the rate of the catalytic at current I, r_o is the open-circuit catalytic

rate, and *F* is Faraday's constant. In all studied cases of the electrochemical promotion $\Lambda >> 1$, and that was the reason why this effect has been called ''non-faradaic.''

Vayenas *et al.*[5, 7-10] explained the electrochemical promotion of a catalyst as an effect of changes in the work function, $e\Delta\Phi$ (e is the electron charge, $\Delta\Phi$ is change of the electron extraction potential), of the catalyst under polarization. The change of the electron extraction potential has been measured to be equal to the applied polarization, *i.e.*

$$\eta = \Delta\Phi \qquad (3.3)$$

It was also suggested that this change in the work function was caused by spillover of the products of the charge transfer from the three-phase boundary to the catalyst-gas interface. The change in the work function was measured using the Kelvin probe technique.

However, it has been found later [11-15] that work function changes of catalyst with different morphology, measured using a Kelvin probe, may be only a part of the applied polarization or do not change at all. Summarizing the results of Refs. [5,7-10,11-15] one can agree with the assumption of Emery *et al.*[13] and Metcalfe[14,15] that

$$\Delta\Phi = \xi\eta \qquad (3.4)$$

Where ξ is a coefficient. Furthermore one can also assume $0 \leq \xi \leq 1$.

The electrochemical potential of the electron in a metal, $\bar{\mu}_i$ (Fermi level), is a sum of the chemical potential of the electron in the metal μ_e and $e\phi$, where ϕ is the inner or Galvani potential (Equs. 1.2, 1.3). The Galvani potential is a sum of an outer (or Volta) potential, Ψ, and a surface potential, χ. The work function of electron, $e\Delta\Phi$, is equal to the electrochemical potential of the uncharged metal ($\Psi = 0$),[16] *i.e.*

$$\Delta\Phi = \Delta\mu + \Delta\chi \qquad (3.5)$$

and $\Delta\Psi \neq 0$ is the reason for the difference between $\Delta\Phi$ and η (Eq. 3.4). The value of ξ is defined by the value of the polarization resistance of the electrochemical reaction at the catalyst/support interface: if this resistance is low, $\xi \approx 1$; if this resistance is high, $\xi \approx 0$ and by polarization we mainly charge the catalyst-support electric double ayer.[13]

Based on the published data and our experimental results[99-102 (A5-A8)], a ***new theory of electrochemical promotion of catalytic reactions*** was developed (compared to the C. Vayenas theory[11]).

The basic principle of electrochemical promotion is that heterogeneous catalytic reaction is promoted by an ***electrochemical change of the Fermi level of the catalyst***.

Three types of electrochemical promotion can be defined depending on values of the faradaic current, ***I***, and the enhancement factor, Λ (Equ. (3.2), p.11):

1. The electric double layer (or catalyst/support) effect (**EDLE**) is characterized by $I = 0$. Charging of the electric double layer at the catalyst-support interface is the only result of the polarization of the catalyst. $\Delta\Psi \neq 0$ and $\Delta\Phi \neq \eta$. However it can dramatically change the catalyst activity because the charging leads to change of structure (or nature) of the catalyst/support interface.
2. The effect of the electrochemically produced promoters (**EEPP**). $I \neq 0$. $\Lambda >> 1$. Electric current carriers from the catalyst support (e.g. H^+, O^{2-}, Na^+) are reduced or oxidized electrochemically at the catalyst support interface and act as the catalyst promoters.
3. The case of electrocatalysis is when reactant (or reactants) of a catalytic reaction are oxidized or reduced electrochemically. $I \neq 0$, $\Lambda = 1$. It means that the catalytic reaction follows the Faraday's low.

In Chapter 5, the results of the study of the electrochemical promotion of catalytic reactions on the Pt (or Pt/Ru)/C/Polybenzimidazol-H_3PO_4 catalyst at 135-170°C obtained by the author will be discussed.

4. DEFINITIONS AND CONCIDERATIONS OF THE CATALYTIC SO_2 OXIDATION ON V_2O_5 CATALYST (CONTACT PROCESS)

In the following chapter I will present the results of the investigation where for the first time we used electrochemistry as a tool in study on the catalytic reaction. This approach was very effective and contributed a lot in our understanding of the effect of the catalyst concentration, water and alkali metal ions on the catalyst activity. For the first time possibility of electrochemical promotion of commercial catalyst was studied and the results are presented in Chapter 4.6.

It is natural to start from the desciption of the state-of-art of this area before an electrochemical technique was used to study the catalytic SO_2 oxidation on the V_2O_5 catalyst.

The molten $V_2O_5 – M_2S_2O_7$ system (M is an alkali metal) on a silica support is used as a catalytic medium for sulfur dioxide oxidation with oxygen or air, and this has been a subject of numerous publications for more than sixty years.[23-27] However, the mechanism of this catalytic process was not clearly understood, the following problems remaining unsolved:

1) The number of the catalytical reaction steps involved has not been defined; two-step [23,28], three-step[24], and four-step[26] mechanisms were proposed.

2) The structure of catalytically active V(V) species has to be elucidated. Neither proposed monomeric[28], nor dimeric [26, 27, 29] structure of the dioxovanadium complexes was convincingly determined.

3) The first unsolved problem also led to a question concerning the possibility of the V(V) two-stage reduction (both to V(IV) and V(III) species). The precipitation of solid V(III) compounds in the liquid-gas $M_2S_2O_7/V_2O_5$-$SO_2/O_2/SO_3/N_2$ system (where M is Na, K, or Cs), has been proven by chemical and x-ray analysis.[26] Electrochemical investigations in $V_2O_5 – M_2S_2O_7$ melt could neither prove nor disprove the V(V) $\rightarrow$ V(III) reduction reaction.[28,31,34]

4) The nature of the promoting effect of alkali ions on the catalytic activity of the $V_2O_5 – M_2S_2O_7$ was unknown. It was found in practice that the efficiency increased with alkali metal atomic number and the presence of sodium cations had a promotive effect at low temperatures (close to the point of catalyst deactivation, i.e., 440°C[24]); and that cesium ions decreased the temperature of deactivation.[26, 32-35]

The promoters, used in modern catalyst for the industrial sulfuric acid production are potassium, cesium, and sodium sulfates (or pyrosulfates).[23,26,32,33,35, 72-81]

If the efficiency of alkali promoters increases with the alkali atomic number (or with the ionic radious), then Cs^+ ions have the strongest promotion effect. This fact was explained on the basis of the increasing ability of the alkali sulfates to react with SO_3 and therefore increasing stability of the alkali pyrosulfates in the series from $Li_2S_2O_7$ to $Cs_2S_2O_7$.

It was also found that the activity and thermal stability of the V_2O_5 catalysts promoted only by sodium salts were much lower than those based on potassium salts.[23,35,81] However small amounts (up to 20 m/o) of sodium salts appeared to increase the activity of the potassium vanadium sulfate catalysts[81], especially in the lower part of the working temperature range. This effect was explained as a result of formation potassium-sodium oxosulfatovanadates (V(V)). Nevetherless there was no clear explanation why such a different cations as Cs^+ and Na^+ have a similar promotive effect on the catalytic activity.

Understanding of the nature of the alkali ion promotion certainly should be based on the mechanism of the SO_2 catalytic oxidation. Therefore it is important to have a more comprehensive understanding of the mechanism of the catalytic SO_2 oxidation. The starting point is *the number of catalytic reaction steps involved and the rate-determining step.* – Numerous researchers in the field of the catalytic SO_2 oxidation believe that the V(IV) oxidation with oxygen is the rate-detemining step.[23,24,35, 73-81] It was also found that the V(IV) concentration in the catalyst is a function of temperature, thickness of the catalyst layer, and the equilibrium V(V) + $SO_2 \leftrightarrow SO_3$ – V(IV).[2,73] The latter depends very much on the SO_2 partial pressure and at low pressures it can become the rate determing step.[72] Many researchers [23,24,72-78] have also shown for K/V catalysts that oxygen diffusion affects the rate-determining step. However, there was still a strong disagreement about the number and nature of steps in the catalytic SO_2 oxidation. Thus Mars and Maessen[23] suggested a 2-step mechanism for both K/V and K,Na/V catalysts. According to them, the SO_2 oxidation proceeds through the fast establishment of equilibrium

$$SO_2 + 2V^{5+} + O^{2-} \leftrightarrow SO_3 + 2V^{4+} \qquad (4.1)$$

And the rate-determining step is V(IV) oxidation with oxygen. They also suggested that at temperatures close to an observed sudden decrease of catalytic activity with temperature, the solubility of SO_2 in the molten catalyst becomes high enough to slow down the reaction (4.12) (break in the Arhenius activation energy – 1/T plot for the reaction).

However, the same researchers did not reject the possibility that this break in the Arhenius plots can be explained by the formation of oxosulfovanadates caused by high concentrations of dissolved SO_3. Mars et al. thought that these oxosulfo groups can inclose and stabilize the V^{4+} ion.

The same considerations were behind the three-step mechanism for the 330-380°C temperature range introduced by Glueck and Kenney.[72] They assumed that the melt containing V^{5+} will absorb SO_2 without liberation of the equivalent amount of SO_3 and therefore two types of V^{4+} particles will be present in the molten catalyst at low temperatures: $(VOSO_4)_2$ and $V_2O_4 \cdot SO_3$. Glueck et al. argued against the conception of the V(IV) oxidation as a rate-determining step, at low operation temperatures: they found no dependence of the catalyst activity on the oxygen pressure in the 330-380°C temperature range. Therefore Glueck et al. could not rule out the possibility that reaction (4.12) could be far from equilibrium and become a rate-determining step in the low temperature range.

The idea about a three-step mechanism and two types of V(IV) particles present in the vanadium catalyst at operating temperatures below 430°C was further developed by Villadsen and Livbjerg.[24] They assumed the following mechanism

$$2X + SO_2 \leftrightarrow 2Y \qquad (4.2)$$

$$2Y \leftrightarrow 2Z + SO_2 \qquad (4.3)$$

$$2Z + \tfrac{1}{2} O_2 \leftrightarrow 2X \qquad (4.4)$$

where X are V(V) species and Y and Z are V(IV) species. Reaction (4.4) assumed to be far from equilibrium in thin films and at equilibrium in thick films of the catalyst on a support. The authors[24,77] also suggested that the V(IV) oxidation is a rate-limiting step due to low solubility of oxygen in the molten catalyst.

Villadsen et al.[2] stated that the precipitation of V(IV) complexes is a reason for a drop in the catalytic activity at low operating temperatures, because when the V(IV) species precipitation was taken into account in the model, the break in the Arhenius plot disappeared.

The mechanism assumed by Villadsen et al.[24] was later supported with experimental data obtained by Doering et al.[32] for K/V and Cs/V catalysts. They agreed with the idea that irreversibility of reaction (4.4) at low operation temperatures can cause high Y concentrations and a drop in the catalytic activity. It was also suggested that presence of Cs^+ in the catalyst decreases formation of inactive V(IV) species. It was found[32] that concentration of V(IV) complex is very dependent on the SO_2 partial pressure and temperature but slightly dependent on

the O_2 partial pressure. Doering et al. insisted on the kinetic model with the V(IV) oxidation as the rate-limiting step.

Boreskov et al.[79] and Bolzhinimaev et al.[80] assumed that an associative mechanism, which did not change the oxidation state of vanadium, was possible. They proposed a six-step mechanism that actually consisted of two types of mechanisms: assotiative (without change in the oxidaxion state of vanadium) and redox (with change in the oxidation state of vanadium).

Than an important progress has been made in the investigation of the structure of the solid vanadium compounds that can be separated from the liquid catalysts at temperatures lower than the point of the activity drop.[26,81-84] Moreover, it was shown that at low operating temperatures V(III) species can be formed by reduction with SO_2.[26]

The $Na_2VO(SO_4)_2$, $Na_3(VO)_2(SO_4)4$, $K_4(VO)_3(SO_4)_5$, $K_3(VO)_2(SO_4)_4$, $Cs_2(VO)_2(SO_4)_3$, β-$VOSO_4$, $VOSO_4(SO_2SO_3)x$ [V(IV) and V(V)] deposites] and $Na_3V(SO_4)_2$, $Na_3V(SO_4)_3$, $KV(SO_4)_2$, $CsV(SO_4)_2$ [V(III) deposits] were assumed to be responsible for the catalyst deactivation.[84] It is also believed that the catalytic activity can be increased by increasing the atomic number of the alkali promoter, mixing of alkali promoters, and decreased vanadium concentration of the catalyst. Eriksen et al. suggested that a mixture of alkali ions, such as Na^+ and K^+ or Na^+, K^+, and Cs^+, would probably lead to higher solubility of the V(IV) and V(III) compounds.

Thus, *the reason of the sudden drop of the catalytic activity at 380-430℃* was explained by most researchers by the precipitation of insoluble V(IV) and V(III) oxosulfo complexes. However there is some disagreement concerning V_2O_5-$Cs_2S_2O_7$ melts. According to Boghosian et al.[26,84] the reason is the same as for other alkali cations contained by vanadia catalysts, i.e. precipitation of the V(IV) and V(III) compounds. Still, Doering et al.[32,33] claimed the absence of the V(IV) precipitation in cesium systems down to 300°C, which was much lower than the point of the activity drop, i.e. 400°C. In this case the drop of the catalytic activity was explained on the basis of a reduced availability of V(V) because of the increased V_2O_4-SO_3 concentation at low temperatures.

Many years ago, Glueck and Kenney[72] gave a very good advice concerning the way of obtaining a precise knowledge about the mechanism of the SO_2 oxidation on the vanadia catalyst: *"It is clear that almost any kinetics can be fitted by*

choosing appropriate values of the different rate constants and it is obviously desirable, if possible, to study the individual reaction steps separately."

By using electrochemical techniques, the oxidation and reduction parts of complex chemical reaction can be separated; moreover, some oxidation and reduction agents (such as O_2, SO_2 and SO_3) can be excluded, thus simplifying the investigation. As a result, useful information for the mechanism could be obtained.

The *electrochemical behavior* of molten potassium pyrosulfate and vanadium pentoxide in different gas atmospheres was discussed in numerous publications. [28-31, 36,37]

From these references, large disagreements could be seen between experimental data and conclusions on the width of the potential window and the nature of the electrochemical reactions involved. Moreover, in the most cases conditions of an electrochemical experiment were far from the conditions of the Contact process. According to[36], the potential window of molten $K_2S_2O_7$ at the gold electrode was 0.41V for acidic melt and 0.51V for basic melt at 430°C:

Acidic: ***Basic:***

$$2S_2O_7^{2-} \leftrightarrow S_3O_{10}^{2-}(SO_3 \text{ solvate in the pyrosulfate melt}) + SO_4^{2-} \qquad (4.5)$$

The difference between cathodic potential limits in the acidic and basic melts was as high as 0.52 V. The anodic limit was assumed to be the gold electrooxidation in the acidic melt, and in the basic melt to the SO_4^{2-} ion oxidation with oxygen evolution. The cathodic limit was assumed to be the reduction of $S_2O_7^{2-}$ (or SO_3).[28] These assumptions have not been tested experimentally, and the difference between the potential windows for the acidic and basic melts seems questionable taking into account the results obtained by Comtat et al.[36], Frank and Winnick,[29] and Dojcinovic et al.[31] Thus, according to Ref.36, it is the same anodic potential limit in the basic electrolyte for Pr and Au electrodes. Frank and Winnick[29] obtained an approximately 0.6 V wide potential window at a gold electrode in N_2, air, SO_2/air, $SO_2/O_2/N_2$ atmospheres, in both acidic and basic molten potassium pyrosulfate. Oxidation of SO_4^{2-} was observed at the anodic limit of 0.8-0.9 V vs. Ag/Ag^+, whereas $S_2O_7^{2-}$ reduction was seen as the cathodic limiting reaction at 0.25 V. However, the experiments in Ref.29 were conducted at 370-400°C, i.e. at temperatures lower than the melting point of dry $K_2S_2O_7$ (418.52°C[38]). This can indicate the presence of water in the melt, and therefore a possible water effect on the electrochemical behavior of

molten potassium pyrosulfate. These consideretions could also explain the 1.0 V difference between the potentials of the cathodic limiting reactions in Ref.29 and Ref.31.

Electrochemistry of molten alkali sulfates was studied more extensively than electrochemistry of molten pyrosulphates.[40-44]

The electrochemical behavior of solutions of V_2O_5 and $VOSO_4 \cdot 3.5\ H_2O$ in acidic and basic molten $K_2S_2O_7$ was investigated at gold electrodes in different gas atmospheres (i.e. N_2, O_2, SO_2/N_2 etc.).[28,29] Franc and Winnick[29] have studied the electrochemistry of V_2O_5 solutions (1-5 w/o) in basic and acidic $K_2S_2O_7$ in N_2, O_2, SO_2/N_2, and $SO_2/O_2/N_2$ atmospheres.

Durand et al.[28] have concluded that in 0.25-1.0 mole % (m/o) concentration range, the $V(V) \leftrightarrow V(IV)$ is a reversible one-electron electrochemical reaction. They therefore assumed that V(V) and V(IV) species were monomeric in both acidic and basic solutions. It has been found that V(IV) species were $VOSO_4$ and $VO(SO_4)_3^{4-}$, and V(V) species were $VO_2SO_4^-$ and $VO_2(SO_4)_2^{3-}$, in the acidic and basic electrolytes, respectively These considerations are in agreement with spectrophotometric, cryoscopic, and potentiometric data obtained in the dilute V_2O_5 solutions in molten $K_2S_2O_7$-K_2SO_4.[38]

It has been found in [29] that electrochemical reaction

$$V(V) \leftrightarrow V(IV) \qquad (4.6)$$

was reversible in the concentration range of 1-5 w/o of V_2O_5. Calculated number of the electrons (***n***) participating in this reaction varied from 1 to 2, and it was decided that 2 is the most probable number. It means that V(V) or V(IV) species or both of them were dimeric.

In the other research [45,46], on the basis of calorimetric, density and electric conductivity data obtained in V_2O_5 solutions in molten $K_2S_2O_7$ (molar fraction of V_2O_5 was 0-0.5266), a conclusion was made, that in concentrated vanadium pentoxide solutions it exists in a form of dimeric ($(VO_2)_2(SO_4)_2S_2O_7^{4-}$) and polymeric $(VO_2SO_4)_n^{n-}$) species.

There is further information which might be used to help unravel "monomeric" and "polymeric" theories:

A monomeric salt, $K_3VO_2SO_4S_2O_7$, was isolated from the $K_2S_2O_7$-V_2O_5 system,[47] and a dimeric compound, $Cs_4(VO)_2O(SO_4)_4$, was found in the $Cs_2S_2O_7$-V_2O_5 system.[48]

A phase diagram with a $3M_2S_2O_7$-$1V_2O_5$ compound "no sign of formation of dimeric V(V) compouns" was presented in[48] (M = 80%K + 20%Na).
In the case of V(IV), both monomeric and polymeric structures seem to exist, although in dilute systems the existence of only monomeric vanadyl complexes was shown[27]. These results are in agreement with the electrochemical data presented in Ref.28.
At high concentrations of V(IV), the polymeric species seem to be predominant.[49]

The disagreements concerning the V(IV) → V(III) reaction,[28,31,34] may be explained on the basis of different contents of water in the melts. The potential window could, depending on the level of moisture, be too narrow to obtain the second vanadium reduction wave (the difference between V(V) → V(IV) and V(IV) → V(III) potentials can exceed 0.68V[49]).

The effect of *water* on the electrochemical behavior of vanadia in the molten V_2O_5-$M_2S_2O_7$ mixture is very important when vanadia catalyst in SO_2 removal from flue gases[24]. Flue gases can contain a significant amount of water (ca. 7% by volume).[25] It is known that water dissolves in molten alkali metal pyrosulfates with formation of hydrogen sulfates:[26,27]

$$H_2O + S_2O_7^{2-} \leftrightarrow 2HSO_4^- \qquad (4.7)$$

Dissolved water (or hydrogen sulfate) may participate in some steps of the Contact process, can even change the whole mechanism of this process. Obviously the physicochemical properties of the melt and possibly the structure of the catalytically active vanadium species depend on the water activity.
Therefore the electrochemistry of $K_2S_2O_7$- $KHSO_4$-V_2O_5 melts was also studied in an attempt to understand the effect of water.
Before my investigation, neither the electrochemistry of V_2O_5 in the molten $K_2S_2O_7$-$KHSO_4$ mixtures, nor the electrochemical behavior of $K_2S_2O_7$- $KHSO_4$ melts has been studied. Hadid et al.[55] investigated the electrochemistry of V_2O_5 in molten NH_4HSO_4 (up to 5.4 m/o of V_2O_5) at 200°C using Pt electrode. It was concluded that vanadium existed only in the oxidation state +5 (i.e. VO_2^+ in the acidic media and $VO_2SO_4^-$ in the basic media) and +4 (i.e. $VOSO_4$ in the acidic media and $VO(SO_4)_2^{2-}$ in the basic media), $VOSO_4$ being slightly soluble in the neutral melt. The equilibrium potential of the V(V)/V(IV) couple was estimated as 0.677 V vs. a Ag/Ag_2SO_4 reference

electrode. The electrochemical V(V) → V(IV) reaction was shown to be a reversible one-electron process at 200°C.

Experimental data obtained in other electrochemical investigations demonstrate the occurrence of vanadium particles with lower than +4 oxidation stages, both in the aqueous electrolytes and in molten salts.[49,56-58] Thus, the electrochemical reduction of V(V) in aqueous solutions can proceed in two steps with formation of V(III) as an end product:[49]

$$VO_2^+ + 2H^+ + e^- \rightarrow VO^{2+} + H_2O \qquad E° = +1.0\ V \qquad (4.8)$$

$$VO^{2+} + 2H^+ + e^- \rightarrow V^{3+} + H_2O \qquad E° = +0.34\ V \qquad (4.9)$$

where E° is the standard potential. The electrochemical reduction of V(III) to V(II) in 2M aqueous H_2SO_4 was used as a cathodic process in the redox flow battery.[56,57] It was shown that V(V) can be chemically reduced to V(III) [in the form of $KV(SO_4)_2$] by SO_2 in molten $K_2S_2O_7$- $KHSO_4$ - V_2O_5 and $KHSO_4$ - V_2O_5 systems at 450°C.[58]

In the molten $K_2S_2O_7$-V_2O_5 systems, catalytically active V(V) (possibly $VO_2SO_4S_2O_7^{3-}$) were found to react with water forming hydrated complexes by the reaction[59]

$$VO_2SO_4S_2O_7^{3-} + 3H_2O \rightarrow VO_2SO_4 \cdot 3H_2O^- + 2HSO_4^- \qquad (4.10)$$

In studies on the structure of V(V) compounds formed in V_2O_5 solutions in concentrated sulfuric acid, disulfuric acid, and oleum at the ambient temperatures, it was shown that $VO(HSO_4)_3$, $VO(OH)(HSO_4)_2$ and $H[VO(HSO_4)_4]$ were the most likely V(V) compounds.[60-62] Gillespie et al.[61] have also found evidence for the formation of dimeric $H[V_2O_3(HSO_4)]_6$ species at high V_2O_5 concentrations.

The electrochemistry of hydrogen reduction on platinum from molten $KHSO_4$ has been studied.[63-65] Electroreduction of hydrogen on bright and platinized Pt was studied in molten $KHSO_4$ at 250°C to 440°C.[63,64] Videla et al. suggested hydrogen bonding in the melt.[63] Arvia et al.[64] assumed that the potential window of molten $KHSO_4$ is limited by the following cathodic and anodic electrochemical reactions

$$2H^+ + 2e^- \leftrightarrow H_2 \qquad (4.11)$$

$$2HSO_4^- \leftrightarrow H_2SO_4 + SO_3 + ½\ O_2 + 2e^- \qquad (4.12)$$

or

$$SO_4^{2-} \leftrightarrow SO_3 + ½\ O_2 + 2e^- \qquad (4.13)$$

The residual EMF after the electrolysis of the $KHSO_4$ melt was measured.[64] It was found to be 0.602 V at 269°C and was assumed to be equal to the potential window of this electrolyte. The hydrogen evolution reaction was studied[65] at a bright Pt electrode at 270-430°C. It was shown that the atom-atom combining step at low polarization is the rate-determining step, and at high polarization ion-atom electrochemical desorption is the rate-determining step. These regions are separated by a transition region. By analogy with aqueous H_2SO_4, it was also shown that PtO_2 formation and reduction took place at 0.8 and 0.4 V, respectively, *vs.* the hydrogen reference electrode.

Equation (4.11) implies a preceding dissociation of HSO_4^-

$$HSO_4^- \rightarrow H^+ + SO_4^{2-} \qquad (4.14)$$

i.e., the presence of more or less "free" protons in molten $KHSO_4$. This assumption is in agreement with the conclusion of Rogers et al.[66] that different particles are responsible for the conductivity and viscous flow in molten alkali hydrogen sulfates: the energy barrier for viscosity involves only the M^+, HSO_4^-, and SO_4^{2-} ions (M = alkali metal), while the conductivity also involves H^+ ions. A considerable higher electroconductivity of molten $K_2S_2O_7$ after addition of $KHSO_4$[67] is also in agreement with a proton hopping mechanism of conductivity for molten $KHSO_4$-$K_2S_2O_7$.

White et al.[68] studied the electrochemical behavior of water dissolved in a molten Li_2SO_4-K_2SO_4-Na_2SO_4 eutectic using a gold electrode at 560°C. It was shown that water is solvated in the sulfate melt, occurring in the form of hydrogenosulfate after the reaction

$$H_2O + M_2SO_4 + SO_3 \leftrightarrow 2MHSO_4 \qquad (4.15)$$

It was also shown that the reduction of the HSO_4^- ion in molten sulfates proceeds at 0.31 and 0.28 V vs. Ag/Ag^+ at 100 and 500 mV/s, respectively.

Almost all electrochemical data for $K_2S_2O_7$ and $K_2S_2O_7$-V_2O_5 melts were obtained at Au electrodes using the Ag/Ag^+ reference electrode; and the electrochemical data for molten $KHSO_4$ were obtained at Pt electrode using primarily the hydrogen reference electrode.

Gold is not catalyst itself in the sulfur oxidation/reduction reaction, and therefore can be use in the study on catalytic activity of V_2O_5.

This review on chemical and electrochemical study of the catalytic SO_2 oxidation on the vanadia catalyst has shown that dispite of numerous publications there were still a lot of questions for chemist and no comprehensive electrochemical study. The result of my study[18-22] will be discussed in this chapter.

4.1. Experimental

Pure and ry $K_2S_2O_7$ was obtained by thermal decomposition of $K_2S_2O_8$ (Merck, Pro Analysi, maximum 0.001%N) as discussed earlier.[38] K_2SO_4 (Merk, Suprapur) and Li_2SO_4 (Sigma, 99%) were dried at 500°C overnight. $KHSO_4$ (Merck, p.a.) was dried at 120°C for 24 hours and then stored in dry box. Cesium pyrosulfate was synthesized from $CsOH{\cdot}H_2O$ (Aldrich, Cs_2CO_3 < 5%), and $(NH_4)_2S_2O_8$ (Merk, > 98%). After filtration, the CsOH and $(NH_4)_2S_2O_8$ aqueous solutions were mixed and left in the ice bath for three hours. The resulting precipitant, long white needle-shaped $Cs_2S_2O_8$ crystals, was washed with ice-cooled water, ethanol and ether. The crystals were than dissolved in the minimal amount of preheated (54°C) water in order to accomplish a further purification. The solution was then left in an ice bath for 3 h and washed twice with ice-cooled water, ethanol and ether. Finally the $Cs_2S_2O_8$ crystals were dried overnight in desiccators and were then heated to 300°C in nitrogen atmosphere to form $Cs_2S_2O_7$ through the reaction

$$Cs_2S_2O_8 \rightarrow Cs_2S_2O_7 + ½\ O_2 \qquad (4.1.1)$$

V_2O_5 from Cerac (99.9% pure) and Ag_2SO_4 were used without further purification. All sample preparation and handling were performed in an argon-filled glove box (Vacuum Atmospheres Inc.), with a measured oxygen and water concentration less than 10 ppm.

Cyclic voltammetry measurements were performed in a vacuum-tight three-electrode quartz cell with an epoxy resin-joined and water-cooled stainless steel head (Fig.4.1.1). The reference electrode was a silver wire placed in a Pyrex cylindric

chamber with a Pyrex frit bottom. A melt of potassium pyrosulfate saturated with silver and potassium sulfates was used as electrolyte in the reference silver electrode chamber. This reference system has been proven to have a stable potential in the studied temperature range.[36]

A gold wire sealed in a Pyrex tube served as the working electrode. A gold-wire spiral served as the counter electrode. It has been shown that gold is chemically stable in the acidic and basic $K_2S_2O_7$ melts.[38]

The electrochemical cell was assembled and filled with electrolyte powder in the dry argon box, than taken out of the box and placed in the verical furnace. Temperature regulation was within ±1ºC.[50] Temperature within the cell was measured by the chromel-alumel thermocouple. Electrochemical measurements were carried out with Schlumberger SI1286 potentiostate, THJ Instrument potentiostat, potentiostat/galvanostat Autolab-PGSTAT 20 and an EG&G PAR 283 potentiostat/galvanostat. The data were corrected for IR drops using current interruption technique.

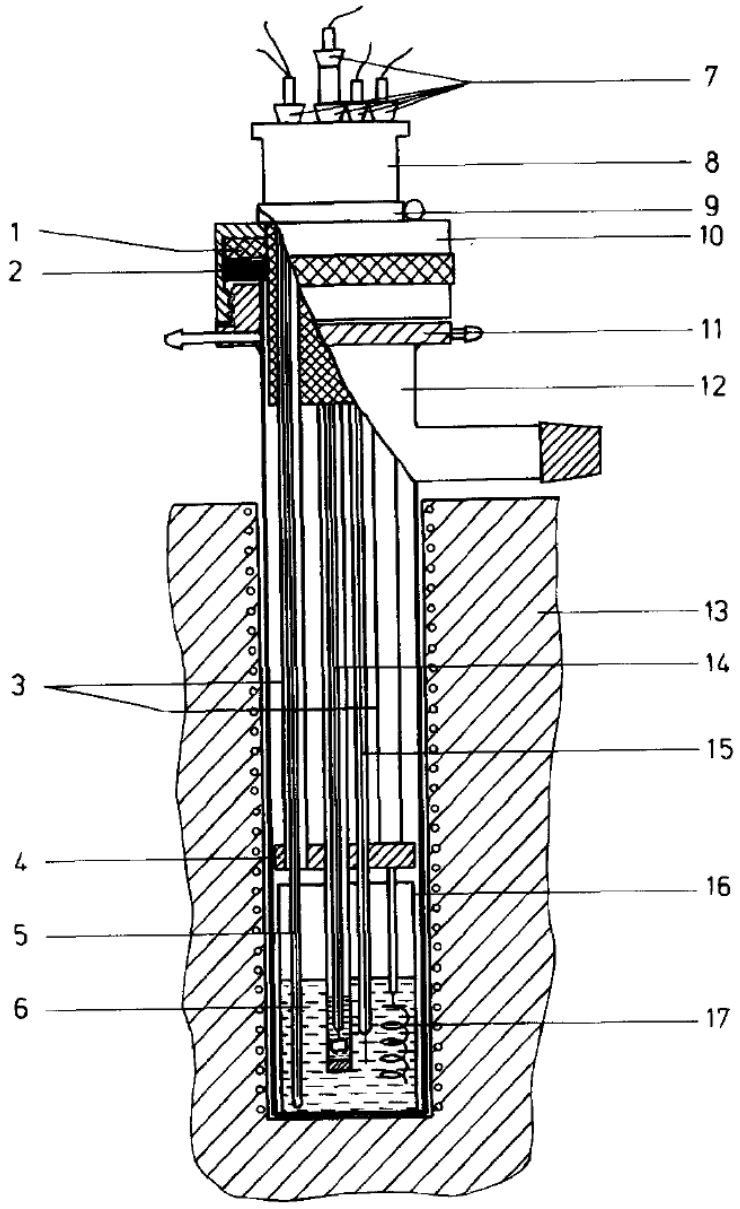

Fig.4.1.1. The electrochemical cell: 1, Teflon ring; 2, Viton ring; 3, ceramic tubes; 4, ceramic screen; 5, thermocouple; 6, electrolyte, 7, silicon rubber stoppers; 8, Teflon lid; 9, fixation ring; 10, stainless steel cover; 11, stainless steel lid; 12, quartz tube; 13, oven; 14, reference electrode; 15, working electrode; 16, Pyrex glass; 17, counter electrode (1)[18]

Several voltammetric measurements were done in a mixture of SO_2 (10 v/o), O_2 (26 v/o), and N_2 (64 v/o), bubbling the gas through the Pyrex tube immersed in the molten electrolyte. Commercial gases were used: SO_2 (>99.9% by volume), O_2 (99.8 v/o + 0.2 v/o N_2 and Ar, and N_2 (<40 ppm of O_2). The $SO_2/O_2/N_2$ was supplied from a mixing system based on gas streams monitored by Brooks mass flowmeters.

The electrochemical cell which was used in the study of electrochemical promotion of the commercial VK-58 catalyst (Haldor Topsoe A/S) with a molar ratio M/V (M = 70 mol % K + 25 mol % Cs + 5 mol % Na) in Fig.4.1.2. The catalyst was used as a powder mixed with $K_2S_2O_7$ and pressed between the upper gold working electrode and the porous quartz diaphragm. Molten potassium pyrosulfate which filled the catalyst and the pores of the diaphragm served as electrolyte between the gold working electrode and the gold counter (and reference) electrode.

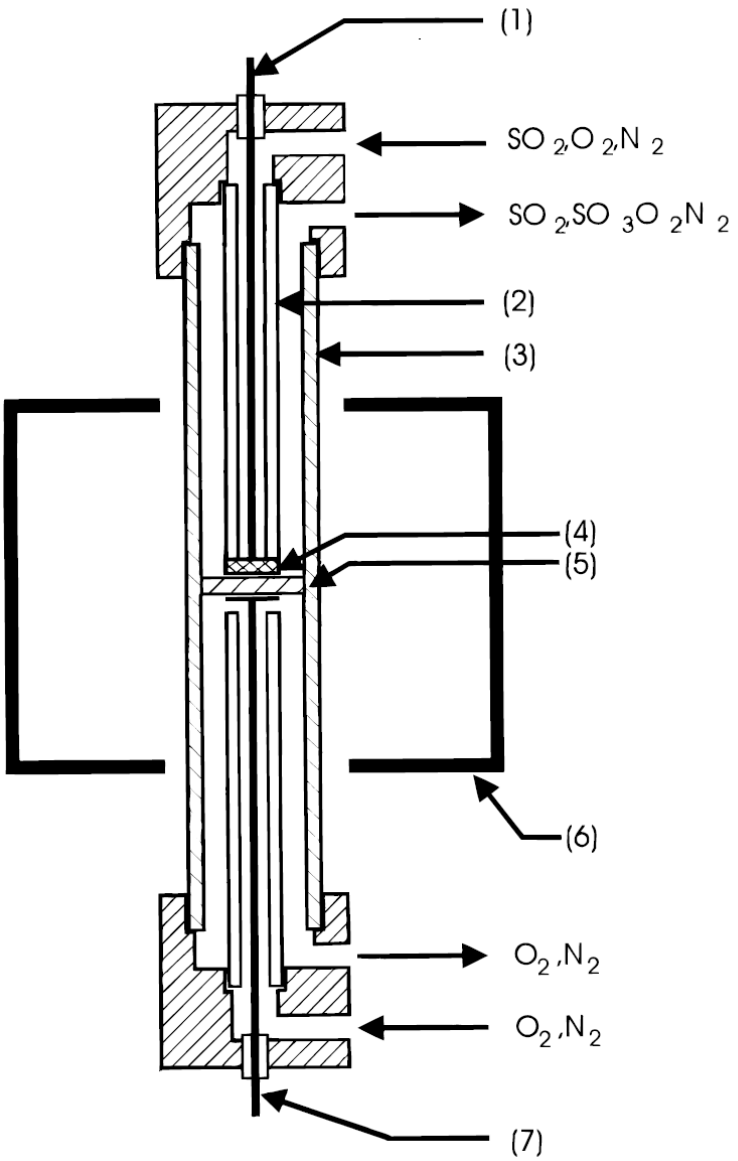

Fig. 4.1.2. Electrochemical cell for study of the polarization effect on the commercial VK-58: (1) Au working electrode, (2) quartz tube, (3) quartz cell, (4) catalyst layer, (5) quartz porous membrane, (6) furnace, (7) Au counter electrode.[22]

It has been shown[18] that in the studied media the potential at the Au electrode is defined by the redox couple V(V) ↔ V(IV). This reaction is reversible and the

reference has a stable potential. The working electrode gas composition was 10%SO_2/18%O_2/72%N_2, and the gas for counter electrode was 20%O_2/80%N_2. Both inlet gas mixtures flow rates were 100 mL/min. The SO_2 concentration in the outlet gas was measured by a Shimadzu GC 8A chromatograph (GC) with a thermal conductivity detector and 8 ft × 1/8 in. stainless steel columns packed with Porapak Q (50-80 mesh before the experiment calibration with known SO_2 was carried out. The carrier was He, and the column and detector temperatures were set at 140 and 160°C, respectively.

The initial (at zero polarization) catalytic activity was measured after the turnover frequency (number of the converted SO_2 moles per mole of V_2O_5 per second) had stabilized, i.e. under a steady-staate conditions. For each value of polarization the measurements were performed after stabilization of turnover frequency (6-24 h). The turnover frequency vs. polarization curves were reproduced for the each studied V_2O_5 concentration and temperature.

A theoretical current value for pure Faradaic SO_2 oxidation was calculated and compared with a value of maximum turnover frequency at positive polarization.

4.2. Voltammetric measurements in the $K_2S_2O_7$ and $K_2S_2O_7$-K_2SO_4 melts at 440°C

Cyclic voltammogramm obtained at a gold electrode in $K_2S_2O_7$ melt in Ar at 50 mV/s is shown in Fig.4.2.1. It can be seen that the potential window for this melt is limited by -1.1 V in the cathodic direction and by 1.0 V in the anodic direction. In addition, four votammetric waves can be seen inside the potential window: three reduction waves (**A**, **B** and **D** in Fig.4.2.1) and one oxidation wave (**C** in Fig.4.2.1). These waves could affect the potential window of the $K_2S_2O_7$ melt, therefore their identification was important.

The effect of potential scan rate ($\boldsymbol{v_E}$) on the ekectrochemical behavior of the $K_2S_2O_7$ melt is shown in Fig.4.2.2. It can be seen from Figs.4.2.3-4.2.4 that, for the waves **A** and **C**, the peak current ($\boldsymbol{i_p}$) is linearly dependent on the square root of the potential scan rate and the peak potentials are the linear functions of the logarithm of the potential scan rate. The same behavior has been demostrated by the wave **B**. It should be noticed that wave **A** decreased during the multiple voltammetric cycling (Fig.4.2.5).

The effect of ***acidity*** of the electrolyte was studied by adding K_2SO_4 to the molten $K_2S_2O_7$. Comparison of the voltammetric behavior of $K_2S_2O_7$ and $K_2S_2O_7$- K_2SO_4 (sat.) melts is given in Fig.4.2.6. It is seen, that in basic melts, the peak potential of wave **C** moves in the positive direction and the peak itself becomes less sharp than in the acidic solution. A new anodic wave **E** appears at approximately 0.9V.
For the reactions **C**, **D** and **E**, the peak currents are the linear functions of square root of the potential scan rate and the peak potentials are independent on the ν_E in the 25-200 mV/s region for the **C** and **D** waves and in the 50-100 mV/s region for the **E** wave (Figs.4.2.7 and 4.2.8).

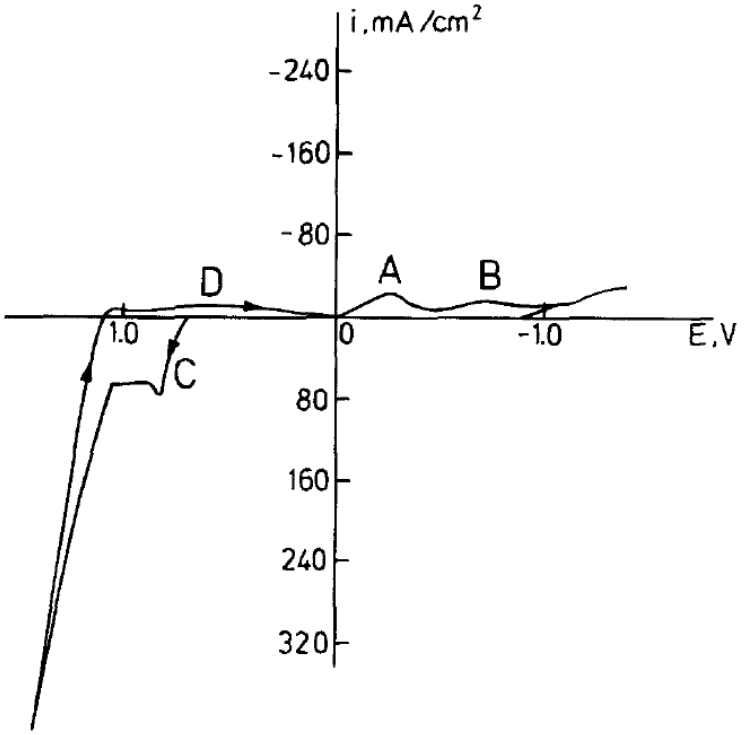

Fig.4.2.1 Cyclic voltammogram obtained at gold electrode in molten $K_2S_2O_7$ at 50 mV/s and 440°C[18]

According to Nicholson and Shain,[51]

$$E_P = E^0 - \frac{RT}{\alpha n_\alpha F}\left[0.78 - \ln k_s + 1/2 \ln \frac{D\alpha n_\alpha F \nu_E}{RT}\right] \qquad (4.2.1)$$

where E_P is the peak potential, E^o is the standard potential, k_s is specific rate constant, α is the transfer coefficient, n_α is the number of electrons, participating in the rate-determining electron-transfer step, D is the diffusion coefficient, R is the gas

constant, ***F*** is the Faraday constant, and ***T*** is the absolute temperature. Equation (4.2.1) is the main (along with the linear dependence between i_p and v_E) diagnostic criteria of kinetics controlled by electron transfer rate (irreversible electrochemical reaction).[51] It means that in the ***acidic*** melt, **A**, **C** and **D** reactions are irreversible, and Equation (4.2.2) can be used to calculate the number of the electrons participating in these reactions:

$$E_P - E_{P/2} = -1.857\frac{RT}{\alpha n_\alpha F} \qquad (4.2.2)$$

(E_P and $E_{P/2}$ are the peak and half-peak potentials, respectively).

The αn_α values for **A**, **C** and **D** electrochemical reactions in the acidic melt are given in Table 4.2.1. Assuming that α is approximately 0.5, the caculated numbers of the electrons participating in **A**, **C**, and **D** are 3, 3, and 2.

The number of electrons, participating in a reversible electrochemical reaction can be calculated using the following equation[51]:

$$E_P - E_{P/2} = -2.20\frac{RT}{nF} \qquad (4.2.3)$$

The numbers of electrons participating in the reversible **C** and **E** electrochemical reactions (***basic*** melt) are given in Table 4.2.1. For reaction **C**, ***n*** was 3, and, for reaction **E**, ***n*** was 2.

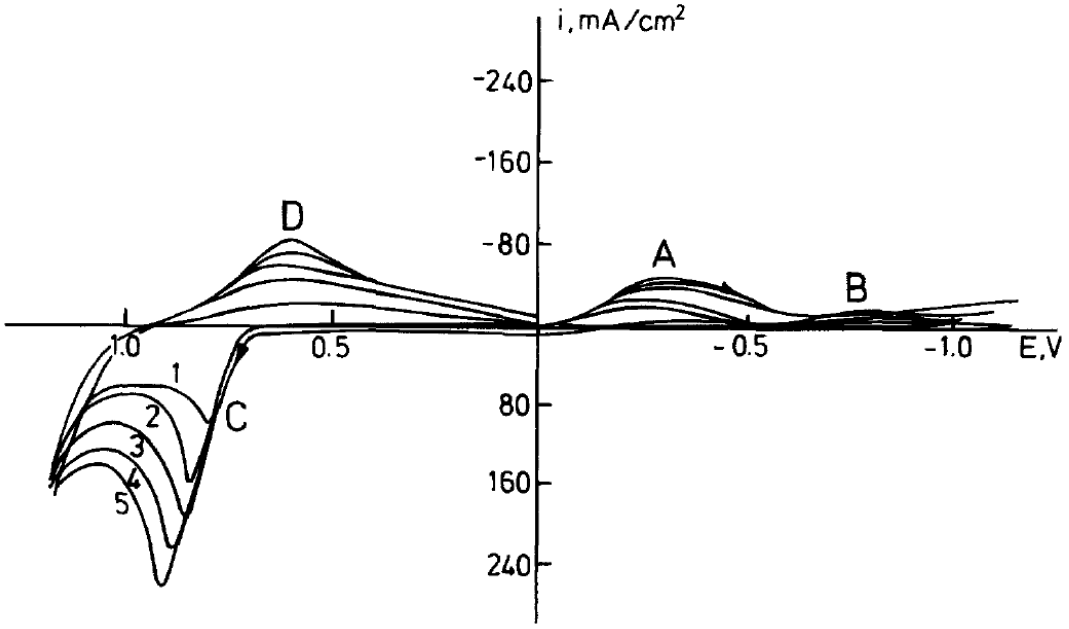

Fig.4.2.2. Cyclic voltammograms obtained at gold electrode in molten $K_2S_2O_7$ at 440°C and 1, 100; 2, 200; 3, 300; 4, 400 and 5, 500 mV/s[18]

The only possible electrochemical reaction with n = 3 (wave C) in the studied electrode/electrolyte system is electrochemical oxidation of gold:

This assumption is in agreement with the data obtained by Durand et al.[37].The reactions (4.2.4A) and (4.2.4B) include chemical step following electrochemical step (EC mechanism).[51]

For acidic melt: $Au + 2nS_2O_7^{2-} \rightarrow Au(SO_4)_n^{3-2n} + nS_3O_{10}^{2-} + 3e^-$ (4.2.4A)

For basic melt: $Au + nSO_4^{2-} \rightarrow Au(SO_4)_n^{3-2n} + 3e^-$ (4.2.4B)

This chemical step is the formation of complex ions of gold. If this step is fast and potential scan rate is low, it can lead to the disapearence of the reverse cathodic reaction. This is probably the case with wave ***C***.

Table 4.2.1. Peak and half-peak potential difference, $E_p - E_{p/2}$, αn_α[a], n_α for the irreversible A, C and D reactions and the number of participating electrons, n, for reversible C and E reactions obtained in molten $K_2S_2O_7$ and $K_2S_2O_7$-K_2SO_4 systems at 440°C[18(A1)]

Electrochemical reaction	Potential scan rate, V/s	$E_p - E_{p/2}$, V	αn_α	n_α, n
A	0.2	0.070	1.637	3.27
	0.3	0.085	1.348	2.70
	0.4	0.085	1.348	2.70
	0.5	0.083	1.380	2.76
C	0.2	0.070	1.637	3.27
	0.3	0.070	1.637	3.27
	0.4	0.080	1.433	2.87
	0.5	0.080	1.433	2.87
D	0.1	0.110	1.042	2.08
	0.2	0.120	0.955	1.91
	0.3	0.130	0.878	1.76
	0.4	0.130	0.878	1.76
C	0.050	0.045		3.04
	0.075	0.040		3.43
	0.100	0.045		3.04
E	0.050	0.060		2.28
	0.100	0.058		2.36

[a] αn_α is a product of transfer coefficient and the number of the electrons participating in the irreversible A, C, D reactions

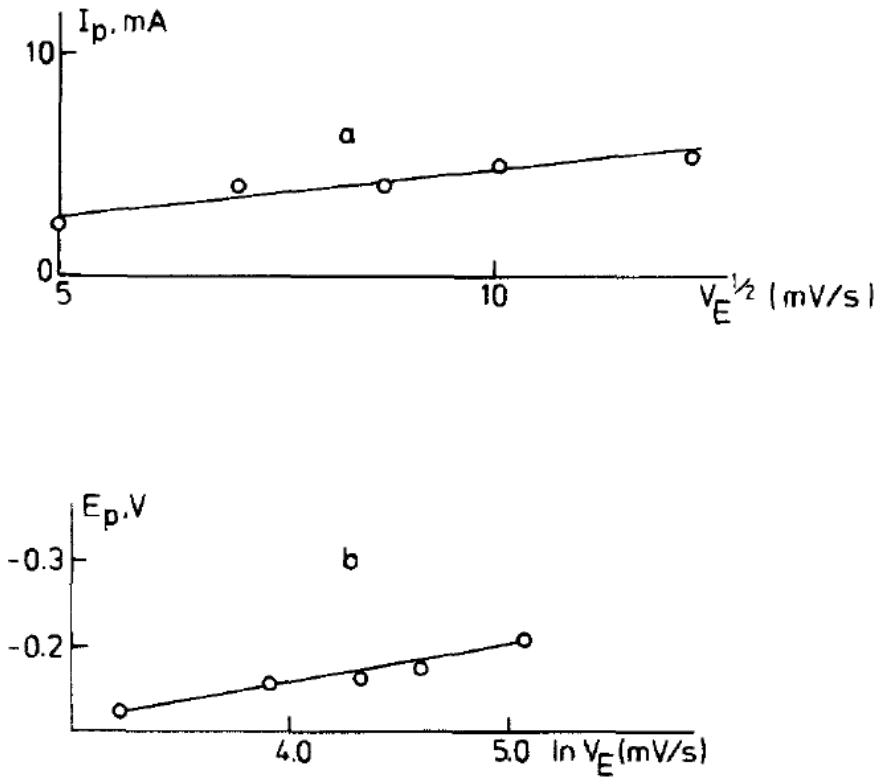

Fig.4.2.3. Peak current (a) and peak potentioal (b) of wave A (Fig.4.2.2) as function of potential scan rate[18]

As seen in Figs.4.2.6 – 4.2.7, the electrochemical reaction ***C*** is irreversible in the acidic melts and reversible in the basic melts. The related cathodic current is absent for the reaction (4.2.4B), and this reaction becomes irreversible at the potential scan rates of ≥ 100 mV/s

Peak current of the wave ***A***, decreases during voltammetric cycling (Fig.4.2.4). It can be safely ascribed to the gold surface oxide reduction:

$$1/2Au_2O_3 + 3/2S_2O_7^{2-} + 3e^- \rightarrow Au + 3SO_4^{2-} \qquad (4.2.5)$$

Wave ***E*** (Fig.4.2.6) appears only in basic melts (containing an excess of sulfate). Wave ***E*** is caused by a 2-electron reaction (Table 4.2.1), reversible at low scan rates and irreversible at high scan rates (Fig. 4.2.8(a)). It is known[40] that sulfate participates in both the cathodic and the anodic limiting reactions in the (Li, $K)_2SO_4$ eutectic melt at 625°C. The anodic limiting process was the oxidation of sulfate ion according to the reaction:

$$SO_4^{2-} \leftrightarrow SO_3(gas) + \tfrac{1}{2} O_2(gas) + 2e \qquad (4.2.6)$$

The cathodic limiting reaction was the reduction of sulfate to sulfite, possibly

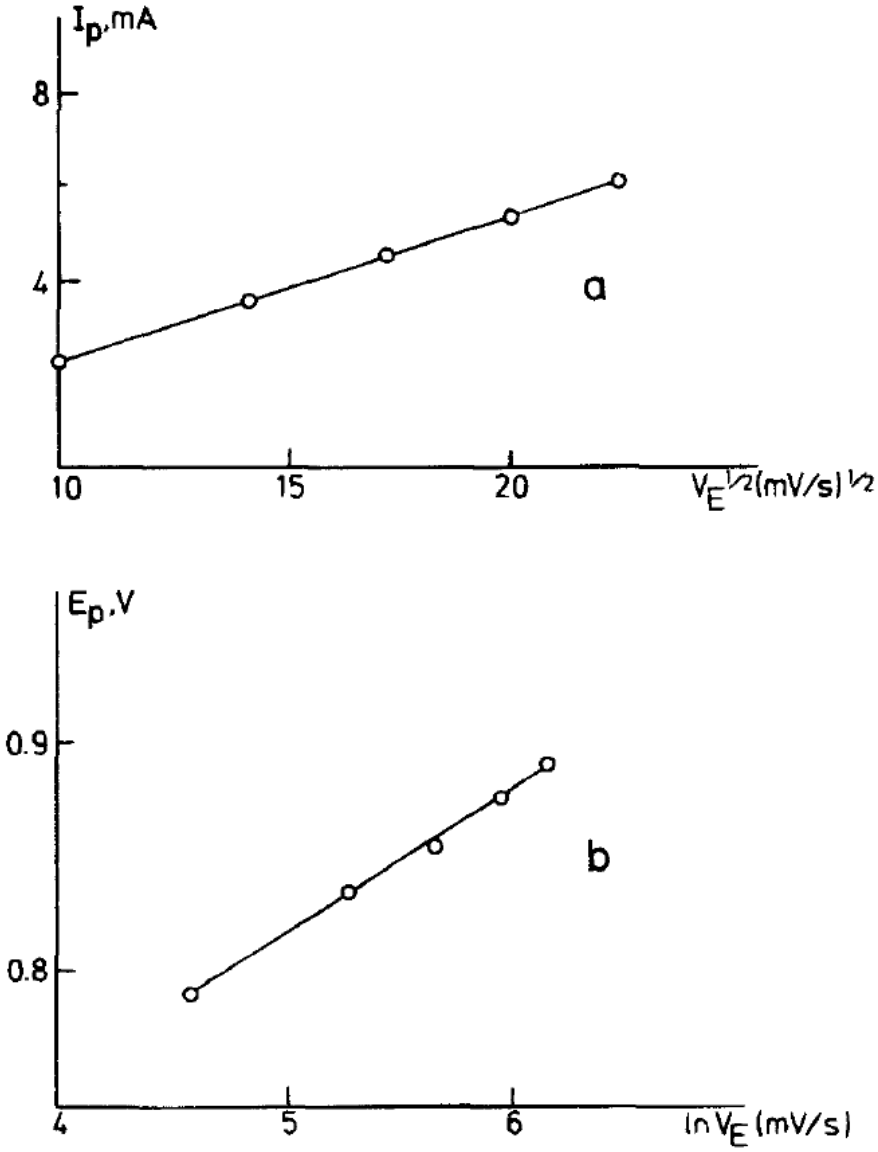

Fig.4.2.4. Peak current (a) and peak potentioal (b) of wave C (Fig.4.3.2) as function of potential scan rate[18]

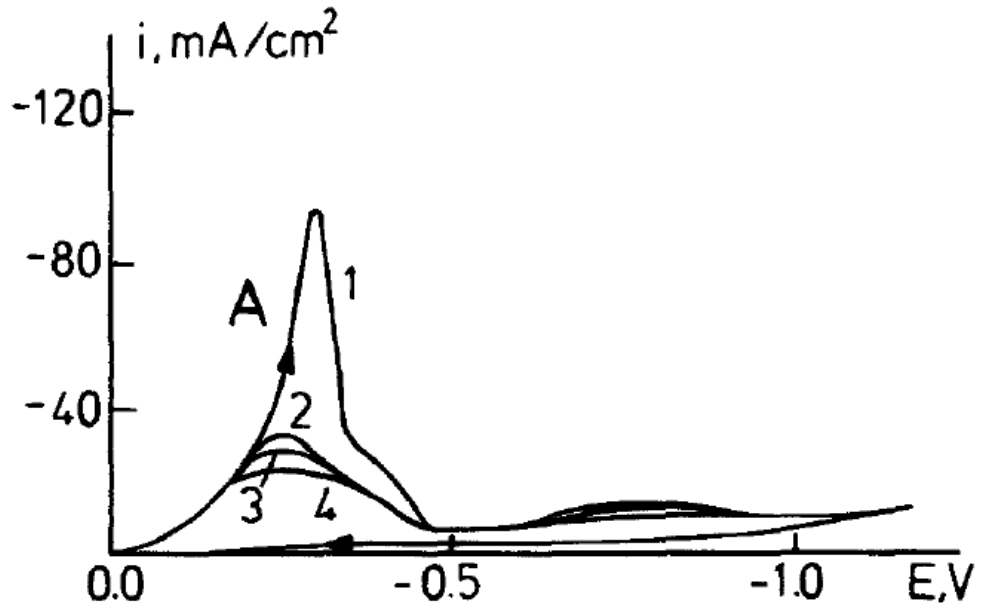

Fig.4.2.5. Consecutive voltammetric cycles obtained at gold electrode in molten $K_2S_2O_7$ at 50 mV/s and 440°C[18]

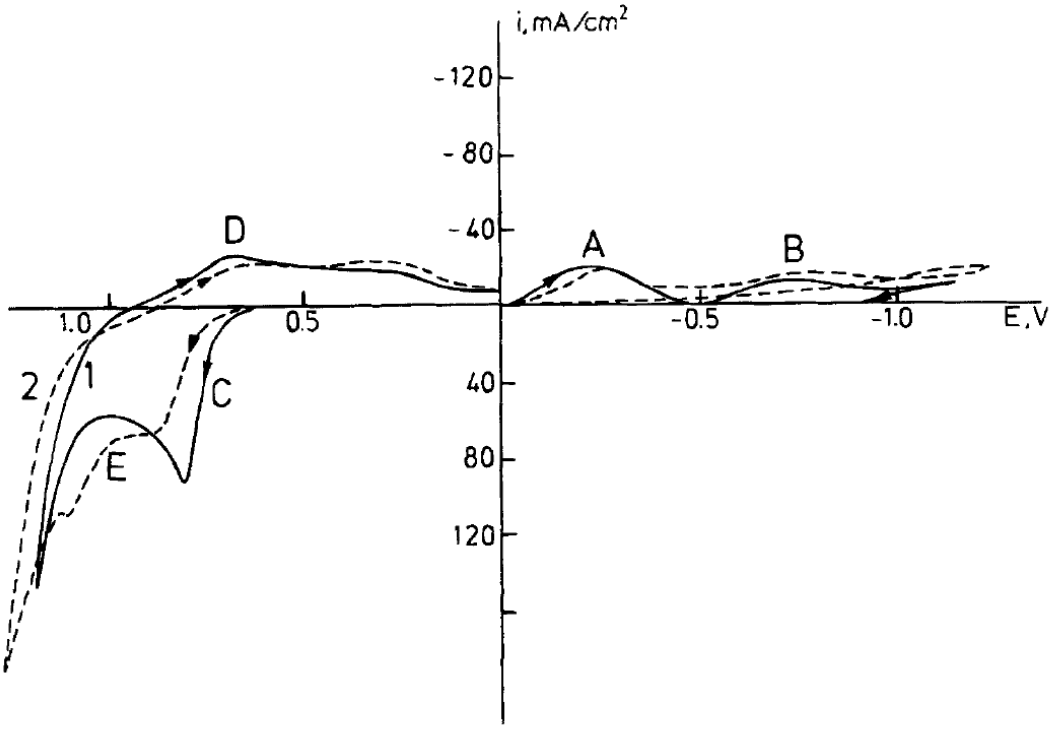

Fig.4.2.6. Cyclic voltammograms obtained at gold electrode at100 mV/s and 440°C in $K_2S_2O_7$ (1) and $K_2S_2O_7$ saturated with K_2SO_4 (2) melts[18]

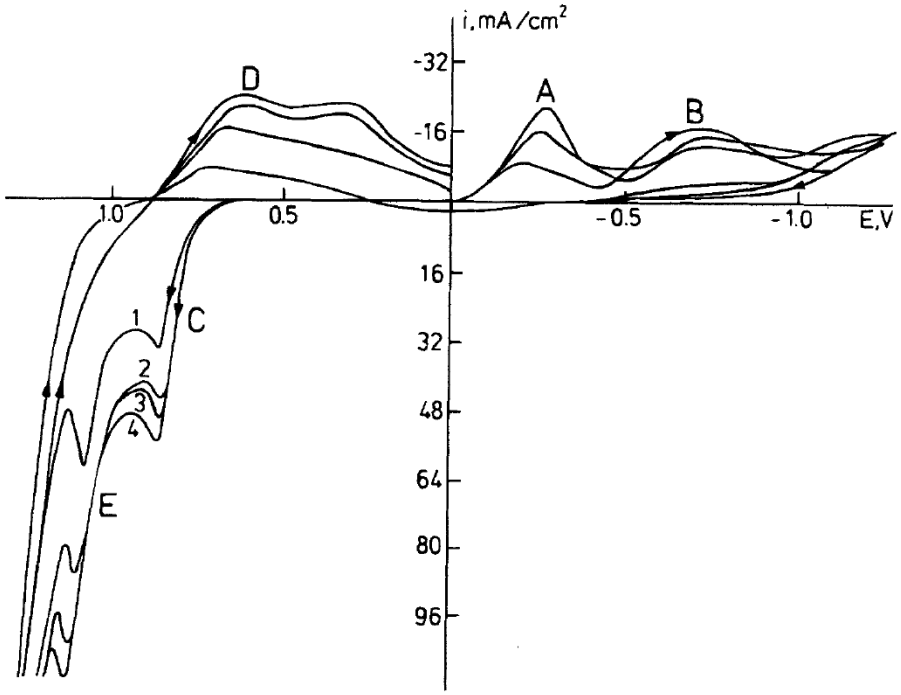

Fig.4.2.7. Cyclic voltammograms obtained at gold electrode in molten $K_2S_2O_7$ saturated with K_2SO_4 at 440°C and 1, 25; 2, 50; 3, 75 and 4, 100 mV/s[18]

followed by additional steps leading to the formation of sulfur, sulfide, or both, depending on the conditions of electrolysis. For anodic reaction the equilibrium potential of 0.9 V vs. Ag^+/Ag was obtained.[41] This value is in agreement with Frank et al. for molten $K_2S_2O_7$.[29] For the platinum electrode, the rest potential of the O_2/O^{2-} couple was between 0.046 V and 0.025 V vs. Ag^+/Ag, depending on the treatment of Pt. Burrows et al.[42] have shown that the potential-determining reaction involves one or more types of oxides of platinum. Apparently no proper oxygen/oxide electrode has been obtained in this melt. Salzano et al.[43] have ascertained that sulfur dioxide and trioxide were electrochemically active in the alkali sulfate melts. Boxall et al.[44] observed a Nerstian behavior of molten sulfates corresponding to the reaction (4.2.6) with equilibrium potential of 0.774 V vs. Ag^+/Ag.

Combining our data with the data presented in Refs. 41 and 43 on the reversible SO_4^{2-} oxidation at 0.9 V in sulfate melt, we can assume that wave ***E*** is caused by the reaction (4.2.6). Process ***D*** is a two-electron electrochemical reaction and proceeds at the potential corresponding to the reduction of O_2/SO_3 gaseous mixture in the sulfate melt[44] (reaction (4.2.6) in the opposite direction). Thefore we can assume this reaction taking place also in $K_2S_2O_7$ melt.

Therefore, the anodic limit in molten potassium pyrosulfide (1.0 V vs. Ag^+/Ag) can be described by the following reactions taking into account that free SO_3 cannot exist in molten pyrosulfates:

For acidic melt: $3S_2O_7^{2-} \rightarrow 2S_3O_{10}^{2-} + ½\ O_2 + 2e^-$ (4.2.7A)

For basic melt: $2SO_4^{2-} \rightarrow S_2O_7^{2-} + ½\ O_2 + 2e^-$ (4.2.7B)

The reduction wave B starts at the same potential as the SO_3 reduction in the sulfate melt[42] i.e., -0.5 V vs. Ag^+/Ag. The shape (of almost limiting current type) of the wave in the acidic melt is typical for the slow preceding chemical reaction, i.e. CE, mechanism.[51] Therefore, wave ***B*** (Fig.4.2.2.) can be ascribed to the electrochemical reduction of solvated SO_3[36]:

$$3S_3O_{10}^{2-} + 2e^- \rightarrow SO_2 + 4S_2O_7^{2-} \quad (4.2.8)$$

The cathodic stability limit (-1.1 V) of potassium pyrosulfate melt can be reduction of the pyrosulfate anion, probably according to the following reaction:

$$2S_2O_7^{2-} + 2e^- \rightarrow SO_2 + 3SO_4^{2-} \quad (4.2.9)$$

4.3. The Electrochemical Behavior of V_2O_5 in Molten $K_2S_2O_7$

The electrochemical behavior of V_2O_5 in molten potassium pyrosulfate at a golden electrode was studied in a wide concentration range. The voltammetric curve obtained 2 mol % of V_2O_5 is shown in Fig.4.3.1. It is seen that two new cathodic waves (***F*** and ***G***) and one anodic wave (***H***, which obviously is an oxidation of the first reaction product) appear in the presence of V_2O_5. The dependence of the ***F***, ***G***, and ***H*** wave parameters on the potential scan rate is shown in Fig.4.3.2. The ***F*** and ***H*** peak currents depend linearly on the sqare root of the potential scan rate, and the peak potentials are independent on the potential scan rate (Figs.4.3.6 and 4.3.7). For a melt with 2 mol % of V_2O_5, the ratio of the first reduction (***F***) and the oxidation (***H***) peak currents is close to unity (Table 4.3.1). The voltammetric characteristics of the $K_2S_2O_7$-V_2O_5 system with the V_2O_5 concentrations up to 20 m/o are shown in Figs. 4.3.3, 4.3.4, 4.3.6, 4.3.7 and in Table 4.3.1.

The ***F*** peak current is linearly dependent on the V_2O_5 concentration. Starting from 5 mol % of V_2O_5, the ***F*** and ***H*** peak potentials depend linearly on the logarithm of the potential scan rate.

The ratio between ***F*** and ***H*** peak currents decreases with the concentration of V_2O_5, having minimum at 5 mol %. The reduction wave ***G***, instead of peak, shows a linear current-potential dependence for high potential scan rates. A new oxidation wave, ***I***, corresponding to the reduction wave ***G***, becomes noticeable at 10 mol % of V_2O_5.

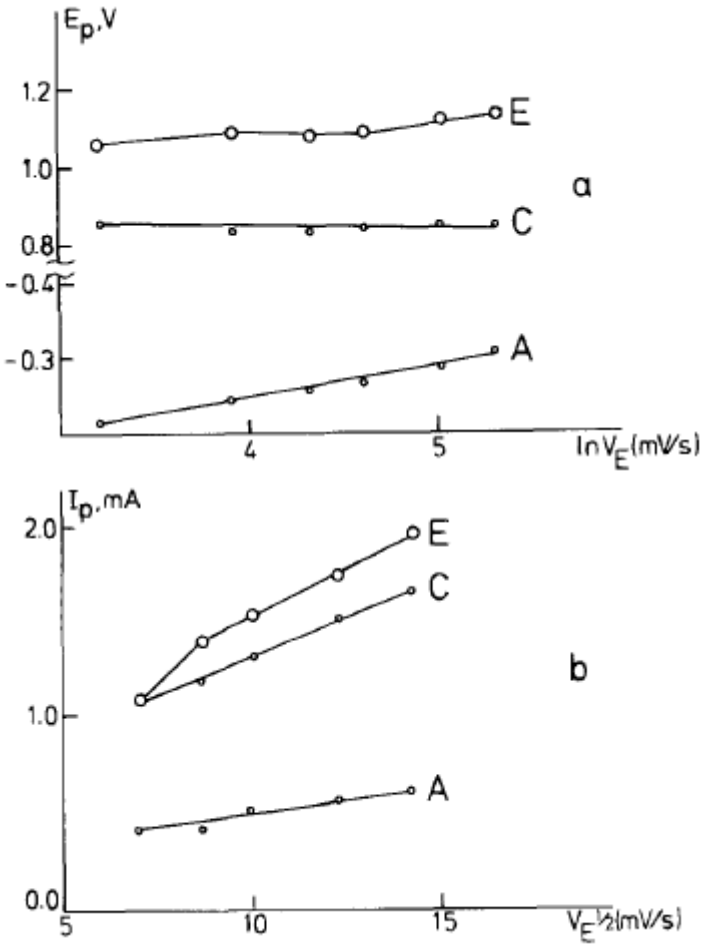

Fig.4.2.8. Peak potential (a) and peak current (b) of wave A, C and E (Fig.8) as function of potential scan rate[18]

Hence, the first reduction-oxidation process (waves ***F*** and ***H***) seems to be reversible below 5 m%o of V_2O_5 but irreversible at higher concentrations. It can be seen from Table 4.3.1 that at all studied concentrations both peaks F and H are ***one-electron*** reactions. It means that these waves are caused by the V(V) →

(V(IV) and V(IV) → V(V) reactions, and that only one vanadium atom participates in these processes.

They may be described by Eq. 4.3.1

For acidic melt $VO(S_2O_7)_2^{2-} + 2S_2O_7^{2-} \leftrightarrow VO_2SO_4S_2O_7^{3-} + S_3O_{10}^{2-} + e^-$ (4.3.1A)

For basic melt $VO(SO_4)_2^{2-} + 2\ SO_4^{2-} \leftrightarrow VO_2(SO_4)_2^{3-} + S_2O_7^{2-} + e^-$ (4.3.1B)

The change in kinetics of the reaction given by Eq. 4.3.1 at V_2O_5 concentrations higher than 5 mol % could be explained by an increase in degree of dimerization or of polymerization of V(IV) species, proceeding via a mechanism of electrochemical desorption, in which a slow charge transfer step is usually involved.[52]

Assuming (*i*) the potential difference between ***F*** and ***G*** reactions,[49] (*ii*) the electrochemical behavior of the V(IV) cathodic materials,[53] and (*iii*) the chemical identification of V(III) species as the products of the reduction of V(V) under the conditions of commercial sulfuric acid production,[26] we can ascribe a V(IV) → V(III) reduction to wave ***G***. The shape of the voltammetric curve can be explaned by the low solubility of the V(IV) and V(III) compouns at 440°C,[26] and therefore one has an ohmic control of reaction ***G***.

Starting from 10 mol % of V_2O_5, a new oxidation wave (wave ***I***) appears on voltammetric curves. This wave can be related to a V(III) → V(IV) reaction considering the reversible performance of the V_2O_5 secondary battery cathodes.[53] Figures 4.3.5-4.3.7 (and Table 4.3.1) demonstrate the voltammetric effect of adding 5.5 mol % Li_2SO_4 to a 10 mol % V_2O_5 solution in a potassium pyrosulfate melt. After addition of lithium sulfate, a white precipitate appeared in the melt. Taking into account the higher solubility of Li_2SO_4 than K_2SO_4 (which is 4.64 m/o at 440°C[44]) in molten $K_2S_2O_7$ and a possible exchange equilibrium (Eq. 4.3.2), in the reciprocal system

$$Li_2SO_4 + K_2S_2O_7 \rightarrow Li_2S_2O_7 + K_2SO_4 \qquad (4.3.2),$$

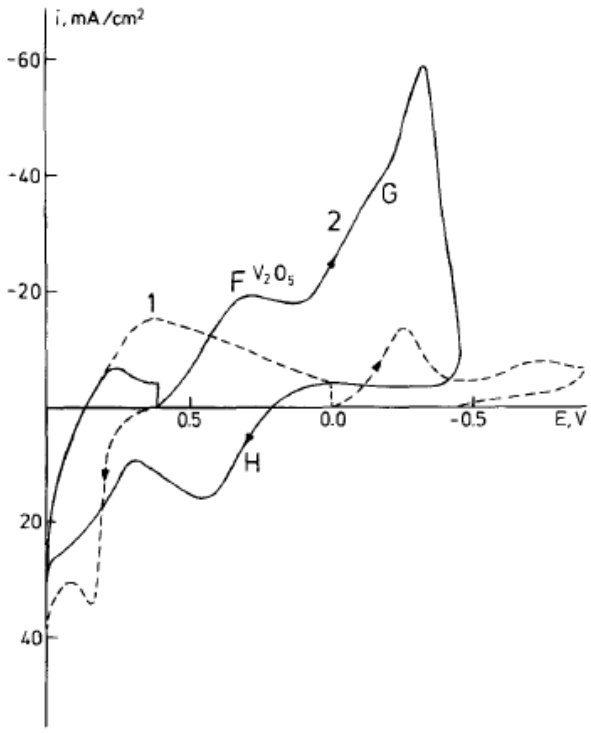

Fig.4.3.1. Cyclic voltammograms obtained at gold electrode at100 mV/s and 440°C in $K_2S_2O_7$ (1) and $K_2S_2O_7$ + 2m/o V_2O_5 (2) melts[18]

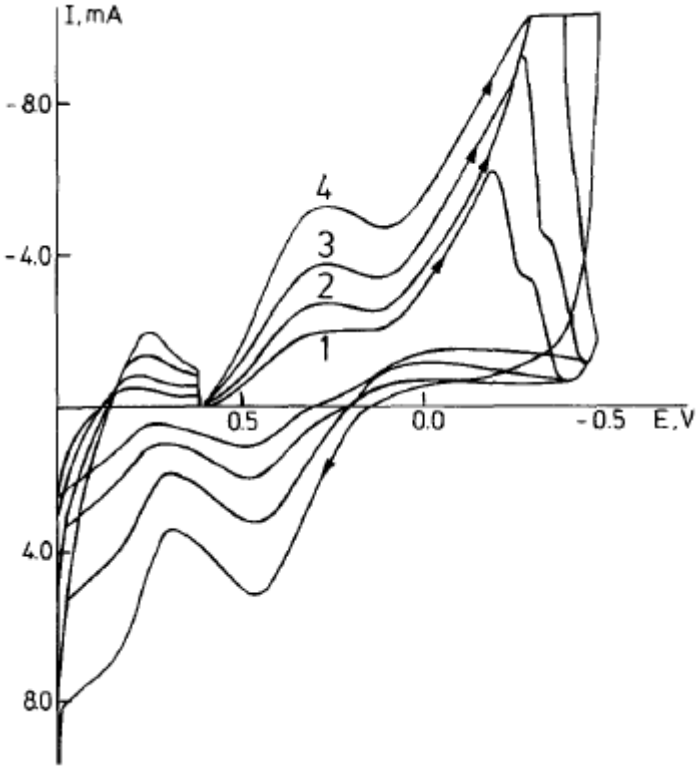

Fig.4.3.2. Cyclic voltammograms obtained at gold electrode in molten $K_2S_2O_7$ + 2 mol % V_2O_5 at 440°C and 1, 25; 2, 50; 3, 100 and 4, 200 mV/s[18]

we assume that all the added lithium sulfate is practically present in the form of lithium pyrosulfate in the $K_2S_2O_7$melt.

It can be seen that the Li^+ ion has a promoting effect on both oxidation and reduction processes, with the depolarization being almost three times higher for the V(V) $\rightarrow$ V(IV) reduction than for the V(IV) $\rightarrow$ V(V) oxidation. The ratio between the anodic and the cathodic peak currents is closer to unity in the presence of Li_2SO_4 in the studied electrolytes. It should also be noted that saturation of a $K_2S_2O_7$ melt by potassium sulfate has only a marginal effect on the V(V) $\leftrightarrow$ V(IV) kinetics. Termodynemical characteristics of the reactions (4.3.1A, 4.3.1.B) depend on the nature of the alkali cation: the smaller the cation radius the higher its polarization effect on the complex vanadium particles. This could cause the weakening of the V-O bond and facilitate the vanadium reduction.

The alkali-ion promotion effect can be qualitatively devided into two types: “large amont promoter”, when the promoter changes physic-chemical properties of the bulk melt (i.e. Cs^+); and “small amount additive”, when the bulk properties are not significantly changed, but the thermodynamics and kinetics of catalytic reaction is changed (Na^+, Li^+).

Mixed with potassium pyrosulfate cesium pyrosulfate (or sulfate) forms a system with low melting point (and therefore viscosity), which gives an increase of the solubility of the participants of the reaction (4.3.1), and in this way accelerates the reaction. $Na^+$and Li^+ are small cations with therefore higher charge density than for K^+ and Cs^+. Naturally the small cations have stronger polarization effect on V-O bond in VO_2^+ and VO^{2+} and in this way affect the thermodynemics and kinetics of the reaction (4.3.1).

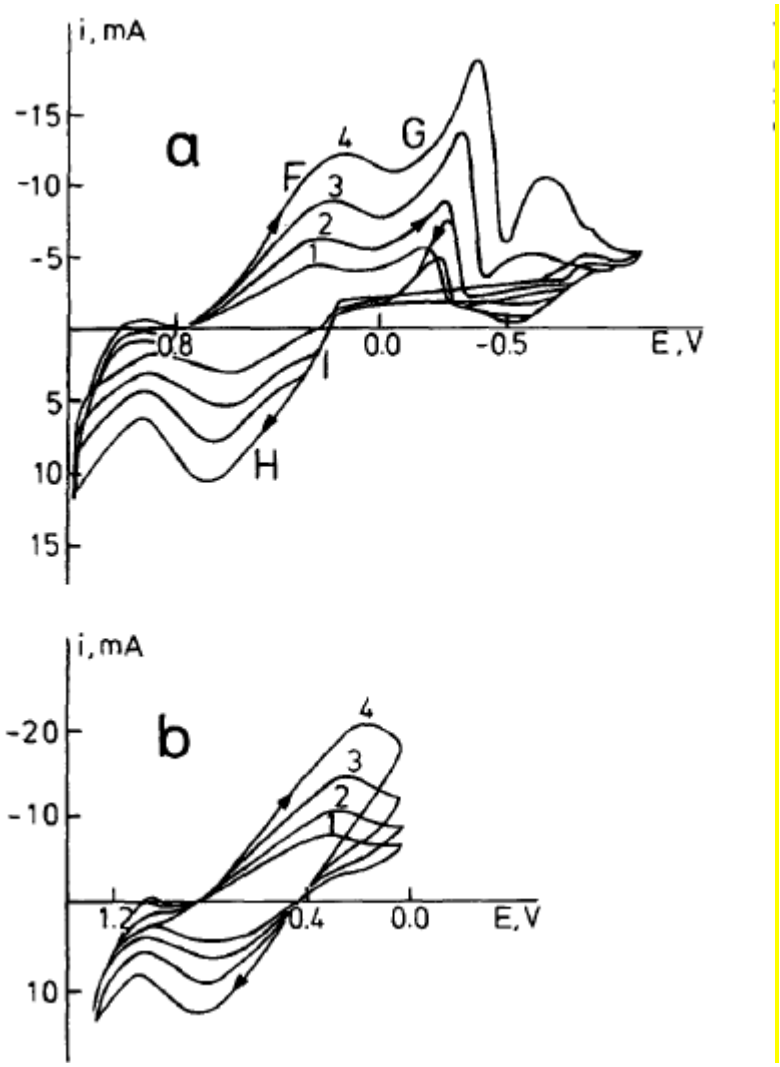

Fig.4.3.3 Cyclic voltammograms obtained at gold electrode in molten $K_2S_2O_7$ + 10 mol % V_2O_5 (a) and molten $K_2S_2O_7$ + 20 mol % V_2O_5 (b) at 440°C and 1, 50; 2, 100; 3, 200 and 4, 400 mV/s[18]

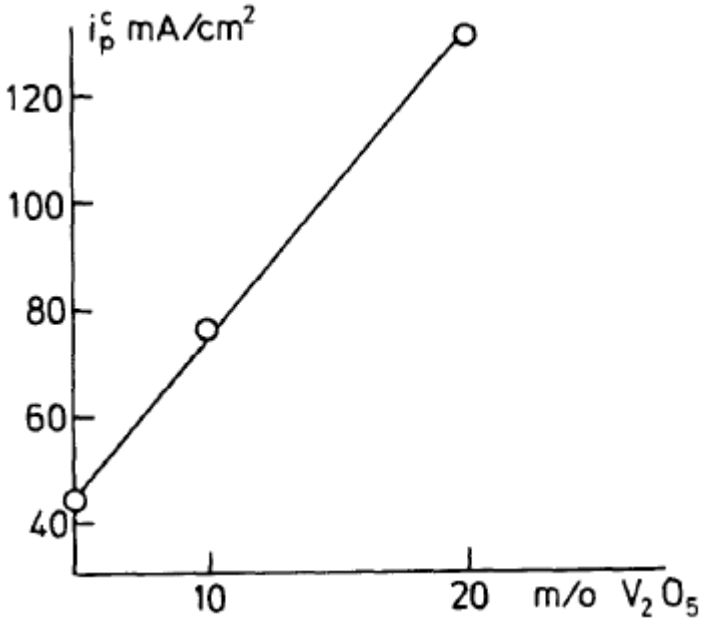

Fig.4.3.4. V(V) → V(IV) reduction peak current vs. V_2O_5 concentration obtained at gold electrode in molten $K_2S_2O_7$ + V_2O_5 at 440°C and 400 mV/s[18]

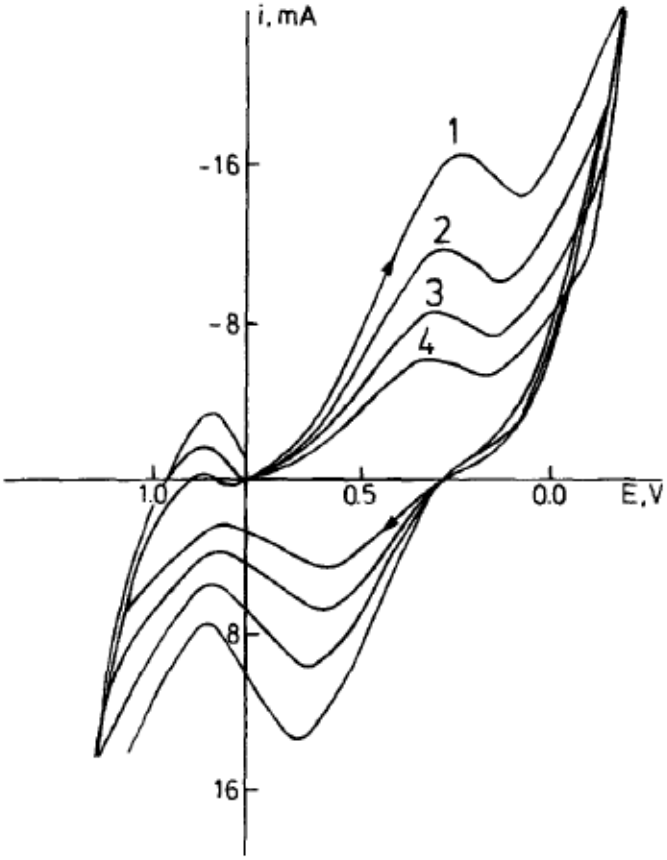

Fig.4.3.5. Cyclic voltammograms obtained at gold electrode in molten $K_2S_2O_7$ + 10 mol % V_2O_5 saturated with Li_2SO_4 at 440°C and 1, 400; 2, 200; 3, 100 and 4, 50 mV/s[18]

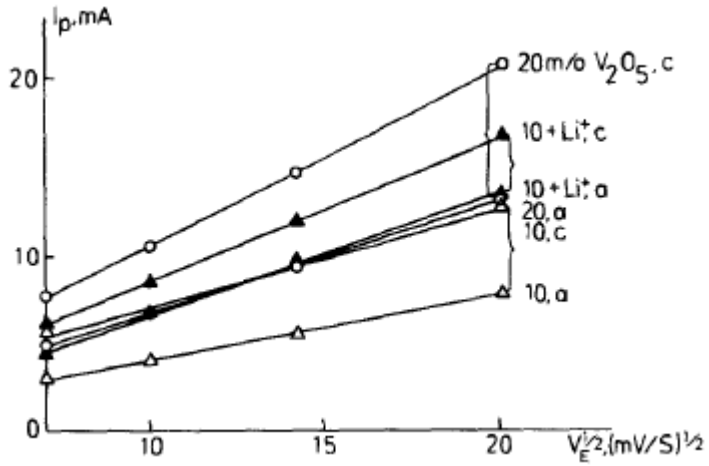

Fig.4.3.6. V(V)→V(IV) and V(IV)→V(V) peak currents as function of potential scan rate obtained in $K_2S_2O_7 – V_2O_5$ and $K_2S_2O_7 – V_2O_5 – Li_2SO_4$ melts at gold electrode and 440°C. c, Cathodic and A, anodic.[18]

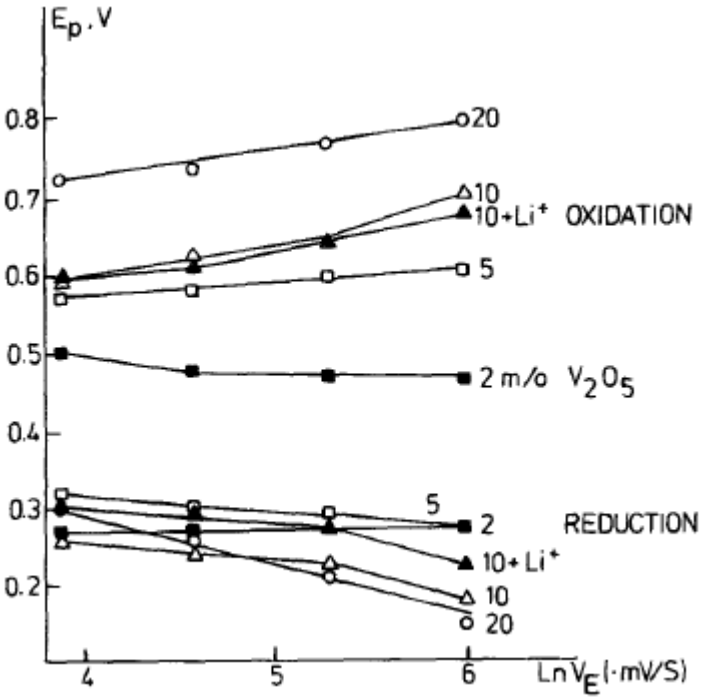

Fig.4.3.7. V(V)→V(IV) and V(IV)→V(V) peak potentials as function of potential scan rate obtained in $K_2S_2O_7 – V_2O_5$ and $K_2S_2O_7 – V_2O_5 – Li_2SO_4$ melts at gold electrode and 440°C.[18]

Table 4.3.1. Peak and half-peak potential difference, $E_p - E_{p/2}$, αn_α[a] for the irreversible and the number of participating electrons, n, for the reversible V(V)□V(IV) reaction in molten $K_2S_2O_7$-V_2O_5 system at 440°C and 100mV/S.

m/o V_2O_5	Reaction	n	αn_α	I_p^a/I_p^c
2	anodic	0.90		
	cathodic	0.75		0.90
3	anodic	0.67		
	cathodic	0.71		0.90
5	anodic		0.76	
	cathodic		0.53	0.55
10	anodic		0.71	
	cathodic		0.45	0.60
20	anodic		0.55	
	cathodic		0.38	0.68
10 5.5 m/o Li_2SO_4	anodic		0.55	
	cathodic		0.38	0.79

[a] αn_α is the product of the transfer coefficient and the number of electrons participating in the reaction.

4.4. Electrochemical study of the promotion of catalytic SO_2 oxidation in the $K_2S_2O_7$--V_2O_5 melts by Na^+ and Cs^+ ions

The effect of Na^+ ions on the electrochemical behavior of V_2O_5 in molten $K_2S_2O_7$ was studied in 2-10 mol. % $Na_2S_2O_7$ concentration range at 440°C in air and Ar atmospheres. The results obtained are given in Figs. 4.4.1-4.4.5. and Tables 4.4.1-4.4.4.

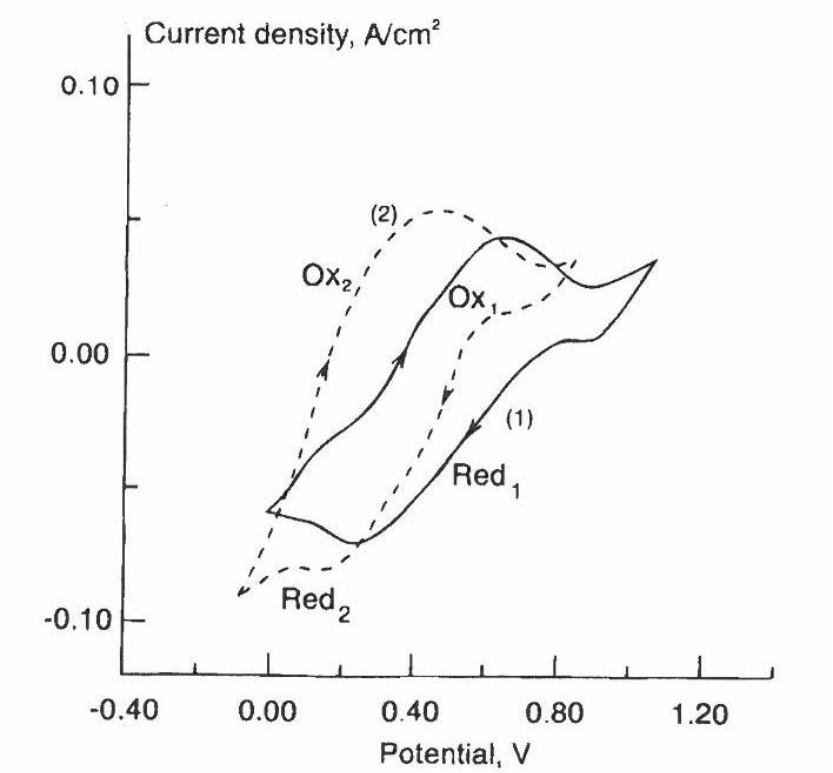

Fig. 4.4.1. Cyclic voltammograms obtained at a gold electrode in a 5 mol % solution of V_2O_5 in (1) a $K_2S_2O_7$ melt, and (2) a $K_2S_2O_7$-$Na_2S_2O_7$ (Na/K = 7.6/91.5) melt at 440°C in dry air atmosphere. The potential scan rate was 0.8 V/s.[21]

Table 4.4.1. The V(IV) → V(V) oxidation for 5.0 mol % V_2O_5 solution in a $K_2S_2O_7$ (93.5 mol %) – $Na_2S_2O_7$ (6.5 mol %) melt in air at 440°C. Peak current, pek potential, and half-peak potential of wave Ox_2 vs. potential scan rate.

Scan rate (V/s)	Peak current (mA)	Peak potential (V)	Half-peak potential, $E_{p/2}$ (V)
1.0	5.89_5 [a]	0.44_5	0.25_9
0.9	5.71_1	0.45_5	0.25_7
0.8	5.43_6	0.44_4	0.27_7
0.7	5.27_1	0.44_1	0.26_1
0.6	4.81_0	0.43_8	0.25_2
0.5	4.38_9	0.43_7	0.25_4
0.4	3.91_8	0.44_0	0.25_1

[a] Subscripts indicate less reliable figures.

Table 4.4.2. The V(IV) → V(V) oxidation for 5.0 mol % V_2O_5 solution in a $K_2S_2O_7$ (92.4 mol %) – $Na_2S_2O_7$ (7.6 mol %) melt in air at 440°C. Peak current, peak potential, and half-peak potential of wave Ox_2 vs. potential scan rate.

Scan rate (V/s)	Peak current (mA)	Peak potential (V)	Half-peak potential, $E_{p/2}$ (V)
1.0	6.58_6	0.47_2	0.24_3
0.9	6.47_6	0.45_2	0.24_8
0.8	6.11_9	0.46_2	0.24_6
0.7	5.87_7	0.46_2	0.24_9
0.6	5.57_8	0.46_4	0.25_0
0.5	5.29_7	0.46_1	0.24_9

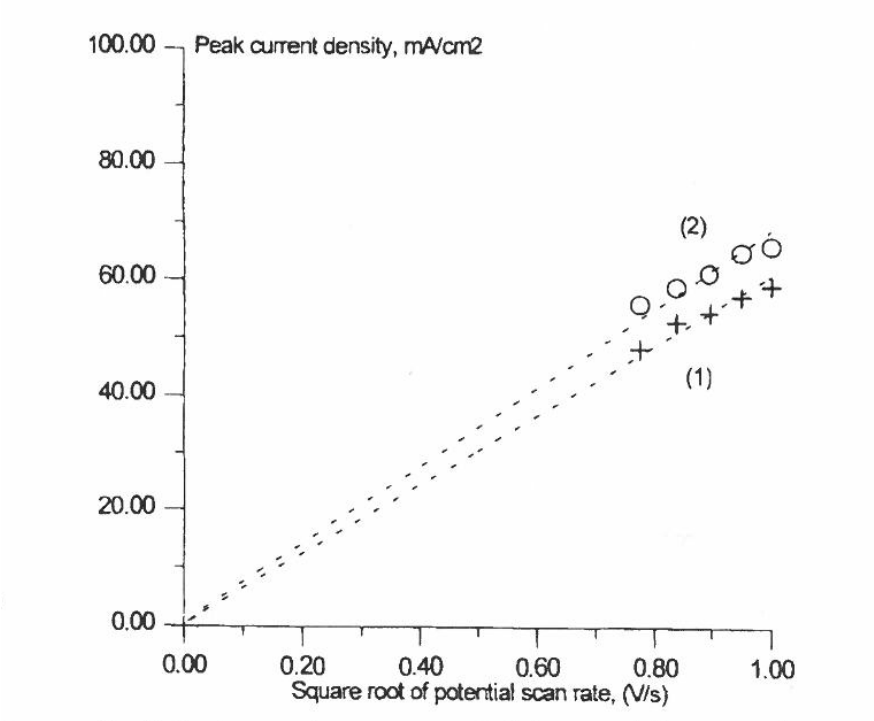

Fig. 4.4.2. Peak current vs. square root of potential scan rate for wave Ox_2 obtained in (1) 5.0 m/o V_2O_5 solution in a $K_2S_2O_7$ (93.5 mol %) – $Na_2S_2O_7$ (6.5 mol %) melt; (2) 5.0 mol % V_2O_5 solution in a $K_2S_2O_7$ (92.4 mol %) – $Na_2S_2O_7$ (7.6 mol %) melt at 440°C in a dry air atmosphere.[21]

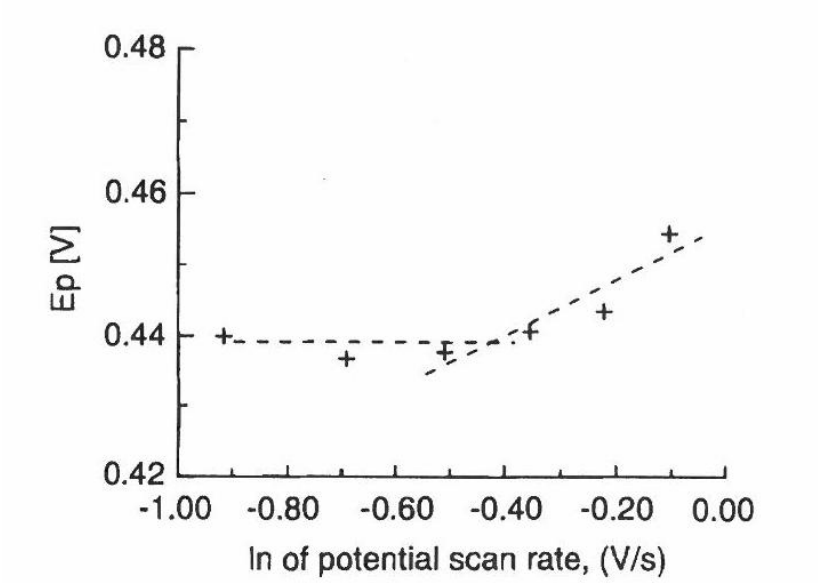

Fig. 4.4.3. Peak potential vs. logarithm of the potential scan rate for wave Ox_2 obtained in 5.0 mol % of V_2O_5 solution in a $K_2S_2O_7$ (93.5 mol %) – $Na_2S_2O_7$ (6.5 mol %) melt at 440°C in a dry air atmosphere.[21]

4.4.1. Cyclic voltammetry of the molten V_2O_5-$Na_2S_2O_7$-$K_2S_2O_7$ system

Comparison of the voltammetric behavior of V_2O_5 (5 mol. %) solution in molten $K_2S_2O_7$ and in molten $K_2S_2O_7$ containing 7.6 mol. % of $Na_2S_2O_7$ in the air atmosphere at 440°C is shown in Fig. 4.4.1. It can be seen, from Fig. 4.4.1, that sodium ions noticeably affect both the V(V) reduction and the V(IV) oxidation. The initial potentials of the both reactions move to the negative directions: for example, at the potential scan rate of 0.8 V/s (Fig. 4.5.1) there was a ≈ -0.26 V shift for the V(IV) oxidation and ≈ -0.17 V sfift for V(V) reduction. These shifts mean a depolarization for the V(IV) oxidation and extra polarization for the V(V) reduction. Moreover, it can be seen that, when Na^+ ions were added to the molten V_2O_5-$K_2S_2O_7$ system, the peak currents of both the V(IV) oxidation and the V(V) reduction waves increased ≥ 25%. This means that both reactions were accelerated by the $Na_2S_2O_7$ addition.

The study on the electrochemical kinetics in the V_2O_5-$Na_2S_2O_7$-$K_2S_2O_7$ has been made only for the V(IV) → V(V) reaction because of the importance of this step in the mechanism of the catalytic oxidation of SO_2.[23,24,32,33,72-80]

The linear I_p -$V_E^{1/2}$ in Fig. 4.5.2 means that the V(IV) → V(V) oxidation is controlled by diffusion of vanadium complexes. It can also be seen that even a little change in the Na^+ ion concentration gives a visible increase in the V(IV) oxidation rate.

A more detailed evaluation of the kinetics of the V(IV) oxidation can be obtained from the E_P (the peak potential) – ln V_E plot (Fig. 4.4.3). It can be seen that the reaction is reversible at low scan rates (peak potential independence on the scan rate) and irreversible at high scan rates (peak potential linear dependence on the logarithm of the potential scan rate). It can also be seen from Fig. 4.4.4 that the addition of Na^+ ion to the V_2O_5-$K_2S_2O_7$ melt change the kinetics of V(IV) oxidation to reversible at all scan rates.

Number of the electrons participating in the reaction, ***n***, was calculated for the case of the irreversible reaction with an assumption that transient coefficient, α, is approximately 0.5.[85] The results of the calculation are given in Tables 4.4.3 and 4.4.4. It can be seen that the number of electrons participating in the V(IV) oxidation was ***one*** at all conditions studied. It means that even if the kinetics of this reaction changes it will not affect the number of the participating electrons.

In electrochemistry, the rate of electrochemical reaction is a linear function of current. Therefore if the addition of Na^+ increased the current, it means that the electrochemical reaction was accelerated. In this connection, it was also important to study the promoting effect as a function of a concentration of a promoter. The concentration dependence of the Na^+ promoting effect on the V(IV) oxidation was studied in the solvent consisting of ***x*** mol % of $Na_2S_2O_7$ and (100 –***x***) mol %$K_2S_2O_7$ with 5 mol % V_2O_5 added and with x in the 2.5-10 concentration range in the air atmosphere. The results are given in Fig. 4.4.5. It can be seen that the maximum anodic peak current was found at a solvent composition of 8.5 mol % $Na_2S_2O_7$ and 91.5 mol % $K_2S_2O_7$.

The results of the investigation of the Na^+ on the V(V) reduction and V(IV) oxidation in a solvent of ***x*** mol % of $Na_2S_2O_7$ and (100 –***x***) mol %$K_2S_2O_7$ with 10 mol % V_2O_5 added and with ***x*** = 5, 10, 15 in an argon atmosphere are given in Fig. 4.5.6. It can be seen that sodium ions affect both current and potential ov the V(V) reduction and V(IV) oxidation in the same way as in the air atmosphere and the optimum concentration of the $Na_2S_2O_7$ promoter is close to what has been found in the air atmosphere. On the basis of the results obtainened in Ar and air, one can conclude that oxygen does not change the effect of Na^+ on the V(V) reduction and V(IV) oxidation.

It is common opinion that the V(IV) $\rightarrow$ V(V) oxidation with oxygen is the rate-determing step of the catalytic SO_2 oxidation,[23,24,32,33,72-80] and it is obvious that electrochemical data reflect the ecceleration of the V(IV) oxidation. This increase

of current was not caused by a difference in the ionic conductivity of the molten electrolyte, because it has been found that the ionic conductivities of V_2O_5-$K_2S_2O_7$ and V_2O_5-$Na_2S_2O_7$ melts are very close.[86] Therefore, the voltammetric response reflects the kinetic changes in the rate-determining step of the catalytic SO_2 oxidation in the presence of alkali promoter. We can conclude that cyclic voltammetry can be used as a technique for the investigation of the nature of the cationic promotion of the V_2O_5 catalyst. Moreover the electrochemical technique can be used for an optimization of the concentration of $Na_2S_2O_7$ promoter. As it has been described earlier, it was assumed that irreversibility of the V(IV) electrooxidation and V(V) electroreduction at V_2O_5 concentrations higher than 5 mol % is caused by formation of the dimeric(or polymeric) vanadium complexes. Threfore, if there is a change of the irreversible mechanism into reversible, then it is probably because of stabilization monomeric vanadium species in the presence of Na^+. Another assumption can be done concerning the role of the slow diffusion of oxygen in the V(IV) oxidation step. The fact that Na^+ has the same promoting effect work both in air and Ar atmospheres (compare Figs. 4.5.1. and 4.5.6) shows that the electron transfer during the V(IV) oxidation is the rate-determining step.

4.4.2. Cyclyc voltammetry of a 5 mol % solution of V_2O_5 in the molten $K_2S_2O_7$-$Cs_2S_2O_7$ system.

The results of a voltammetric investigation of a 5 mol % V_2O_5 in a $K_2S_2O_7$: $Cs_2S_2O_7$ (1: 1) melt in the air atmosphere at 440°C are given in Figs. 4.4.7- 4.4.9. The voltammetric peak parameters for the anodic wave are given in Table 4.4.5. It can be seen from Fig. 4.4.7, that in the presence of Cs^+ a signicant change takes place in the kinetics of the V(V) reduction and the V(IV), especially in the case of the oxidation. The increase in the anodic peak current (i.e. acceleration) is approximately 58% compared to the V_2O_5-$K_2S_2O_7$ system. This means that the acceleration effect caused by Cs^+ ions is more than twice as strong as the promoting effect of Na^+ ions. As in the case of V_2O_5-$Na_2S_2O_7$-$K_2S_2O_7$ melt, the V(IV) oxidation proceeds with depolarization (at more negative potentials) in the presence of Cs^+ ions. There is no significant change in the initial potential of the V(V) reduction, however, instead of the peak shape, the cathodic V(V) reduction wave *Red*$_3$ (Fig. 4.4.7) is more similar to a steady-state voltammetric wave with a limiting diffusion current.

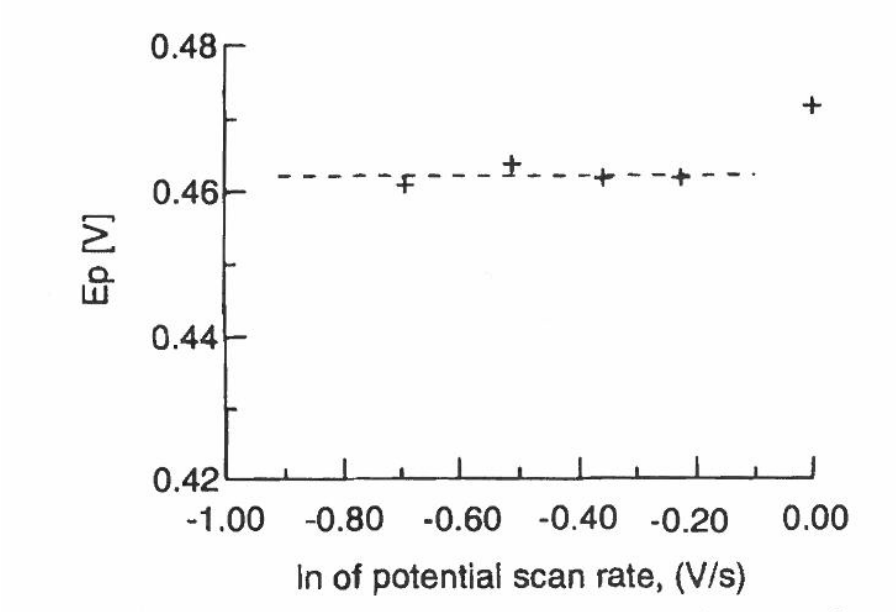

Fig. 4.4.4. Peak potential vs. logarithm of the potential scan rate for wave Ox_2 obtained in 5.0 mol % V_2O_5 solution in a $K_2S_2O_7$ (92.4 mol %) – $Na_2S_2O_7$ (7.6 mol %) melt at 440°C in a dry air atmosphere.[21]

Table 4.4.3. The V(IV) → V(V) oxidation for 5.0 mol % V_2O_5 solution in a $K_2S_2O_7$ (93.5 mol %) – $Na_2S_2O_7$ (6.5 mol %) melt in air at 440°C. Type of the kinetics and number of the electron participating in the oxidation.

Scan rate (V/s)	Kinetics	Number of electrons, n
0.9	Irreversible	1.15
0.8	Irreversible	1.22
0.7	Quasi-reversible	-
0.6	Quasi-reversible	-
0.5	Reversibe	0.74
0.4	Reversible	0.72

Table 4.4.4. The V(IV) → V(V) oxidation for 5.0 mol % V_2O_5 solution in a $K_2S_2O_7$ (92.4 m/o) – $Na_2S_2O_7$ (7.6 m/o) melt in air at 440°C. Type of the kinetics and number of the electron participating in the oxidation.

Scan rate (V/s)	Kinetics	Numberof electrons, n
1.0	Quasi-reversible	-
0.9	Quasi-reversible	-
0.8	Reversible	0.63
0.7	Reversible	0.63
0.6	Reversible	0.63
0.5	Reversible	0.64

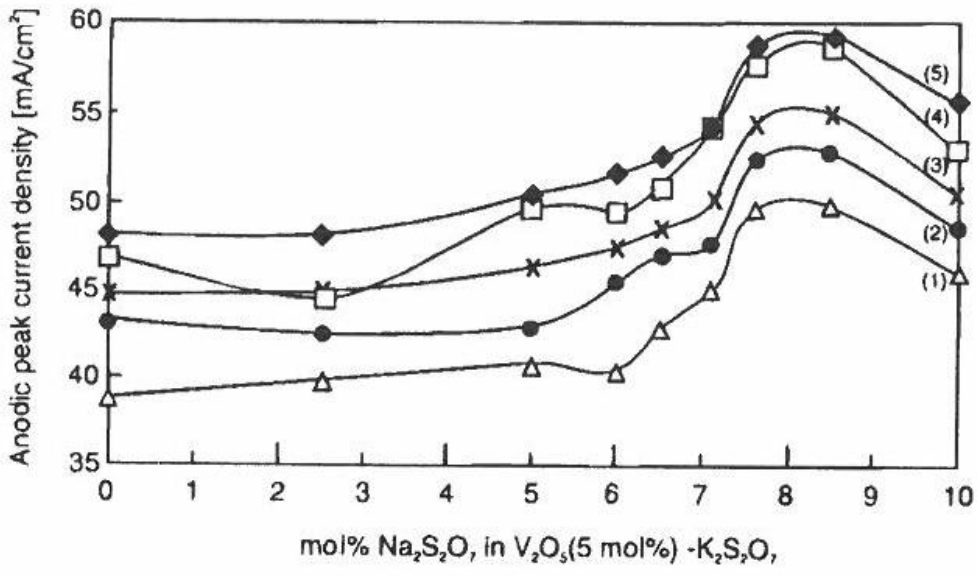

Fig. 4.4.5. Dependence of the peak current of wave Ox_2 on the $Na_2S_2O_7$ content in a V_2O_5-$Na_2S_2O_7$-$K_2S_2O_7$ (5 mol % V_2O_5) melt in dry air atmosphere at 440°C and (1) 0.6; (2) 0.7; (3) 0.8; (4) 0.9; (5) 1.0 V/s, respectively.[21(A3)]

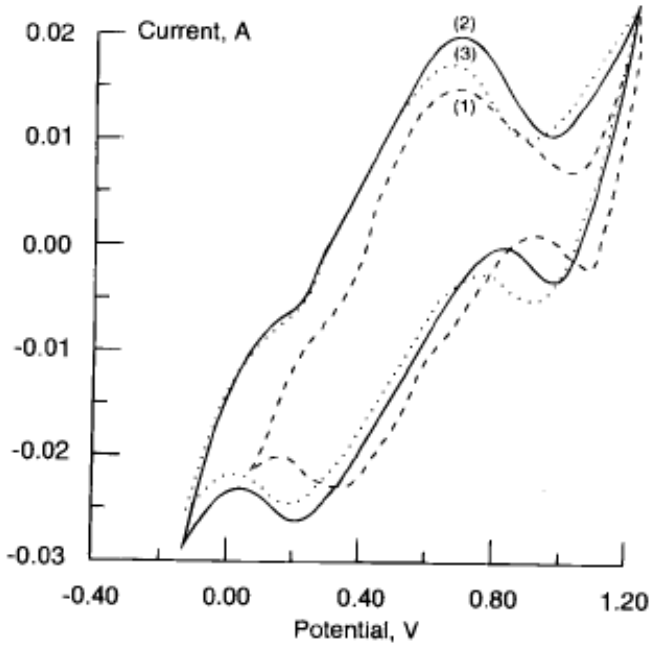

Fig. 4.4.6. Cyclic voltammograms obtained at a gold electrode in a V_2O_5 (10 m/o) - x mol % $Na_2S_2O_7$ – (90 – x) mol % $K_2S_2O_7$ system in Ar atmosphere for x = (1) 5; (2) 10 and (3) 15 at 500 V/s and 440°C.[21]

As in the case of V_2O_5-$Na_2S_2O_7$-$K_2S_2O_7$ melt, the kinetics of the V(IV) electrooxidation was analyzed. The results are given in Figs. 4.4.8 and 4.4.9 and in Table 4.4.5. It can be seen that the ratio $I_P/V_E^{1/2}$ is linearly dependent on the square root of the potential scan rate and decreases with increasing scan rate (Fig. 4.4.8). The peak potential of wave Ox_3 is linearly dependent on the logarithm of the potential scan rate, but, unlike what it would be in the case of an irreversible electrochemical reaction, E_P moves in the negative direction with increase in the potential scan rate. These are clear diagnostic criteria of a mechanism with slow preceding chemical reaction.[85] It has been found that this negative shift for the anodic peak potential (ΔE_{Pa}) equals ca. 60/n mV per hundredfold increase in V_E for a reversible electrochemical step of the reaction at 25°C, i.e.

$$\Delta E_{Pa} = \frac{RT}{nF}\ln(10)\,mV \qquad (4.4.1)$$

per hundredfold increase of V_E and if the increase in the potential scan rate was not hundredfold, then

$$\Delta E_{Pa} = \frac{1}{X}\frac{RT}{nF}\ln(10)\,mV \qquad (4.4.2)$$

per hundredfold$^{1/X}$ increase of V_E, where X is the constant.

It can be seen from Table 4.4.5 that the maximum increase in scan rate in the present study was from 0.6 to 1.0 V/s, or 1.67. X can be found using Fig. 4.5.9: $1.67 = 100^{1/X} \rightarrow X = 9.015$. Therefore at 440°C and for potential scan rate increase of 1.67 times:

$$\Delta E_{Pa} = \frac{1}{9.015}\frac{8.314 \cdot 713}{n \cdot 96485}\ln(10) = \frac{15.7}{n}\,mV \qquad (4.4.3)$$

Using Equ. 4.4.3, we can calculate ***n*** for the V(IV) → V(V) oxidation. An ***n*** value of 0.78 was obtained, which means that the number of electrons participating in the reaction should be one.

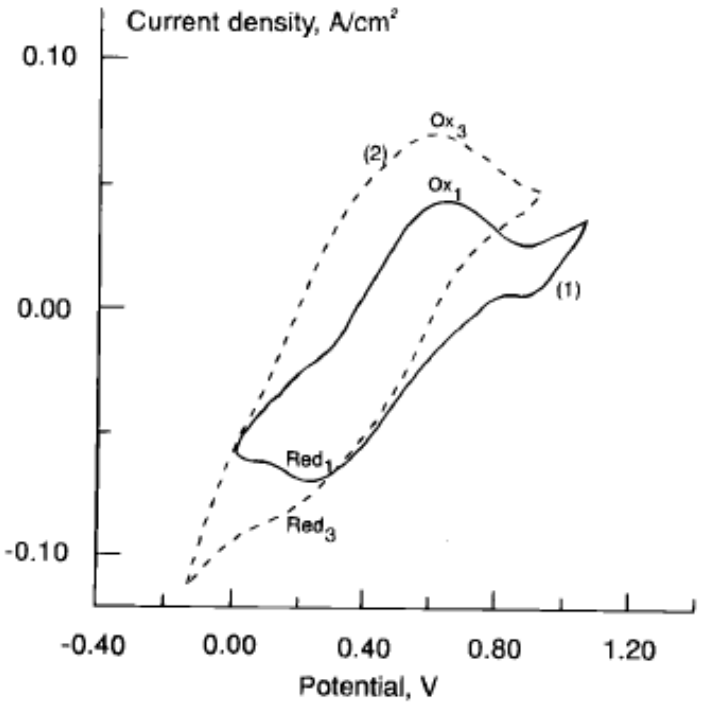

Fig. 4.4.7. Cyclic voltammograms obtained at a gold electrode in a 5 mol % solution of V_2O_5 in (1) a $K_2S_2O_7$ melt and (2) a $Cs_2S_2O_7$- $K_2S_2O_7$ (Cs/K = 1/1) melt, both at 440°C in a dry air atmosphere. The potential scan rate was 0.8 V/s.[21]

Table 4.4.5. The V(IV) → V(V) oxidation for 5.0 mol % V_2O_5 solution in a $Cs_2S_2O_7$- $K_2S_2O_7$ (Cs/K = 1/1) melt at 440°C in a dry air atmosphere. Peak current and peak potential of wave Ox_3 vs. potential scan rate.

Scan rate (V/s)	Peak current (mA)	Peak potential (V)
1.0	9.31_9	0.59_6
0.9	9.13_4	0.60_6
0.8	8.70_5	0.60_4
0.7	8.35_6	0.60_8
0.6	7.82_3	0.60_6

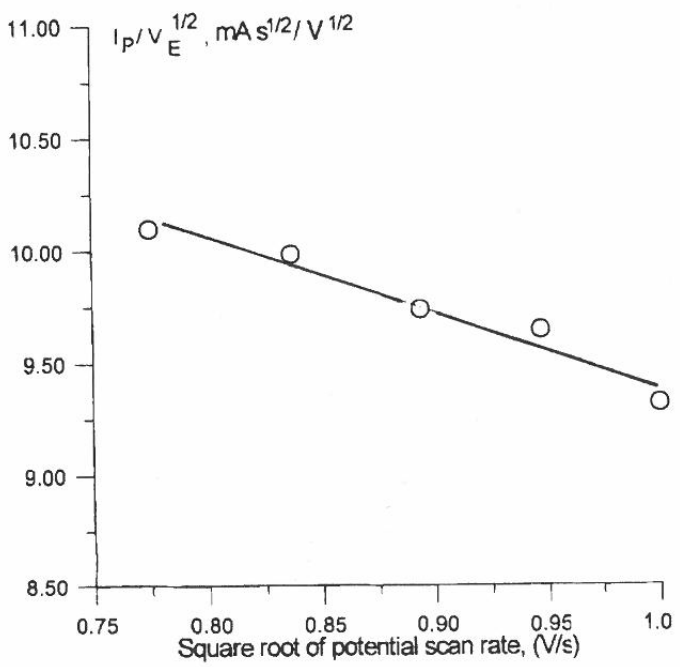

Fig. 4.4.8. Peak current vs. square root of potential scan rate for wave Ox_3 obtained in a 5.0 mol % V_2O_5 solution in a $Cs_2S_2O_7$- $K_2S_2O_7$ (Cs/K = 1/1) melt at 440°C in a dry air atmosphere.[21]

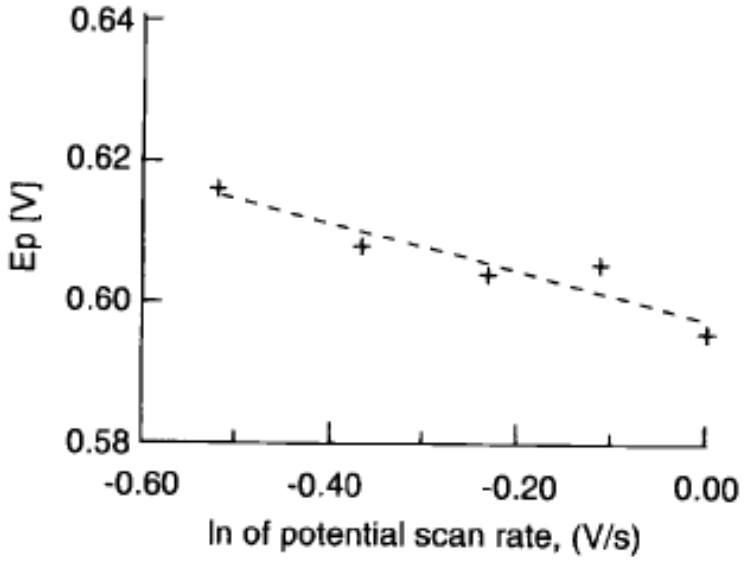

Fig. 4.4.9. Peak potential vs. logarithm of the potential scan rate of wave Ox_3 obtained for a 5 mol % solution of V_20_5 in a $Cs_2S_20_7$- $K_2S_20_7$ (Cs/K = 1/1) melt at 440°C in a dry air atmosphere.[21]

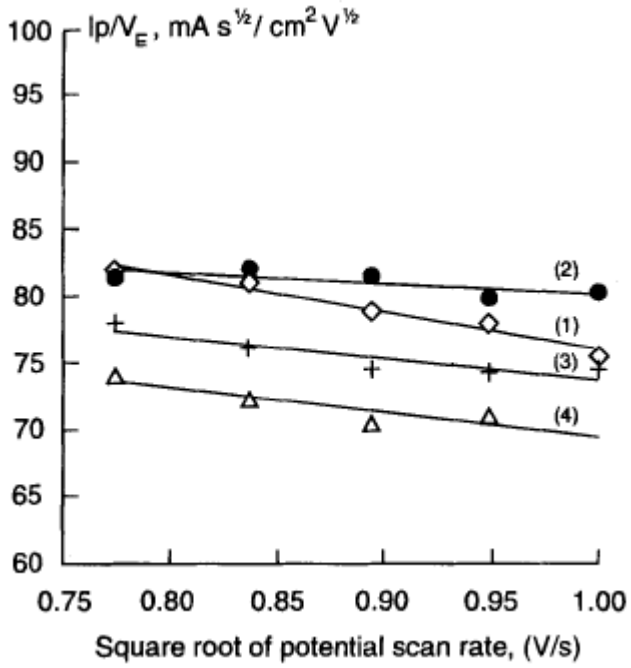

Fig. 4.4.10. Peak current vs. square root of potential scan rate for the V(IV) → V(V) wave obtained in a 5.0 mol % V_2O_5 solution in a $Cs_2S_2O_7$- $K_2S_2O_7$ (Cs/K = 1/1) melt containing (1) 0; (2) 3; (3) 5; (4) 7 mol % of $Na_2S_2O_7$ at 440°C in a dry air atmosphere.[21]

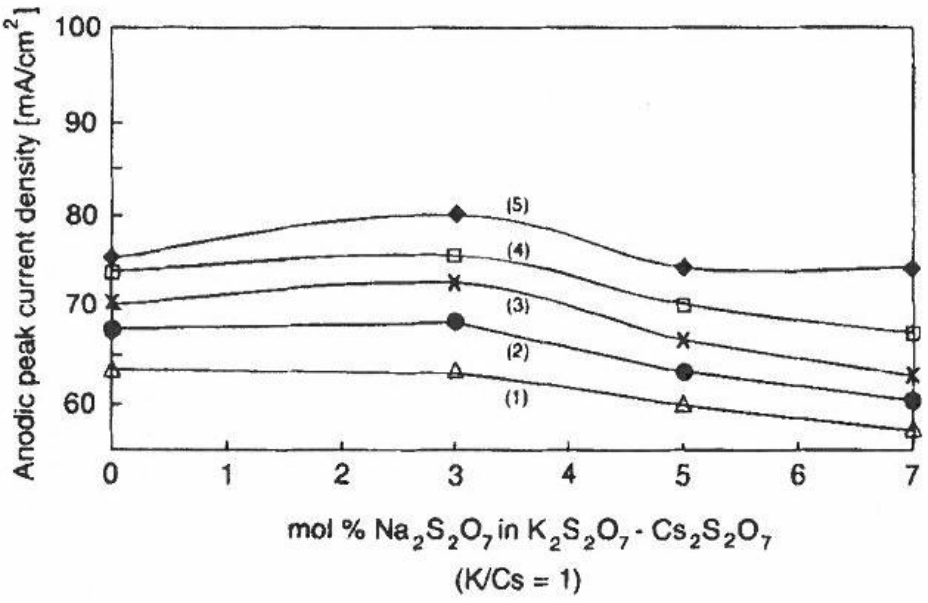

Fig. 4.4.11. Dependence of the peak current of the V(IV) → V(V) wave on the $Na_2S_2O_7$ content in a V_2O_5-$Na_2S_2O_7$- $Cs_2S_2O_7$ - $K_2S_2O_7$ (5 m/o V_2O_5) melt in dry air atmosphere at 440°C and (1) 0.6; (2) 0.7; (3) 0.8; (4) 0.9; (5) 1.0 V/s, respectively.[21]

4.4.3. Cyclic voltammetry of a 5 mol % V_2O_5 solution in molten $Na_2S_2O_7$-$K_2S_2O_7$-$Cs_2S_2O_7$ system.

The effect of Na^+ ions on the electrochemical behavior of V_2O_5 in molten $K_2S_2O_7$: $Cs_2S_2O_7$ (1:1) was studied in the 0-7 mol % $Na_2S_2O_7$ concentration range at 440°C in the air atmosphere. The results are given in Figs. 4.4.10, 4.4.11.

It can be seen in Figs. 4.4.10 and 4.4.11 that small concentrations of Na^+ can further accelerate the V(IV) oxidation, which was already accelerated by Cs^+ ions. Moreover even small concentrations of Na^+ notably changed the kinetics of the V(IV) oxidation. $I_P/V_E^{1/2}$ was still linearly dependent on $V_E^{1/2}$ (Fig. 4.4.10), i.e., it is stil a mechanism with a reversible electron-transfer step and slow preceding chemical step, but these plots changed significantly after the addition of $Na_2S_2O_7$ to the $K_2S_2O_7$-$Cs_2S_2O_7$ melt. This can mean a change of the preceding chemical step or of the type of the V(IV) complex formed. It can be seen from Fig. 4.4.10 that at small Na^+ concentrations [i.e., 3 mol % of $Na_2S_2O_7$, line (2)] this participation may even cause a slight acceleration of the V(IV) oxidation, however higher Na^+ concentrations slow down the reaction (Figs. 4.4.10 and 4.4.11). We

can conclude that the values for the optimum $Na_2S_2O_7$ concentration are different for the V_2O_5-$K_2S_2O_7$-$Na_2S_2O_7$ and for the V_2O_5-$Cs_2S_2O_7$-$K_2S_2O_7$-$Na_2S_2O_7$ systems. These concentration values are possibly defined by the stoichiometry of the active V(V) and V(IV) complexes in the studied melts.

We can assume that the presence of Cs^+ ions does not change the number of vanadium atoms in the active V(IV) and V(V) particles participating in the V(IV) $\rightarrow$ V(V) oxidation. However, Cs^+ ions significantly change the mechanism of this reacton compared to the V_2O_5-$K_2S_2O_7$ melt. The promoting effect of both Na^+ and Cs^+ ions shows that their participation in the V(V) and V(IV) complex structures, stabilize in this way the monomeric particles and in this way accelerate the V(V) $\leftrightarrow$ V(IV) reaction.

Based on the experimental data, we can conclude that:

- Voltammetry can be used as a reliable tool for study of a mechanism of the cationic promotion of the SO_2 catalytic oxidation and for an optimization of the amount of the promoter.
- The alkali-ion promotion effect can be qualitatively devided into two types: *"large amont promoter"*, when the promoter changes physic-chemical properties of the bulk melt (i.e. Cs^+); and *"small amount additive"*, when the bulk properties are not significantly changed, but the thermodynamics and kinetics of catalytic reaction is changed (Na^+, Li^+).
- Mixed with potassium pyrosulfate cesium pyrosulfate (or sulfate) forms the system with the low melting point (and therefore viscosity), which gives an increase of the solubility of the participants of the catalytic reaction, and in this way accelerates the reaction. *$Na^+$and Li^+* are small cations with therefore higher charge density than for *K^+ and Cs^+*. Naturally the small cations have stronger polarization effect on V-O bond in VO_2^+ and VO^{2+} and in this way affect the thermodynemics and kinetics of the catalytic reaction.
- It was found that Li^+, Na^+ and Cs^+ help to restore the reversibility of the V(V) $\leftrightarrow$ V(IV) reaction and thus accelerate it.
- Addition of $Na_2S_2O_7$ to the V_2O_5-$Cs_2S_2O_7$-$K_2S_2O_7$ melt caused a slight increase (< 5%) of the anodic V(IV) $\rightarrow$ V(V) peak current for the $Na_2S_2O_7$ concentration lower than 3 mol %. At higher Na+ concentration the V(IV) oxidation rate decreased.

4.5. Effect of water on the electrochemical behaviour of V_2O_5 in molten $K_2S_2O_7$

4.5.1. Voltammetric measurements on Pt and Au electrodes in melts of $KHSO_4$ and $K_2S_2O_7$-$KHSO_4$ at 265 and 440°C.

The voltammogram obtained with the gold electrode in the molten $K_2S_2O_7$ and its mixtures with 7.5 and 10 m/o of $KHSO_4$, at 700 and 1000 mV/s at 440°C are given in Figs. 4.5.1 and 4.5.2.

After addition of $KHSO_4$ to the $K_2S_2O_7$ melt, the reduction wave R_1 and the oxidation wave Ox_1 appear in the voltammetric curves at potentials 0.26 and 0.04 V (300 mV/s), respectively. The R_1 peak current depends on the concentration of $KHSO_4$ and the cathodic limit of the potential window moves toward more positive potentials. The oxidation wave Ox_2 and reduction wave R_4 are gradually suppressed with the increasing concentration of $KHSO_4$.

It has already been shown[18] that wave R_2 is due to the reduction of the gold oxide to gold according to the reaction described by the Eq.4.2.5.

Wave Ox_2, according to Ref. 18, 29 is the electrochemical dissolution of the gold electrode which can be described by the Eq. 4.2.4A.

Wave Ox_3 is the electrochemical oxidation of $S_2O_7^{2-}$ according to the Eq.4.2.7A and wave R_3 is the electrochemical reduction of solvated SO_3 mixed with oxygen (reaction 4.2.7A in the backword direction).[18] Wave R_4 appears only at high potential scan rates and can be ascribed to the electrochemical reduction of gold complexes because it is decreasing simultaneously with wave Ox_2 after the additions of $KHSO_4$. Wave R_1 is clearly due to $KHSO_4$. To identify the electrochemical reactions, we need information about the electrochemical behavior of molten $KHSO_4$. We also compare the electrochemical behavior of the much investigated Pt electrode to the Au electrode under the same conditions. The results are given in Fig.4.5.3. Wave R_1 at approximately 0.25V and wave Ox_5 at 1.3V corresponds to the cathodic and anodic limiting reactions, respectively.of the potential window of the $KHSO_4$ melt. Acording to Arvia et al.,[64] the residual EMF, after electrolysis of the molten $KHSO_4$, was 0.602 V at 269°C. This EMF was identified with the potential window of molten potassium bisulfate on the basis of reversibility of the reactions (4.11) and (4.12), i.e. it was much lower than in our experiment. However, it is obvious from Fig. 4.5.3, that

reaction Ox_5 is irreversible. The only "available" cathodic reaction to form an electrochemical couple with hydrogen after molten $KHSO_4$ electrolysis is reaction R_5 (Fig. 4.5.3). This fact can explain the low values of residual EMF obtained by Arvia *et* al.[64] Wave R_5 can be ascribed to the reduction of platinum oxide, taking into account the electrochemical behavior of (i) platinum in dilute sulfuric acid[70] (platinum oxide formation and reduction region occurring between 0.4V and 1.1V *vs.* hydrogen electrode), (ii) platinum in concentrated sulfuric acid solutions[71] (platinum oxide formation and reduction region occurring between 0 and 0.6 V *vs.* the h:ydrogen electrode), and (iii) the experimental data obtamed by Gilroy[65] (platinum oxide reduction in the molten $KHSO_4$ takes place at 0.4 V *vs.* the hydrogen electrode).

The gold electrode voltammogram for molten $KHSO_4$ under Ar atmosphere and at 265°C was characterized by a 0.26 V cathodic limit (wave R_1) and a 0.96 V anodic limit (wave Ox_5) at 300 mV/s (Fig. 4.5.3, solid line). The cathodic wave R_6 is obviously the electrochemical reduction of the product of the reaction Ox_4.

As the cathodic limiting reaction (and taking into account the data obtained with Pt electrode) wave R_1 can be ascribed to H^+ or HSO_4^- reduction on Au (Equ. 4.7).

It was found that the value of the peak current of wave R_6 depends upon the duration of the anodic electrolysis during the corresponding oxidation wave Ox_4. At high potential scan rates it is possible to scan the potential to more positive values to reach (similar to Pt) the anodic oxidation of HSO_4^- ion at 1.45 V, i.e. wave Ox_5 (Fig. 4.5.4).

Experimental data on the electrochemical behavior of gold in $KHSO_4$ melts and comparison of the voltammograms obtained in molten $K_2S_20_7$ and $KHSO_4$ electrolytes at 440°C (Fig. 4.5.5) show that the cathodic wave R_1 on the $K_2S_2O_7$- $KHSO_4$ voltammogram (Fig. 4.5.1) can be ascribed to proton reduction and the anodic wave Ox_1 to the oxidation of the adsosorbed hydrogen (Eq. 4.11 in the opposite direction). It can also be seen from Fig. 4.5.5, that the anodic dissolution of gold in molten $KHSO_4$ proceeds at more positive potentials than in molten $K_2S_2O_7$, i.e. Au is more stable in the molten potassium bisulfate.

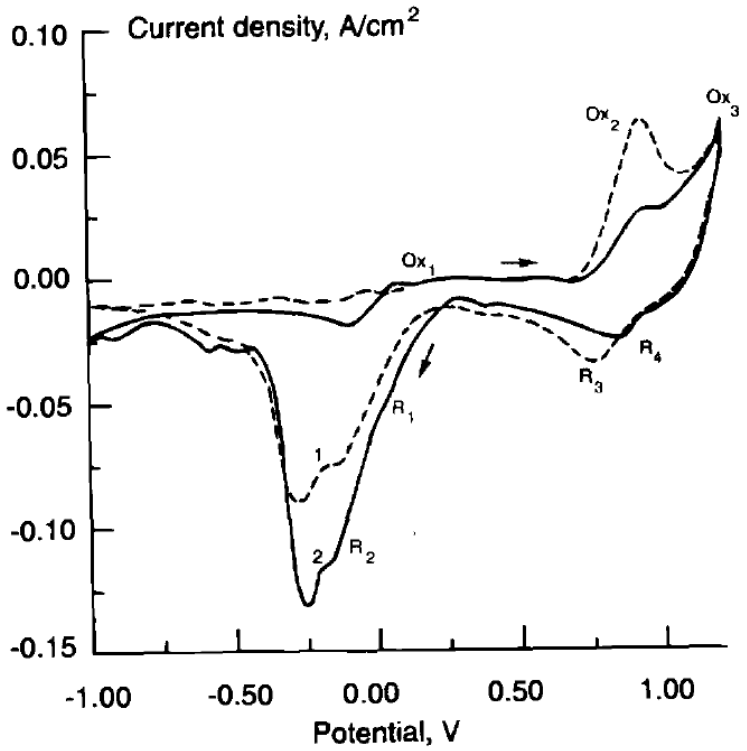

Fig.4.5.1. Voltammetric curves obtained with a gold electrode in molten $K_2S_2O_7$ (1); and $K_2S_2O_7$ + 7.5 m/o $KHSO_4$ (2) at 800 mV/s and 440°C in Ar.[19]

We can conclude, that potential window of molten $KHSO_4$ is limited at the cathodic end by the hydrogen evolution reaction (HER), Equ. (4.11) on both Pt and Au electrodes. At the anodic end it is limited by oxygen evolution reaction (OER), Equ. (4.12), at Pt electrode and electrochemical dissolution of gold (Equ. 4.2.4B) at Au electrode.

atmosphere.[19(A2)]

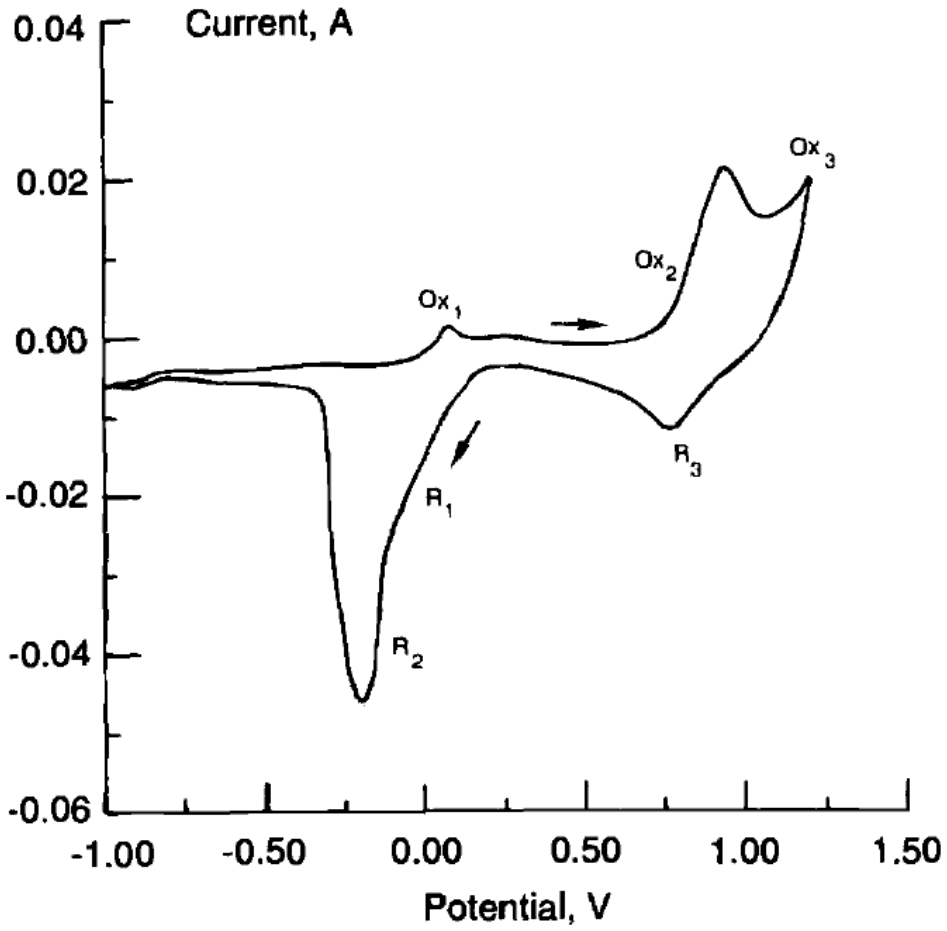

Fig.4.5.2. Voltammetric curve obtained with a gold electrode in molten $K_2S_2O_7$ + 10 m/o $KHSO_4$ at 1000 mV/s and 440°C in Ar atmosphere.[19]

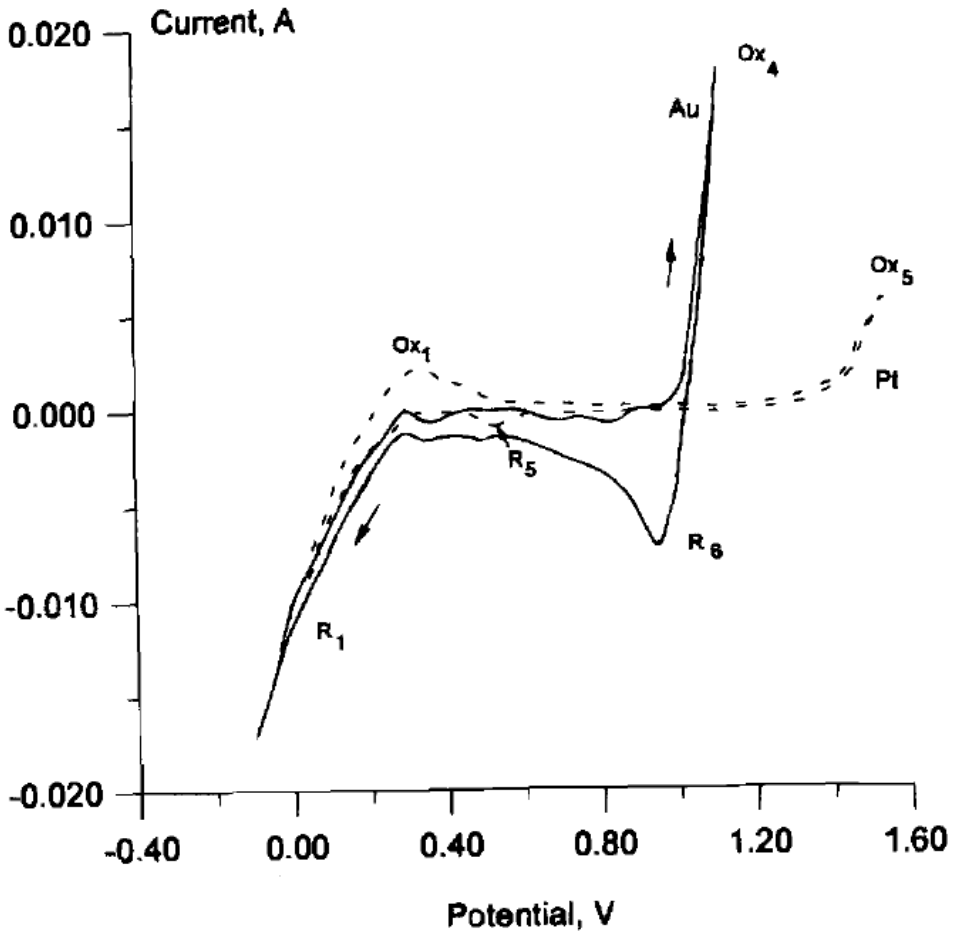

Fig.4.5.3. Comparison of voltammetric curves for different electrode materials, platinum (Pt) and gold (Au) in molten $KHSO_4$ at 300 mV/s and 265°C in Ar atmosphere.[19]

4.5.2. Voltammetric measurements on a gold electrode in the molten $K_2S_2O_7$-V_2O_4, $K_2S_2O_7$-$KHSO_4$ -V_2O_4 and $K_2S_2O_7$-$KHSO_4$ -V_2O_5 systems at 440°C in Ar atmosphere

In order to perform the effective study on water effect on the kinetics of the V(V)/V(IV) couple, especially V(IV) oxidation, we decided to start from the V_2O_4 solutions in molten $K_2S_2O_7$ and $K_2S_2O_7$-$KHSO_4$. It can be seen, from Fig.4.5.6, that when V_2O_4 was added to potassium pyrosulfate and after the first voltammetric cycle (when V(V) was produced), four new waves appeared at the voltammogram, i.e. reduction waves R_{10} and R_{11} and oxidation waves Ox_9 and Ox_{10}. Taking into account the results obtained in Ref. 18(A1), we can define R_{10} as V(V)→V(IV) reduction, R_{11} as V(IV)→V(III) reduction, Ox_{10} as V(IV)→V(V) oxidation and Ox_9 as V(III)→V(IV) oxidation.

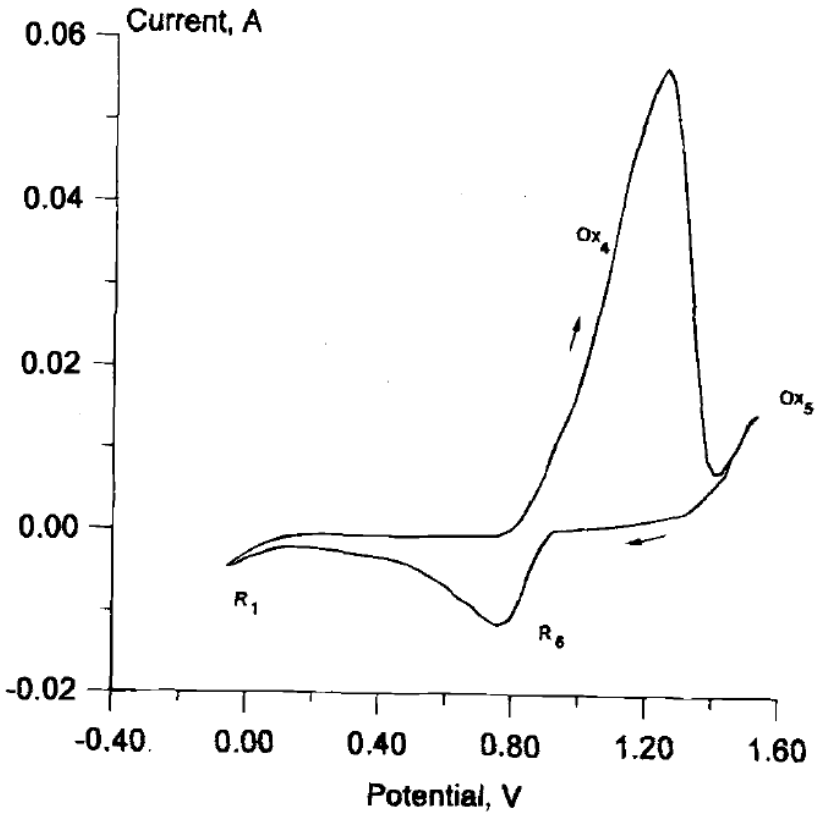

Fig.4.5.4. Voltammetric curves obtained with a gold electrode in molten $KHSO_4$ at 1000 mV/s and 265°C in Ar atmosphere.[19]

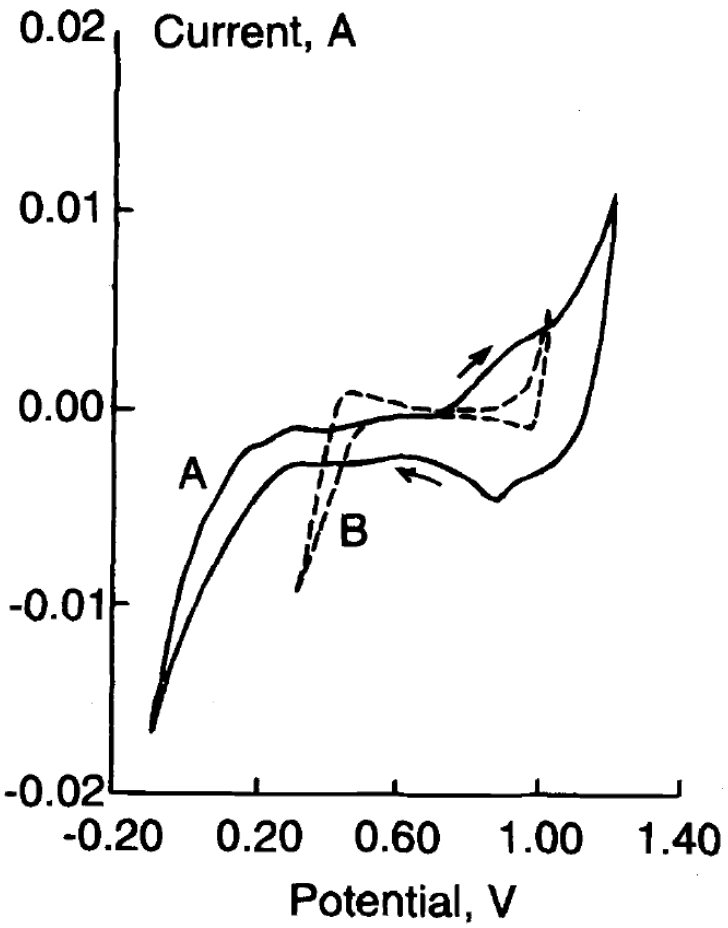

Fig. 4.5.5. Comparison of voltammetric curves obtained with a gold electrode in molten $K_2S_2O_7$ (A) and molten $KHSO_4$ (B) at 1000 mV/s and 440°C in Ar atmosphere.[19]

The results of the voltammetric measurements in $K_2S_2O_7$-$KHSO_4$ (10 mol %) - V_2O_4 (sat.) melt are given in Figs. 4.5.7, 4.5.8. It can be seen, that new reduction wave (R_{12}) appears between V(V) → V(IV) (R_{10}) and V(IV) → V(III) (R_{11}) reduction waves. Wave R_{12} and wave R_1 (Fig. 4.5.2) appeared in the same potential range. Therefore we can assume that R_{12} is H^+ (or HSO_4^-) reduction. The fact that hydrogen evolution (R_{12}) proceeds at more positive potential than V(IV) → V(III) reduction (R_{11}) helps us to understand the reason for the absence of the second vanadium electroreduction step in the previous publications about the electrochemical behavior of $K_2S_2O_7$-V_2O_5 melts containing water. [28,29]

It can be seen from Fig.4.4.7, that addition of $KHSO_4$ causes a higher concentration of V(III). This can be achieved either through the promotion of the V(IV) → V(III) electroreduction by protons (Eq.4.5)[49] or by a chemical reduction of V(IV) by hydrogen formed during proton reduction.

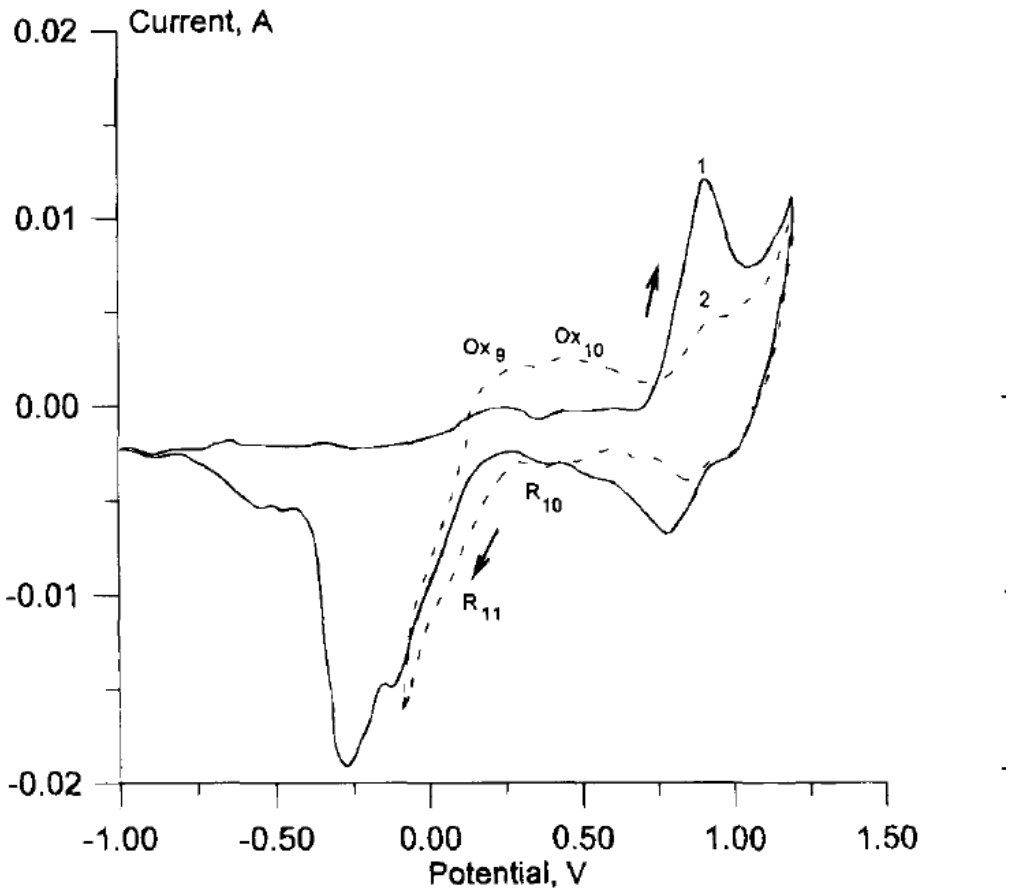

Fig. 4.5.6. Comparison of voltammetric curves obtained with a gold electrode in molten $K_2S_2O_7$ (1) and molten $K_2S_2O_7$-V_2O_4 (sat.), 2nd cycle (2) at 1000 mV/s and 440°C in Ar atmosphere.[19]

4.5.3. Electrochemical of vanadium pentoxide in molten $K_2S_2O_7$-$KHSO_4$.

The voltammetric data obtained at a gold electrode in a $K_2S_2O_7$-$KHSO_4$ (10 mol %)-V_2O_5 (10 mol %) melt are given in Figs.4.5.9-4.5.12 and in Table 4.4.1; the votammogram obtained in the "dry" $K_2S_2O_7$-V_2O_5 (10 mol %) melt is also presented for a comparison. It can be seen that the addition of $KHSO_4$ does not affect V(V) → V(IV) reduction significantly but the peak potential of the V(IV) → V(V) oxidation moves to more positive potentials. For both V(V) → V(IV) and V(IV) → V(V) reactions, peak currents depend linearly on the square root of the potential sca rate (Fig.4.5.11). The peak potentials (E_p) are linearly dependent on the logarithm (ln) of the potential scan rate (V_E) (Fig.4.5.12), i.e. the V(V) → V(IV) reaction is irreversible, and Eq.4.2.2 can be used to calculate the number of electrons (n_α) participating in the reaction.

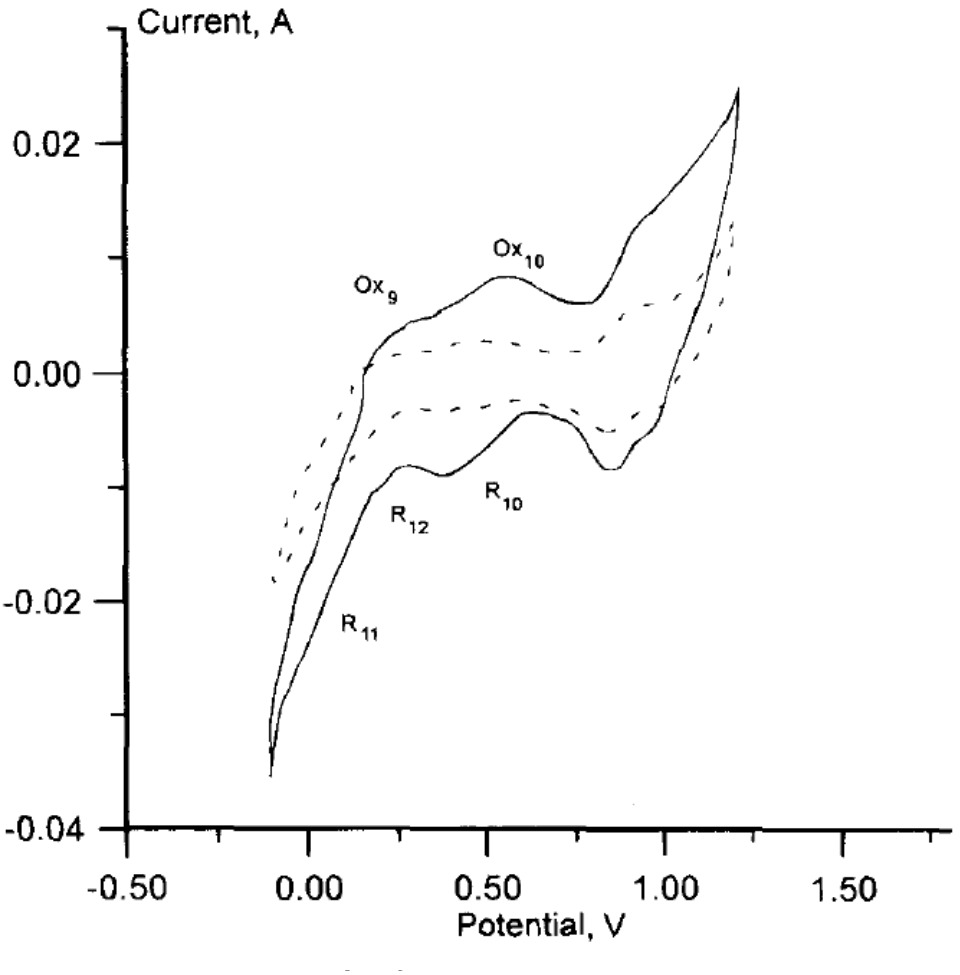

Fig.4.5.7. Comparison of voltammetric curves obtained with a gold electrode in molten $K_2S_2O_7$ – V_2O_4 (sat.) (dashed curve) and in molten $K_2S_2O_7$ – $KHSO_4$ (10 mol %) – V_2O_4 (sat.) (solid curve) at 1000 mV/s and 440°C in Ar atmosphere.[19]

It was assumed that the transfer coefficient, α, equals 0.5. Calculated n_α was 1 (Table 4.5.1), i.e. similar to the "dry" melt. The more positive peak potentials for the V(IV) oxidation is a result of a slow down of the kinetics of this reaction.[29] This change can be cused by formation of stable hydrate $VOSO_4 \cdot 3H_2O$. Participation of the water in formation of the electric double layer can be the reason of this change.

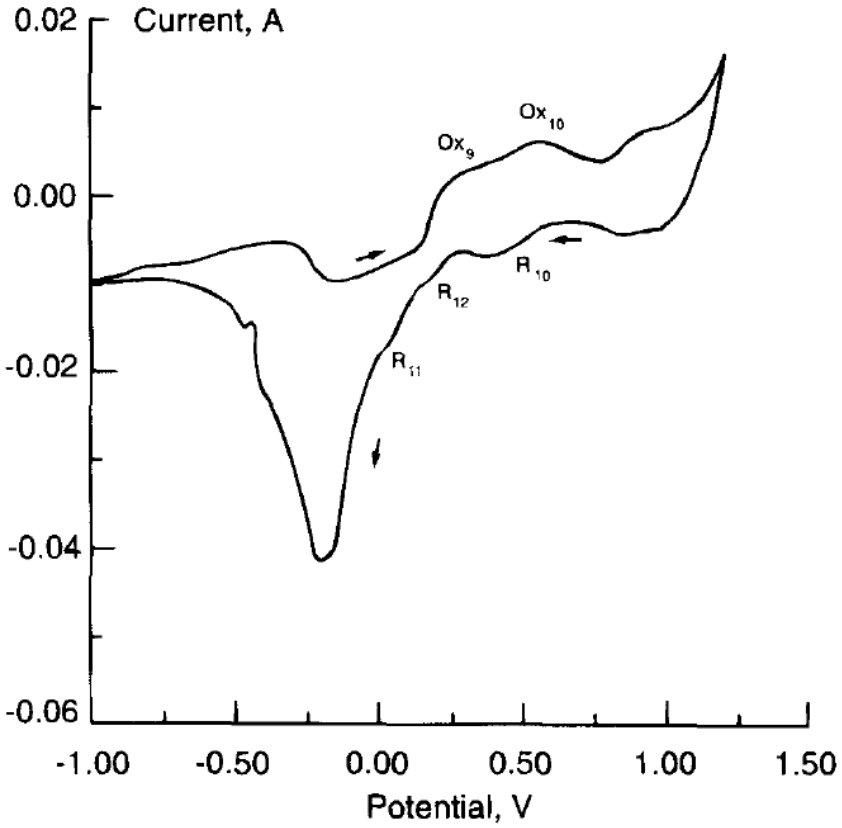

Fig.4.5.8. Voltammetric curve obtained with a gold electrode in molten $K_2S_2O_7$ – $KHSO_4$ (10 mol %) – V_2O_4 (sat.) at 400 mV/s and at 440°C in Ar atmosphere.[19]

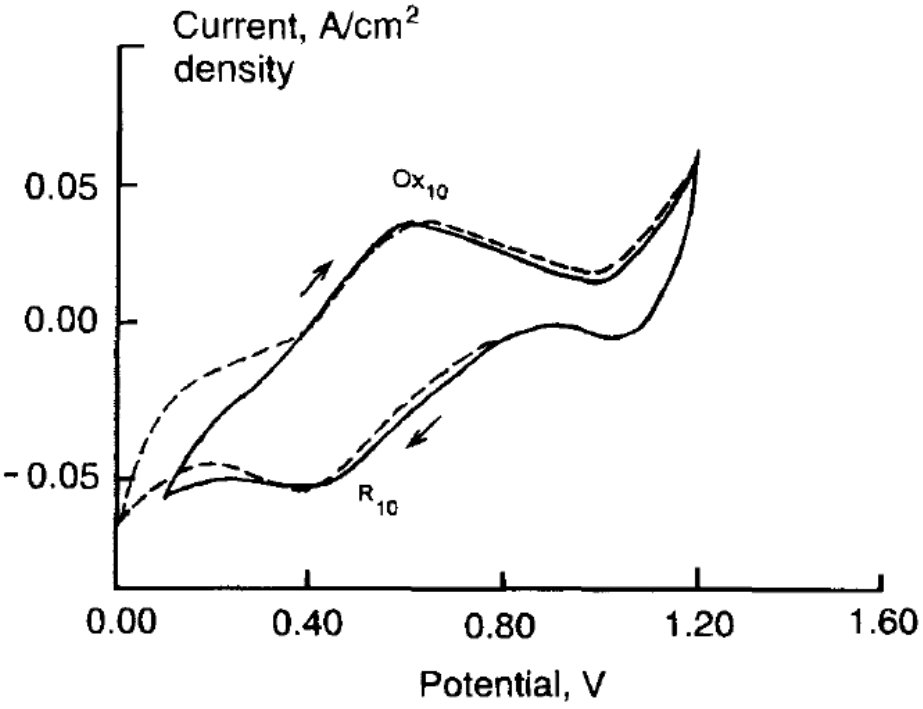

Fig.4.5.9. Voltammetric curves obtained with a gold electrode in molten $K_2S_2O_7$ – 10 mol % V_2O_5 (solid line) and molten $K_2S_2O_7$ – 10 mol % V_2O_5 – 10 mol % $KHSO_4$ (dashed line) at 100 mV/s and 440°C in Ar atmosphere.[19(A2)]

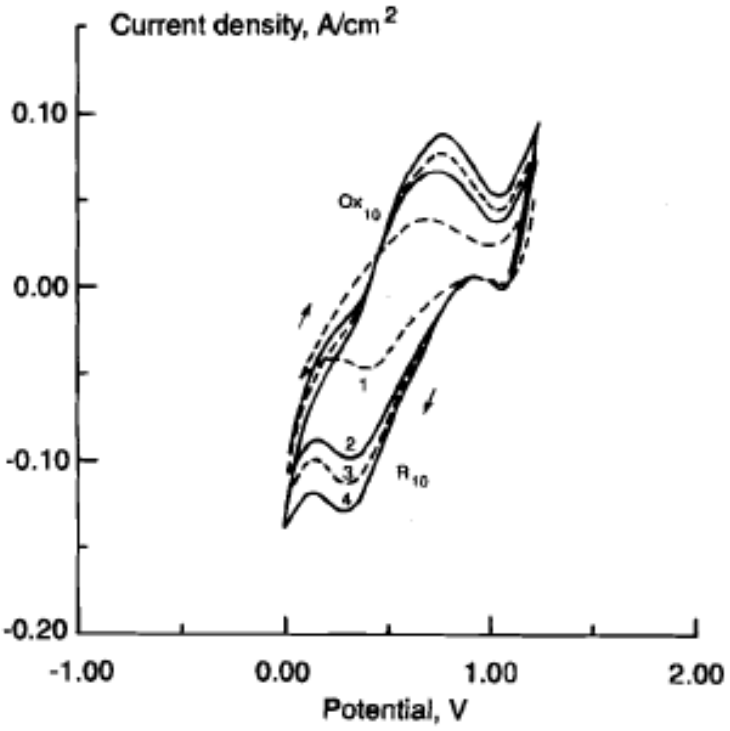

Fig. 4.5.10. Effect of the potential scan rate on the voltammetric curves obtained with a gold electrode in $K_2S_2O_7$ – 10 mol % V_2O_5 – 10 mol % $KHSO_4$: 1, 100; 2, 500 3, 700; and 4, 1000 mV/s at 440°C in Ar atmosphere. [19]

4.5.4. Voltammetric measurements on a gold electrode in the molten $K_2S_2O_7$--V_2O_5 and $K_2S_2O_7$-$KHSO_4$ -V_2O_5 systems at 440°C in SO_2/air atmosphere.

The two-phase liquid $K_2S_2O_7/V_2O_5$ – gas $SO_2/O_2/N_2$ system is close simulation of the catalytic conditions of the industrial sulfuric acid production. Therefore the additional measurements were made in the molten $K_2S_2O_7$-V_2O_4, $K_2S_2O_7$--V_2O_5 and $K_2S_2O_7$-$KHSO_4$ -V_2O_5 systems at 440°C in SO_2/air atmosphere. The experimental results are given in Figs. 4.5.13, 4.5.14. It can be seen that V(IV) → V(V) oxidation in the SO_2/air atmosphere proceeds at lower polarization than in the Ar atmosphere (compare Figs. 4.4.12 and 4.4.14). Similarly to what was found in the Ar, the presence of water (or $KHSO_4$) has no significant effect on the V(V) reduction, but it visibly changes the polarization of the V(IV) oxidation, the effect being more pronounced in SO_2/air atmosphere than in Ar.

The V(IV) → V(V) oxidation kinetics in the "dry" $K_2S_2O_7$--V_2O_5 changes from slow charge transfer[18] in Ar to slow preceding chemical reaction in SO_2/O_2 (Fig.

4.5.14). Fig. 4.5.14A demonstrates the well-known criterion for the slow preceding chemical reaction mechanism[51]: oxidation peak potential moves in the negative direction with the growth of the potential scan rate. After the addition of water (or $KHSO_4$), the V(IV) → V(V) oxidation kinetics, like in the argon atmosphere, becomes a slow charge-transfer kinetics. (Fig. 4.5.14B). Therefore it is easier to detect the inhibiting water effect on the V(IV) → V(V) oxidation in the SO_2/air atmosphere than in Ar. Neither the SO_2/O_2 nor the water change the type of the kinetics of V(V) → V(IV) reduction (Figs. 4.5.12 and 4.5.14). However, there is a small positive change of V(V) → V(IV) peak potential after $KHSO_4$ addition in the SO_2/air atmosphere. The effect disappears at high potential scan rates.

Taking into account considerable changes in the mechanism of the V(IV) → V(V) oxidation and absence of the effect for the V(V) → V(IV) reduction at high potential scan rates, the described water effects are rather caused by change in the structure of the active vanadium complexes in the presence of water, than adsorbed water molecules at the surface of the gold electrode.

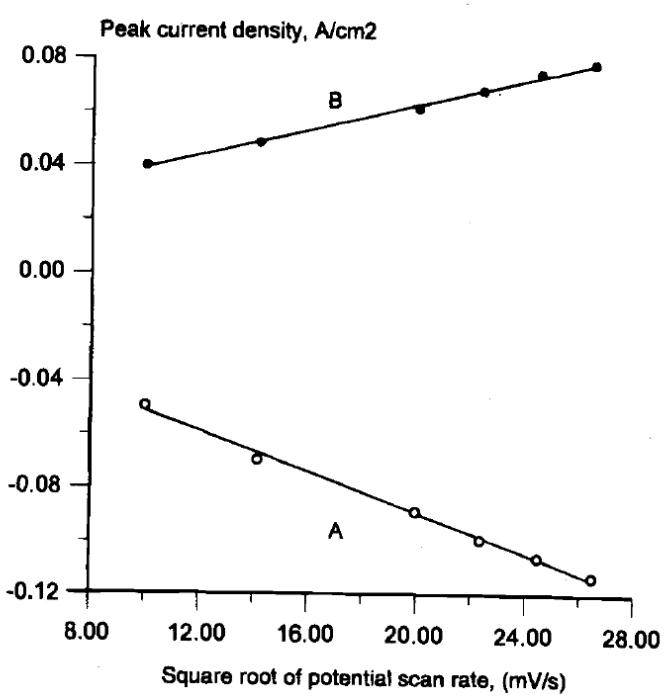

Fig. 4.5.11. Peak currents of R_{10} (A) and Ox_{10} waves (Fig. 4.5.10) vs. the square root of the potential scan rate.[19]

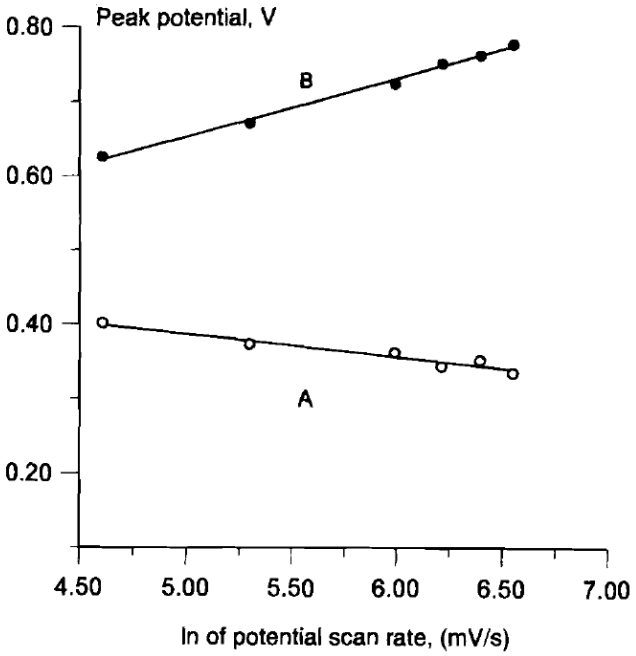

Fig. 4.5.12. Peak potentials of R_{10} (A) and Ox_{10} (B) waves (Fig. 4.5.10) vs. logarithm of the potential scan rate.[19]

Table 4.5.1. Potential difference between peak and "half-peak" potentials; $E_p - E_{p/2}$, and the number of participating electrons, n_α, for the V(V) → V(IV) and V(IV) → V(V), obtained in molten $K_2S_2O_7$ containing $KHSO_4$ (10 m/o) V_2O_5 (10 m/o) with Au electrode at 440°C.

Electrochemical wave designation	Potential scan rate (V/s)	$E_p - E_{p/2}$ (V)	n_α
Ox_{10}	0.7	0.23_1	0.99
R_{10}	0.7	0.23_0	1.14
Ox_{10}	0.5	0.19_2	1.19
Red_{10}	0.5	0.17_6	1.30
Ox_{10}	0.2	0.23_1	0.99
Red_{10}	0.2	0.16_9	1.28
Ox_{10}	0.1	0.22_4	1.02
Red_{10}	0.1	0.20_8	1.10

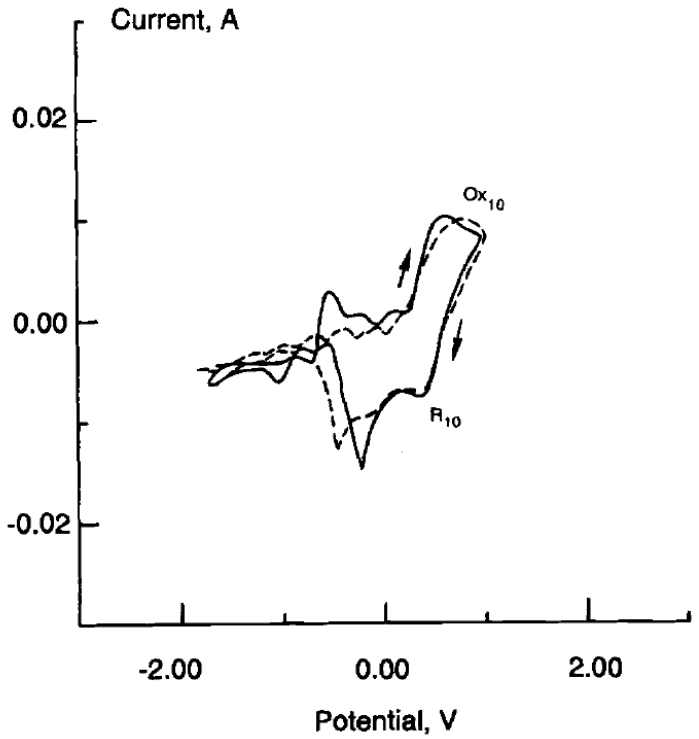

Fig. 4.5.13. Voltammetric curves obtained with a gold electrode in molten $K_2S_2O_7$ – 10 m/o V_2O_5 (solid line) and molten $K_2S_2O_7$ – 10 m/o V_2O_5 – 10 m/o $KHSO_4$ (dashed line) at 500 mV/s and 440°C in SO_2/air atmosphere.[19]

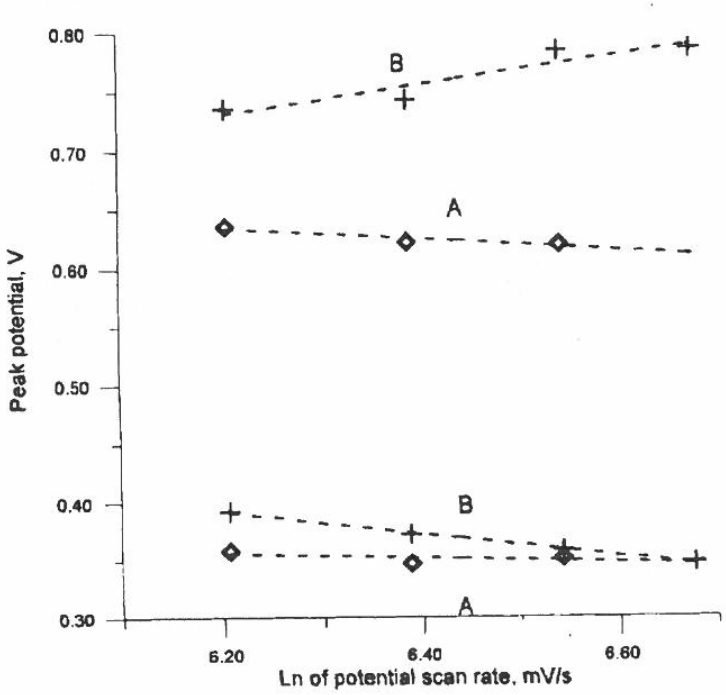

Dependence of peak potentials of the V(V)→V(IV) reduction and V(IV)→V(V) oxidation voltammetric waves on the logarithm of the potential scan rate obtained in molten $K_2S_2O_7$ -10 mol % V_20_5(A) and molten $K_2S_2O_7$ -10 mol % V_20_5-10mol % $KHSO_4$ (B) at 440°C $S0_2$/air atmosphere.[19]

4.6. Electrochemical promotion of sulfur dioxide catalytic oxidation

Possibility of an electrochemical promotion of the V_2O_5-$K_2S_2O_7$ catalyst for the SO_2 oxidation was studied in Ref.22 (A4).

It was shown with the industrial VK-58 catalyst (Haldor Topsoe A/S) with a molar ratio M/V = 4.25 (M = 70 mol % K + 25 mol % Cs + 5 mol % Na), using the cell demonstrated in Fig. 4.1.2. The cell was used in the vertical position. The catalyst was a powder mixed with $K_2S_2O_7$ and pressed between the upper gold working electrode and the porous quartz diaphragm. Molten potassium pyrosulfate which filled the catalyst and the diaphragm served as an electrolyte between the Au working and the Au counter electrode. The open-circuit potential of the SO_2, O_2/Au working electrode was -0.287 V against O_2/Au counter electrode.

It was shown that the catalyst activity can be increased up to four times by low (below -0.2 V) negative polarization (Fig. 4.6.1). The highest promotion effect took place at a potentials corresponding to the the V(V) $\rightarrow$ V(IV) reduction (Fig.4.6.2).[18(A1)]

It can be assumed that by electrochemical acceleration of the most important step of the catalytic reaction, i.e. V(V) $\leftrightarrow$ V(IV), the whole reaction can be promoted.

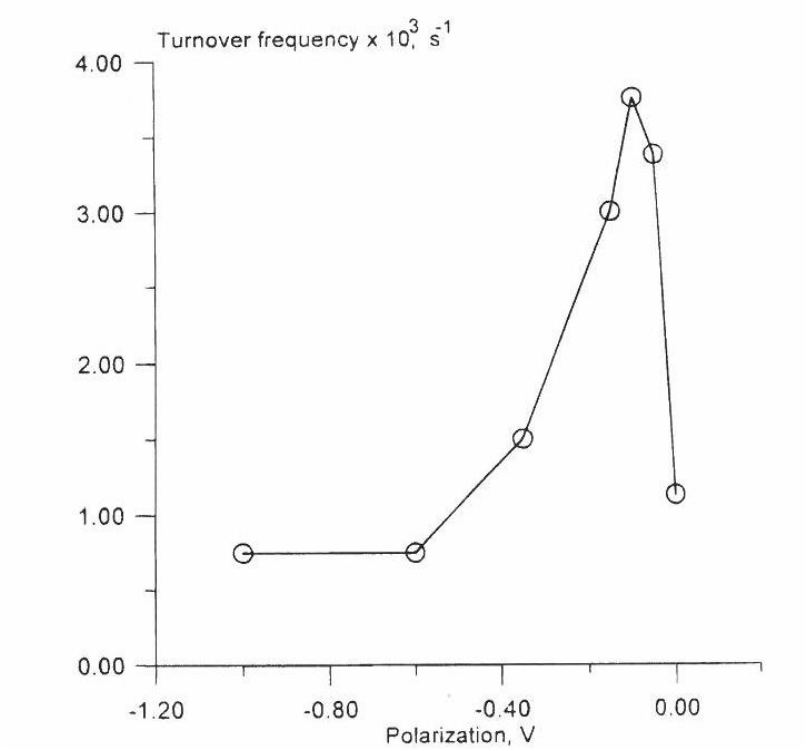

Fig. 4.6.1. Turnover frequency of the SO_2 catalytic oxidation for oxidation [mol SO_2 (conv.)/ mol V_2O_5/ s] vs. working electrode polarization for the VK-58 catalyst (Haldor Topsøe A/S) at 400°C[22].

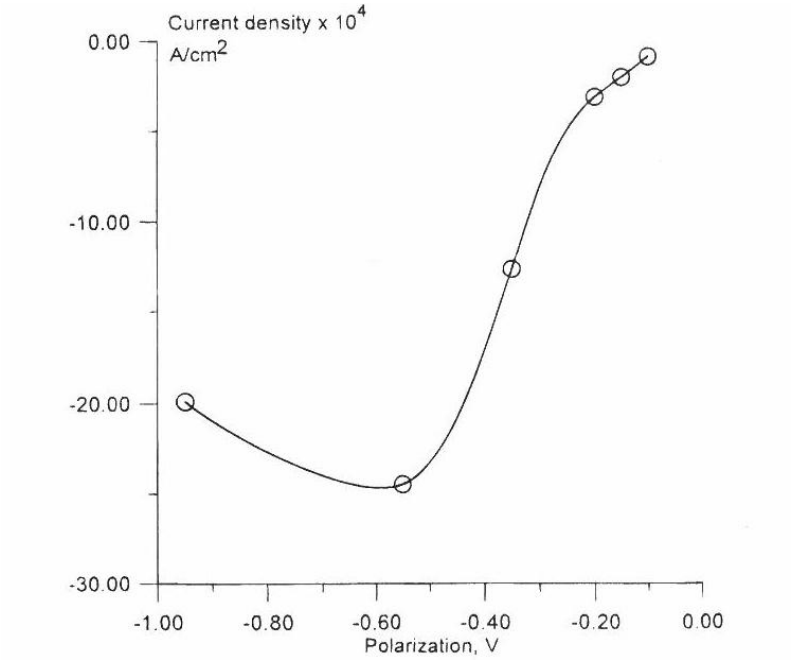

Fig. 4.6.2. A steady state voltammetric curve obtained during the electrochemical experiment with the VK-58 catalyst (Haldor Topsøe A/S) at 440°C[22].

5. ELECTROCHEMICAL PROMOTION OF HETEROGENEOUS CATALYTIC REACTIONS ON PT(RU)/C/POLYBENZIMIDAZOL-H_3PO_4 CATALYST AT 135-170°C

5.1. Electrochemical promotion of oxidative coupling of methane on Pt/PBI catalyst

Electrochemical promotion of catalytic methane oxidation was studied using a following electrochemical cell

(CH_4, O_2, Ar) /Polybenzimidazole (PBI)-H_3PO_4 /Pt, (H_2, Ar)

The PBI-H_3PO_4 electrolyte was chosen because it is stable at temperatures higher then 100°C, at which Pt catalyst has much higher tolerance to CO poisoning.[103]

Experimental

The setup for study of electrochemical promotion of the catalytic methane oxidation is given in Fig. 5.1.1. A carbon-supported Pt catalyst with Pt load around 0.5 mg/cm^2 was used in the investigation.[99] The morphology of the catalyst and the structure of the three-phase (Pt-electrolyte-gas) boundary are given in Fig. 5.1.2. The electrolyte was PBI doped with H_3PO_4. The techniques of preparing the PBI(H_3PO_4) membrane electrolyte and the Pt, C/PBI (H_3PO_4)/Pt,C assembly (the working electrode area is 5 cm^2) were developed in our group as well as by others.[103, 104] Graphite plates with gas channels were used as holders and current collectors. Two aluminum end plates with attached heaters were used to clamp the graphite plates. Temperature was controlled by a homemade controller. Mass flowmeters (5850 S Brookssmart) and 0154 Brooks Instrument controllers were used to control the inlet gas composition. The outlet gas composition was measured by an on-line quadrupole mass spectrometer (QMS 421, Pfeiffer) with a secondary electron multiplier detector and a cross-beam ion source with a rhenium filament. The ionization voltage was 70 V. The outlet gases were admitted to the mass spectrometer from the fuel cell through a 0.8 mm stainless steel capillary.

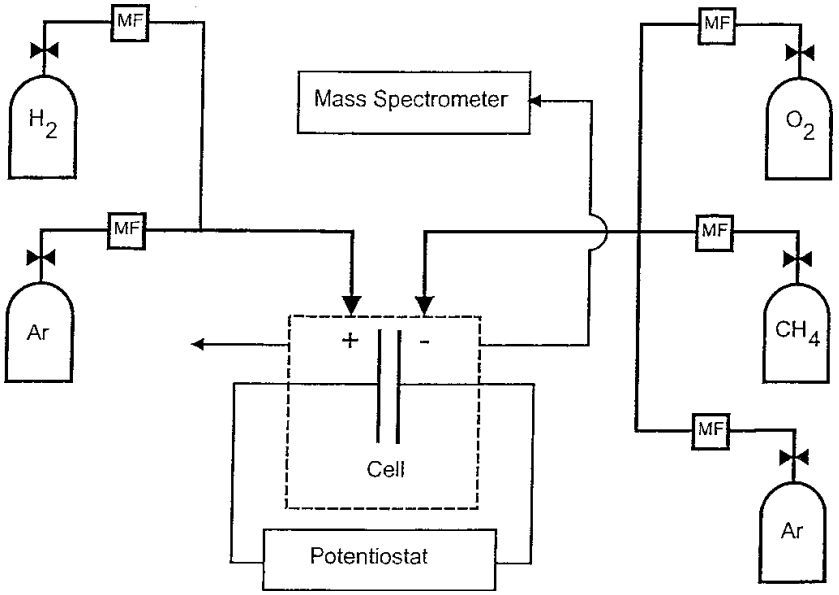

Fig. 5.1.1. Setup for study of electrochemical promotion of catalytic methane oxidation.[99]

The mixture of methane and oxygen, diluted by Ar (CH_4/O_2/Ar = 34/17/70 mL/min), was used as a working mixture at one electrode, and hydrogen or hydrogen/argon mixture (usually H_2/Ar was 50/50 vol %) was used as reference and counter gas at the other electrode. The gas flow rate at both electrodes was 120 mL/min. The temperature was 135-137°C.

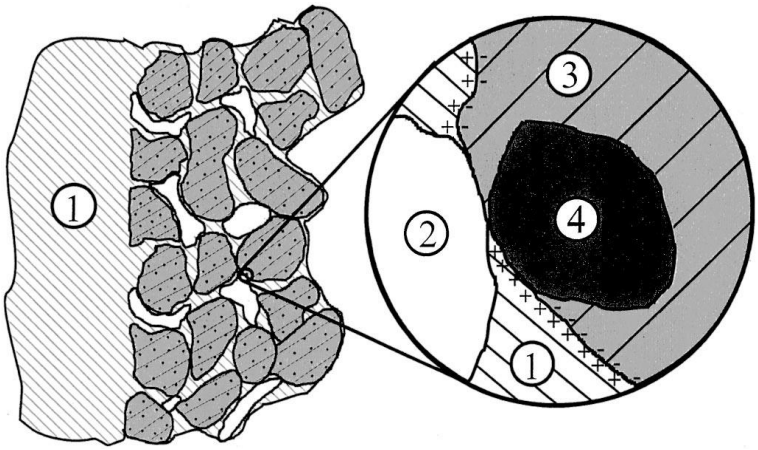

Fig. 5.1.2. Reactant-catalyst-electrolyte boundary: (1) PBI-H_3PO_4 electrolyte; (2) CH_4/O_2/Ar gas phase; (3) carbon support of the Pt catalyst; and (4) Pt catalyst.[99]

Commercial gases CH_4 (99.95%), H_2 (99.9%, ≤ 10 ppm O_2, ≤ 15 ppm H_2O), O_2 (99.8% O_2 + 0.2% N_2 and Ar), and N_2 (<40 ppm O_2 + H_2O) were used.

An EG&G Instruments (Princeton Applied Research) 283 potentiostat/galvanostat and homemade potentiostat controlled by 352 SoftCorr^{TM} III software and homemade software were used for electrode polarization and steady-state voltammetric measurements. The initial (at zero polarization) catalytic activity was measured after the yield of gas products had stabilized, *i.e.*, under steady-state conditions. For each value of polarization the measurements were performed after stabilization of the yield of gas products (1-1.5 h). Turnover frequency *vs.* polarization curves were reproduced for each studied product and temperature.

Results and Discussion

The results of the investigation of the electrochemical promotion of the catalytic methane oxidation are given in Fig.5.1.3-5.1.7.

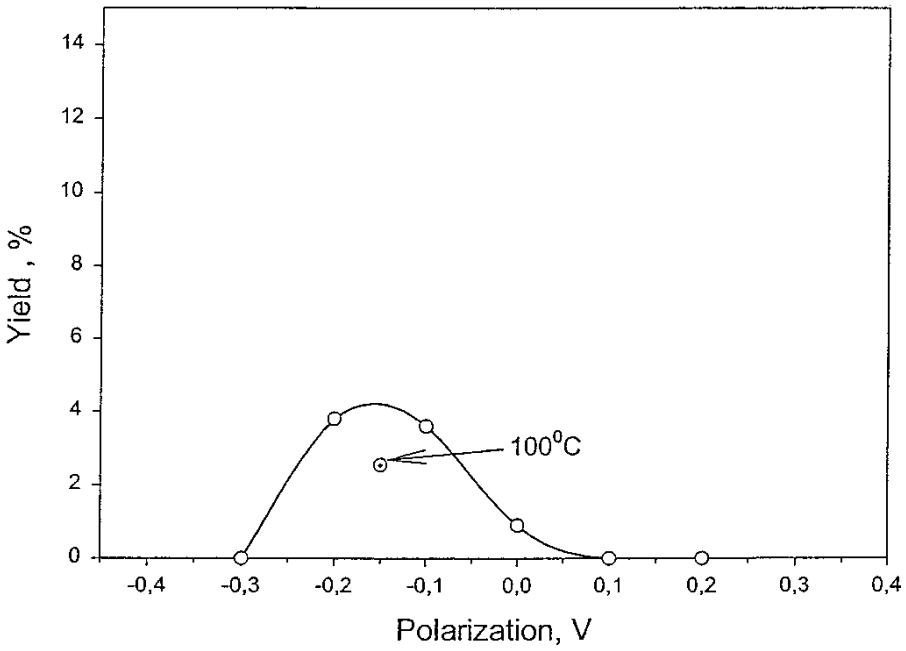

Fig. 5.1.3. Dependence of C_2H_2 yield on polarization obtained in (CH_4, O_2, Ar), Pt/PBI-H_3PO_4/Pt,(H_2, Ar) fuel cell at 135°C.[99]

It has been found that C_2H_2, CO_2, and water are the main oxidation products. Without polarization the yield of C_2H_2 was 0.9% (Fig.5.1.3) and the yield of CO_2 was 7.3% (Fig. 5.1.4). This means that C_2 open-circuit selectivity was approximately 11%. The open-circuit voltage (OCV) was around 0.6 V. The reactions are assumed to be

$$\boldsymbol{CH_4 + 2O_2 \rightarrow CO_2 + 2H_2O} \qquad (5.1.1)$$

$$\boldsymbol{2CH_4 + 3/2\ O_2 \rightarrow C_2H_2 + 3H_2O} \qquad (5.1.2)$$

The oxidative coupling of methane (OCM) is a relatively widely studied catalytic reaction.[105,106] However, in most OCM cases the major products are C_2H_6, C_2H_4, and CO_2. It is also known that direct pyrolysis of methane to acetylene takes place at temperatures close to 2000°C with 30% methane conversion.[107] An alternative route for direct conversion of methane into acetylene can be made through the activation in a two-stage burner by a hydrogen/oxygen flame.[108] Thus, in an alumina reactor, acetylene can be produced from the preheated (700°C) $CH_4/O_2/H_2$ gaseous mixture with a yield of ~17%. It was found in Liu et al. investigation[109] that the plasma catalytic conversion of methane produces acetylene with high selectivity and yield under atmospheric pressure in the temperature range 70-500°C. The highest yield of C_2 hydrocarbons (about 20% C_2 yield and more than 85% selectivity toward acetylene) was obtained in the hydrogen-containing plasma. Lower temperature favors the formation of acetylene, while no acetylene is formed at higher temperatures (more than 300°C).

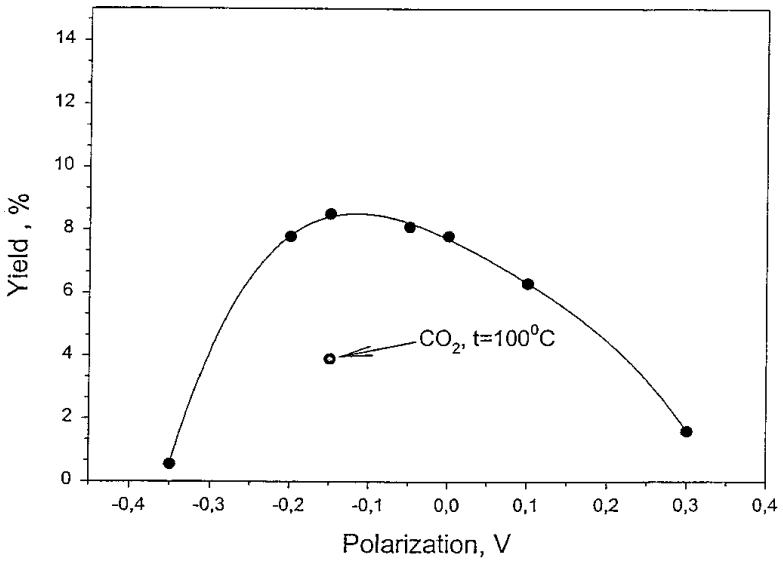

Fig. 5.1.4. Dependence of CO_2 yield on polarization obtained in (CH_4, O_2, Ar), Pt/PBI-H_3PO_4/Pt,(H_2, Ar) fuel cell at 135°C.[99]

It can be concluded that presence of hydrogen in the reactant mixture at low temperature increases the C_2H_2 yield of OCM. Therefore, the most probable explanation of the unusual $CH_4 \rightarrow C_2H_2$ conversion in the present study is based on proton conductivity of the Pt catalyst support. It can be assumed that there is an $H^+ \rightleftharpoons H_{ads}$ equilibrium at the three-phase boundary of the catalyst, and this equilibrium is a source of the H_{ads} active centers for the $CH_4 \rightarrow C_2H_2$ conversion.

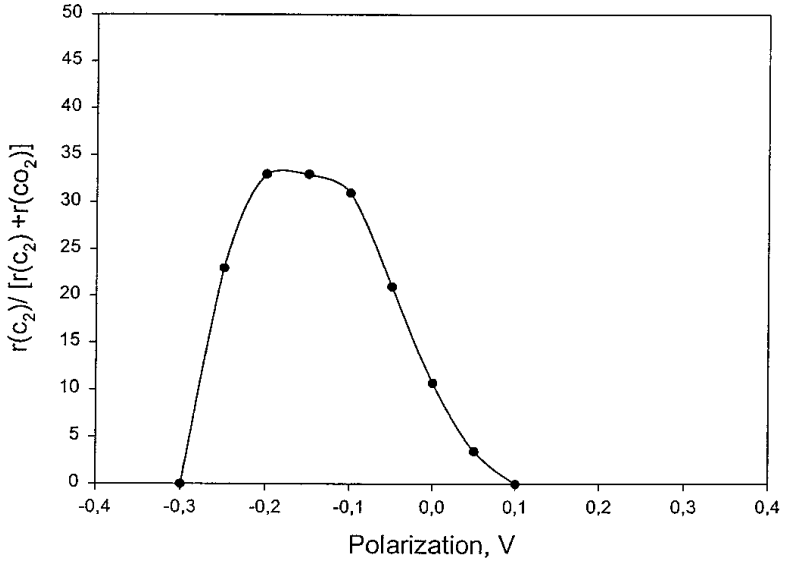

Fig. 5.1.5. Dependence of $r(C_2)/[r(C_2) + r(CO_2)]$ ratio on polarization obtained in (CH_4, O_2, Ar), Pt/PBI-H_3PO_4/Pt,(H_2, Ar) fuel cell at 135°C.[99]

Dependence of the C_2H_2 yield on polarization is given in Fig.5.1.3. It can be seen that the $CH_4 \rightarrow C_2H_2$ catalytic reaction can be electrochemically promoted at negative polarization and exhibits a clear "volcano-type" promotion behaviour.[7] It means that there is a maximum promotion effect at a polarization of –0.15 V, or 0.45 V catalyst potential *vs.* the hydrogen electrode (3.8% C_2H_2 yield). The catalytic rate enhancement ratio, $r(C_2)/r_o(C_2)$ (Ref.10), at this maximum is 4.2. It can also be seen from Fig. 5.1.3, that there is no C_2H_2 production at polarizations more positive than 0.1 V and more negative than –0.3 V. The yield of C_2H_2 decreases with decreasing of the temperature (Fig. 5.1.3). The value of Λ calculated for the case of maximum promotion effect was 7.9×10^3, *i.e.*, $\Lambda >> 1$. This means that the electrochemical promotion for the CH_4-C_2H_2 route has an electrochemical nature.

Dependence of CO_2 yield on polarization is given in Fig.5.1.4. This dependence also shows a volcano-type behavior with maximum yield of 8.3% at –0.15 V, *i.e.*, at the same potential as for C_2H_2 production. The catalytic rate enhancement ratio for CO_2 production, $r(CO_2)/r_o(CO_2)$, at this maximum is 1.1, which means that this catalytic reaction is only slightly affected by the electrochemical polarization. This also means

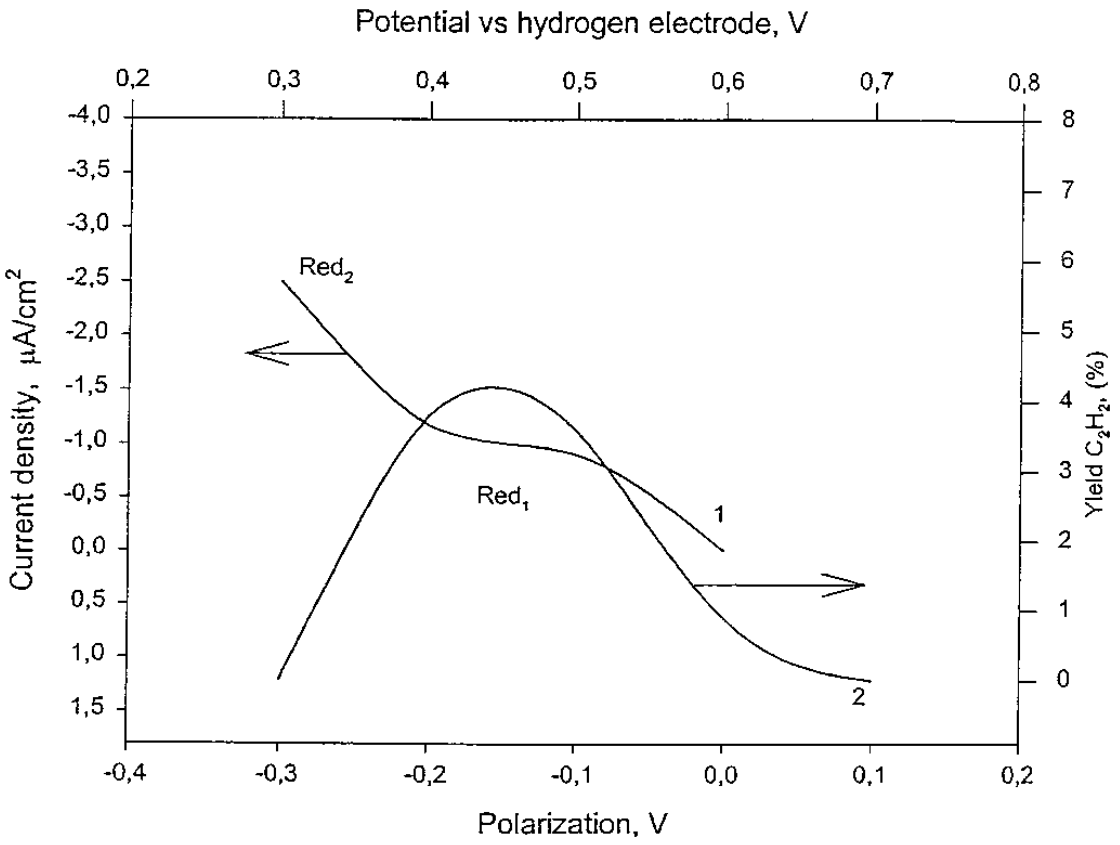

Fig. 5.1.6. Steady-state voltammetric curve (1) obtained at Pt catalyst and dependence of C_2H_2 yield on polarization (2) obtained in (CH_4, O_2, Ar), Pt/PBI-H_3PO_4/Pt,(H_2, Ar) fuel cell at 135°C.[99]

that the polarization affects the C_2 selectivity more than the CO_2 selectivity. Figure 5.1.5 shows the "volcanic" nature of the dependence of the ratio between $r(C_2)$ and $r(C_2) + r(CO_2)$ with a maximum at –0.2 V. Similar to the C_2H_2 path, CO_2 production is inhibited at very positive and very negative polarizations and decreases with a temperature decrease from 135 to 100°C (Fig.5.1.4). The value of Λ calculated for the case of maximum promotion effect was 2.7×10^3, *i.e.*, $\Lambda >> 1$, meaning that it is the electrochemical promotion for the CH_4-CO_2 route (as in the case of the CH_4-C_2H_2 route) and not an electrocatalytic reaction.

The same potential of maximum promotion for both C_2H_2 and CO_2 paths shows that polarization probably has the same effect on the rate-determining steps of these paths. It would therefore be useful to review the published data on electrochemical conversion of methane. Since the 1960s there have been many publications on the electrocatalytic oxidation of methane in connection with the development of phosphoric acid fuel cells.[105] This reaction was mainly studied on platinum and platinum group metal catalysts. In most of the studied cases there was a complete

electrocatalytic oxidation of methane to CO_2.[105] It has been shown that the rate-determining step of this reaction is dissociative chemisorption of methane at the catalyst-electrolyte interface. Moreover, it has been found that on a Pt-black catalyst in 4.3 M $HClO_3$ at 65°C the maximum amount of methane is adsorbed at 0.3 V *vs.* the standard hydrogen electrode (SHE).[110]

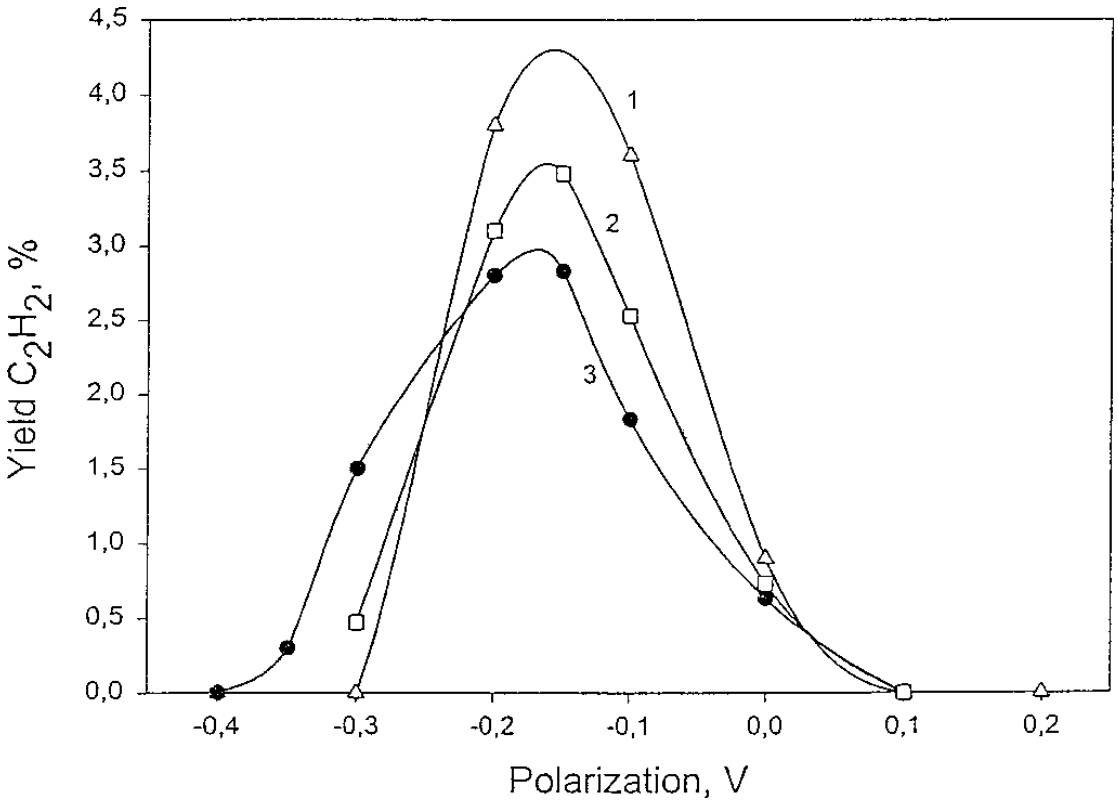

Fig. 5.1.7. Dependence of electrochemical promotion on the partial pressure of hydrogen at the counter electrode obtained in (CH_4, O_2, Ar), Pt/PBI-H_3PO_4/Pt,(H_2, Ar) fuel cell at 135°C (1) 100 vol %; (2) 50 vol %; (3) 0 vol % H_2).[99]

The only studied electrochemical system that provided the oxidative coupling of methane was a high-temperature fuel cell with zirconia-based solid electrolytes.[105] The effect of polarization on the oxidative methane coupling in the CH_4,O_2/Ag/YSZ/Pt/O_2 fuel cell at 800°C was studied by Seimanides and Stoukides.[111] They have shown that "oxygen pumping" at positive polarization promotes methane conversion to CO_2 and that negative polarization slightly promotes the OCM to C_2H_4 and C_2H_6, therefore promoting C_2 selectivity.

In order to explain similarities and differences in the electrochemical promotion of methane conversion in CH_4, O_2/Pt/PBI-H_3PO_4/Pt, H_2, and CH_4,O_2/Ag/YSZ/Pt/O_2 fuel cell systems we should compare the open-circuit potentials of the Pt and Ag catalysts in these systems. In our study for the Pt catalyst it was 0.6 V *vs.* the hydrogen

electrode and in Ref. 113 it was –0.45 V *vs.* the oxygen electrode, *i.e.*, approximately 0.6-0.8 V against the hydrogen electrode. Considering the value of the potential of the maximum CH_4 adsorption, *i.e.*, 0.3 V *vs.* SHE,[110] the catalyst potentials in both electrochemical cells should be moved in the negative direction in order to achieve this maximum. The data obtained in Ref.99 on OCM and C_2 selectivity is in agreement with this assumption. Moreover, the much stronger promotion effect in the CH_4, O_2/Pt/PBI-H_3PO_4/Pt,H_2 system can be explained on the basis of the difference in the current carriers in this system and the CH_4, O_2/Ag/YSZ/Pt/O_2 fuel cell, protons and oxide ions, respectively.

A steady-state voltammetric curve obtained at the Pt catalyst (curve 1) and C_2H_2 yield *vs.* polarization dependence (curve 2) are given in Fig.5.1.6. It can be seen that the polarization range of the C_2H_2 production (0.3-0.6 V *vs.* the hydrogen electrode) is the potential range of the reduction wave Red_1. This wave has a limiting current plateau at around 1 $\mu A/cm^2$ at the potentials of the maximum promotion effect. It has been found[112] that during the electrochemical reduction of H^+ in 0.1 M H_3PO_4 at 25°C at a Pt rotating disk electrode, covered by PBI thin film, so-called strongly adsorbed hydrogen is produced in the region of 0.2-0.4 V *vs.* the reversible hydrogen electrode. It is natural to assume that wave Red_1 is caused by the electrochemical production of strongly adsorbed hydrogen. The combination of the maximum CH_4 adsorption and electrochemical production of the Pt-H active sites (in the same potential region), which stabilize C_2 products, can provide a strong promotion effect at the CH_4, O_2/Pt/PBI/H_3PO_4 boundary. In the case of the CH_4, O_2/Ag/YSZ/Pt/O_2 electrochemical cell, this effect is much weaker because of the absence of the proton current carriers in the solid electrolyte. Taking into account faradays current, reduction of the current carriers at the potential of maximum promotion effect we can conclude that it is an obvious EEPP type of promotion effect.

It was found that electrochemical conversion of CH_4 into CO_2 proceeds through the formation of the so-called O-type products of the dissociative adsorption of methane, *i.e.*, $\equiv$COH, $-$CHO.[105] This means that in this case parameters of the oxygen adsorption should play an important role in the kinetics of the methane conversion. Positive polarization of the Ag catalyst probably provides the optimum potential for the oxygen adsorption at the catalyst-gas interface[111].

We can also assume that through the reversible[112] electrochemical production of Pt-H sites we can create a new OCM route for catalytic CH_4 oxidation.

The experimental data given in Fig. 5.1.7 are also in agreement with the assumption about the EEPP nature of the promotion of C_2H_2 production. Reversibility of the $H^+ \leftrightarrow H_{ads}$ electrochemical reaction means that this reaction proceeds under diffusion control. Therefore, by changing the H^+ concentration gradient across the PBI electrolyte we should affect the H^+ diffusion rate and in this way the electrochemical H^+ reduction rate and the rate of OCM. It can be seen from Fig.5.1.7, that the zero hydrogen pressure at the counter electrode, which should provide a lower H^+ concentration gradient across the electrolyte, also provides a weaker promotion effect on the methane conversion into C_2H_2.

5.2. Electrochemical promotion of the catalytic NO reduction with hydrogen.

The electrochemical promotion of catalytic NO reduction by hydrogen was studied using a ***(NO, H_2, Ar), Pt polybenzimidazole (PBI)-H_3PO_4\|Pt, (H_2, Ar)*** electrochemical cell at 135°C.[100] A mixture of $NO/H_2/Ar$ was used as the working mixture at one electrode and a mixture of H_2/Ar was used as reference and counter gas at the other electrode.

In other studies of electrochemical promotion of the catalytic NO reduction, Na was pumped to the surface of the catalyst using electrochemical reduction of Na^+ ions from Na β''-alumina support.[92-95] This supply of Na greatly enhanced the reduction of NO on Pt, Pd, Rh, and several other catalytic materials with a reaction rate enhancement as high as two orders of magnitude. Simultaneously the selectivity of production of N_2 against N_2O increased. Lambert *et al.*[92-95] showed that the effect of electrochemical promotion is equivalent to the effect seen from depositing Na chemically on the catalyst surface. It means that the effect had a pure EEPP nature.

The reason for NO reduction being promoted so remarkably is that the supply of Na to the catalytic surface changes the electronic properties of the surface. This happens in a way that strengthens the N-catalyst bond at the expense of the N-O bond, thereby

facilitating the dissociation of NO, which is the limiting step of the whole reaction.[113] As N_2O is produced by NO + N(ads) $\rightarrow$ N_2O, the fast dissociation of NO diminishes the production of N_2O.[113]

The electrochemical promotion of NO reduction is increased with the loading of Na until a certain point, where the supply of any more Na leads to a poisoning of the system.[93] This poisoning happens because when too much Na is present, it and O_{ads} from the NO dissociation begin to cover most of the active centers blocking out new NO molecules.

Electrochemical promotion of NO reduction also took place when the catalyst support was an O^{2-} conducter. For this kind of system, an increase in NO reduction rate (up to $\lambda = 700$) was obtained when O^{2-} was removed from (or in some cases added to) the catalytic surface.[90,91,96,97]

Our purpose was to study the possibility of promoting NO reduction with the adsorbed hydrogen atoms produced electrochemically.

Experimental

The setup for study of electrochemical promotion of the catalytic NO reduction is given in Fig.5.2.1. The carbon-supported Pt catalyst with Pt load around 0.5 mg/cm^2 was used in this investigation. The electrolyte was PBI doped with H_3PO_4. The techniques of preparing the PBI(H_3PO_4) membrane electrolyte and the Pt, C/PBI (H_3PO_4)/Pt, C assembly (the working electrode area is 5 cm^2) and the setup were described ealier.[99(A5)]

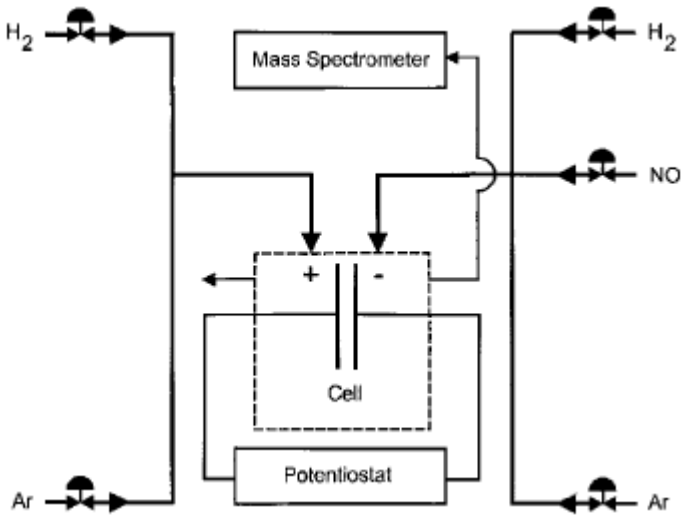

Fig. 5.2.1. Setup for study of electrochemical promotion of catalytic reduction.[100]

The mixture of NO and hydrogen, diluted by Ar ($NO/H_2/Ar$ = 17 mL/min; 17 and 354 mL/min; or 17 mL/min; 17 and 140 mL/min, respectively, at atmospheric pressure) was used as a working mixture at one electrode and hydrogen/argon mixture (H_2/Ar was 17 and 371 mL/min or 17 and 140 mL/min, respectively) was used as a reference and a counter gas at the other electrode. The temperature was 135-137°C.

Commercial gases NO (99.9%), H_2 (99.9%, ≤ 10 ppm of O_2, ≤ 15 ppm of H_2O), and Ar (<40 ppm O_2 + H_2O) were used.

An EG&G Instrument (Princeton Applied Research) 283 potentiostat/galvanostat controlled by 352 SoftCorr™ III Software was used for electrode polarization and steady-state voltammetric measurements. The initial (at zero polarization) catalytic activity was measured after the yield of gas products had stabilized, *i.e.*, under steady-state conditions. For each value of polarization the measurements were performed after stabilization of the yield of gas products (1-1.5 h). NO conversion *vs.* polarization curves were reproduced for each studied product and temperature. The open-circuit potential of the working electrode was approximately 0.14 V.

Results and Discussion

The results of the investigation of the electrochemical promotion of the catalytic NO reduction are given in Fig.5.2.2-5.2.5 . The presented data has been obtained at high and low gas flow rates to create the conditions where there are, respectively, an

underproduction and an overproduction of the Pt-H_{ads} and Pt-H^{+}_{ads} sites at the catalyst-gas interface through the chemical reaction.

Data in Fig.5.2.3 and 5.2.3 were obtained at high gas flow rate after the catalyst was first polarized 0.1 V positively and then negatively to –0.3 V. Nitrogen and water are the NO reduction products. Without polarization the NO conversion was 2% (Fig.5.2.2). The reaction is assumed to be

$$2NO + 2H_2 \rightarrow N_2 + 2H_2O \qquad (5.2.1)$$

Dependence of the NO conversion on polarization is given in Fig.5.2.2. It can be seen that Reaction 5.2.1 can be electrochemically promoted at negative polarization and exhibits a clear "volcano"-type promotion behavior.[10] This means that there is a maximum promotion effect (9.3% NO conversion) at a polarization of approximately –0.15 V, or –0.01 V catalyst potential *vs.* the reversible hydrogen electrode, RHE. The catalytic rate enhancement ratio at this maximum is 4.65. Figure 5.2.2 shows no NO conversion at a polarization more positive than 0.1 and more negative –0.3 V.

There are obvious anodic and cathodic faradaic reactions inside this potential region (presence of the voltammetric waves, Fig.5.2.3). The anodic current at the potential of maximum effect was 0.2 mA/cm^2. The value of Λ calculated for the maximum promotion effect was 1.26×10^3, *i.e.*, $\Lambda >> 1$. This means that this effect has an electrochemical promotion nature. The type of this promotion is obviously an EEPP type.

The closest published example of an electrochemically promoted catalytic reaction is the catalytic oxidation of CO by O_2 at the Pt catalyst on YSZ support.[12] According to Belyaev *et al.*, this catalytic reaction is promoted by ZO_2^- oxygen species which are the products of the interaction between electrochemically produced ZO^- species and chemically adsorbed oxygen species Z_oO (where Z are the catalyst active sites at the catalyst-support-gas interface and Z_o are the catalyst active sites at the catalyst-gas interface). We can assume here that both electrochemically produced ZH and

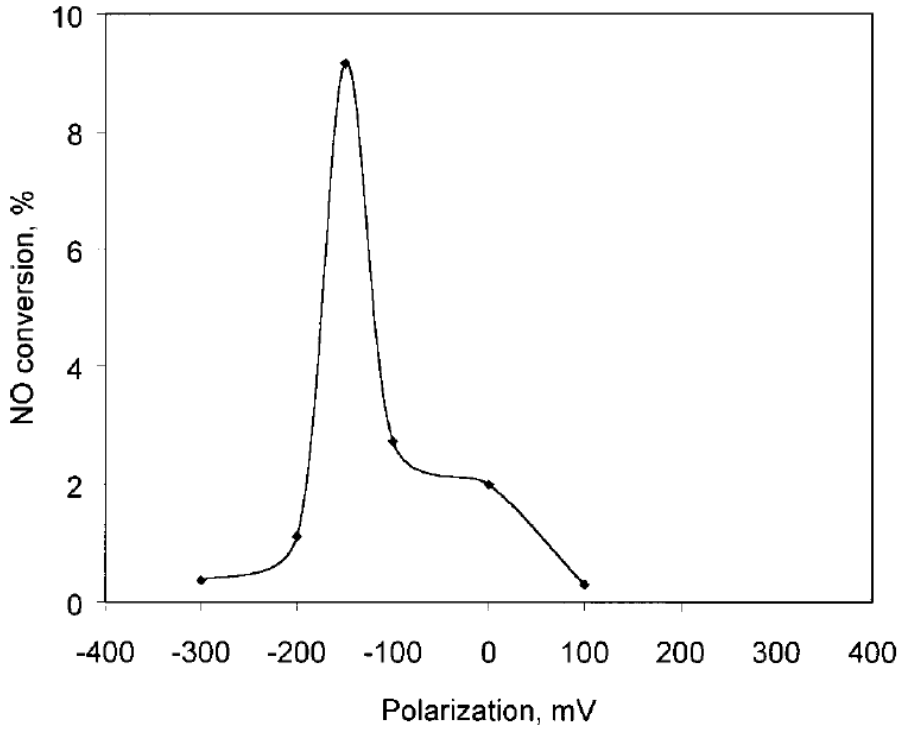

Fig. 5.2.2. Dependence of NO conversion on polarization obtained in (NO, H_2, Ar), Pt/polybenzimidazole (PBI)-H_3PO_4/Pt, (H_2, Ar) fuel cell at high NO + H_2 + Ar flow rate (17 mL/min; 17 and 354 mL/min, respectively, at atmospheric pressure) and at 135°C.[100]

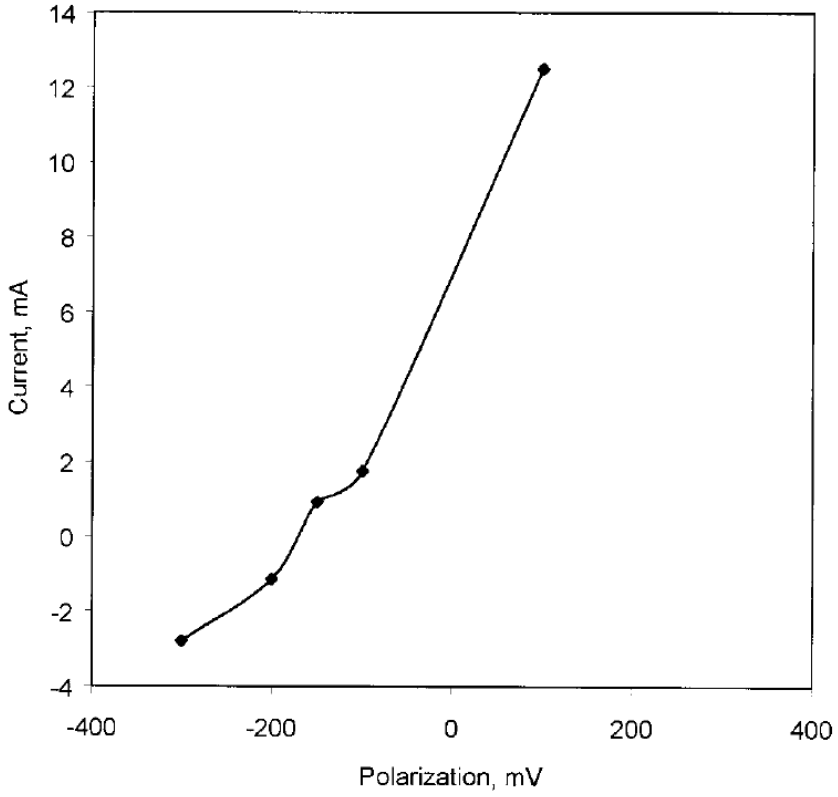

Fig. 5.2.3. Steady-state voltammetric curve obtained at Pt catalyst at high NO + H_2 + Ar flow rate (17 mL/min; 17 and 354 mL/min, respectively, at atmospheric pressure) and at 135°C.[100]

chemically produced Z_oH species, and also the possible product of their interaction with H^+, ZH_2^+, can promote the NO catalytic reduction. The reaction

$$ZH \leftrightarrow Z + H^+ + e \qquad (5.2.2)$$

takes place in the potential range between 0 and 0.4 V *vs.* RHE,[112] *i.e.*, at the potentials of the electrochemical promotion of NO reduction (Fig.5.2.2). The nature of promotion of NO reduction by the adsorbed hydrogen species is probably the same as the nature of the promotion of the same reaction by the adsorbed Na atoms.[92-95] It has been shown that the rate-determining step of the catalytic NO reduction at a Pt catalyst is dissociative chemisorption of NO because Pt is relatively ineffective at this step.[113] Adsorbed hydrogen species can act to increase the adsorption strength of electronegative adsorbates (NO) and weaken the N-O bond in the adsorbed molecule and therefore promote NO dissociation.[94]

Data in Fig. 5.2.4 and 5.2.5 were obtained at low gas flow rate after the catalyst was first polarized –0.3 V negatively and then positively to 0.2 V. It can be seen from comparison of Fig. 5.2.2 and 5.2.4 that NO reduction is increased 20 times even without polarization. Moreover, under these conditions negative polarization decreased the rate of NO reduction (*i.e.*, an opposite effect to what was found at high gas flow rates). It can also be seen that the electrochemical promotion effect did occur at a positive polarization with maximum increase at approximately 0.08 V polarization and with 1.5 times the zero polarization value.

The steady-state voltammetric behavior of the catalyst at a low gas flow rate is shown in Fig.5.2.5. It is obvious from Fig. 5.2.5 that in the potential range of the promotion effect faradaic current is absent. This means that the promotion effect has an EDLE nature. Increase of the NO conversion under open-circuit conditions and changes in the nature of the promotion effect can be explained by a high concentration of Pt-H sites at the low gas flow rates. The increased number of the adsorbed hydrogen species (as in the NO promotion with Na[93, 112]) can complicate the NO (electronegative adsorbate) chemisorption, especially at negative polarization. At positive polarization, however, the charge-induced change of the strength of chemisorptive bonds can take place (EDLE effect).

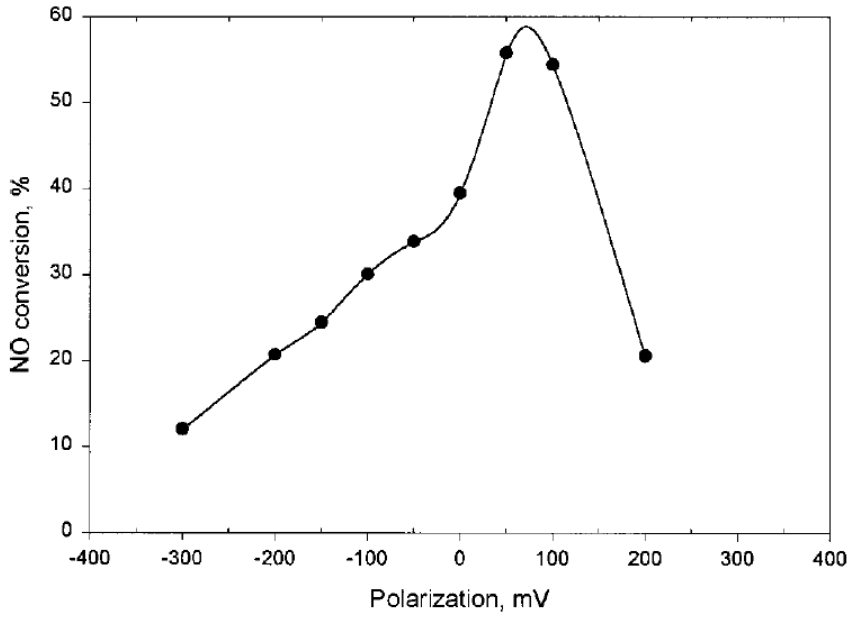

Fig. 5.2.4. Dependence of NO conversion on polarization obtained in (NO, H_2, Ar), Pt/polybenzimidazole (PBI)-H_3PO_4/Pt, (H_2, Ar) fuel cell at low NO + H_2 + Ar flow rate (17 mL/min; 17 and 140 mL/min, respectively, at atmospheric pressure) and at 135°C.[100]

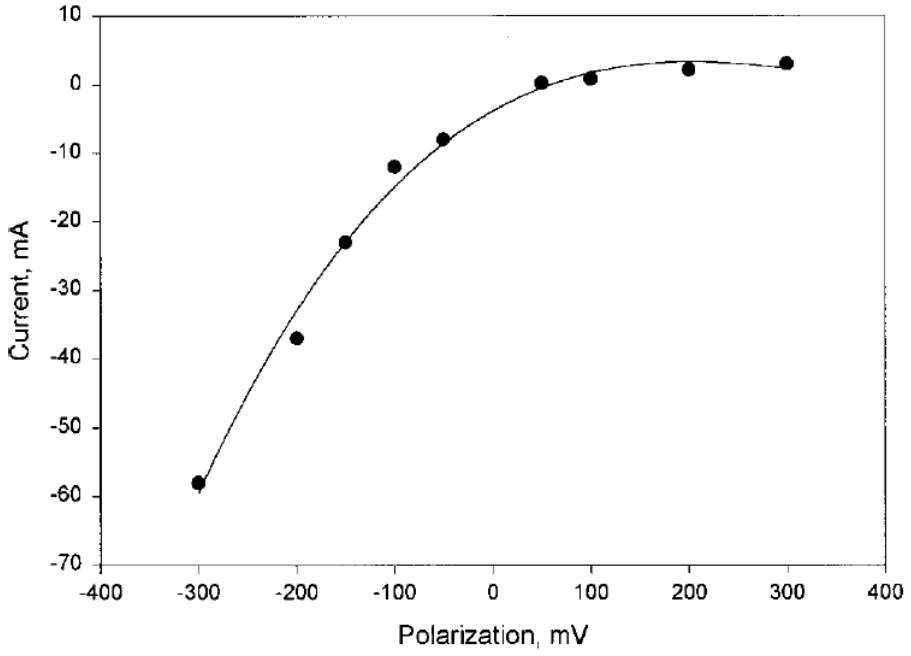

Fig. 5.2.5. Steady-state voltammetric curve obtained at Pt catalyst at low NO + H_2 + Ar flow rate (17 mL/min; 17 and 140 mL/min, respectively, at atmospheric pressure) and at 135°C.[100]

5.3. Catalytic NO reduction with methane

The catalytic reduction of N_xO_y plays a very important role in pollution control. Although there is already a developed industrial process for selective catalytic

reduction of N_xO_y with NH_3, the use of hydrocarbons has attracted much attention, because their cost is much lower than that of NH_3. Particular methane would be convenient because the development of natural gas-powered vehicles will require the development of more active catalysts to remove N_xO_y from the exhaust.[114-116]

In the studies of an electrochemical promotion of the catalytic NO reduction by propene at 375°C, Na was pumped to the surface of the catalyst using electrochemical reduction of Na^+ ions from Na β''-alumina support.[92,93,95] This supply of Na was seen to greatly enhance (2–3 times for N_2 production) the reduction of NO on the Pt (or Rh) catalyst. Simultaneously, the selectivity of production of N_2 against N_2O was seen to increase. It has been shown by Lambert *et al.*[92,93,95] that the effect of electrochemical promotion is equivalent to the effect seen from depositing Na chemically on the catalyst surface. It means that the effect had an EEPP nature.

Yentekakis *et al.* also studied an effect of sodium (chemical promotion) on the Pd/yttria-stabilized zirconia (YSZ)-catalyzed reduction of NO by methane at 347–497°C. It has been found that unlike the reduction of NO by propene,[92,93,95] the reduction of NO by methane is strongly poisoned by sodium.[117]

Electrochemical promotion of NO reduction by C_3H_6 (or CO) was also found to take place when the catalyst support was an O^{2-} conductor, i.e., Rh (or Pd)/YSZ catalyst. For this kind of system, an increase in the NO reduction rate was obtained when O^{2-} was removed from (or in some cases added to) the catalytic surface.[90,91,96,98]

Later the electrochemical NO reduction was studied on the Pt electrode of the (NO, O_2), Pt | Nafion | Pt, (H_2O)[118] (70°C) and (NO, O_2, Ar), Pt/C|In^{3+}-doped SnP_2O_7|Pt/C (Air, H_2O)[119] (150–300°C) electrochemical cells. In these papers the electrochemical cell with proton-conducting electrolytes were shown as effective "electrochemical NO filters" even in the presence of oxygen. In both cases the reaction had an electrocatalytic nature with participation of H^+ from the electrolytes or electrochemically produced H atoms.

In our work we made an attempt to study the catalytic reduction of NO by methane on a Pt/PBI(H_3PO_4) catalyst at 135 and 165°C during the catalyst polarization. Taking into account the diversity of the mechanisms described above, one of our main aims was an investigation of the mechanism of the NO reduction by methane.

Experimental

The usual[99,100 (A5,A6)] experimental setup is shown in Fig.5.3.1. A transmission electron microscopy (TEM) image of the Pt/C catalyst is given in Fig.5.3.2. The TEM images were obtained using a Philips 430 TEM microscope.

The PBI used was poly 2,2′-*m*-(phenylene)-5,5′-bibenzimidazole, synthesized from 3, 3′-diaminobenzidine tetrahydrochloride (Aldrich) and isophthalic acid (Aldrich) by polymerization in polyphosphoric acid (PPA) at 170–200°C, as described in Ref.120. The membranes were doped by immersing them in 75% phosphoric acid solutions for at least a week at room temperature. This doping procedure gives an acid-doping level of about 5.6 mol H_3PO_4 per repeating unit of the polymer and a doped thickness of 80 μm. The conductivity of the membranes at 135°C was measured at 0.03 S cm^{-1}.

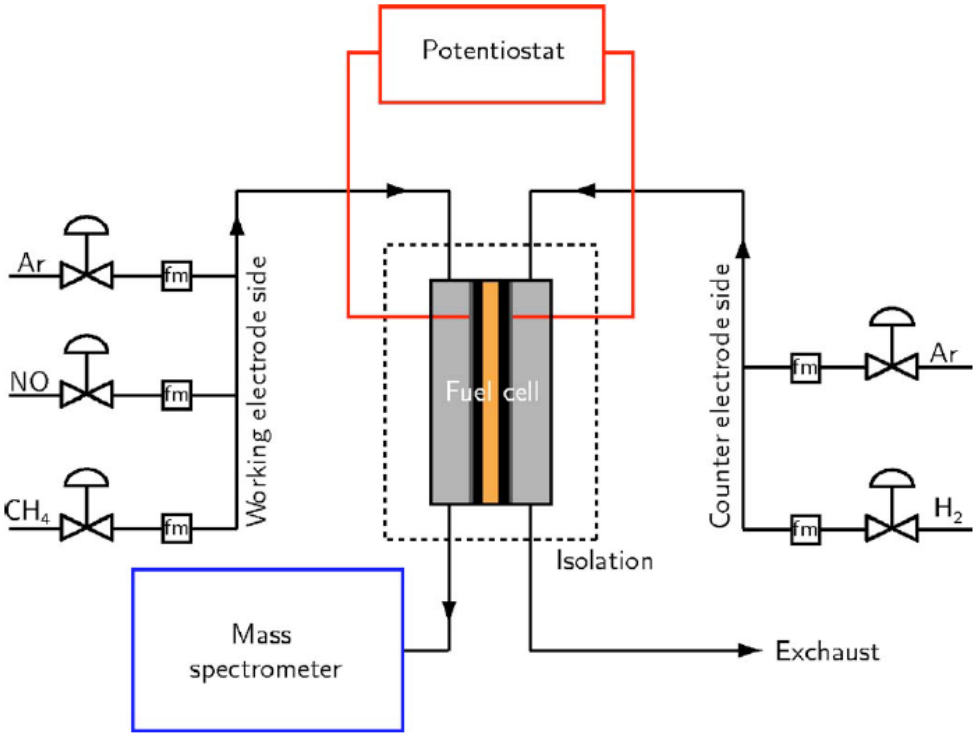

Fig.5.3.1. Experimental setup.[101]

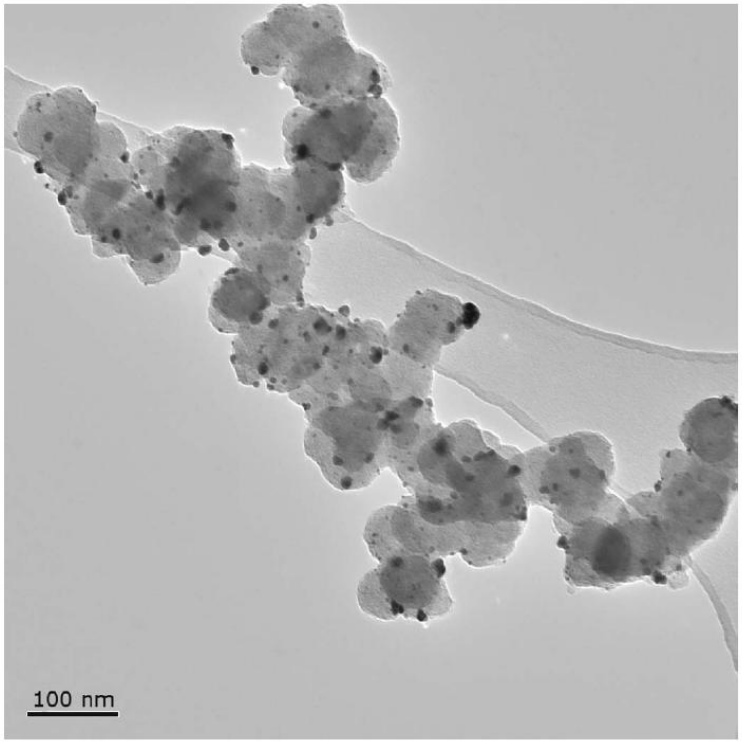

Fig 5.3.2. TEM image of the Pt/C catalyst; black spots are the Pt particles.[101]

Electrodes were prepared using a tape casting method and subsequently hot pressed to the PBI membrane to form a membrane electrode assembly (MEA). The complete procedure for electrode preparation is described in detail in Ref.121.

Mass-flow meters (5850 S Brookssmart) and 0154 Brooks Instrument controllers were used to control the inlet gas composition. The outlet gas composition was measured by an online quadrupole mass spectrometer (QMS 421, Pfeiffer) with a secondary electron multiplier detector and a cross-beam ion source with a rhenium filament. The ionization voltage was 70 V. The catalytic reaction products were also identified with a gas chromatograph HP 6890 with the HP-MOLESIEVE column (30 m×0.32 mm×250 μm).

The mixture of NO and methane diluted by Ar (CH_4, NO, and Ar=17, 17, and 354 mL/min, respectively) was used as a working mixture at one electrode and hydrogen/argon mixture (H_2 and Ar were 17 and 371 mL/min, respectively) was used as a reference and a counter gas at the other electrode; the counter gas was humidified by bubbling it through ionized water. The temperature was 135 and 165°C and all experiments were done at atmospheric pressure.

Commercial gases H_2 (>99.9%, ≤ 10 ppm of O_2, ≤ 15 ppm of H_2O) (from Strandmøllen A/S), Ar (<40 ppm O_2+H_2O), CH_4 (≥ 99.5%), and NO (>99.9%) from AirLiquid-Alphagas were used.

An EG&G Instrument (Princeton Applied Research) 283 potentiostat/galvanostat controlled by 352 SoftCorr III software and homemade cyclic voltammetry software was used in the electrochemical measurements. The measurements of the catalytic activity were performed at potentiostatic conditions. The catalytic activity at open-circuit voltage (OCV) was measured after the yield of gas products had stabilized, i.e., under steady-state conditions. For each value of voltage the measurements were performed after stabilization of the yield of gas products and current (0.5–1.0 h), i.e., at steady-state conditions. Because of the relatively high conductivity of the membrane and the low currents observed, the maximum internal resistance (iR) drop is calculated to be 0.2 mV (at 4 mA). Therefore, no correction for iR losses was performed.

Results and Discussion

According to the gas chromatography analysis, the products of catalytic reduction of NO with methane were nitrogen, ethylene, and water. It therefore can be assumed that the following catalytic reaction takes place

$$2CH_4 + 2NO \rightarrow C_2H_4 + 2H_2O + N_2 \qquad (5.3.1)$$

This means that an oxidative coupling of methane (OCM) takes place during the reduction of NO with methane in (NO, CH_4, Ar), Pt|PBI|Pt, (H_2, Ar) electrochemical cell at 135°C. This result is not in agreement with the data obtained in the study of the same catalytic reaction on Pt-group metals where the methane oxidation to carbon dioxide took place.[114-117] It should be taken into account, however, that the catalytic reduction of NO by methane on Pt-group catalysts was proved to have a Langmuir–Hinhelwood-type kinetics at 347–497°C,[117] and with high probability this is valid at lower temperatures as well.[114,115] This kinetics means competitive adsorption of NO and methane on the catalyst surface, with NO adsorption being much more

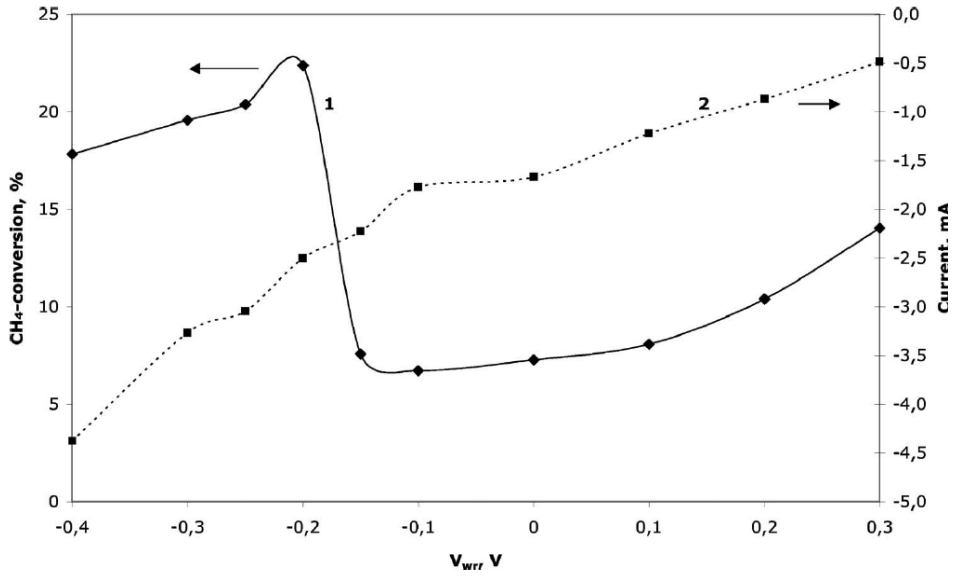

Fig. 5.3.3. CH_4 conversion vs V_{WR} obtained in the (NO,CH4,Ar), Pt/PBI–H_3PO_4/Pt, (H_2,Ar) electrochemical cell cell at 135°C and atmospheric pressure (curve 1) Steady-state voltammetric curve obtained in the same conditions (curve 2). This was the 1st polarization run.[101]

pronounced than CH_4 adsorption. This also means that the reaction kinetics and mechanism are very sensitive to the NO/CH_4 ratio, oxygen presence, temperature, and, of course, the catalyst.

OCM was one of the two main mechanisms of the methane oxidation by oxygen which we discovered using the PBI electrochemical cell at 135°C, but acetylene was was an OCM product.[99] Ethylene was the main OCM product if a solid oxide electrochemical cell (SOEC) with YSZ electrolyte was used.[122-126] In this case methane and oxygen were separated by the electrolyte; CH_4 passed over the positive electrode and O_2 passed over the negative electrode. The oxygen was electrochemically reduced. The oxide ions were pumped to the positive electrode and oxidized again to oxygen. The methane was oxidized by this oxygen. The described mechanism was a classic electrocatalytic reaction (or version of an oxygen pump). The reaction proceeded at 600–900°C and was studied at numerous catalysts.[122-126]

The results of the first polarization run of the (NO,CH_4, Ar), Pt|PBI|Pt, (H_2,Ar) system at 135°C are given in Fig.5.3.3. The CH_4 conversion was calculated on the basis of mass spectral data, and the mass spectrometer was calibrated with flows containing a known composition of CH_4.

There is a difference between most of the electrochemical systems used in EP experiments[10] and the electrochemical cell used in the present paper. In the former

case the membrane (solid electrolyte)/electrodes assembly is placed in a tightly closed cell with the working gas atmosphere in it and, therefore, the voltage between working and reference (or working and counter) electrodes is zero. In our case there are different gases at the working and the reference (counter) electrodes. Therefore, an electrochemical promotion effect can be obtained even without inforced polarization, using e.g. potentiostat.

Before the first steady-state polarization the OCV of the cell was 0.372 V. The methane conversion at the OCV was 13.6%.

It can be seen from Fig.5.3.3 (curve 1) that the methane conversion drops to 6.8% during the negative polarization from 0.372 V to -0.14 V. It is also clear that there is a promotion effect which starts at approximately −0.14 V and has a maximum (23% methane conversion, ρ=3.1) at V_{WR} (voltage between the working and the counter (reference) electrodes) = −0.15 (Fig.5.3.3, curve 1). Comparison of curve 1 (CH_4 conversion) and curve 2 (steady-state voltammetric curve) in Fig. 5.2.3 shows that there are electroreduction processes both in the case of the methane conversion drop in the beginning of the polarization and in the case of the promotion of the catalytic reaction. The latter takes place in the same voltage area as the EP effect in our previous study on the methane catalytic oxidation by oxygen[99] and the NO reduction with hydrogen[100] in the PBI electrochemical celll. It was assumed in our previous papers that these two reactions were promoted by electrochemically produced hydrogen. In order to distinquish between catalytic and electrocatalytic reaction, we have also studied an electrochemical behaviour of the cell with only Ar gas at the working electrode during its polarization. The results are presented in Fig.5.3.4. It can be seen from Fig. 5.3.4, that there is an electroreduction reaction which starts at approximately −0.15 V, i.e., at the same voltage at which the promotion effect takes place in Ref.99, 100 and in Fig.5.2.3. In pure Ar atmosphere the only possible electrochemical reaction is the electrochemical hydrogen reduction.

$$H^+ + e \rightarrow H \qquad (5.3.2)$$

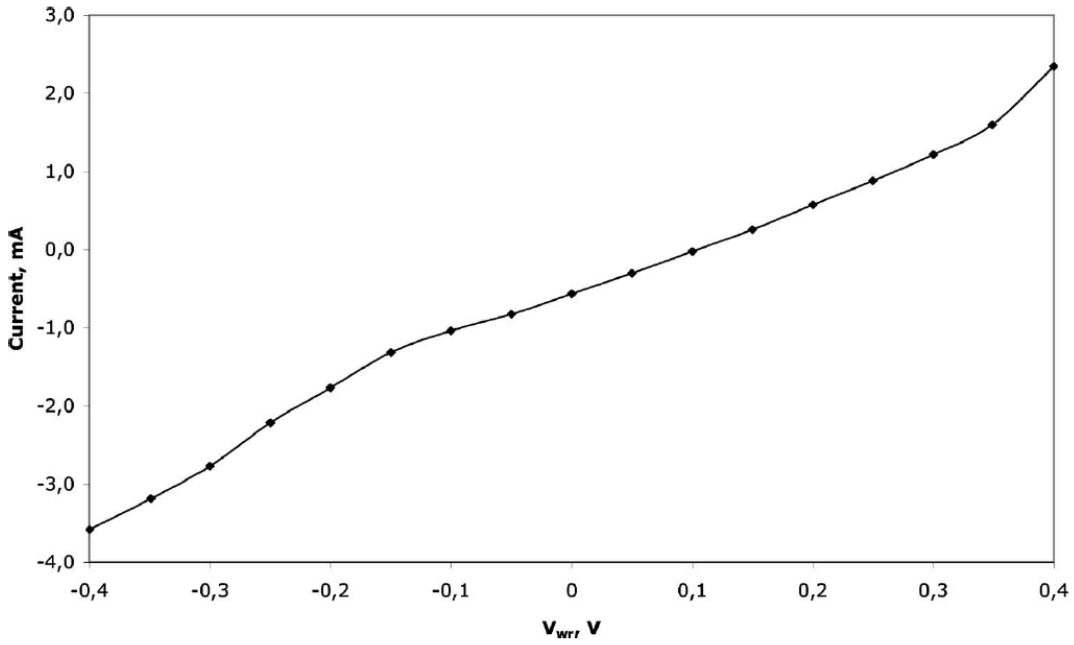

Fig. 5.3.4. Steady-state voltammetric curve obtained in the (Ar,Pt/PBI-H_3PO_4/Pt, (H_2, Ar) electrochemical cell at 135°C.[101]

The drop in the methane conversion at the start of the polarization of the catalyst can be safely explained by a decrease of the adsorbed methane on the catalyst. It has been found on a Pt-black catalyst in 4.3 M $HClO_3$ at 65°C the maximum amount of methane is adsorbed at 0.3 V vs. the standard hydrogen electrode (SHE).[112] At the potentials more negative than -0.15 V, the electrochemical reduction of hydrogen takes place. The hydrogen atoms promote the CH_4 oxidative coupling and the NO reduction, and therefore the reaction (5.3.1). Therefore the mechanism of the promotion is EEPP.

We can assume that the electrochemical reduction reaction which took place at the potentials close to the OCV is the electrochemical reduction of NO. To calculate the amount of the electrochemically reduced NO, we assumed that the following electrochemical reaction takes place

$$NO + 2H^+ + 2e \rightarrow 1/2N_2 + H_2O \qquad (5.3.3)$$

100% faradaic efficiency was also assumed. In the presence of methane, only 3.4% of NO was oxidized electrochemically.

5.4. Electrochemical promotion of Fischer-Tropsh synthesis.

Electrochemical promotion (EP) of Fischer-Tropsh synthesis (FTS) studied in the ***CO, H_2, Ar//Pt/Ru/C/Polybenzimidazol-H_3PO_4/Pt/H_2,Ar*** cell at 170°C. The Pt/Ru catalyst was chosen because Ru was known to be an active FTS catalyst.[127]

The open circuit potential of the working electrode was -0.304 V against the counter electrode. The results of the EP study are shown in Fig.5.4.1. The main product of synthesis was methane. No change in the product composition was seen at different polarization. Only trace amount of higher carbon compound was observed.

Therefore we can assume that the main reaction is

$$CO + 3H_2 \rightarrow CH_4 + H_2O \qquad (5.4.1)$$

Fig.5.4.1 shows a "volcano" type dependence of the CO conversion on the working electrode potential (V_{WR}) against the counter (reference) hydrogen electrode. The maximum promotion was found between -0.050 V and 0 V and showed 11.1% or a CO conversion rate of 1.38×10^{-6} mol/s.

The electrochemical promotion of FTS was first studied using solid-electrolyte membrane reactor (an yttria stabilized zirconia electrolyte) by Gür and Huggins at 500-1090°C.[128,129] This reactor was used in the mixed flow (co-fed) mode. Ni (Co, Fe) (the catalyst) and Pt were used as the electrodes. The idea was based on the knowledge that the rate-determining step for the FTS is the dissociation of CO adsorbed by the catalyst. Therefore the electrochemically promoted O^{2-} transport from the catalyst/electrolyte interface should promote the reaction. Indeed, the methane production increased significantly (up to 5 times) by the negative polarization of the Ni (Co or Fe) catalyst. The highest CH_4 production rate under the negative polarization (5.01×10^{-8} moles CH_4/s) was obtained at the Ni catalyst at 700°C.[128,129]

Later a study on electrochemical promotion of the FTS at Ru catalyst, has been performed by Lambert et al. at 200°C.[130] In this work sodium was used as a promoter, supplied by a Na-β-Al_2O_3 electrolyte. CH_4, C_2H_4, C_2H_6, C_3H_6 and C_3H_8 were the FTS products. The highest obtained for methane production was 3.75×10^{-15} mol/s (and it was higher than for the other products), i.e. lower than obtained in the our study.[101(A7)]

We can assume that this case of electrochemical promotion had EDLE mechanism of electrochemical promotion, because it takes place during a positive polarization of the catalyst, i.e. there was no electrochemical production of promoter (H atoms) and probably in this way the oxidation of gaseous hydrogen was accelerated and conditions of CO adsorption were improved.

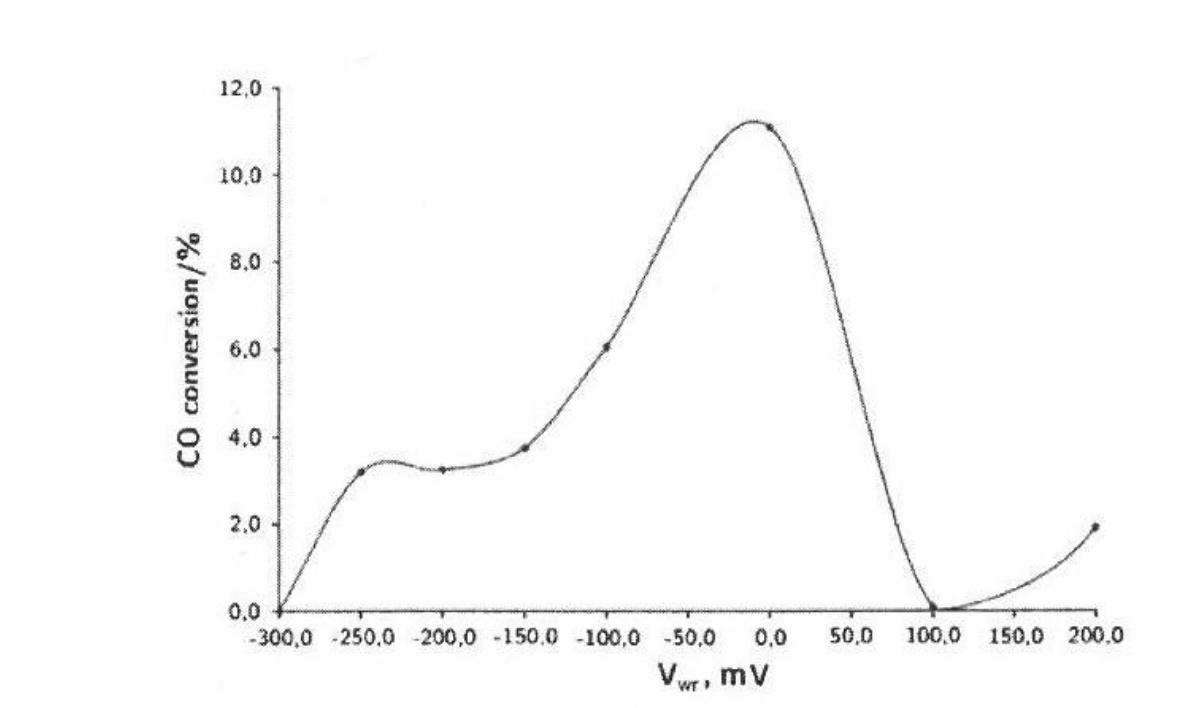

Fig.5.4.1. Dependence of CO conversion to methane on the catalyst potential obtained in (CO,H_2,Ar),Pt/Ru/PBI-H_3PO_4/Pt/Ru, (H_2,Ar) cell at CO/H_2/Ar flow rate (17, 17 and 354 mL/min, respectively, at atmospheric pressure) and at 170 °C.[102]

6. CATALYSTS FOR THE HIGH TEMPERATURE PROTON EXCHANGE MEMBRANE (PEM) WATER ELECTROLYSIS

The experimental data on the development of the catalysts for high-temperature PEM water electrolyzersare given in Chapter 6.

6.1. Preparation and study of IrO_2/SiC/Si supported anode catalyst for high temperature PEM steam electrolysers

Introduction

Some of the future aspirations of the "hydrogen energy cycle" involve the splitting of water by means of electrolysis and using the evolved hydrogen as a fuel. One way to do this would be by using a PEM electrolyser.[135] The electrolysis of steam instead of liquid water is favourable in several ways. The thermodynamic demands are lower at higher temperatures, waste heat can be utilized (effective cooling due to temperature gradient) and water management is simplified in such systems (avoiding two-phase seperation). Elevated working temperatures involve increased demands for corrosion resistance of catalysts and construction materials (bipolar plates and current collectors), while the contact resistance in gas diffusion layer (GDL) should remain reasonable. For conventional PEM water electrolysers, Nafion® is commonly used as an electrolyte.[136-138] The conductivity of such membranes decreases significantly at temperatures above 80°C, which is associated with the evaporation of water.[139] Sufficient efficiency is achieved using polybenzimidazole (PBI) membranes doped with phosphoric acid in PEM fuel cells at temperatures up to 200°C under ambient pressure.[139-140] Doped membranes are potential electrolytes for use in PEM steam electrolyser systems. Nevertheless, one of the main problems in such systems still remains the extremely low pH combined with elevated temperatures and high overpotentials at the anodic compartment. These conditions impose serious limitations on the materials which can be used. The applicable electrocatalysts for the oxygen evolution reaction (OER) are still limited to Ir, Ru and their oxides.[141] The anodes used in research and in industry are mostly based on mixtures of an electrocatalyst and a stabilising agent, e.g. TiO_2. Such kinds of electrodes are known as dimensionally stable anodes (DSA) and were first developed by Beer.[142-144] For Nafion-based systems, porous Ti usually serves as an anode bipolar plate and GDL material.[138,145] Unfortunately, previous studies have shown that titanium can not be used in systems that involve phosphoric acid containing electrolytes.[146,147] Ruthenium oxide is known as the most active catalyst for the OER. However it is not dimentionally stable under the conditions of PEM electrolyzer.[148] Instability of Ru-based anodes at high overpotentials in acidic conditions has been proved by several studies. The mechanism of corrosion is explained by the conversion of RuO_2 to soluble, non-conductive and volatile RuO_4, with a boiling point of 130°C.[149-151] The

facts mentioned above present Ru and its oxides as unsuitable catalysts for the OER in high temperature PEM steam electrolysers.

Several studies[152,153] devoted to improving of the stability of RuO_2 during anodic oxygen evolution by mixing the catalyst with IrO_2. This causes a decrease in the corrosion rate of RuO_2 dependant on the IrO_2 content in the mixture. IrO_2 appears to have greater stability and a reasonable activity compared with Ru-based electrocatalysts for such systems.[141]

Moreover, IrO_2 is the most stable OER catalyst for PEM water electrolysers studied until now. Unfortunately, high loadings of noble metals or their oxides puts considerable commercial limitations on a wider application of PEM electrolysers and a significant reduction of such metal loadings should be achieved[154]. In search for an electrode with lower loading requirement for the electrocatalyst, two main strategies can be followed:

The first includes doping of active oxides with other, more available materials, such as SnO_2, SbO_2, TaO_2, Mo_xO_y etc.[135,155-157] This approach involves introduction of a dopant precursor on the initial stage of catalyst synthesis. Following this method, composite binary or ternary catalytic oxides are usually obtained.

The second approach includes the use of a support material which would improve the specific surface area of the electrocatalyst and prevent particle agglomeration, thus increasing the specific surface area of the electrode.

Ideally, raw materials for the preparation of inert anode support should be cheap and readily available.

Carbon is a widely used catalyst support material for PBI fuel cells. On the other hand, one of the main reasons for fuel cell catalyst degradation is the corrosion of the carbon support, which occurs at potentials higher than 0.207 V (vs. SHE).[139,140] In electrolysis mode the corrosion of carbon would be much faster than in fuel cell mode due to the higher anodic overpotentials of the OER. For this reason, carbon cannot be considered as a potential durable support for anode electrocatalyst in PEM electrolysers. The corrosion stability and durability of the OER electrocatalyst support appears to be one of the greatest challenges in the field.

In conclusion, only a dimensionally and chemically stable, as well as readily available and reasonably conductive material should be used for this application. Among others, ceramic materials are potentially promising candidates.[159] However, most ceramics have relatively low electrical conductivity. The value of the acceptable electrical conductivity of catalytic layers is discussed elsewhere.[160]

Nevertheless, some of the materials with low electrical conductivity can be used as catalyst support in acidic systems.[161] In this study, p-Si was employed as a substrate for thermal deposition of the active IrO_2 and results showed that this material can be used for the preparation of DSA-type electrodes.

Silicon carbide, produced by the Acheson process is known as a hard, refractory and chemically inert material.[162] Electrical conductivity of this material is quite poor, however doping with appropriate elements can significantly improve this property.[163] Considering a possible electrochemical application of silicon carbide, the main advantage among others is its high stability in phosphoric acid solutions.[164]

Several studies have been published, reporting the successful use of silicon carbide as a catalyst support for PEM fuel cells.[165,166] However, at present there are almost no publications covering catalyst support investigations for electrolyzers.[167] Indeed, this area of research is more challenging and the material choice is highly limited, which is directly connected with the increased cell voltages applied in the electrolyzer mode. In our study a refractory silicon carbide-silicon material (Si content was less than 22%) was used as a support for the active OER catalyst IrO_2. The aim was to find a stable support and introduce it to the active catalyst.

Experimental part

SiC-Si/IrO_2 powder catalyst preparation

The sintered SiC/Si material was provided by the "State Powder Metallurgy Plant", Brovary, Ukraine. Catalyst support powder was prepared according to the following procedure: the as-received plate was cut with a diamond saw into squared samples with 1 cm side. The thickness of the plates was 2 mm. The prepared plates were cleaned in an ultrasonic bath, degreased with acetone, washed with demineralised water and finally dried at 80°C. The silicon carbide-silicon plates were milled in a planetary ball mill (Fritsch, Pulverisette 7). Since SiC is a material with high hardness, a mill made of conventional steels could not be used for this procedure. This is due to the relative softness of the steel, and associated risk of contamination of the sample by self abrasion of the steel balls and a possible tribochemical reaction. Therefore, two 45 ml steel vials, covered with tungsten carbide wear resistant lining were used. Milling was performed in the vial, which contained 6 WC balls, each 15

mm in diameter. The working vial contained 2 g of the starting material. The mill was operated at 730 r.p.m. for 10 min.

The product of the milling was introduced at the initial stage of the Adams fusion method of IrO_2 synthesis.[168] The iridium oxide content in the prepared catalyst was varied from 0 to 100 wt.% in steps of 10 wt.%. As the support was added to the initial solution of the catalyst precursor, it was expected that the catalyst would adhere to the surface of the support. Chemical inertness of SiC/Si during synthesis was confirmed by XRD analysis. The calcinated products appeared to be fine powders, changing colour from black to more greyish with increasing content of silicon carbide in the composition.

The electrochemical characterization. Corrosion stability tests

For investigation of the corrosion stability of material, plates prepared as described in the previous section were used. The corrosion stability test of the the material was performed in a specially designed cell, used in our work on corrosion resistence of construction materials for high-temperature PEM electrolyzer (Fig.6.1.1).[146(A10)]

Preparation of Nafion bonded electrodes for CV investigation

In order to estimate the electrochemical performance of the obtained electrocatalyst powder, the following procedure was performed.

A tantalum cylinder, accurately embedded in a Teflon/PTFE body, was used as a working electrode. The diameter of the cylinder was 7.5 mm which corresponded to an active surface area of 0.44 cm^2. Tantalum was chosen because of its superior corrosion resistance in hot phosphoric acid solutions, while having necessary conductivity and mechanical strength to support the electrocatalyst.[146(A10),169] Silicon carbide abrasive paper was used for polishing, followed by polycrystalline diamond powder (Struers A/S (Denmark)) with a particle size less than 0.25 mm. Finally, the surface was degreased with acetone and rinsed with demineralised water. The catalyst suspensions were prepared by adding of a 1 mg portion of prepared powder to 1 mL of demineralised water. The suspension was dispersed in an ultrasonic bath for 1 h. Immediately after this procedure, a 30 μL portion of the suspension was applied on the surface of the working electrode, following by the drying of the catalyst layer under nitrogen protective atmosphere.

A second suspension, consisting of a 1% solution in water of commercial

5 wt.% Nafion® (by DuPont) was applied on top of the catalyst layer and dried in the same manner. Therefore, each electrode contained 30 μg of sample powder. All 11 test electrodes were prepared in the same manner, using equal amount of applied test powder, while ranging in its composition of active IrO_2 from 0 to 100% with a step of 10%.

The performance investigations of the supported electrocatalyst were conducted in a specially designed three-electrode cell, described in Ref.146 (A10). (Fig. 6.1.1.).

A commercial platinum counter electrode and a KCl-saturated calomel reference electrode (SCE), connected to the system through a Luggin capillary were provided by Radiometer Analytical SAS.

The CV experiments were performed in the potential window between 0 and 1.2 V against the SCE. This allowed the observation of the reversible redox behaviour of IrO_2 while avoiding the formation of significant amounts of oxygen which could detach the catalyst layer from the working electrode. This also permitted the use of the same sample for experiments at elevated temperatures.

As it is necessary to evaluate the catalyst performance at the conditions close to those in a PEM cell, in our work the 85% phosphoric acid (analytical purity) was used as electrolyte. The range of temperatures was from room temperature (ca. 23°C) to 80°C, 120°C and 150°C, with the experiments performed from lower to higher temperatures. The temperature tolerance allowed during the cyclic voltammetry experiments was ±3°C. Temperature was controlled by a k-type thermocouple, covered with Teflon/PTFE and inserted into the working cell (Omega Co.). For each temperature, a series of scans at different speeds were carried out in the following sequence: 200, 100, 50, 20, 10 mV/s. The CV scan started at 0.0 V, going to the vertex potential of +1.2 V and reversing back to the initial value of 0.0 V (all potentials vs. SCE). An open circuit of 10 s was maintained between each experiment. The experimental apparatus used for electrochemical studies was a VersaSTAT 3 potentiostat and VersaStudio software by Princeton Applied Research.

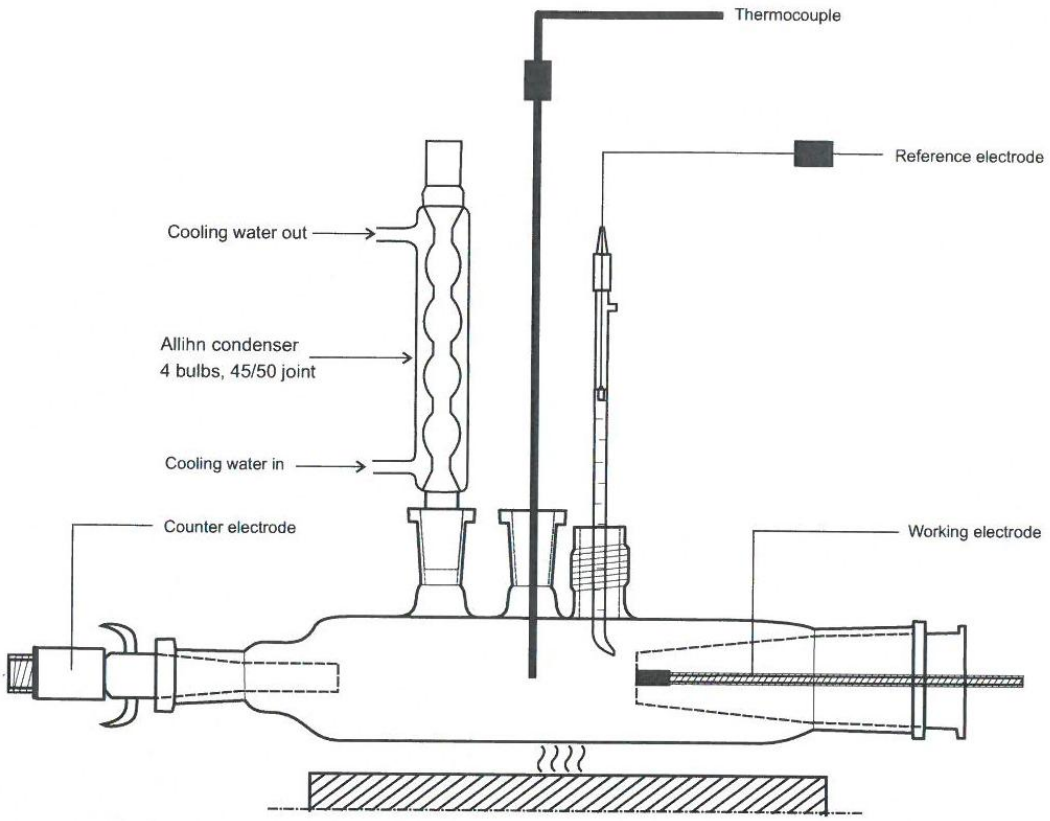

Fig. 6.1.1. The electrochemical cell.[131]

Physico-chemical characterisation

The prepared powder samples were studied using scanning electron microscopy (SEM) and energy-dispersive x-ray spectroscopy (EDX). The catalyst powder was dispersed in ethanol and the suspension was kept for 1 h in an ultrasonic bath. 20 μL portions of this solution, containing 20 μg of the catalyst were afterwards applied to both a sticky carbon disk and polished golden holders, which were correspondingly used for SEM and EDX investigations. SEM measurements were made with an FEI Quanta 200F scanning electron microscope. The EDX-system used was INCA from Oxford Instruments (accelerating voltage 5 kV, working distance 5.1 mm). The as-milled SiC/Si powder as well as other samples were characterized with x-ray powder diffraction (XRD) using a Huber D670 diffractometer (Cu-K α x-ray source, α = 1.5405981 Å).

The BET method was used to evaluate the specific surface area of the catalysts. Automated Gemini 2375 surface area analyser by Micromeritics was used in our work.

Results and discussion

Structural and electrical properties. X-ray diffraction

The x-ray diffractogram for the IrO_2 prepared without the support is shown in Fig. 6.1.2. The supported catalysts showed the characteristic signals of IrO_2, SiC and Si (Fig. 6.1.3). However, small peaks of WC were detected in the diffractogram of the support powder (Fig. 6.1.4). This contamination originates from the ball milling procedure. The catalyst consisted of a physical mixture of IrO_2 and support material with no any other substances produced during the synthesis process, e.g. during the firing at 500°C. As other compounds were not detected in the samples (Fig. 9.1.3), the composite samples can be considered as physical mixtures of IrO_2 and support. The peak at around 55° and the width of IrO_2 peaks for different samples were chosen for calculation of the average crystal size, on the basis of the Scherrer equation[170]:

$$\tau = \frac{K\lambda}{\beta \cos\theta} \qquad (6.1.1)$$

where K is a shape factor, usually taken as 0.9; λ is the x-ray wavelength; β is the peak width in radian; and θ is the Bragg angle of the peak.

The supported catalysts showed smaller crystal sizes than those for pure IrO_2, as can be seen in Fig. 6.1.5. Since the synthesis method and conditions were the same for all samples, these results indicate an effect of the support on the IrO_2 crystal growth during the catalyst synthesis.

BET surface area

The IrO_2 powder surface area was 121 m^2/g. In contrast, the support had only approximately 6 m^2/g. The BET area of the supported catalysts follows approximately the rule of mixtures. However, the BET area of pure IrO_2 is significantly lower than that of 80% and 90% IrO_2 samples (Fig. 6.1.6).

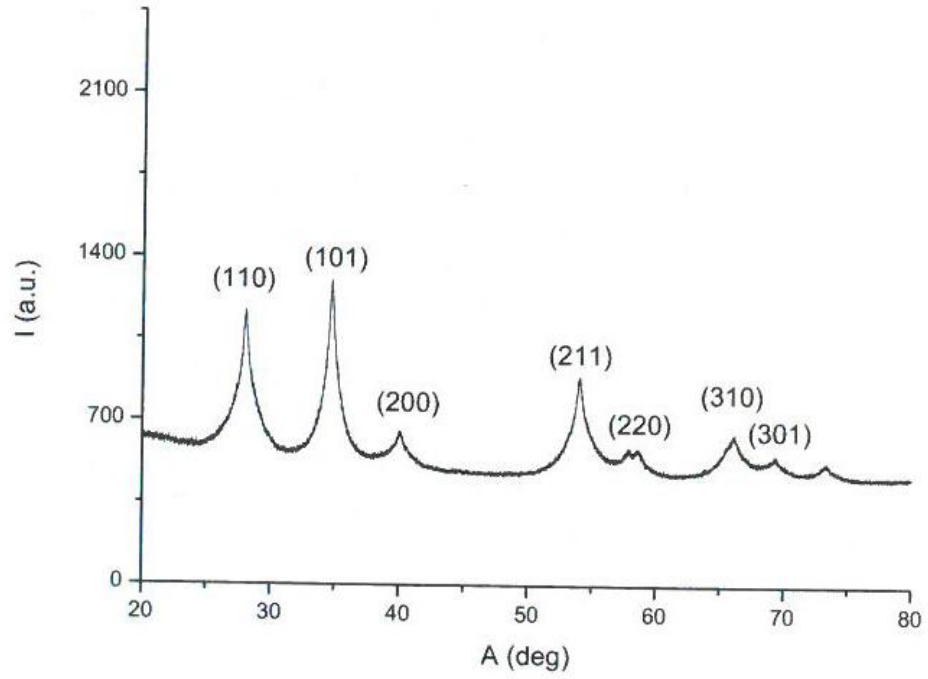

Fig. 6.1.2. XRD spectrum for IrO_2.[131]

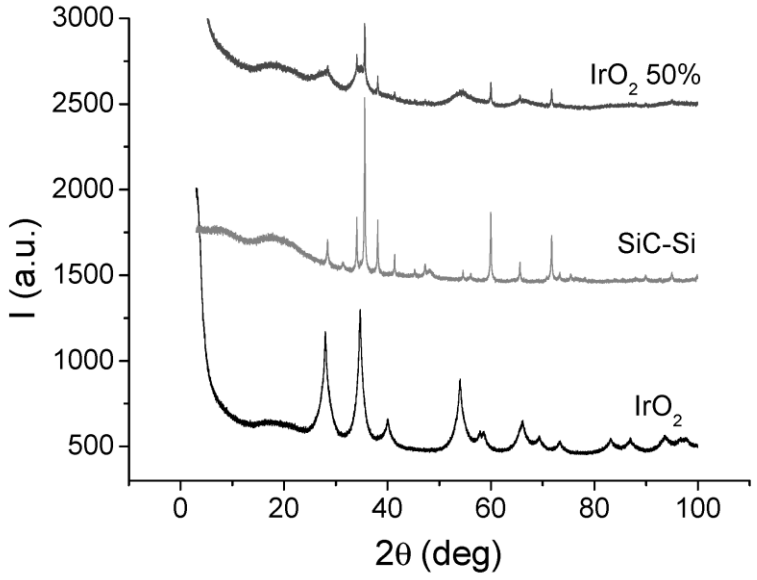

Fig. 6.1.3. XRD spectra for IrO2, SiC-Si support, and a 50% of the catalyst.[131]

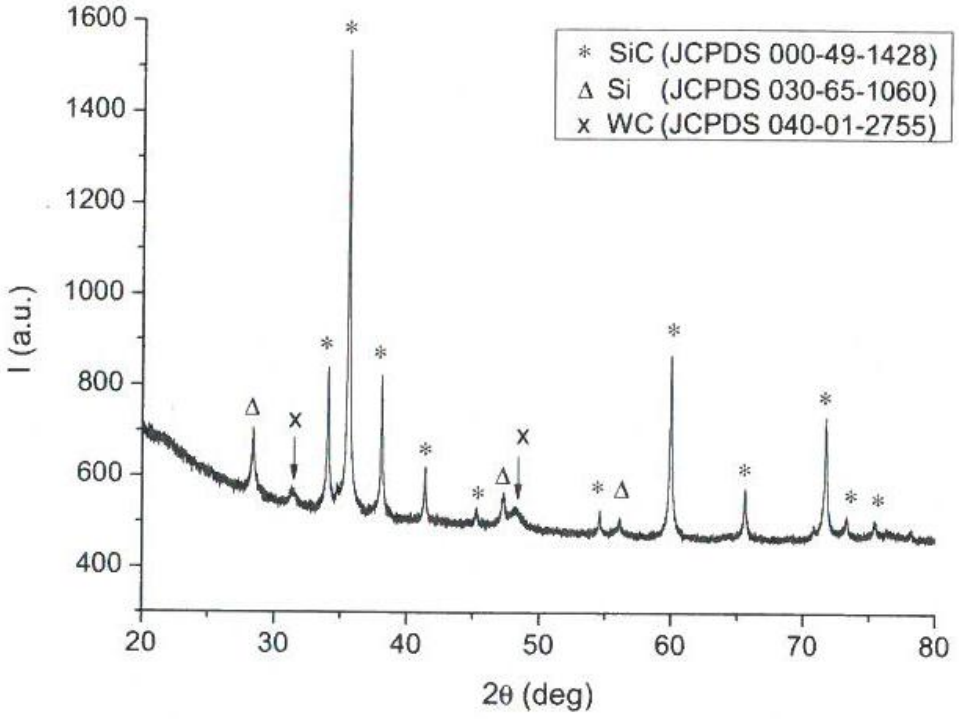

Fig. 6.1.4. XRD spectra for the prepared support powder.[131]

This difference can be due to stabilization of smaller IrO_2 particles by the SiC/Si support.

SEM and EDX analysis

Scanning electron microscopy was performed on a selected sample containing 60% IrO_2 and 40% SiC/Si support. The images were obtained with an incident electron energy of 5 kV (Fig. 6.1.7). SEM results resolved that the active component was distributed evenly over the surface of the support. In the SEM micrograph two groups of particles can be seen. There are larger particles, between 5 and 10 μm in size which are most likely support particles. On these there are smaller agglomerate particles of IrO_2. The distribution of the IrO_2 particles on the support material seems to be quite homogeneous. This distribution suggests that the IrO_2 particles are formed on the support particles, which could provide nucleation sites for the formation of IrO_2. This could explain the results observed in the XRD and BET experiments, where the IrO_2 particles in the supported catalysts tend to be smaller than in the pure material (Figs. 6.1.5 and 6.1.6). On Fig. 6.1.8 and Table 6.1.1 the results of the EDX quantative analysis, performed at low voltage (5 kV) are presented.

Powder conductivity

The conductivities of all sample powders were measured using a technique, described previously by Marshall.[171] Measurements were conducted in air at room temperature.

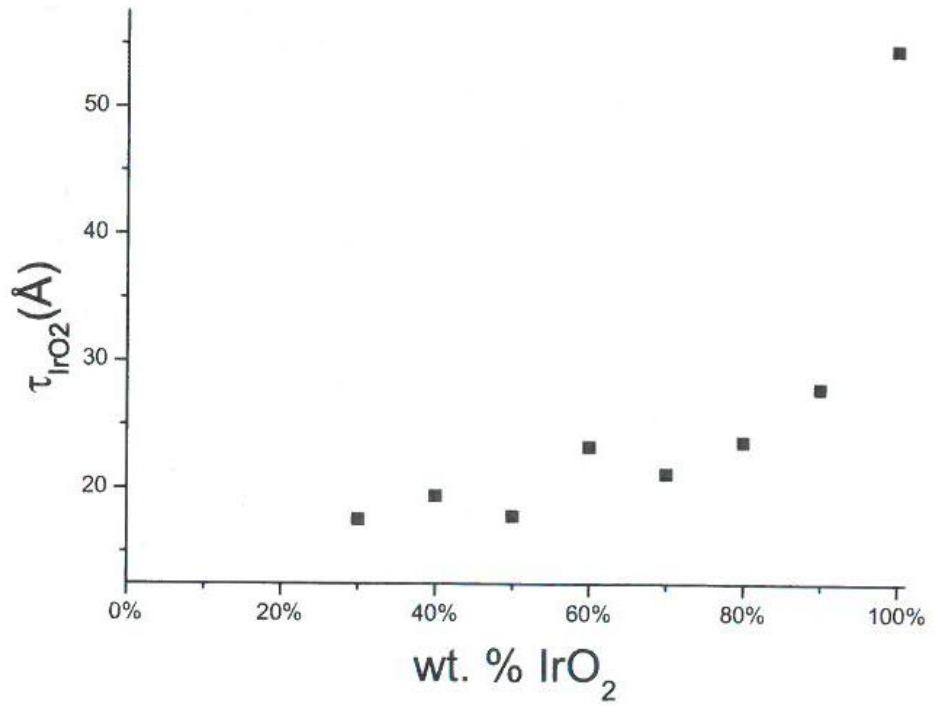

Fig. 6.1.5. Calculated average crystal sizes for different samples.[131]

To this end, the resistance of powder samples with different thickness was measured (Fig. 6.1.9). It can be seen that the change of the resistance with the powder thickness is quite linear. The conductivity results are shown in Fig. 6.1.10. The IrO_2 conductivity is 67 S/cm, i.e. much higher than for the support, which is 1.8×10^{-5} S/cm. It can be thus assumed that almost all the current passes through the IrO_2 particles. The dependency of conductivity on the sample composition is not linear, levelling off and increasing again with the mass fraction of IrO_2. The effect of the support on the conductivity of the composite powders is obviously negative.

It has been proposed that the conduction of current through powders depends strongly on the contact resistance between particles.[172] The presence of a step in conductivity around 60% of IrO_2 seems to support this hypothesis. If we take into account the great difference in conductivity of the support and IrO_2, it is clear that the contact between IrO_2 particles is very important for the conductivity of the catalyst.

Although the conductivity changes slowly with composition, there is an increase from 90 wt.% to 100 wt.% IrO_2. This suggests that there must be another factor influencing particle contact. For instance, the inclusion of the support particles, with very different size and shape, could alter the packing of the IrO_2 particles in the powder. This could also be another effect of a different IrO_2 particle growth in the presence of the support, as mentioned above.

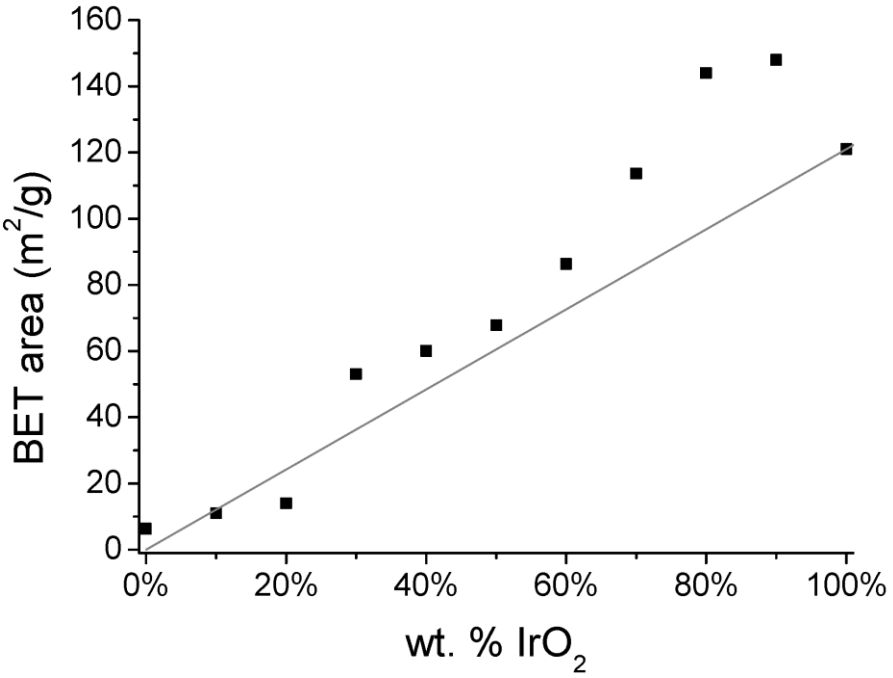

Fig. 6.1.6. BET surface area of all samples.[131]

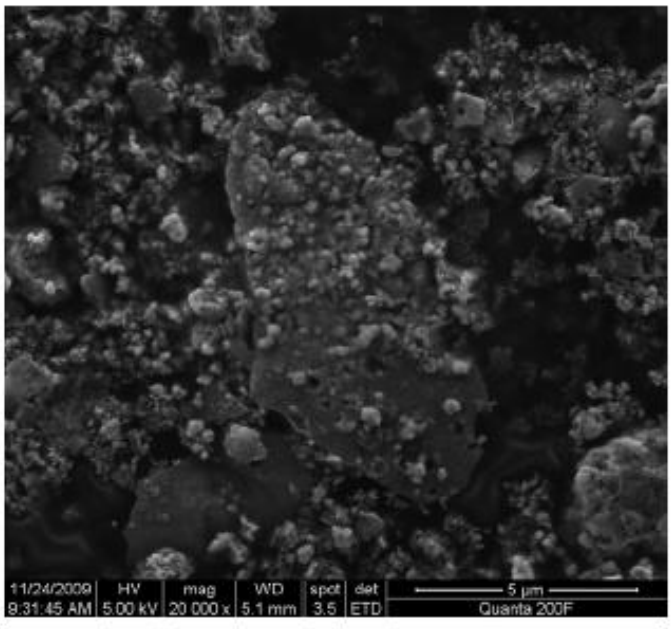

Fig. 6.1.7. SEM micrograph of a sample with composition 60% IrO_2 and 40% SiC/Si support.[131]

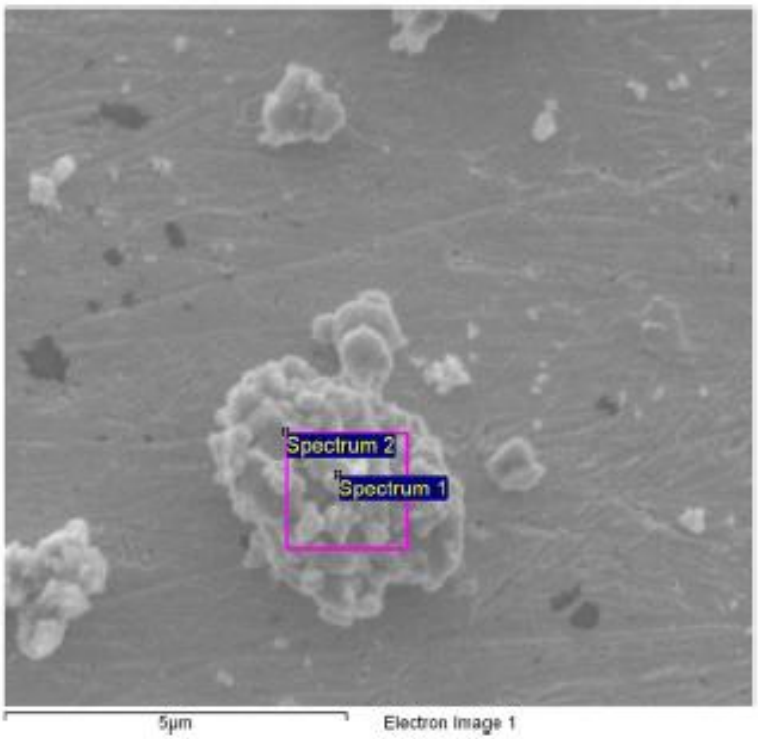

Fig. 6.1.8 SEM micrograph for EDX analysis at 5 kV on a gold plate. Sample composition: 60% IrO_2 and 40% SiC/Si support.[131]

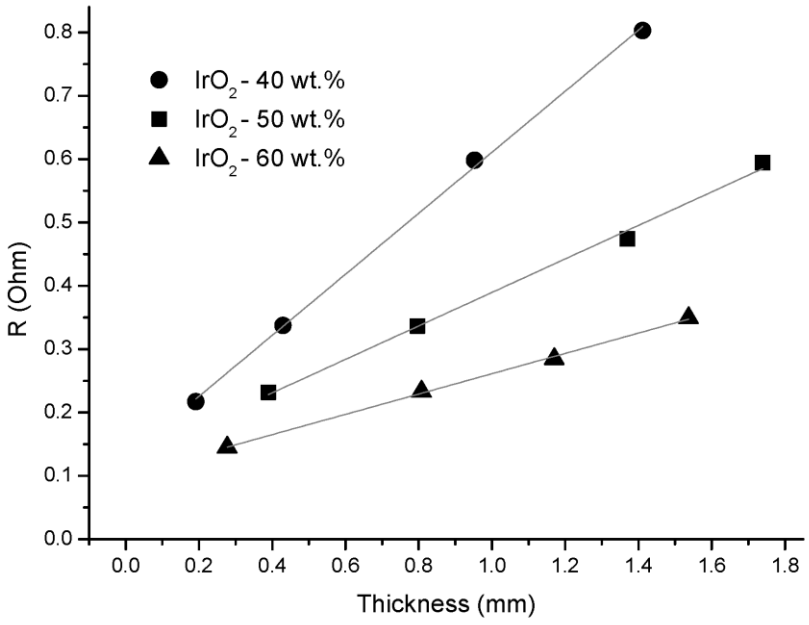

Fig. 6.1.9. Evolution of resistance with powder thickness for some samples.[131]

Table 6.1.1. EDX data for SiC/Si/IrO_2 (SiC/Si : IrO_2)

Spectrum	Composition, wt.%							
	C	O	Na	Si	Fe	Mo	Ir	Total
1	7.0	20.4	3.1	13.3	2.6	0.9	52.8	100.0
2	6.5	19.6	2.3	15.5		2.0	57.0	100.0

Electrochemical characterization.The corrosion stability of the support at high temperatures

Corrosion stability of the support material was tested using the electrochemical cyclic Tafel voltammetry technique. [146] Fig. 6.1.11 presents the Tafel plot for a SiC/Si plate. The potential shifts to more positive values after the anodic sweep, which shows the passivation of the material in the studied media. The corresponding corrosion current measured from the curve was 0.005 mA, dropping to 0.002 mA during the backward

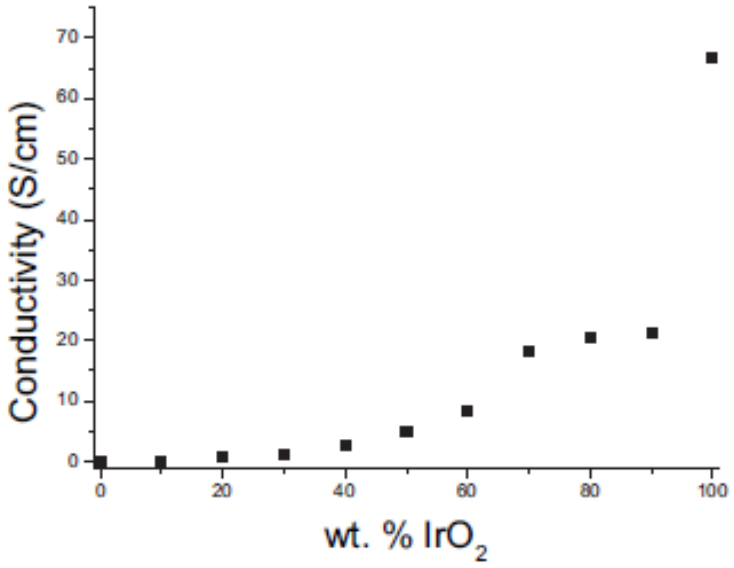

Fig. 6.1.10. Powder conductivities of all samples.[131]

scan, which is at least one order of magnitude less than for all alloy materials tested before in similar conditions.[146]

Cyclic voltammetry experiments. Room temperature.

Even though the SiC/Si support is considered to be inert under the chosen conditions, an additional experiment was performed for the tantalum working electrode and

support material, in order to identify any considerable background current which could also originate from WC impurities, detected earlier by the X-Ray diffraction.

Thus, in the supported catalysts, almost all the signal comes from the IrO_2 particles (Fig. 6.1.12). Catalysts with different loadings were characterised with cyclic voltammetry at potential scan rate of 20 mV/s. IrO_2 shows a pseudocapacitive behaviour, with a broad reduction and oxidation peaks. This has been attributed to reversible oxidation and reduction of Ir^{141} on the electrode surface. This feature allows integration of the charge under the anodic peak in order to compare the relative activity of the different catalysts. The background current under corresponding anodic peaks was subtracted prior to integration. Fig. 6.1.13 shows cyclic voltammograms, recorded with the supported and unsupported iridium oxide on tantalum electrodes. There is an evident increase in associated voltammetric capacitance value corresponding to the supported catalyst compared to the pure catalyst material. The peak charges of all samples are plotted against the IrO_2 loading in Fig. 6.1.14. The activity of samples with higher IrO_2 loading tend to show greater values. However, the activity of 80 wt.% and 90wt.% samples is higher than that of pure IrO_2. In theory, the activity should be proportional to the IrO_2 fraction.

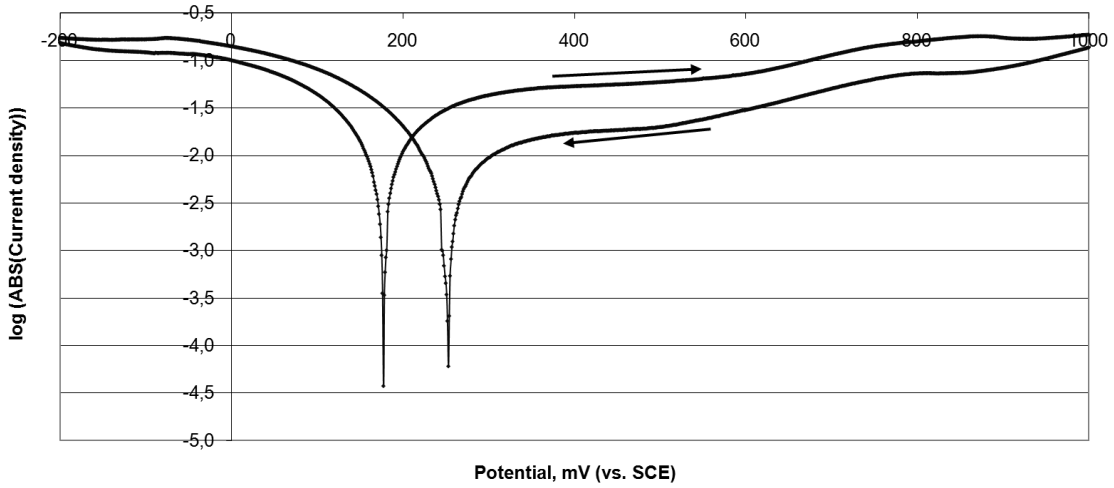

Fig. 6.1.11. The Tafel plot for a SiC/Si plate. Scan rate 1 mV/s, electrolyte 85% H_3PO_4, 120°C.[131]

As shown by the powder conductivity tests, the support has a very low conductivity compared to the active phase, so this cannot be the reason for the improvement in activity. Therefore, it can be assumed that the improvement of catalyst activity with

the addition of the support must be related to particle growth during the synthesis of IrO_2. Taking into account the results of the XRD and BET experiments, a reason for the improvement could be a smaller IrO_2 particle size for the supported catalysts, compared with the pure oxide. The smaller the IrO_2 particles are, the greater the specific surface area thus giving higher electrochemical activity.

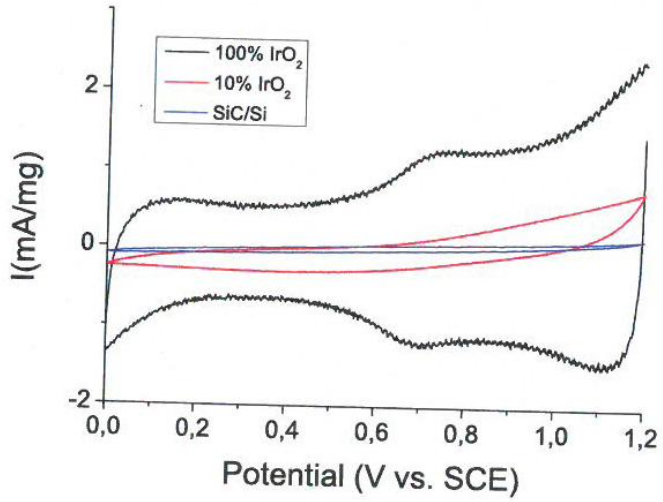

Fig. 6.1.12. Comparison of the voltammograms of the support and some samples. Scan rate 20 mV/s.[131]

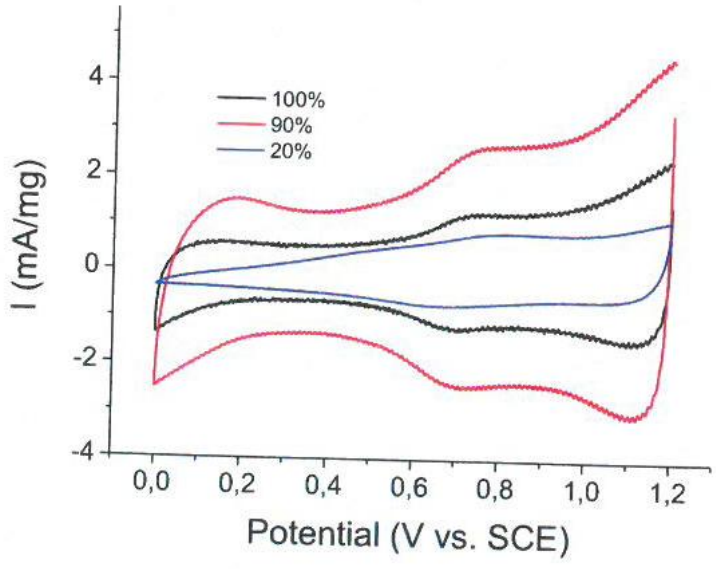

Fig. 6.1.13. CV experiments of several supported catalysts, in 85% H_3PO_4 at room temperature. Scan rate 20 mV/s.[131]

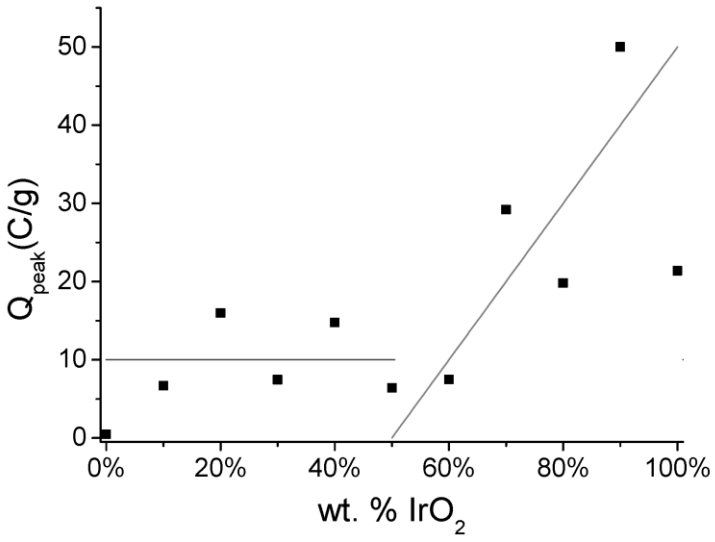

Fig. 6.1.14 Integrated peak charge of all samples, in 85% H_3PO_4 at room temperature. Scan rate 20 mV/s.[131]

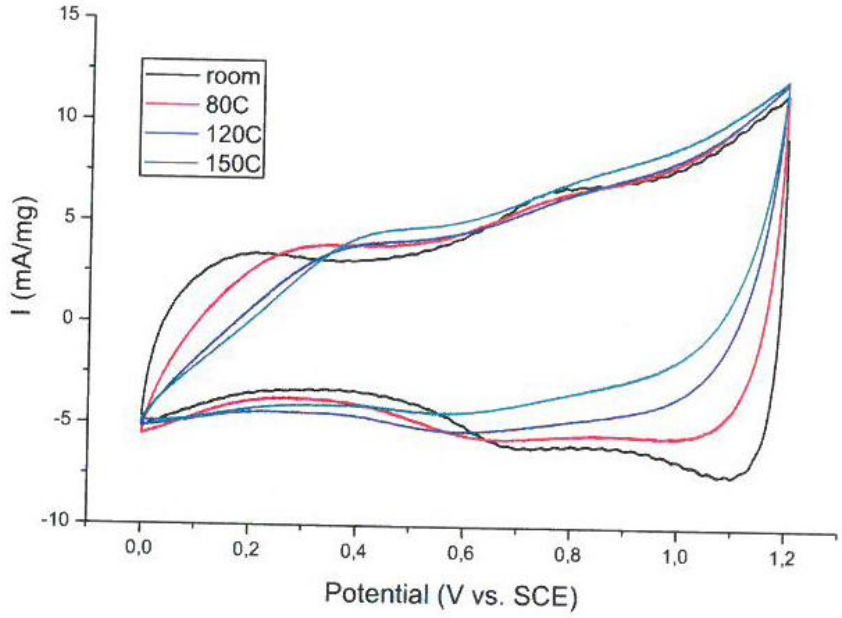

Fig. 6.1.15. CV experiments for 90% IrO_2 at different temperatures, in 85% H_3PO_4. Scan rate 20 mV/s.[131]

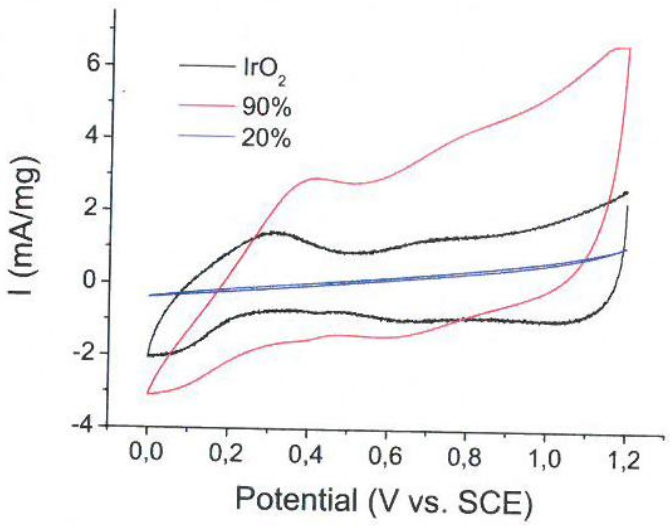

Fig. 6.1.16. CV experiments for some samples at 150°C, in 85% H_3PO_4. Scan rate 20 mV/s.[131]

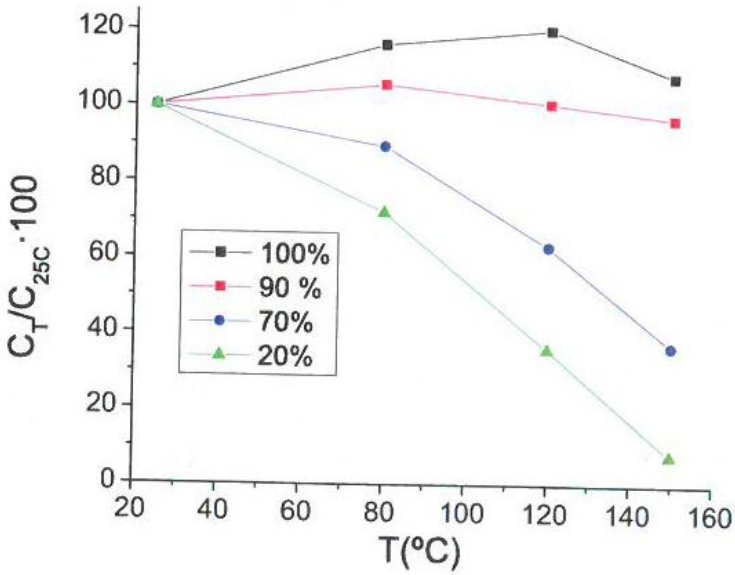

Fig. 6.1.17. Evolution of capacitance with temperature for some samples, in 85% H_3PO_4. Scan rate 20 mV/s.[131]

Cyclic voltammetry. High temperature.

Cyclic voltammetry experiments were carried at 80, 120 and 150°C. The rest of the experimental conditions were the same as for room temperature. In Fig. 6.1.15, change of CV curves for 90 wt.% IrO_2 electrodes with temperature is shown. The activity tends to decrease at higher temperatures, with less pronounced peaks and

smaller area under the voltammogram curve. This activity loss seems to be more pronounced for samples with low IrO_2 loading (Figs. 6.1.16 and 6.1.17).
Considering the transition state theory of reaction kinetics applied to electrode reactions, the catalyst activity should increase with temperature. The evolution of activity with temperature is different for each sample, with an apparent influence of the composition. This suggests a problem of loss of the catalyst, rather than an activity loss of the catalyst itself. Perhaps the samples with high support content have poor interaction with the electrode, thus losing catalyst particles over time. This process could be accelerated by convection during heating between experiments at different temperatures.

6.2. Tantalum carbide as a novel support material for anode electrocatalysts in polymer electrolyte membrane water electrolysers

Introduction

This work was focused on ceramic materials other than SiC/Si as possible support for IrO_2 catalyst. Four ceramic materials potentially suitable for this application were identified in the literature[173]: TaC, Si_3N_4, WB and Mo_2B_5. These materials were chosen because they are stable in harsh environments and also, in some cases, are electrically conductive. To select the most stable material in this group, a quick and easy preliminary stability test was developed, based on exposing the prospective support material to a mixture of trifluoromethanesulfonic acid (TFMSA) and hydrogen peroxide at 130°C. After a defined time, the liquid phase is analysed for the presence of ions originating from the dissolved support material. TFMSA was chosen because it provides a high level
of acidity without any unwanted complexing or chelating effects. The hydrogen peroxide provides an oxidative environment to simulate the anodic polarization in a PEM water electrolysis (PEMWE).
Overall, the conditions chosen were harsher than conditions in a PEM water electrolysis because this is an accelerated test which should provide the required information on material stability in a relatively short time.
Electronic conductivity represents another important parameter that influences electrocatalyst performance. At this point a distinction has to be made between the conductivity of the support itself and of the entire composite material, consisting of the support and IrO_2. It should be kept in mind that the conductivity of IrO_2 alone is

sufficient for the operation of a PEMWE when IrO_2 covers most of the support. Therefore, even a non-conductive support may be acceptable for the process. However, it is necessary to use high IrO_2 loading and at the same time a support material with a relatively low specific surface area to allow formation of a coherent conductive surface film of IrO_2. Finally, the electrical conductivity of the support is very welcome since it can reduce the ohmic drop in the PEMWE[171], but it is not a critical quality.

Several methods for the synthesis of electrocatalysts have been described in the literature. The most common is the Adams fusion method[168], which produces metal oxides.[131,141,157,171] The other methods used are the polyol method (also known as the colloid method)[141,171], simple thermal decomposition of the corresponding metal chlorides.[177] The polyol method and chemical reduction are usually followed by the oxidation of the resulting metal particles, either anodically or by simple calcinations in air.

In our study a modified version of the Adams fusion method was used for the synthesis of IrO_2 supported on TaC. This method was selected because it provides IrO_2 particles straight from the synthesis and because it allows direct comparison with the results of the preceding work.[131] The electrochemical activity of the prepared supported IrO_2 lectrocatalysts was compared with that of an unsupported IrO_2 electrocatalyst.

Thus, for the first time, the use of TaC as a support material for IrO_2-based lectrocatalysts for PEMWEs was reported.

Experimental

Support stability testing. Starting materials

Based on the published data,[173] the following materials were tested as potential electrocatalyst supports: TaC (SigmaeAldrich, 99%), Si_3N_4 (Goodfellow, >85%), WB (Alfa Aesar, 99%) and Mo_2B_5 (Cerac Inc., 99.5%). To remove any surface contamination, approximately 200 mg of each material was first etched in 50 mL of boiling 2% HCl for 15 min. After cooling down to room temperature, each suspension was washed five times with demineralised water on a centrifuge to remove chlorides. Final washing was followed by evaporation under argon.

Chemical stability test of the support

A mixture of the four support materials was created by taking 50 mg of each one. Then, 5 mL of concentrated TFMSA (Sigma-Aldrich, 98%) was poured into the mixture before 1.67 mL of 30% hydrogen peroxide was added drop-wise. The mixture was kept stirred at 130°C in a glass vessel, at the top of which a reflux condenser was attached. After 48 h, the mixture was cooled down to room temperature and diluted to 50 mL with demineralised water. The remaining powder was separated using a centrifuge and a 5 mL aliquot was taken as a sample. To prevent the ions from precipitating, 100 mg of NaF was added to the sample and the mixture was heated in a closed vessel at 80°C for 1 h.

Inductively coupled plasma mass spectrometry (ICP-MS) analysis

The sample containing the dissolved ions was analysed using a Perkin-Elmer Elan 6000 ICP-MS with a dual-stage detector with a high-concentration setting. All standards for the calibration line were purchased from Fluka. The calibration line was designed with a lower limit corresponding to 0.1% of the dissolved support material.

Electrocatalysts preparation

From the stability test, TaC was chosen as the preferred electrocatalyst support. The electrocatalysts with varying content of IrO_2 were prepared, using a modified version of the Adams fusion method.[168] The chemical reactions (6.2.1, 6.2.2), corresponding to the Adams fusion suggested by Marshall et al.[171], are shown below:

$$H_2IrCl_6 + 6NaNO_3 \rightarrow 6NaCl + Ir(NO_3)_4 + 2HNO_3 \quad (6.2.1)$$

$$Ir(NO_3)_4 \rightarrow IrO_2 + 4NO_2 + O_2 \quad (6.2.2)$$

The TaC support and a metal precursor ($H_2IrCl_6 \cdot 4H_2O$, Alfa Aesar, 99%) were dded to 10 mL of isopropanol and stirred for 1 h to ensure complete dissolution of the iridium salt. After the addition of finely ground $NaNO_3$ (16.7 × molar excess), the salt mixture was heated in air to 70°C and the solvent was evaporated.

Then, the mixture was placed into a furnace and heated up to 500°C at a rate of 250°C/h. It remained at 500°C for 1 h before cooling to room temperature overnight. The fused product was washed six times with demineralised water and separated on a centrifuge. Finally, the powder was dried in air at 90°C.

Electrocatalysts were prepared with concentrations of 10, 30, 50, 70, 90 and 100 wt.% IrO_2 and are labelled as $(IrO_2)_x(TaC)_{1-x}$, where *x* is the mass fraction of IrO_2. Like all Adams fusion processes, our modified version provided a yield of almost 100%.[171] The modified Adams fusion process was also applied to pure TaC to see if the process had any impact on its properties.

Physico-chemical characterisation

Scanning electron microscope (SEM) images of the electrocatalysts were taken on a JEOL JSM-5910 (10 kV acceleration voltage, 7 mm working distance). The SEM was equipped with an energy-dispersive X-ray spectrometer (EDX) that was used to collect an element map of the electrocatalyst. The EDX itself consisted of an Oxford Instruments X-Max silicon drift detector (SDD) controlled by Oxford Instruments INCA software.

A Netzsch STA 409 PC was used to perform thermogravimmetric and differential thermal analysis on the TaC. In a synthetic air atmosphere (20.8% O_2, 79.2% N_2, AGA GAS AB), the temperature was increased from room temperature to 1000°C at a rate of 5°C/min.

All electrocatalyst samples were analysed on a Huber D670 X-ray powder diffractometer (Cu-K_α, α= 1.5405981 Å).

Using a Micromeritics Gemini 2375 analyser, the specific surface areas of the electrocatalysts and the TaC were measured by the Brunauer-Emmett-Teller (BET) method.

Powder conductivity measurements were performed in the setup described before.[131] Conductivity values were obtained from the slope of the resistance vs. powder thickness plot.

Electrochemical characterisation

To evaluate the electrochemical performance of the electrocatalysts, working electrodes were prepared using the thin film method.[174] A glassy-carbon disk embedded in PTFE casing was used as the working electrode. The exposed part consisted of a 5 mm diameter circle onto which was pipetted 8 μL of electrocatalyst dispersion in demineralised water, the dispersion having been ultrasonically homogenised for 1 h beforehand. For all samples, the IrO_2 concentration in the

dispersion was 1 mg per mL. The electrocatalyst loading on the working electrode was 40 μg of IrO_2/cm^2. The electrocatalyst layer was fixed with an 8 μL drop of diluted Nafion solution (1 mg dry basis/mL) in isopropanol/demineralised water (3:1, w/w).

Electrochemical measurements were carried out in a three-necked electrochemical cell with a platinum wire counter-electrode and a saturated calomel reference electrode (SCE) connected to the cell via a liquid junction. All potentials in this article refer to this electrode. The electrolyte was 0.5 M H_2SO_4 at room temperature (23 ± 2°C).

A VersaSTAT 4 potentiostat running VersaStudio 2.0 software (Princeton Applied Research) was used for all electrochemical experiments. Cyclic voltammetry experiments were conducted between 0 and 1.2 V at scan rates of 500, 300, 100 and 50 mV/s. Tafel experiments were performed from 1.1 to 1.3 V at a scan rate of 1 mV/s.

Results and discussion

Support stability test

The solution analysis detected the most unstable compound of the four analysed to be Mo_2B_5, which had the highest dissolution extent of 93.3%. On the other hand only 3.3% of WB dissolved in 48 h. This material thus proved to be relatively stable under test conditions. But although such a relatively slow dissolution was detected, it may represent a problem in PEMWE, where the material must be able to withstand thousands of runtime hours. According to the analysis, only 0.5% of Si_3N_4 dissolved within 48 h of exposure. This suggests that it is highly stable. Additionally, the effect of the nitrogen present in the air and Si from the glass reaction vessel walls on the analysis results has to be considered. This material thus represents a promising candidate for the electrocatalyst support. But the results of the ICP-MS analysis showed that TaC, with no ions detected in the solution (Table 6.2.1), was the most resistant material of those under study. Therefore TaC was chosen as the support for IrO_2 in this study.

To confirm the thermal stability of TaC selected as the electrocatalyst support, TGA and DTA curves were recorded for the as-received sample of this material (Fig. 6.2.1). TaC showed a steady weight gain above 200°C as it was oxidized to Ta_2O_5. At 330°C, oxidation to Ta_2O_5 had reached an extent of 1 wt.%. More rapid oxidation

started at temperatures above 600°C and finished at 790°C. At this point TaC was quantitatively oxidised to Ta_2O_5. Theoretically, 100% TaC oxidised to Ta_2O_5 should show a weight gain of 14.5 wt.%. A gain of 14.9 wt.%, calculated as the difference between the lowest and highest recorded mass, was observed within this study. This discrepancy may have been caused by the nonstoichiometric composition of the TaC used.[175] Thus, TaC appears to be highly stable within the temperature range foreseen for the PEMWE, i.e. below 200°C. The situation is less clear with respect to electrocatalyst synthesis by Adams fusion. Here Ta_2O_5 formation has to be considered as a possible option.

Table 6.2.1. Extent of dissolution of tested materials in TFMSA/H_2O_2 (3:1, w/w). Temperature 130°C. Duration 48 h.

Compound	Dissolved portion (%)
TaC	Below quantification limit (<0.1)
Si_3N_4	0.5
WB	3.3
Mo_2B_5	93.3

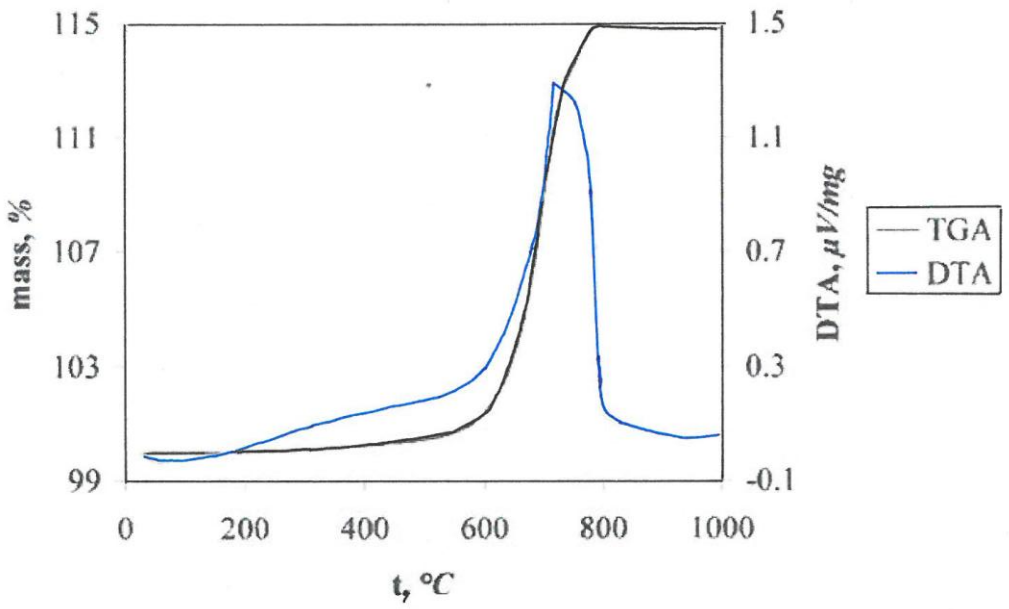

Fig. 6.2.1. Thermogravimmetric and differential thermal analysis curves of TaC in synthetic air. Heating rate 5 °C/min.[132]

Physico-chemical characterization. X-ray diffraction

X-ray diffractograms of series of the electrocatalysts based on TaC supported IrO_2 are shown in Fig.6.2.2. As expected, all diffractograms show well-defined lines of IrO_2 and TaC (except the one for pure IrO_2). Besides these lines, an additional component, identified as $NaTaO_3$ (green lines), was observed in the diffraction spectra of the supported electrocatalyst: it is a perovskite-type semiconductor with a band gap of 4.0 eV.[176] Its origin lies in oxidation of the TaC support by $NaNO_3$ during the Adams fusion process. Diffraction lines of this component are scarcely visible for the electrocatalyst containing 90% of IrO_2. This is due to its small content in this particular sample. However, closer inspection reveals a definite diffraction line at $2\theta = 22.8°$.

The Scherrer equation[170] was used to calculate the average crystallite size of the IrO_2 in the electrocatalysts for different contents of IrO_2 (Fig. 6.2.3); the IrO_2 peak located at $2\theta = 28°$ (110) was used for this purpose (see inset in Fig. 6.2.2). The accuracy of this size determination was better than 10%. The peak recorded for the 10 wt.% $\pm$ IrO_2 electrocatalyst was too weak. Therefore, the crystallite size could not be determined for this composition. The data shown in Fig. 6.2.3 have to be discussed as two sets of data obtained under different conditions. Whereas the pure IrO_2 was synthesised in an initially homogeneous phase of molten salts, samples with the electrocatalyst support represent a heterogeneous reaction system where the support participates in the synthesis as a solid phase. Pure IrO_2 has to overcome a significant energy barrier during nucleation of the first crystallites in the homogeneous liquid phase. Once the nucleation centres have formed, it is energetically favourable for the IrO_2 phase to deposit continuously on already existing crystallites. On the other hand, the presence of the electrocatalyst support introduces a high number of potential IrO_2 nucleation centres on the defects of its structure. Logically, pure IrO_2 forms larger crystallites when compared to the supported electrocatalysts.

Another interesting observation is that the smallest crystallites were observed for the 90 wt.% IrO_2 electrocatalyst. The higher the concentration of the support, the larger the crystallite size with pronounced enlargement starting at 50 wt.% IrO_2. The same trend has been reported elsewhere.[171] Such behaviour may be explained by the driving force for the nucleation of the IrO_2 phase: for the 90 wt.% IrO_2 electrocatalyst, the concentration of the iridium oxide precursor in the reaction system is the highest,

resulting in the formation of the highest number of nucleation centres. Therefore, it leads to the formation of smaller crystallites. With decreasing content of the iridium oxide precursor, this driving force, and thus the number of nucleation centres formed, decreases.

SEM and EDX analysis

SEM pictures of the TaC supported electrocatalyst containing 50 wt.% IrO_2 (Fig. 6.2.4) and the pure IrO_2 electrocatalyst (not shown) were recorded. The morphology of the two samples is similar, both showing IrO_2 present in the form of agglomerates ranging from 50 to 500 nm in diameter. Owing to the rounded shape of the agglomerates, the surface-to-mass ratio is relatively high, enabling high electrocatalytic activity. The homogeneity of the IrO_2 distribution is confirmed by the EDX element map (Fig. 6.2.5).

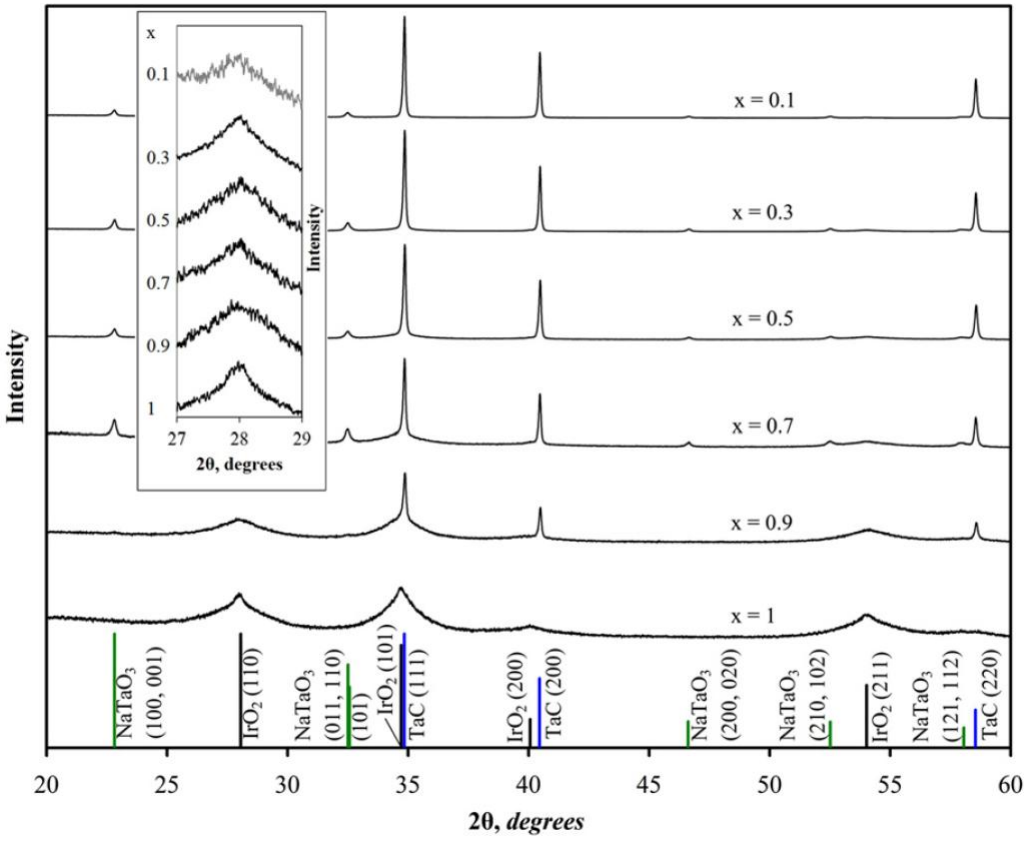

Fig. 6.2.2. X-ray diffractograms of electrocatalysts prepared with mass-based composition $(IrO_2)_x(TaC)_{1-x}$. Figures in parentheses indicate corresponding h, k, l Miller indices of the crystal planes. The inset graph shows zoomed region around 28° where the characteristic peak of IrO_2 has been used to calculate the crystallite size.[132]

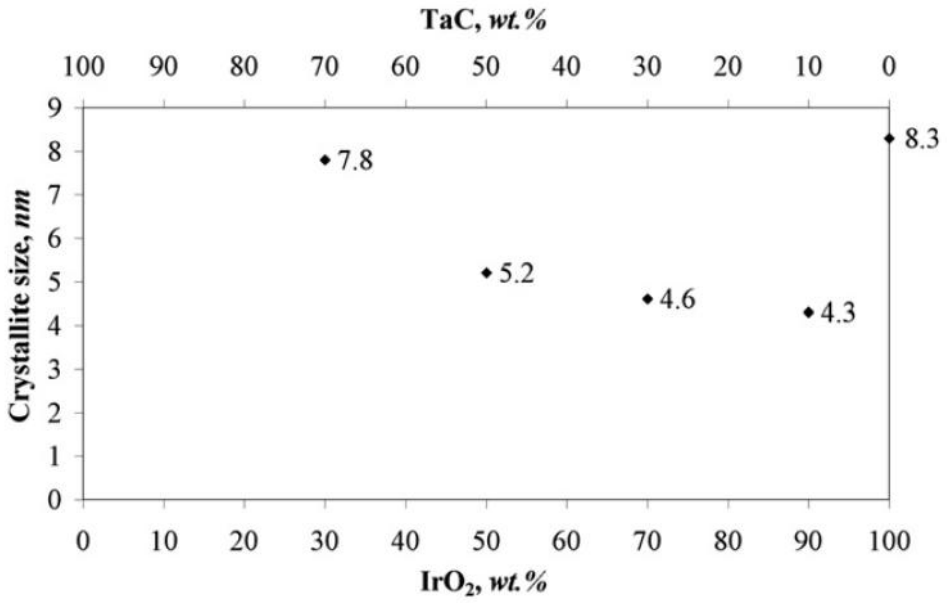

Fig. 6.2.3. Average crystallite sizes of the prepared electrocatalysts as calculated from the XRD spectra.[132]

The sodium content was determined to confirm the presence of the $NaTaO_3$ phase formed during Adams fusion and identified by XRD experiments. Homogeneous distribution over the support surface was proven (Fig. 6.2.5).

Specific surface area

Of the materials studied, pure IrO_2 had the highest specific surface area (SSA) of 121 m^2/g, while pure TaC had the lowest one at only 2.4 m^2/g for TaC after synthesis (Fig. 6.2.6) and 0.7 m^2/g as-received (not shown). The remaining samples followed the rule of mixing, i.e. the SSA was linearly dependent on the content of IrO_2 in the sample. No relation between crystallite size and SSA was observed. This was further confirmed by the SSA of the IrO_2 part in the supported electrocatalyst calculated from the known SSA of the support and composition of the sample. The results (Fig. 6.2.6) indicate no dependence on the size of the IrO_2 crystallites. From the SEM image (Fig. 6.2.4) and XRD analysis (Fig. 6.2.3), it can be concluded that the individual crystallites are 1-2 orders of magnitude smaller than the agglomerates. Since no relation between SSA and crystallite size was found, it is concluded that the agglomerates are not porous and the adsorbent gas cannot access inner surfaces. Furthermore, with respect to the size variations observed (Fig. 6.2.3), it appears that crystallite size does not influence the shape and morphology of the agglomerates and, therefore, does not affect the SSA.

Powder conductivity

First of all, when comparing the presented results with published data it should be kept in mind that powder conductivity is strongly dependent on the conditions under which it is obtained. This is because the transition resistance between the individual powder particles plays a decisive role. From this, it follows that the most important aspect is particle dimensions and compressive force. Therefore, for instance, for bulk TaC a conductivity of 23-34 $\times 10^3$ S/cm has been reported.[173] The conductivity of the as-received TaC powder used in this study was 118 S/cm. This difference is clearly due to the fact that TaC was used in powdered form. Compared to pure IrO_2 powder, which had a conductivity of 62 S/cm, the asreceived TaC powder was twice as conductive. Unfortunately, after synthesis, the conductivity of the TaC decreased by 10 orders of magnitude. Coming back to the above reported data, the drop in conductivity can be explained by the surface layer of a semiconductive $NaTaO_3$ formed during IrO_2 synthesis by Adams fusion. Since surface oxidation is directly linked to the use of this synthesis method, the employment of a different method may reduce or even prevent this drop in conductivity entirely. The dependence of materials-specific conductivity on its composition is summarised in Fig. 6.2.7. As shown in the logarithmic scale presented in the figure inset, the most pronounced conductivity increase occurs with the first IrO_2 addition to the support. This could be due to the interaction of the $NaTaO_3$ covering the support surface with Ir atoms, most probably directly during the fusion. Even though the increase in conductivity had already reached several orders of magnitude at this stage, sufficient conductivity values of at least 10% of the conductivity of pure IrO_2 were first obtained with an IrO_2 content of 50 wt.%. This corresponds to the formation of a conductive IrO_2 film covering the surface of the support.

Electrochemical characterization. Cyclic voltammetry

The cyclic voltammograms of the IrO_2-based electrocatalysts (Fig. 6.2.8) had the overall shape that has been reported by other researchers.[177,178] This shape is characterised by an absence of any well-defined peaks, although the total anodic charge recorded is related to the total number of active sites.[179] A reliable, generally accepted electrochemical method of determining the active area, as it has for example been established for platinum, has not yet been found for iridium oxide.

In the potential region between 0.4 and 1.2 V, the anodic and cathodic parts of the voltammograms display a high degree of symmetry. The predominant influence of IrO_2 on the voltammetric response of the electrode is indicated by the anodic-to-cathodic charge ratio (Q_a/Q_c) being close to unity.[180] In our study this charge was obtained for the potential range between 0.4 and 1.2 V, where the polarisation curve is not influenced by gas evolution reactions or adsorption processes. Polarisation curves obtained at a scan rate 500 mV/s were used to obtain higher current densities and thus a lower relative error of the experimental data.

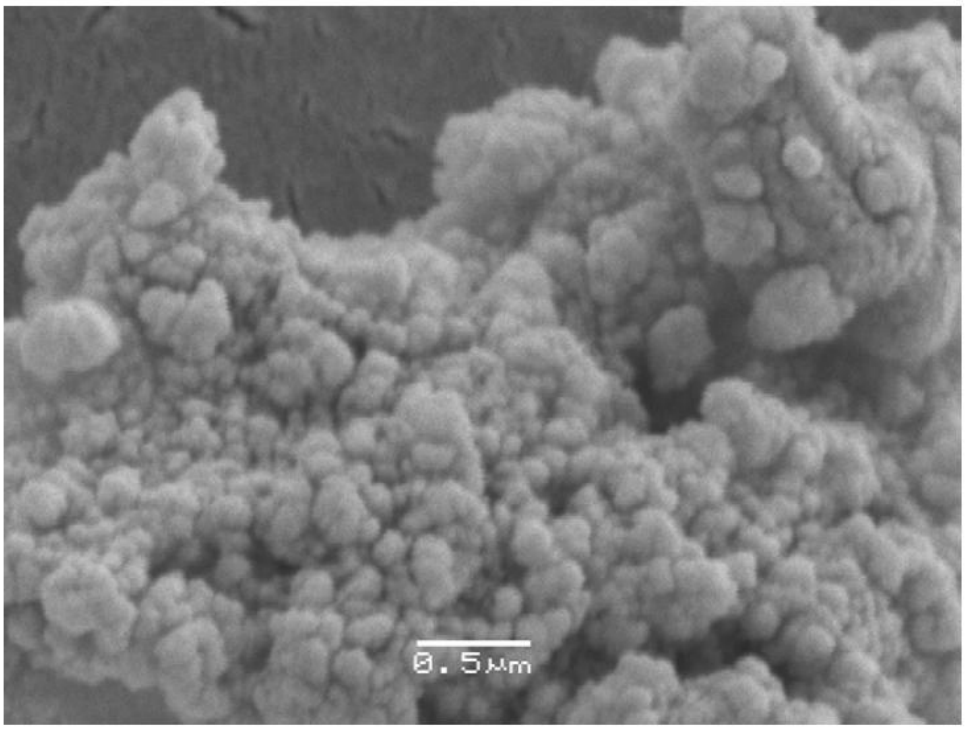

Fig. 6.2.4. Detailed SEM image of 50 wt.% IrO2 electrocatalyst. Accelerating voltage 10 kV, working distance 7 mm.[132]

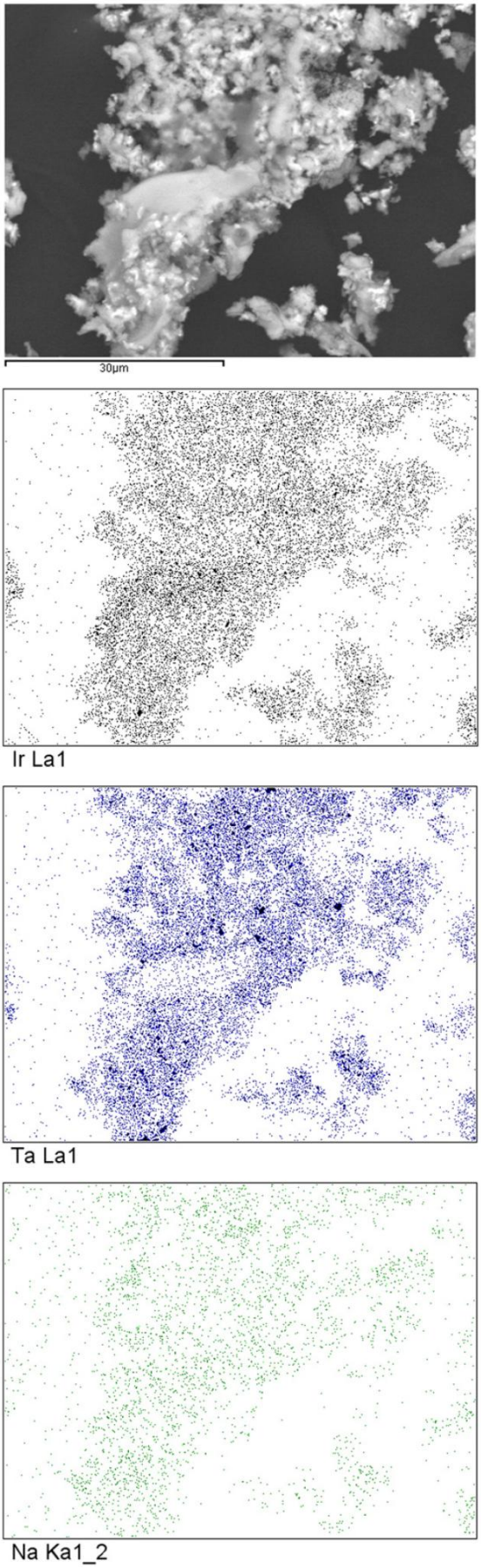

Fig. 6.2.5. SEM/EDX element map for 50 wt.% IrO_2 electrocatalyst (Under each map element and detector mode are presented.).[132]

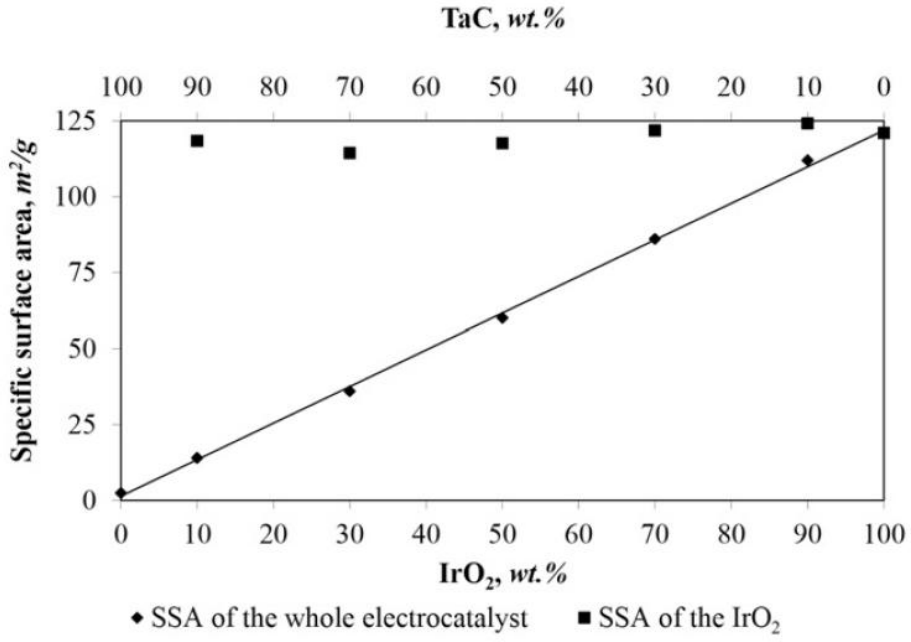

Fig. 6.2.6. BET specific surface area of the prepared electrocatalysts.[132(A12)]

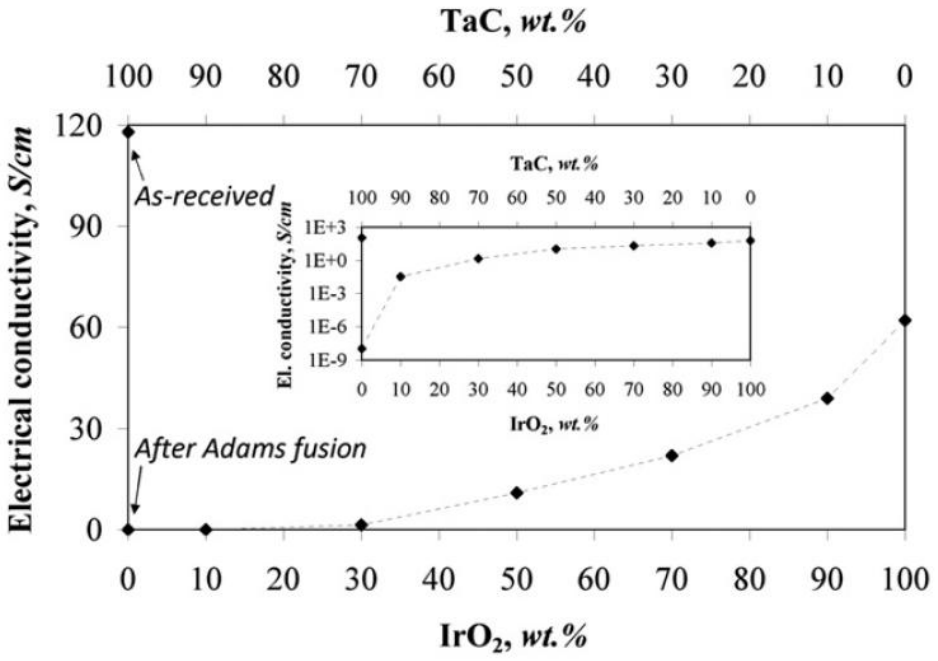

Fig. 6.2.7. Powder conductivities of the prepared electrocatalysts. The inset graph shows conductivities with a logarithmically scaled y-axis.[132]

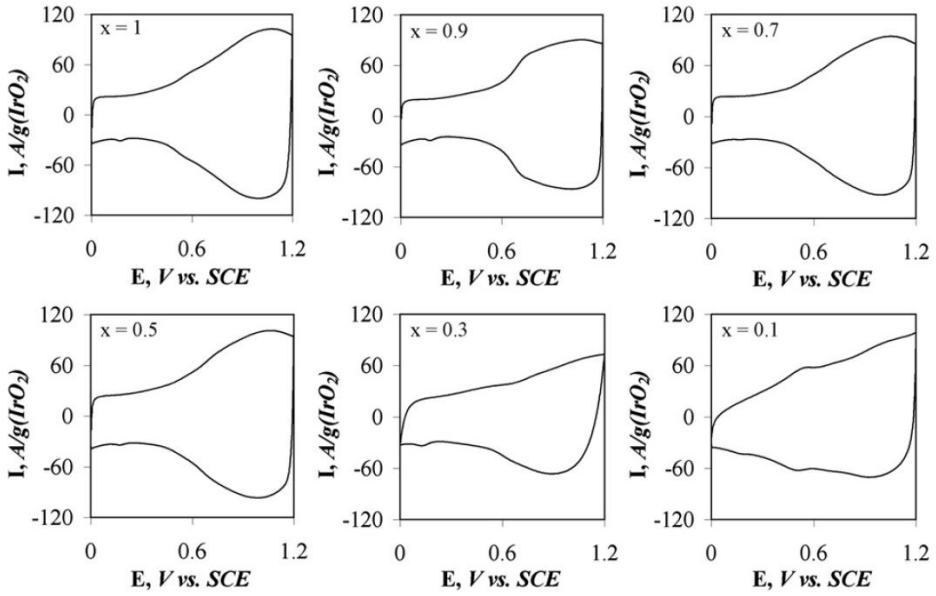

Fig. 6.2.8. Cyclic voltammograms normalised to IrO_2 mass-specific current. Mass-based compositions correspond to general formula $(IrO_2)_x(TaC)_{1-x}$. Potential sweep rate 500 mV/s, 0.5 M H_2SO_4 at room temperature.[132]

The results are summarised in Fig. 6.2.9. They are in agreement with the work of Marshall et al.[171], who observed that the higher the scan rate, the higher the differences between the charge ratios of the electrocatalysts being compared. In the present case, the ratio value was close to unity for electrocatalysts with 50 wt.% of IrO_2. The ratio was very close to that of pure IrO_2.When the content of the IrO_2 was reduced below 50 wt.%, the ratio increased, indicating enhanced interaction of the support with the electrolyte. This result correlates well with the conductivity measurements.

Tafel experiments

Steady-state linear sweep voltammetry was used to determine the Tafel slopes for the individual electrocatalysts (Fig. 6.2.10). Tafel slopes are an indicator of electrocatalyst quality: the lower the Tafel slope, the faster the kinetics of the reaction and the more active the electrocatalyst (under constant electrocatalyst load conditions). Electrocatalyst activity towards oxygen evolution as a desired electrode reaction was measured.

In acidic electrolyte, several possible reaction mechanisms of the oxygen evolution reaction have been proposed.[180,181]

The Tafel slope cannot be used to directly identify the reaction pathway, but it may be used to determine the rate-determining step in an assumed mechanism. However, this

is not straight forward as the transfer coefficient in the kinetic equations is usually not known and the considered value of 0.5 is not necessarily accurate under the conditions studied.[181]

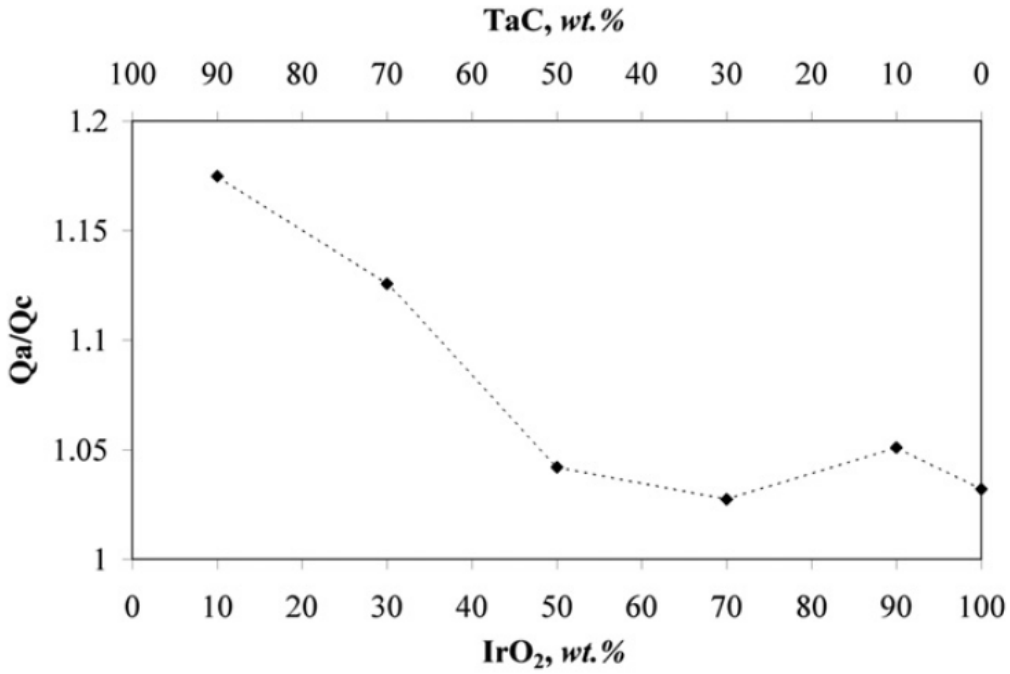

Fig. 6.2.9. Ratio of anodic-to-cathodic charge between 0.4 and 1.2 V. Potential sweep rate 500 mV/s, 0.5 M H_2SO_4 at room temperature.[132]

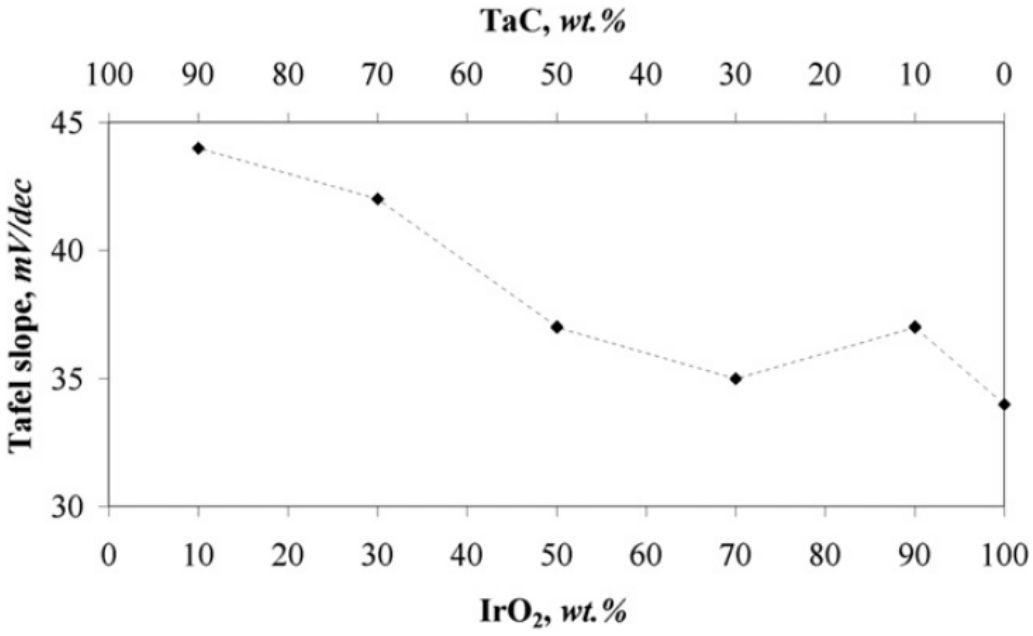

Fig. 6.2.10. Tafel slopes of the prepared electrocatalysts. From linear part of the polarisation curve in Tafel plot between 1.1 and 1.3 V. Potential sweep rate 1 mV/s, 0.5 M H_2SO_4 at room temperature.[132]

A Tafel slope of 30 mV/dec points to the second step in the "oxide path", reaction (6.2.4),[182] and a Tafel slope of 40 mV/dec suggests that the second step in the "electrochemical oxide path", reaction (6.2.6),[182] is rate-determining.
Oxide path[181]:

$$S + H_2O \rightarrow S\text{-}OH + H^+ + e^- \quad (6.2.3)$$

$$2S\text{-}OH \rightarrow S\text{-}O + S + H_2O \quad (6.2.4)$$

$$2S\text{-}O \rightarrow 2S + O_2 \quad (6.2.5)$$

The electrochemical and oxide paths have identical steps (6.2.3) and (6.2.5). They differ in step (2), which in this case can be described by reactions (6.2.4) and (6.2.6)[181]:

$$S\text{-}OH \rightarrow S\text{-}O + H^+ + e^- \quad (6.2.6)$$

Again, when the IrO_2 content ranged from 50 to 100 wt.%, the Tafel slopes obtained were similar for all electrocatalysts under study (34-37 mV/dec). But when the IrO_2 concentration was 10 or 30 wt.%, the Tafel slope increased to above 40 mV/dec, indicating a different rate-determining step. This increase correlates with the conductivity and cyclic voltammetry measurements. A similar effect was also observed by Marshall et al..[171]

6.3. WC as a non-platinum hydrogen evolution electrocatalyst for high temperature PEM water electrolysers

Introduction

PEM electrolysers have more requirements for the components, especially for the electrocatalysts, where in contrary to alkaline systems, noble metals and their oxides present the state of art for PEM technology.Therefore there is an evident need for non-noble alternative materials both for the oxygen and hydrogen electrodes.
One of the approaches includes the use of WC as a support for the platinum electrocatalyst, as their common catalytic properties are attributed to similarities in the electronic structures.[183,184]

However, this approach still does not solve a problem of the HER electrocatalyst, as the reserves of platinum are limited and the demand for this material is increasing due to rapid development of PEM fuel cells and electrolysers.

Therefore, it is essential to find an alternative material It has been shown earlier, that the catalytic behaviour of tungsten carbide is "platinum-like", which is not found for metallic tungsten.[185] This behaviour was explained by the change of the surface electronic properties of the lattice in the way, where they resemble those of platinum. Therefore, WC shows outstanding performance in several reactions of organic synthesis, substituting platinum.[185] Even though, attempts are being made to find a substitution for platinum with a cheaper metal electrocatalyst for the HER in PEM water electrolysers,[186,187] none of the possible candidates have found any commercial application. It can be connected with the fact that most of research of alternative electrocatalysts for the HER is done at room temperatures, even for those materials, which are intended to be used at elevated temperatures in such systems like PEM water electrolysers.[188]

Investigations on the WC electrocatalytic activity in hot phosphoric acid solutions have been done previously.[189] However, the catalytic activity of tungsten carbide was not tested for the HER in this electrolyte and a comparison with the platinum electrode was not done. However, it was reported that WC exhibits good stability in acidic media.[183] It is higher for stoichiometric WC, than for W_2C.[190] Therefore, in our work tungsten monocarbide was prepared and investigated.

A plasma synthesis method was used, followed by carburization. The effect of temperature on the electrocatalytic activity of WC for the HER was investigated and compared with the effect of temperature on the behaviour of Pt electrocatalyst.

Experimental part

The powder electrocatalyst was produced by means of the original method, developed at the Baikov Institute of Metallurgy and Material Science of Russian Academy of Science.[191]

The powder was synthesized using an experimental plasma reactor based on a DC plasma torch with up to 20 kW capacity that ensures generation of the thermal plasma jet with up to 20 MJ/kg bulk enthalpy.

Tungsten carbide nanopowder was synthesized using WO_3 as a precursor and CH_4 as a carburizing agent, which was introduced in the plasma jet along with WO_3. This was

followed by heat treatment in hydrogen of the produced nanopowders.[192-196] The synthesized mixed nanopowder of W, W_2C, WC_{1-x} compositions was further subjected to heat treatment under hydrogen for the production of monocarbide WC. The powder, produced in the plasma process was characterized using a number of techniques. X-ray phase analysis was performed on the DRON-3M diffractometer. Powder specific surface area was measured with the use of the Micrometrics TriStar 3000 specific surface and porosity analyzer. The surface imaging was done on JEOL transmission and scanning electron microscopes. The total and free carbon content was determined on the LECO CS-400 analyzer.

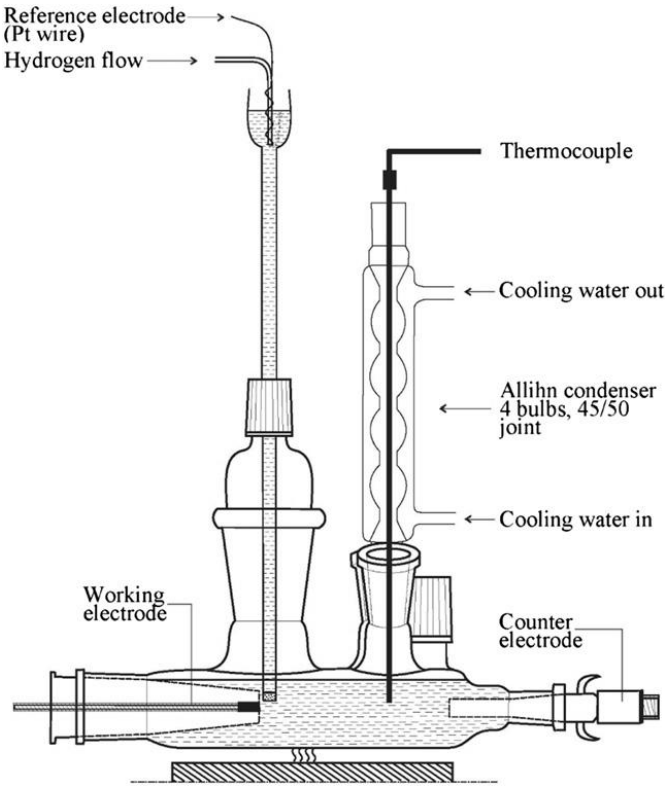

Fig. 6.3.1. The scheme of the electrochemical cell, used to characterize the behaviour of WC electrode.[133]

The electrochemical performance of the prepared electrocatalyst powder was estimated from the cell, shown in Fig. 6.3.1. The working electrode was the same, as used in Ref.131 and consisted of a tantalum cylinder, accurately embedded in a Teflon/PTFE body. The diameter of the cylinder was 7.5 mm, which corresponded to the active surface area of the electrode of 0.44 cm^2. The surface of the electrode was polished prior the experiment with silicon carbide abrasive paper, followed by polycrystalline diamond powder (Struers A/S, Denmark) with a particle size less than 0.25 μm. Afterwards, the surface was degreased with acetone and rinsed with

demineralized water, after which a WC electrocatalyst suspension was prepared by adding a 10 mg portion of the powder to 1 mL of demineralized water. The suspension was then dispersed in an ultrasonic bath for 1 h (model Branson 1510). Immediately after that, a 40 μL portion of the suspension was applied on the surface of the electrode, followed by drying of the electrocatalyst layer under nitrogen protective atmosphere. Thus, the loading of the active electrocatalyst on the electrode was 400 μg. A second suspension, consisting of a 1% solution in water of commercial 5 wt.% Nafion® (by DuPont) was applied on top of the catalyst layer and dried in the same manner. The application of the second layer was used in order to fix the loose powder of the catalyst on the plain surface of the tantalum electrode.

The three-electrode cell, used in this study was able to withstand temperatures up to at least 200°C and the heating of the cell was provided by an external heating plate. A commercial platinum counter electrode was provided by Radiometer Analytical SAS. Hydrogen gas was bubbled through a platinum wire electrode, and was connected through the Luggin capillary and served as a pseudo-reference electrode with potential -0.077 V vs. SHE (to which the values are further referred). The concentrated 85% phosphoric acid was used as an electrolyte in this work.

The cyclic voltammetry experiments were performed in the potential window between -0.227 and 0.273 V vs. the Standard Hydrogen Electrode (SHE). The scan rate was 1 mV/s in all experiments. The range of temperatures was from room temperature (ca. 22°C) to 80°C, 120°C and 150°C, with the experiments performed from lower to higher temperatures. The temperature deviation during the experiments was within ±3°C. Temperature was controlled by a k-type thermocouple, covered with Teflon PTFE (by Omega Co.) and inserted into the working cell. VersaSTAT 3 potentiostat and VersaStudio software by Princeton Applied Research were used in our research.

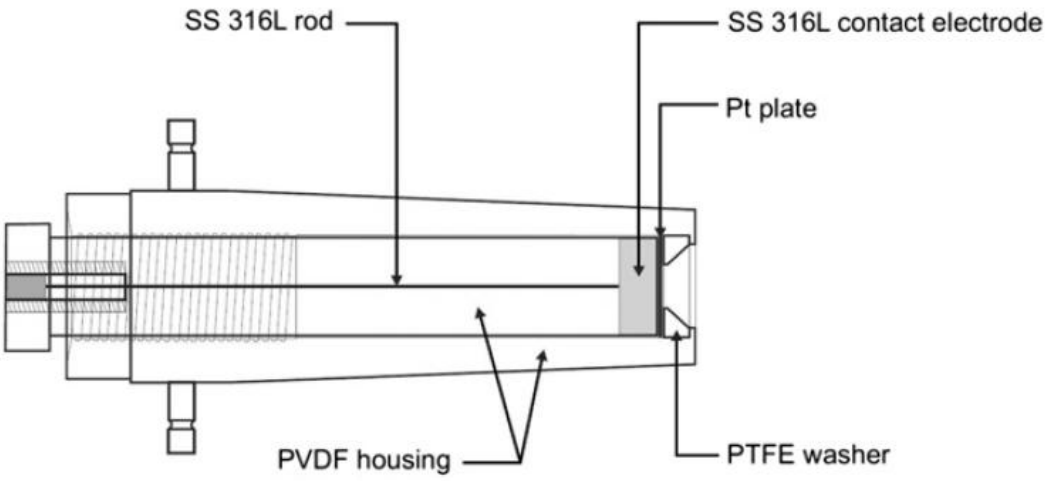

Fig. 6.3.2 The electrode, used for characterization of electrocatalytic behaviour of a Pt plate.[133]

The Pt electrode was made from platinum foil (by Good Fellow Cambridge Limited, England), with thickness 0.1 mm and was cut into a round plate of 15 mm in diameter.

The Pt plate was mounted in the electrode holder, presented in Fig. 6.3.2 and protected from penetration of electrolyte by the PTFE washer, having 6 mm opening, as shown in the drawing. The electrode holder was made from the Symalit PVDF 1000 plastic, provided by Vink Plast A/S (Denmark). It was then used in the cell, earlier depicted cell on Fig. 6.3.1.

Results and discussion

Based on the TEM image of plasma synthesis products, it is established that they are nanopowders with the maximum size of the particles reaching 20 nm (Fig. 6.3.3), which can also be confirmed by SEM image (Figs. 6.3.6, 6.3.7). BET measurements have shown a specific surface area of 27 m^2/g. It can also be seen from the TEM results, that a carbon layer is present on the surface of the tungsten particles. The WC particles were found smaller in size, than in earlier published works.[197] The yield of nanopowder was 95-98% relative to tungsten trioxide input. According to X-ray phase analysis results, nanopowders consist of the W, W_2C, WC_{1-x} mixtures (Fig. 6.3.5). Chemical analysis shows the presence of free carbon. The total carbon content in the nanopowders was 6.5 wt.% and the free carbon content was 3.3 wt.%. The main parameter determining the total carbon content in the nanopowders is the initial atomic element ratio C/W and initial WO_3 flow rate.

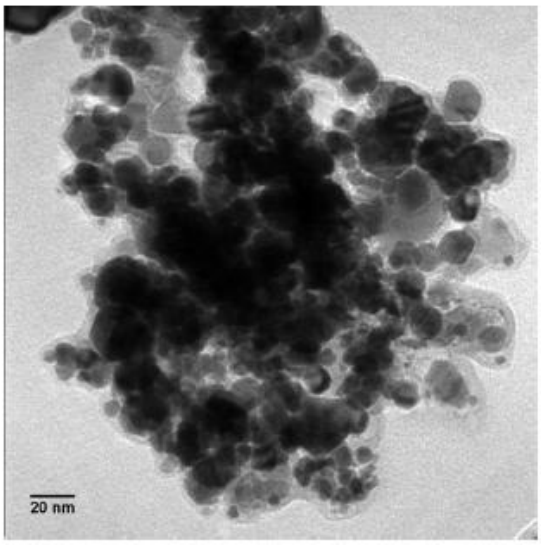

Fig. 6.3.3.TEM image of W-C system nanopowder, produced in plasma reactor, before carburization.[133]

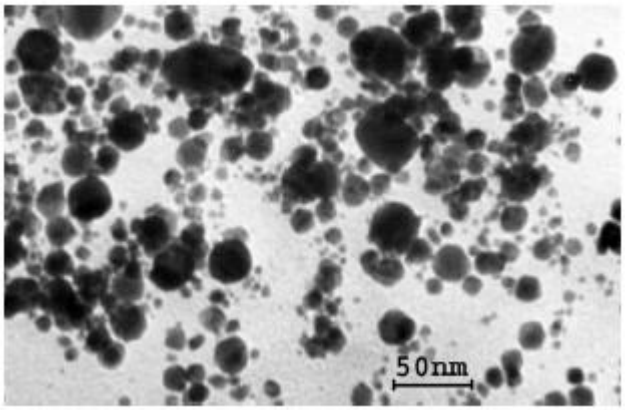

Fig. 6.3.4. TEM image of WC powder, produced in plasma reactor, after carburization.[133]

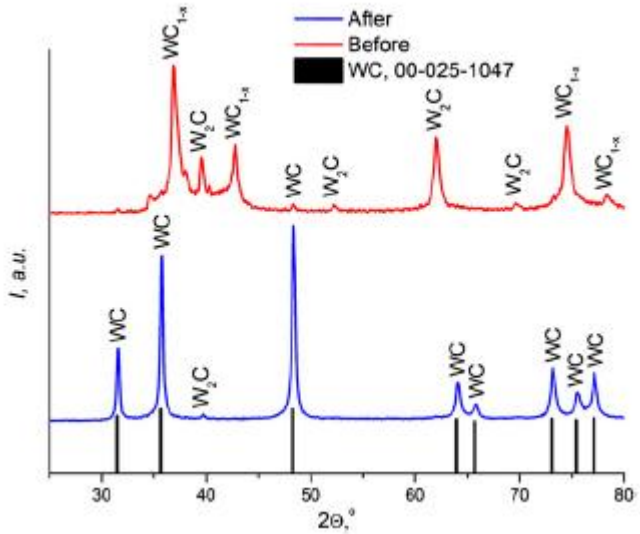

Fig. 6.3.5. XRD patterns for W-C nanopowders before and after carburization.[133]

The specific surface value of nanopowders correlates with the total carbon content: nanopowders with the larger carbon content have the larger specific surface values. The produced multiphase nanopowders were subjected to heat treatment in hydrogen at 900-1150°C. The goal of this treatment was to produce tungsten monocarbide WC nanopowder using carburization with attendant carbon of tungsten nanoparticles and its lower carbides. Consequently, hexagonal tungsten monocarbide powders with the main phase content up to 98 wt.% and specific surface value in the range of 6.8 m^2/g were produced. This related to the average particles size about 55 nm (Figs. 6.3.4 and 6.3.7). As it was shown in Ref.131, the tantalum support of the tested electrocatalyst is electrochemically inactive at studied conditions, and therefore has no effect on the electrochemical data. In Fig. 6.3.8, the dependence of the voltammetric behaviour of Pt electrode on temperature is demonstrated.

The catalytic activity of platinum increases with temperature. In order to evaluate the relative increase of activity during the steady state polarization, the current densities were compared at the fixed potential of -0.15 V vs.SHE and the data is presented in Fig. 6.3.10. It can be seen from Fig. 9.3.9, that hydrogen reduction takes place at the WC electrode. It means that WC acts as a catalyst in the lectrochemical reduction. Similar to the Pt electrode, there is an increase in current density (i.e. activity of the catalyst) at -0.15 V with temperature (Fig. 6.3.10).

However, below 150°C, the electroreduction of the protons at the WC electrode takes place at more negative potentials (with more overpolarization), than at the Pt electrode (Figs. 6.3.8 and 6.3.9).

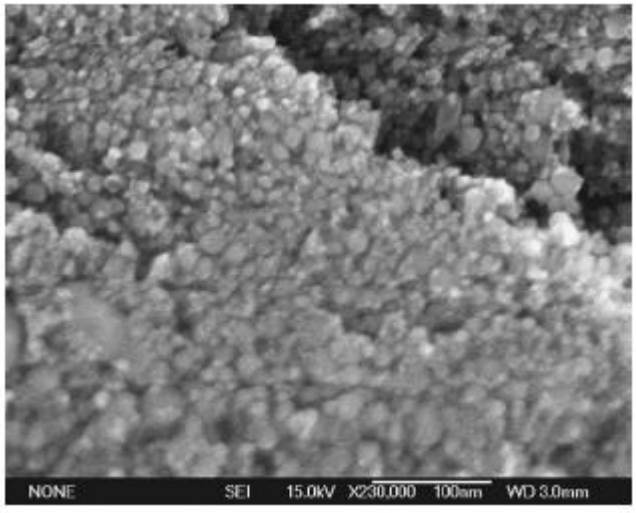

Fig. 6.3.6. SEM image of W-C powder, produced in plasma reactor, before carburization.[133]

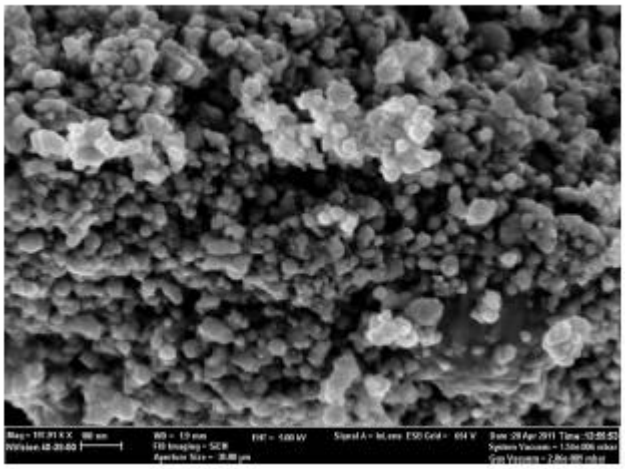

Fig. 6.3.7. SEM image of WC powder, produced in plasma reactor, after carburization.[133]

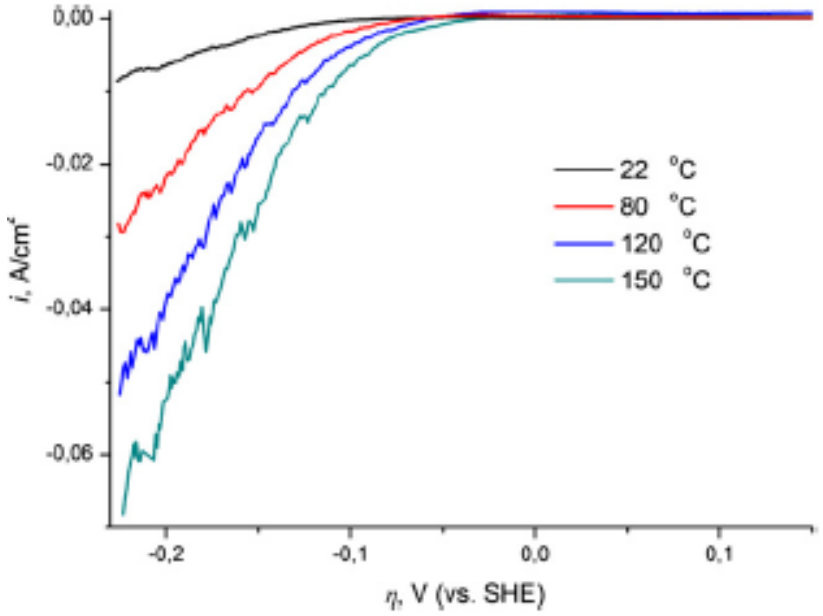

Fig. 6.3.8. Steady-state voltammetric curves obtained at the platinum electrode in 85% phosphoric acid at 22, 80, 120 and 150°C (potential scan rate 1 mV/s).[133]

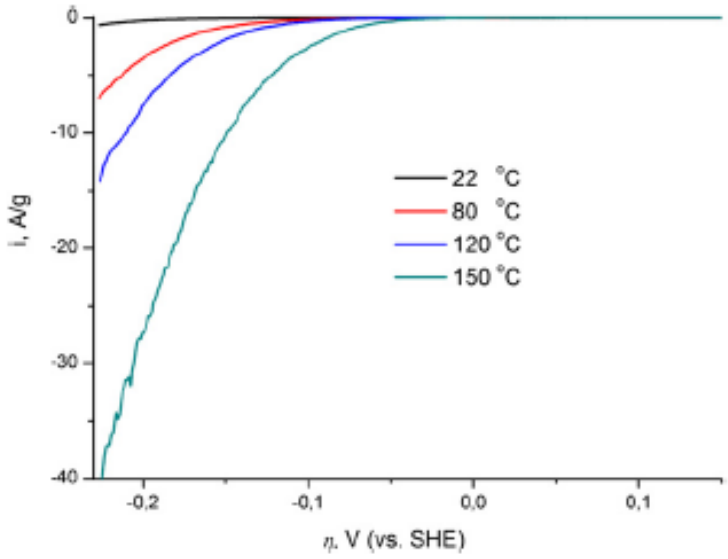

Fig. 6.3.9. Steady-state voltammetric curves obtained at the WC electrode in 85% phosphoric acid at 22, 80, 120 and 150°C (potential scan rate 1 mV/s).[133]

At 150°C the WC electrochemical activity changes dramatically, approaching the Pt activity. It can be seen from comparison of the potentials of hydrogen reduction at the WC and Pt electrodes. But it is especially evident from Fig. 6.3.10: the growth of the WC catalytic activity at 150°C is much more significant for WC than for Pt. More precise calculations of the electrocatalytic activity (the values of the exchange current density) of the WC and Pt electrodes and the equilibrium potentials of the hydrogen reduction at these electrodes can be obtained from the Tafel curves (Figs. 6.3.11 and 6.3.12). The results of the calculations are presented in Table 6.3.1 and in Fig. 6.3.13. The most important fact here is the decrease in Pt catalytic activity when the temperature is changed from 120°C to 150°C, and the dramatic increase of WC activity at the same time. As a result, at 150°C the relative development of electrocatalytic activity of WC is higher than that of Pt at 150°C. This fact is in agreement with more positive potential of the hydrogen electroreduction atWC than that at Pt (Table 6.3.1). It should be noticed, that for WC, the development of the position of the equilibrium potential for HER is not linearly dependent on temperature in the studied temperature range (Fig. 6.3.11). It can be due to the different reaction mechanism for the HER, taking place at 80°C and 120°C. This fact needs further investigation.

The values of the exchange currents were calculated from the Tafel plots and the relative development of exchange current densities both for the Pt and the WC electrodes can be found in Fig. 6.3.13. It can be seen that the relative increase of values of exchange currents is more significant for the WC electrode. Equally, as in Fig. 6.3.10, the relative difference in development of activity starts to differ considerably after 80°C and reaches its highest values at 150°C.

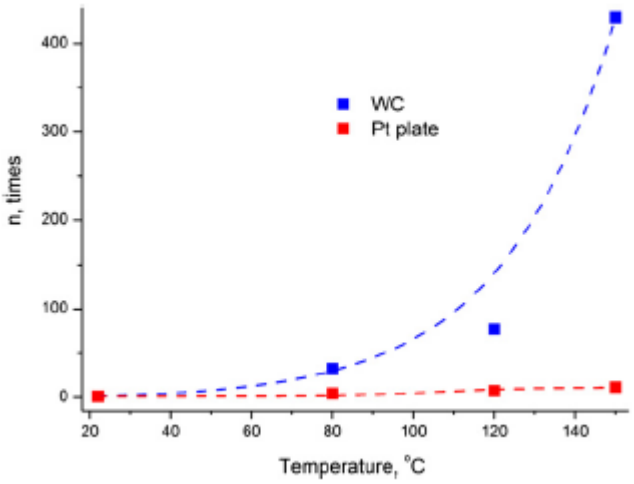

Fig. 6.3.10. Relative growth of current density (at -0.15 V) for the WC and Pt plate electrodes. n stands for the relative increase of i at specific temperature vs. i at 22°C. Calculated from data, presented in Figs. 6.3.8 and 6.3.9.[133]

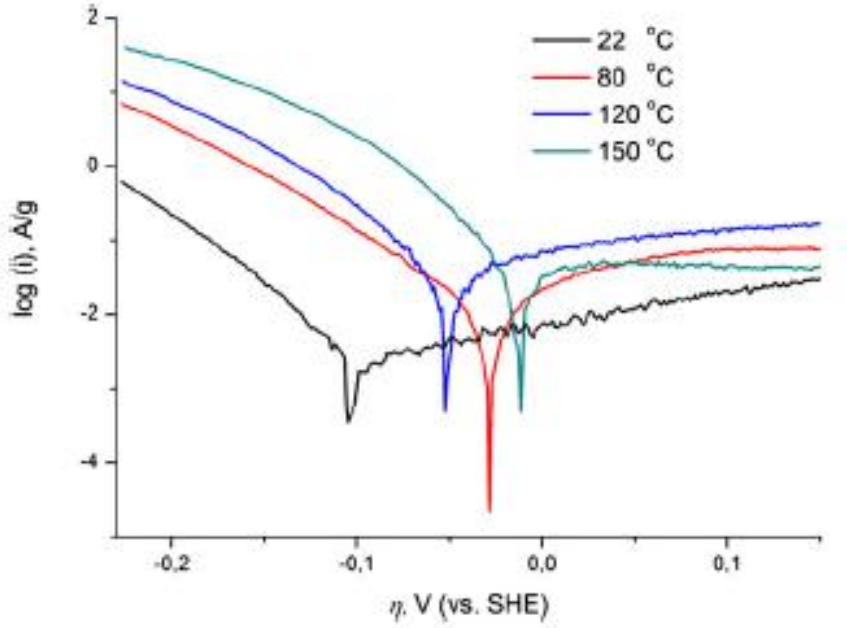

Fig. 6.3.11. Tafel curves obtained for WC electrode at different temperatures. 85% phosphoric acid, scan speed 1 mV/s.[133]

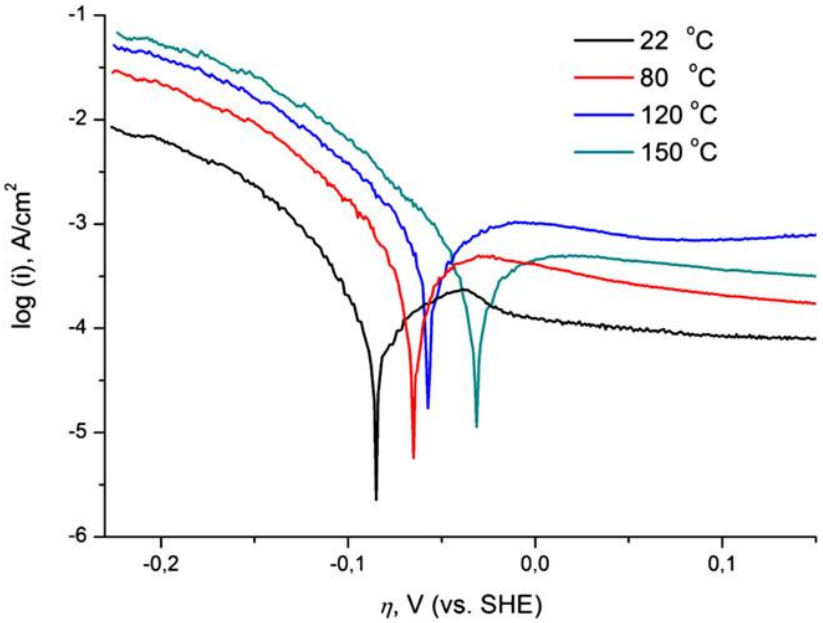

Fig.6.3.12. Tafel curves obtained for platinum electrode at different temperatures. 85% phosphoric acid, scan speed 1 mV/s.[133]

Table 6.3.1. The HER reversible potentials at different temperatures for WC and Pt electrodes.

	Reversible potential, mV vs. SHE			
Temperature, °C	22	80	120	150
WC powder	-105	-28	-50	-11
Pt plate	-85	-65	-57	-31

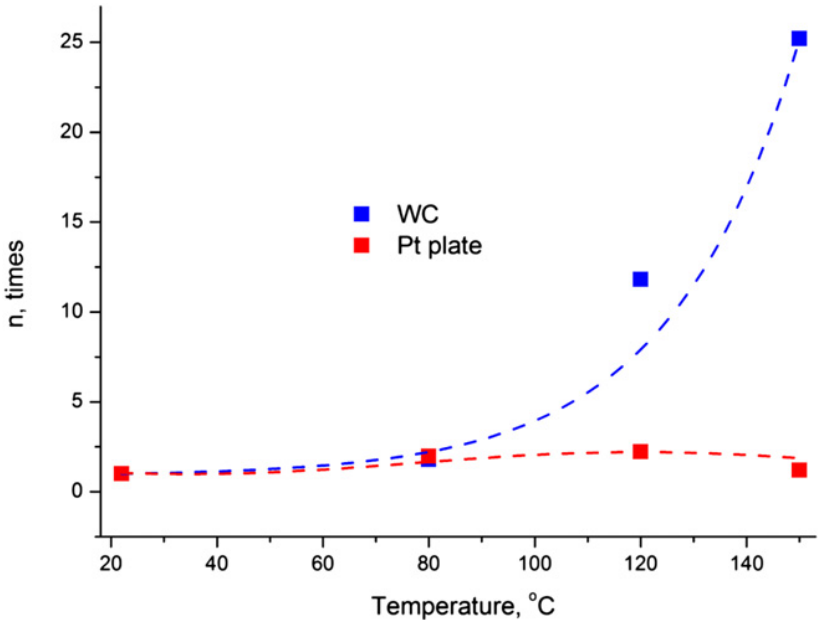

Fig. 6.3.13. The relative development of exchange current densities for the WC and Pt plate electrodes towards the HER with temperature. n stands for the relative increase of I at specific temperature vs. ***i*** at 22°C. Calculated from data, presented in Figs. 6.3.11 and 6.3.12.[133(A13)]

7. TRANSITION METAL CARBIDES (WC, Mo_2C, TaC, NbC) AS POTENTIAL ELECTROCATALYSTS FOR THE HYDROGEN EVOLUTION REACTION (HER) AT MEDIUM TEMPERATURES

.

Introduction

By efficiently converting electricity to chemical energy, many of the current problems of energy storage could be solved and hydrogen produced from water electrolysis is generally considered to be the essential platform molecule for this approach.[198,199] It can on the one hand drive electric engines by fuel cells[200-202] and on the other hand it can be employed as a reactant for the production of more complex molecules such as methane[203-204] or ammonia.[205-207] So far, large scale water electrolysis was commercially not interesting because of too high production costs. Efficient acidic electrolysis can only be performed when suitable electrocatalysts are applied for both the hydrogen (HER) and oxygen (OER) evolution reactions, lowering kinetic barriers. The best known catalysts unfortunately are scarce and expensive metals, namely Pt and IrO_2 or RuO_2 for the HER[208,209] and the OER[210,211] , respectively. Since catalyst prices contribute significantly to the overall operating costs of acidic electrolysers, considerable efforts are being made to find alternative electrocatalysts based on more abundant elements.[212,213]

Transition metal carbides are amongst the most often proposed replacements for the Pt cathode catalyst for the HER.[214] Most established is probably WC since it was first demonstrated for HER use already in 1964.[215] In water, WC is passivated by a WO_3 layer[216] but only anodic potentials > 0.7 V (vs. SHE) lead to bulk oxidation.[217-220] The WO_3 formed dissolves slowly in H_2SO_4 solutions[221,222] and faster in presence of PO_4^{3-} anions by the formation of heteropolytungstates.[223,224] Under anodic potentials, WC electrodes consequently degrade; under cathodic potentials however, the surface is essentially free from WO_3 in these electrolytes. Chen *et al.* extensively studied the surface chemistry of carbides and found that the HER activity of WC increases significantly by Pt or Pd addition.[225,226] One monolayer of Pt on WC exhibited the same overpotential as bulk Pt.[183,227,229] The activity of pure WC is thereby not influenced by small amounts of surface carbon (1-2 monolayers), only thicker layers result in a decreased HER performance.[229]

Besides its influence on supported Pt[230,231], pure WC was found to be a promising HER catalyst by itself. In a screening approach of various transition metal carbide, nitride, sulphide, silicide and boride powders in 100 mM H_2SO_4 solution by Schröder *et al.*, WC was found to be the most active non-Pt HER catalyst.[232] In the past, the same group investigated catalysts with mixed phases of WC, W_2C, W and WO_2 and could correlate HER activity to the WC content.[224] The other phases were attributed to be of minor importance. Later, nanocrystalline WC was found to have a low HER overpotential of -75 mV (vs. RHE) in 0.5 M H_2SO_4.[233]

Due to its chemical similarity to WC, also Mo_2C has attracted considerable attention for electrocatalysis applications. It has been employed in the HER as mixed W-Mo carbide[234], as bulk Mo_2C[235,236] as well as supported on graphtic carbon[237] or carbon nanotubes.[238] No HER data on pure TaC and NbC are available beside the screening of Schröder *et al.*.[233] These carbides showed less activity than WC and Mo_2C.

The HER activity of transition metal carbide catalysts strongly depends on the reaction temperature as was shown by a WC catalyst in 85% H_3PO_4 solution.[133] In the range of 25 °C to 150 °C, the HER activity of WC increased significantly. Generally, the reversible cell voltage of water electrolysers decreases with increasing temperature due to the positive entropy of the water splitting reaction.[239] Medium temperature (200-400°C) acidic electrolysis benefits on the one hand from these thermodynamic and additional kinetic advantages and on the other hand avoids the disadvantages (rapid degradation off cell components) of solid oxide electrolyser cells, operating at 600-900°C. Since commonly used electrolytes for polymer electrolyte membrane (PEM) electrolysers (e.g. Nafion®) are no longer stable under the medium temperature conditions, many new electrolytes have been explored.[240-243] Promising results were especially obtained with the solid acid CsH_2PO_4.[244,245] Its proton conductivity however strongly depends on many parameters such as temperature and humidification.[246] Electrocatalytic measurements with powder electrodes consequently are often only hardly comparable because of too many influencing factors.

In our work, we reported our approaches to meet these challenges connected with the measurement of intrinsic electrocatalytic properties of various transition metal carbides for the HER at intermediate temperature. First, molten KH_2PO_4 was applied as electrolyte for the simulation of solid acid CsH_2PO_4 membranes at elevated temperatures. Second, by using coated transition metal wires as electrodes

we aimed to assess the intrinsic electrocatalytic properties of the catalysts in a better way than by powder catalysts. Ohmic losses due to contact problems are significantly reduced. The temperature range for the HER can be extended to 260 °C this way. So far, measurements on carbide catalysts have been limited by the boiling point of 100% H_3PO_4 to 185 °C.[247]

Experimental

Carbide coating of transition metal wires

Carbide coating of transition metal wires with the respective carbides was performed by temperature programmed reduction of a pre-oxidised metal surface layer. W, Mo, Ta and Nb wires (ChemPur GmbH, Germany, ∅ = 1 mm) have been treated with a mixture of 20% O_2 in Ar at 700 °C (W), 600 °C (Mo), 550 °C (Ta) and 450 °C (Nb), respectively for 3 h (5 K min^{-1} heating rate), followed by carburization with a mixture of 25% CH_4 in H_2 at 950°C (Ta), 900°C (W, Nb) and 750°C (Mo) for 3 h (5 K min^{-1} heating rate).

Material characterisation

For X-ray diffraction analysis of wire coatings, the outer layer of the wires was removed mechanically and grounded. The obtained powders were analysed using a STOE Stadi P diffractometer with Cu $K\alpha_1$ irradiation in the range of 10 to 70°2θ. Optical microscopy images were obtained by the use of a Celestron HDM Pro handheld microscope.

For scanning electron microscopy (SEM), cross-sections of wire samples have been prepared by mounting small wire pieces in a PolyFast phenolic hot mounting resin with a carbon filler, provided by Struers A/S (Denmark). The embedded wires were polished using SiC abrasive paper. SEM measurements of the cross-cuts were performed on a Carl Zeiss EVO MA10 microscope.

Electrocatalytic testing

Electrochemical measurements were performed in molten KH_2PO_4 (Sigma Aldrich, p.a.) in air atmosphere. A thermocouple inside the electrolyte melt assured accuracy of the applied temperature of 260°C.[248] A Pt wire, sealed in a Pyrex tube, was employed as a counter electrode and an Ag wire, placed in a Pyrex chamber with molten, Ag_2SO_4saturated, $KHSO_4$ and fritted bottom (grade 4) was used as a reference electrode.

The coated transition metal wires, used as working electrodes, were sealed in alumina tubes, using CC180W coating paste provided by CeProTec (Germany) as shown in Fig.7.1. Voltammetric measurements were performed with a VersaSTAT 3 potentiostat by Princeton Applied Research at a scan rate of 1 mVs^{-1}. A Pt wire provided by Dansk Aedelmetal (Denmark) with a diameter of 0.4 mm was used for comparison of catalytic activities.

Results and Discussion

Preparation and characterisation of transition metal carbide coated wires

For the coating of transition metal wires with the respective carbides, a two-step approach was pursued and optimised for the various metals and carbides. First, the wires were subjected to treatment under 20% O_2 in Ar for 3h for surface oxidation. It was found that appropriate temperatures were 700 °C for the oxidation of W to WO_3 and 600 °C for Mo oxidation to MoO_3. The group V metals Ta and Nb were oxidised at 550 °C and 450 °C, respectively (5 K min^{-1} heating rate in all cases). As can be seen on the optical micrographs in Fig. 7.2, the colour of the metal wires changed during oxidative treatment. The metallic shine of the metals is lost in all cases and homogeneous layers of yellow WO_3 and white Ta_2O_5 and Nb_2O_5 can be observed.

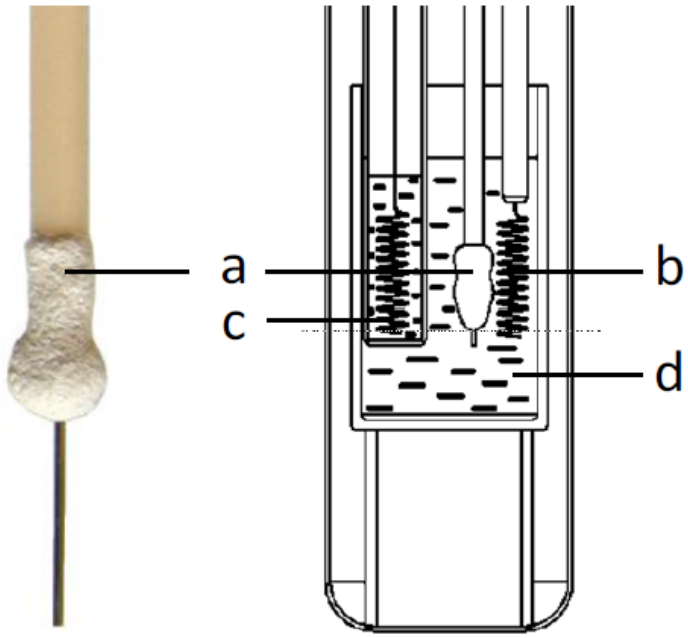

Fig. 7.1. Schematic representation of the electrolysis setup: a) working electrode, b) counter electrode (Pt), c) reference electrode (Ag/Ag_2SO_4 in $KHSO_4$) and d) electrolyte (molten KH_2PO_4).[134]

Yellow MoO_3 cannot be seen, the reason being a thinner oxide layer on the Mo wire than on the other ones. A thicker MoO_3 layer could not be obtained by increasing the reaction temperature. MoO_3 started to sublimate at 650°C and precipitated in form of yellow needles in colder parts of the used tube furnace. At 700°C, the Mo wire was quantitatively oxidised, going along with complete loss of the wire shape.
The temperatures for the conversion of the oxide layers to the respective carbides were optimised by analogously carburizing oxide powders. Quantitative carbide formation was obtained at 950 °C for TaC, 900 °C for WC and NbC and 750 °C for Mo_2C. During the carburization treatment, the surface colour of the wires changed to gray (Mo_2C, TaC) or black (WC, NbC), implying successful oxide-carbide conversion.
For phase analysis of the prepared carbide coatings, the outer layer of each wire was mechanically removed and ground. XRD was measured on the resulting powders; the results are shown in Fig. 7.3. The obtained diffraction pattern of each wire and the respective reference pattern are in excellent agreement. No crystalline impurities can be detected for any of the coatings. The high reflex intensities indicate good crystallinity of the samples. As apparent from the very similar diffraction patterns of TaC and NbC, both carbides exist in the same crystal structure which is of rock salt

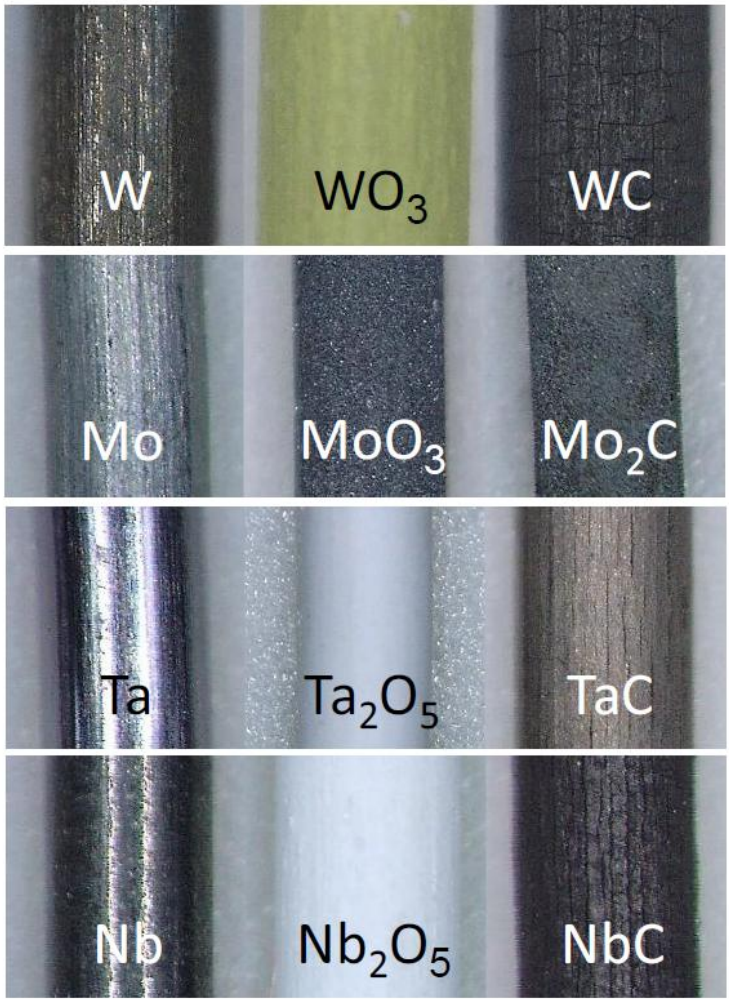

Fig. 7.2. Optical microscopy images of the coated wires; left: pure metal wires, middle: surface-oxidized and right: carbide-coated.[134]

type.[249] WC and Mo_2C have hexagonal structures with different stacking sequences of the metal atoms. In WC, carbon occupies trigonal-prismatic interstices, whereas it occupies octahedral interstices in Mo_2C which is the only stable molybdenum carbide at ambient conditions.

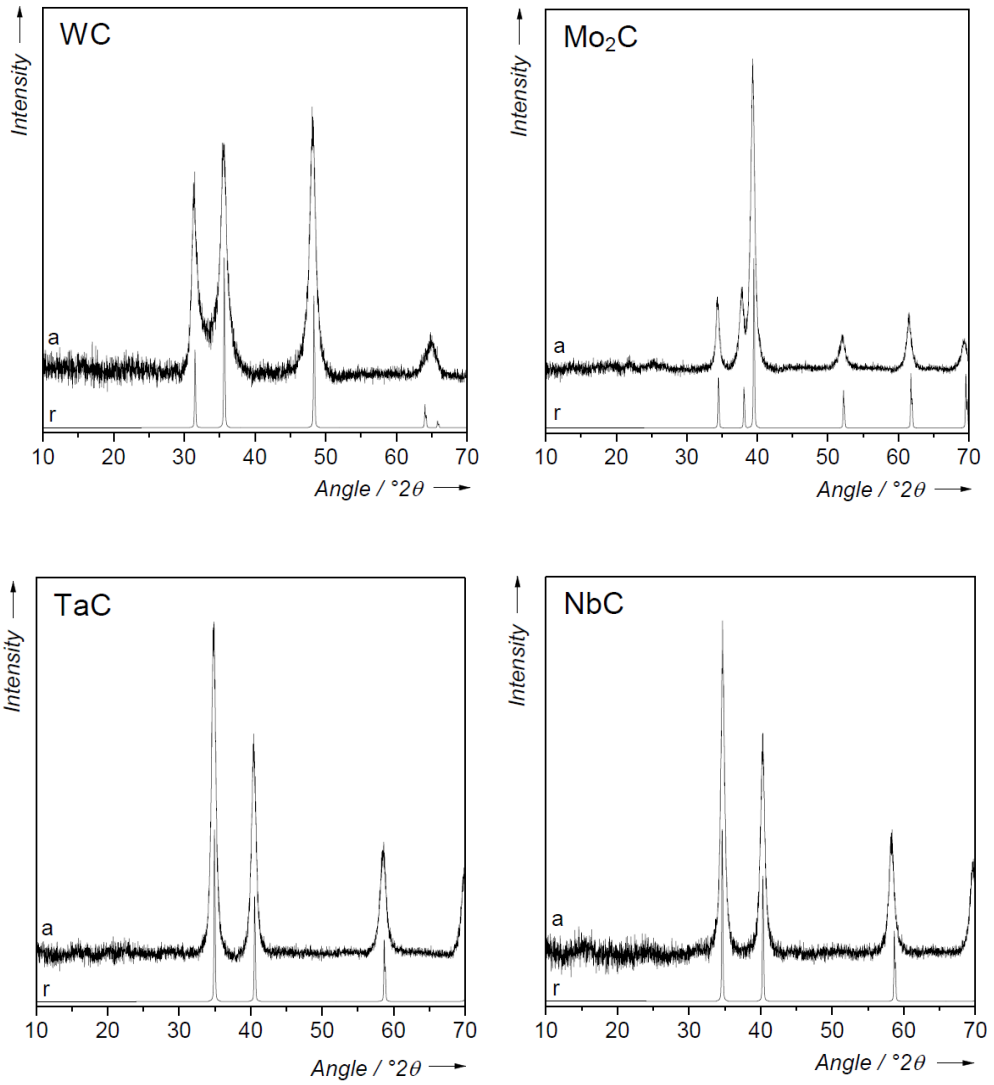

Fig. 7.3. XRD patterns of the wire coatings, obtained after mechanical removal from the wires and measurement of the resulting powder: a) pattern of the respective carbide and r) reference pattern from the ICDD database for comparison.[134]

For determination of the thicknesses of the carbide layers, SEM micrographs of wire cross section have been measured. As shown in Fig. 7.4, the carbide coatings appear with a different contrast compared to the bare metal cores. The layers of WC, TaC and NbC have similar thicknesses between 42 and 53 µm. The Mo_2C layer on the contrary is much thinner as already discussed above based on optical microscopy images. It is estimated to have a thickness of about 6 µm. Pronounced crack formation in the layers of WC and NbC can be observed, whereas the wires coated with TaC and Mo_2C have a smoother surface. The cracks are formed because of volume changes during the preparation processes. The intermediate transition metal oxides have lower densities than the bare metals and therefore a

volume expansion takes place during the oxidation procedure. The carbides have a higher density than the oxides and hence volume shrinking occurs during carburization, leading to the observed crack formation.

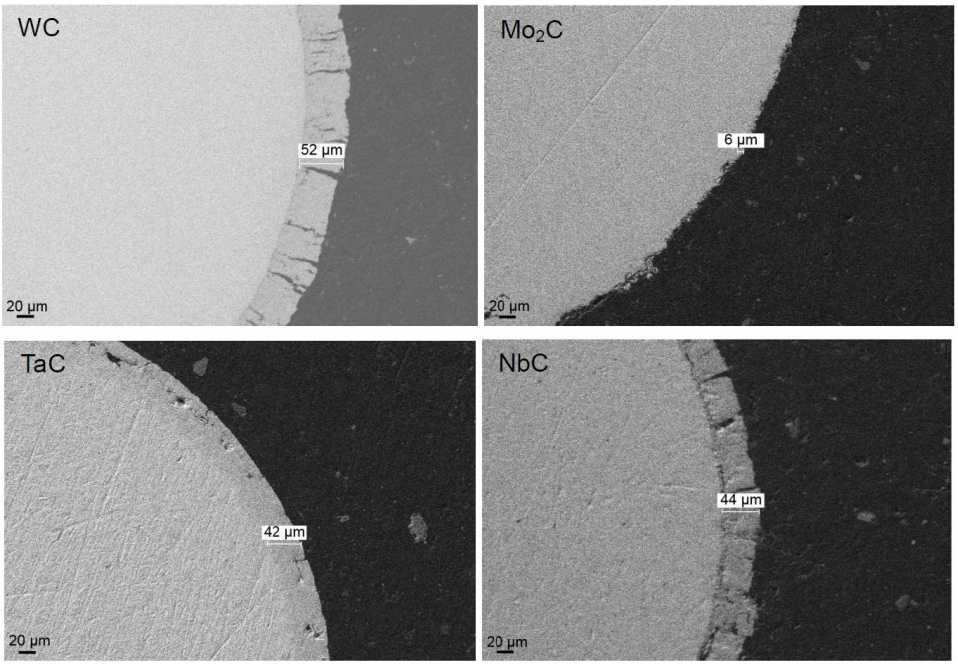

Fig. 7.4: SEM micrographs of the wire cross-sections at a magnification of 500, obtained after embedding the wires in an epoxy paste and polishing; coating thicknesses are given.[134]

Electrochemical characterisation

As discussed above, the electrochemical properties of the carbide coated wires were evaluated in molten KH_2PO_4 as a simulation for solid acid membranes such as the often employed CsH_2PO_4. The temperature was kept constant at 260 °C, slightly above the KH_2PO_4 melting point of 253 °C. Steady state voltammetric measurements were performed from -1.0 V to -0.3 V (vs. Ag/Ag_2SO_4). A Pt wire was used for comparison. In all cases, a strong reduction at negative potentials is observed which is assigned to the HER according to equation (7.1).

$$2H^+ + 2e^- \rightarrow H_2 \qquad (7.1)$$

The protons reduced are a product of the dissociation of the $H_2PO_4^-$ anion in the molten KH_2PO_4 (equation (2)).

$$H_2PO_4^- \rightleftharpoons H^+ + HPO_4^{2-} \rightleftharpoons 2H^+ + PO_4^{3-} \qquad (7.2)$$

Figure 7.5 shows the voltammograms of the four carbides and Pt. To ensure that no reduction processes beside the HER were measured, the curves were taken from negative to positive potentials after an initial reduction from positive to negative potentials. It can be seen that the onset reduction potential which is a measure for electrocatalytic activity, decreases in the following order: WC > Pt ≈ Mo_2C > NbC > TaC. Except for the position of Pt, this result is similar to analogous studies at room temperature and in 0.1 M H_2SO_4[232], proving the reliability of the setup. The assumption that the observed reduction corresponds to the HER is further supported by the observation of bubble formation on the electrodes.

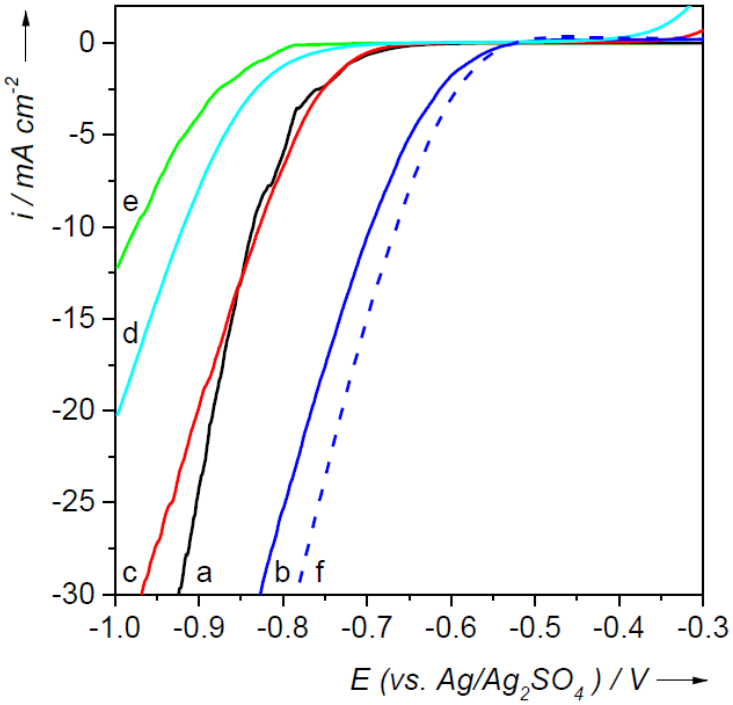

Fig. 7.5. Steady-state voltammetric curves obtained with a) Pt, b) WC, c) Mo_2C, d) NbC and e) TaC electrodes in molten KH_2PO_4 at 260 °C and 1 mV s^{-1}. Curve f) represents the WC catalyst after three cycles. The currents are normalized to geometrical electrode surface areas.[134]

At lower temperatures, Pt was always found to be the most active catalyst although a remarkable tendency of increasing HER activity of WC with temperature was observed before.[133(A12)] According to the present results, the onset potential for the HER is about 150 mV more positive for a WC catalyst than for Pt at 260 °C under the applied conditions. With increasing reaction time, residual WO_3, resulting from surface passivation in air, is dissolved from the catalyst surface. After three cycles, a slight increase of the WC catalytic activity can hence be observed, as depicted by

curve f) in Fig. 7.5.

It was calculated with density functional theory that a clean WC surface binds hydrogen with an energy of 4.0 eV.[250] Pt which is on top of volcano curves at room temperature, binds hydrogen with 2.6 eV and consequently hydrogen desorption limits the HER on WC at ambient conditions. It is supposed that under the present high temperatures, hydrogen desorption is facilitated, leading to higher rates for the WC catalyst compared to Pt. The temperature increase consequently shifts the maximum of the volcano curve for the HER to higher hydrogen binding energies. This also explains the good catalytic activity of Mo_2C. A complete mechanistic picture can however not be given for the moment and is a subject of further investigation.

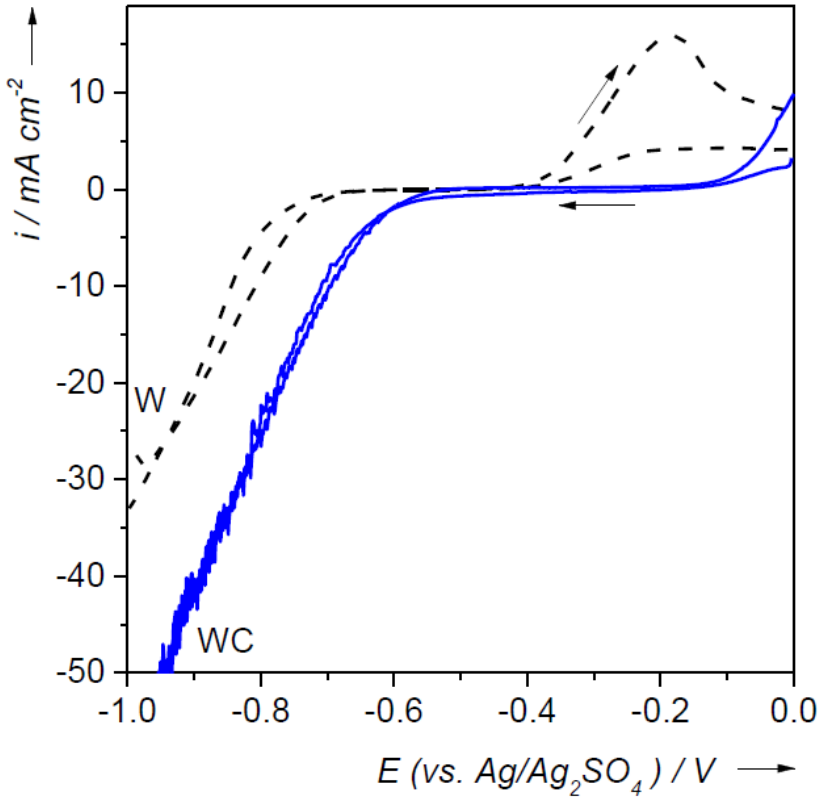

Fig. 7.6. Steady-state voltammetric curves obtained with W and WC electrodes in molten KH_2PO_4 at 260 °C and 1 mV s^{-1}. The currents are normalized to geometrical electrode surface areas.[134]

Figure 7.6 shows the steady state voltammogram of WC in comparison to metallic tungsten. From the more negative onset potential for the W electrode it can be seen that carbon alloying to the metal is crucial for the activity towards HER. The

comparison further proves the successful coating of the W wire with a WC layer, despite the cracks observed in the SEM micrographs. At anodic potentials, both W and WC are oxidised according to the positive currents measured from -0.4 V for W and -0.1 V (vs. Ag/Ag_2SO_4) for WC, respectively. Both materials consequently are not suitable for anode application under the chosen conditions although WC is more stable against oxidation than pure W.

8. CONCLUSIONS

The main common characteristic of heterogeneous catalytic reactions and electrochemical reactions is defined. It is the Fermi level of the catalyst, which is also electrochemical potential of the electrode. According to the Newns-Anderson theory, ***Fermi level*** of catalysts affects (or even define) their activity. The electrochemical potential can be measured and changed by polarization in electrochemical experiment.

The nature of the ***electrocatalytic reaction*** is dicussed, including my theory of ***electrochemical promotion***. This theory is based on electrochemical change of Fermi level of catalyst. It aso states that that there are two types of electrochemical promotion:

First type is based on change of the Fermi level through the charge of the electric double layer (EDL) between catalyst and its support without electrochemical reaction. This effect was abbreviated as EDLE.

Second type is based on change of Fermi level by electrochemical production of promoters, reducing or oxidizing current carriers of the catalyst support (O^{2-}, H^{+}, Na^{+}). This type was abbreviated as EEPP.

The results of my research are given as examples of use of electrochemistry as a tool for study, promotion and development of catalysts.

I. *Use of electrochemical technique (cyclic voltammetry) in study of the mechanism of chemical catalytic reactions (catalytic SO_2 oxidation to SO_3 on vanadia catalyst, Contact process), nature of the cationic promotion of this process, the effect of water on the catalytic activity of vanadia.*

It has been shown that the Contact process can be simulated by the solution of V_2O_5 in molten $M_2S_2O_7$ (M is an alkali metal) and the electrochemical behavior of the V(V) $\leftrightarrow$ V(IV) couple ideally reflects catalytic activity of the vanadia catalyst.

If the V(V) $\leftrightarrow$ V(IV) is reversible, than vanadia catalyst is highly active.

Using cyclic voltammetry, it has been shown that the reaction is reversible (fast) up to a fraction of 5 m/o of V_2O_5 and is a one-electron reaction at all studied concentrations (i.e., up to 20 m/o of V_2O_5). This was in agreement with the published data on the vanadia catalyst and also in agreement with the publications concluded that V(V) complexes are monomeric (one-electrone redox reaction).

The presence of ***Li^+, Na^+*** and ***Cs^+ ions*** cause a noticeable acceleration of V(V) ↔ V(IV) reaction (the V(V)/V(IV) electrochemical couple kinetics changed from irreversible to reversible. Therefore voltammetry can be used as a reliable tool for study of a mechanism of the cationic promotion of the SO_2 catalytic oxidation and for an optimization of the amount of the promoter.

It was concluded that the alkali-ion promotion effect can be qualitatively devided into two types: *"large amount promoter"*, when the promoter changes physic-chemical properties of the bulk melt (i.e. Cs^+); and *"small amount additive"*, when the bulk properties are not significantly changed, but the thermodynamics and kinetics of catalytic reaction is changed (Na^+, Li^+).

The ***effect of water*** on the electrochemical behavior of V_2O_5 was studied in $K_2S_2O_7$-$KHSO_4$ -V_2O_5 and $K_2S_2O_7$-$KHSO_4$ -V_2O_4 melts in argon and SO_2/air atmospheres with a gold electrode at 440°C.

It was shown that the water has a promoting effect on the V(IV) → V(III) reduction increasing the concentration of V(III) species in the studied melts.

Both reactions, the V(V) → V(IV) reduction and the V(IV) oxidation, remain one-electron electrochemical reactions with increasing concentration of $KHSO_4$ in the molten $K_2S_2O_7$-$KHSO_4$ -V_2O_5 system.

Water had no noticeable effect on the kinetics of the V(V) → V(IV) reduction, but caused higher polarizations (i.e. inhibition) of the V(IV) → V(V) oxidation reaction both in the Ar and SO_2/air atmospheres.

II. Study of electrochemical promotion of heterogeneous catalytic reactions on Pt/C/Polybenzimidazol-H_3PO_4 catalyst at 135-170℃).

In this study, for the first time polymeric proton-conducting electrolyte, i.e. polybenzimidazole/H_3PO_4 was used as a catalyst support for promotion of heterogeneous catalytic reactions. The following catalytic reactions were studied: ***oxidative coupling of methane (OCM), NO reduction with hydrogen and methane and Fischer-Tropsh synthesis (FTS).***

Possibility of creation of a new OCM route for catalytic CH_4 oxidation by the electrochemical production of Pt-H centers at the Pt-PBI(H_3PO_4)-gas boundary has been demonstrated.

It has been shown that Pt catalyst activity and selectivity toward the $CH_4 \rightarrow C_2H_2$ reaction can be electrochemically promoted with the maximum promotion effect (3.8% C_2H_2 yield, 135°C) at -0.15 V. The promotion effect had an EEPP nature. Possibility of the electrochemical promotion of the catalytic NO reduction by hydrogen at the Pt-PBI(H_3PO_4)-gas boundary has been demonstrated. It has also been shown that the nature of this promotion effect can vary depending on the flow rate of the NO/H_2 /Ar gas mixture. At high NO/ H_2/ Ar flow rate (17 mL/min; 17 and 354 mL/min, respectively, at atmospheric pressure), it has been found that NO reduction can be electrochemically promoted at negative polarization with maximum (9.3% of NO conversion to N_2 at 135°C) at approximately -0.15 V, *i.e.*, close to the potential found for the maximum promotion of CH_4 oxidation at the same catalyst. The maximum rate enhancement ratio was 4.65. The value of Λ calculated for maximum promotion effect conditions was 1.26×10^3, *i.e.*, $\Lambda >> 1$. This means that this effect has an EEPP nature, the catalytic reaction was promoted by the electrochemically produced adsorbed hydrogen species.

At low NO/ H_2/ Ar flow rate (17 mL/min; 17 and 140 mL/min, respectively, at atmospheric pressure), NO reduction increased 20 times even without polarization. Moreover, under these conditions negative polarization decreased the rate of NO reduction ~*i.e.*, an opposite effect to what was found at high gas flow rates. However, the electrochemical promotion effect did occur at positive polarization with maximum increase (close to 60% NO conversion at 135°C) at approximately 0.08 V and with 1.5 times the zero polarization value. In the potential range of the promotion effect faradaic current is absent. It means that the promotion effect has an EDLE nature.

The reduction of NO by methane was studied in (NO,CH_4, Ar), Pt|PBI–H_3PO_4|Pt, (H_2,Ar) fuel cell at 135 and 165°C. It has been shown that in this system NO can be reduced chemically by methane to N_2. Maximum promotion effect on NO conversion reached 46.5% methane conversion at 135°C . The NO reduction was affected by negative polarization of the catalyst and was maximum at the potentials of the electrochemical reduction of protons. Therefore, the promotion effect had EEPP nature. There was no significant effect of temperature increase (from 135 to 165°C) on the catalyst activity in the NO reduction by methane.

Electrochemical promotion (EP) of FTS studied in the *CO, H_2, Ar // Pt/Ru/ C/Polybenzimidazol-H_3PO_4/Pt/H_2,Ar* cell at 170°C. The Pt/Ru catalyst was chosen because Ru was known to be an active FTS catalyst. The FTS product was methane.

The maximum promotion was found between -0.050 V and 0 V and showed 11.1% or a CO conversion rateof 1.38×10^{-6} mol/s.

This case of electrochemical promotion had EDLE, because it took place during a positive polarization of the catalyst, i.e. there was no electrochemical production of promoter (H atoms) and probably in this way the oxidation of gaseous hydrogen was accelerated and conditions of CO adsorption were improved.

III. Development of catalysts for the high temperature proton exchange membrane (PEM) water electrolysis.

The catalysts composed of ***IrO_2 on a SiC/Si support*** have been studied in hot phosphoric acid (simulation of high temperature PEM electrolyte.

The electrochemical activity of IrO_2 was found to be improved in the presence of the support. The activity of 80 wt.% and 90 wt.% samples was found to be higher than that of unsupported catalyst. This was attributed to the improved surface properties of IrO_2 in the presence of the support, rather than to a better conductivity or surface area of the support itself, which possesses rather poor properties compared to IrO_2.

Based on the above results, the SiC/Si compound has been recommende as a potential candidate as a support of an anode electrocatalyst for phosphoric acid doped membrane steam electrolysers.

It has been shown that ***TaC represents a promising candidate for application as an IrO_2 electrocatalyst support*** for the anodic oxygen evolution reaction in the high-temperature PEM water electrolysis. The negative aspect represented by the formation of a surface film of $NaTaO_3$, characterised by low conductivity, may be overcome by applying a sufficient amount of IrO_2, in this particular case 50 wt.% or more. Such a supported electrocatalyst has shown properties similar to those of pure $_{IrO2}$, including electrocatalytic activity and the rate-determining step of the oxygen evolution reaction.

The data on ***electrochemical behaviour of WC as a hydrogen reduction electrocatalyst*** for high temperature PEM water electrolysis have been discussed. That behaviour has been compared with platinum and it was shown that the relative increase of the electrochemical activity of WC towards the HER as a function of temperature is more pronounced, than for Pt and this has been especially observed in the temperature range from 120°C to 150°C. Therefore there is a probability that at higher temperatures WC can substitute platinum for the hydrogen reduction reaction in high temperature PEM water electrolysers. This assumption was proved during the

study of catalytic activity of WC, Mo_2C, TaC, NbC and Pt at 260°C in molten KH_2PO_4.

IV. Transition metal carbides (WC, Mo_2C, TaC, NbC) as potential electrocatalysts for the hydrogen evolution reaction (HER) at medium temperatures.

The results of the investigation of ***catalytic activity of WC, Mo_2C, TaC, NbC and Pt at 260 °C in molten KH_2PO_4*** were presented and discussed. Molten KH_2PO_4 proved to be a good model system for simulation of solid acid-based electrolyzer cells at medium temperatures. Optimised two-step oxidationcarburization reactions on transition metal wire surfaces lead to transition metal carbide coated electrodes, suitable for measurement of the intrinsic electrocatalytic properties. Problems due to contact and varying morphology can thus be avoided.

Under the conditions chosen (260 °C, 1 atm), WC is more active towards the HER than platinum. The catalytic activity increase in the row: TaC < NbC < Mo_2C = Pt < WC.

9. OUTLOOK OF FUTURE RESEARCH

Electrochemical study of Contact process[A1-A4] has shown that this approach can be very effective not only in homogeneous catalysis, where it is frequently used recently (e.g. Refs. 251, 252), but also in study of heterogeneous catalytic reactions. Especially, in the case when use of usual chemical and physic-chemical techniques is very complicated and the results do not have a straight forward explanation. However, in order to do it, several conditions should take place:

1. Redox step should be the rate-determining step.
2. The redox couple should be an ionic conductor or can be dissolved in an ionic conductor.
3. The working electrode should be made from a non-catalytic material (e.g. gold in our case or glassy carbon.

My electrochemical approach in study of catalytic reaction can also be used in the area of homogeneous catalysis. This assumption can be backed by a great interest to

my Contact process of my recent lecture in Technical University of Munich from the researchers specialized in homogeneous catalysis.[253]

Particular interest in future research create the resultst obtained in the study of electrochemical promotion of heterogeneous catalytic reactions on Pt/C/Polybenzimidazol-H_3PO_4 catalyst at 135-170°C, especially for the oxidative coupling of methane, NO reduction and Fischer-Tropsch synethis (FTS).[A5-A9] This research, if renewed, can bring important results, especially at different temperature and with different catalyst support, e.g. supported KH_2PO_4.

Moreover, instead of FTS electrochemical promotion, the CO reduction by hydrogen, electrochemically produced in the same electrochemical cell, i.e. CO/(Pt/Ru)/PBI(H_3PO_4)/Pt/H_2, can be performed. It was already done by us during the project on electrochemical promotion and very promising results were obtained.[254] [(A9)] Maximum CO conversion was 20.6% (3.04×10^{-5} mol/min) at 150°C. Almost half of it (1.43×10^{-5} mol/min) was CO conversion to methane, the rest was conversion to carbon.

It is very important to mention that recently this area attracted very strong interest from scientific community.[255]

Thus, K. Xie et al., using $BaCe_{0.5}Zr_{0.3}Y_{0.16}Zn_{0.04}O_{3-\delta}$ proton conducting electrolyte in co-electrolysis of water and CO_2 convert 1-2% of the CO_2 into methane at 650°C.[256]

M. Mogensen et al. currently work at the development of co-electrolysis of water and CO_2 in solid oxide electrolyzers at 800°C.[255] During the electrolysis, CO_2 get reduced to CO and with hydrogen from water electrolysis (syngas) is forwarded to FTS reactor to produce hydrocarbons.

Obvious interest for future research is about transition metals and their carbides as catalysts for hydrogen evolution reaction (HER) in intermediate-temperature (200-400°C) water electrolysis.[A14, 15] I am currently participating in this research. The future plans are to develop an effective WC catalyst and to develope a water electrolyzer with supported molten KH_2PO_4 electrolyte.

10. REFERENCES

1. D.M. Newns, *Phys.Rev*. **178**, 1123 (1969).

2. P.W. Anderson, *Phys.Rev*. **124**, 41 (1961).

3. Chorkendorff, J.W. Niemantsverdriet, *Concepts of Modern Catalysis and Kinetics*, 2007, Wiley-VCH Verlag GmbH&Co. KGaA.

4. C. Wagner, *Adv. Catal*., **21**, 323 (1970).

5. C. G. Vayenas, S. Bebelis, and S. Ladas, *Nature*, **343**, 625 (1990).

6. J. Pritchard, *Nature*, **343**, 592 (1990),.

7. C. G. Vayenas, M. M. Jakis, S. I. Bebelis, and S. G. Neophytides, in *Modern Aspects of Electrochemistry* N29, J. O'M. Bockris, B. E. Conway, and R. E. White, Editors, pp. 57-202, Plenum Press, New York (1996).

8. C. G. Vayenas and S. Bebelis, *Catal. Today*, **51**, 581 (1999).

9. S. Bebelis, M. Makri, A. Buekenhoudt, J. Luyten, S. Brosda, P. Petrolekas, C. Pliangos, and C. G. Vayenas, *Solid State Ionics*, **129**, 33 (2000).

10. C. G. Vayenas, S. Bebelis, C. Pliangos, S. Brosda, and D. Tsiplakides, *Electrochemical Activation of Catalysis: Promotion, Electrochemical Promotion and Metal-Support Interactions*, Kluwer Academic/Plenum Publishers, New York (2001).

11. J. Poppe, S. Volkening, A. Schaak, E. Schutz, J. Janek, and R. Imbihl, *Phys. Chem.Chem. Phys*., **1**, 5241 (1999).

12. V. D. Belyaev, T. I. Politova, and V. A. Sobyanin, *Solid State Ionics*, **136-137**, 721 (2000),

13. D. A. Emery, R. J. C. Luke, P. H. Middleton, and I. S. Metcalfe, *J. Electrochem.Soc.*, **146,** 2188 (1999).

14. S. Metcalfe, *J. Catal*., **199**, 247 (2001).

15. S. Metcalfe, *J. Catal*., **199**, 259 (2001).

16. R. B. Anderson, *Experimental Methods in Catalytic Research*, Academic Press, New York (1968).

17. I.Petrushina, N.J.Bjerrum, R.W.Berg, *European Research Conferences, Euchem Conference on Molten Salts*, Bad Herrenalb, Germany, 21-26 August (1994).

18. N.J. Bjerrum, I.M. Petrushina, and R.W. Berg, *J. Electrochem. Soc*., **142**, 1805 (1995).

19. I.M. Petrushina, N.J. Bjerrum, R.W. Berg, and F. Cappeln, *J.Electrochem.Soc*., **144,** 532 (1997).
20. I.M. Petrushina, N.J. Bjerrum, R.W. Berg, and F. Cappeln, Abstract 1142, p. 1416, *The Electrochemical Society Meeting Abstracts*, Vol. **96-1**, Los Angeles, CA, May 5-10, 1996.
21. I.M. Petrushina, N.J. Bjerrum, and F. Cappeln, *J. Electrochem. Soc*., **145**, 3721 (1998).
22. I.M. Petrushina, V.A. Bandur, F. Cappeln, and N.J. Bjerrum, *J. Electrochem. Soc.*, **147**, 3010 (2000).
23. P.Mars and J.G.H. Maessen, *J. Catal*., **10**, 1 (1968).
24. J. Villadsen and H. Livbjerg, *Catal. Rev. Sci. Eng*., **17**, 203 (1978).
25. C.N. Kenney, *Catalysis (London*), **3**, 123 (1980).
26. S. Boghosian, R. Fehrmann, B.J. Bjerrum, and G.N. Papatheodorou, *J. Catal*., **119**, 121 (1989).
27. D.A. Karydis, K.M. Eriksen, R. Fehrmann, and S. Boghosian, in *Molten Salt Chemistry and Technology* 1993, M.-L. Saboungi and H. Kojima, Editors, PV **93-9**, p.390, The Electrochemical Society Proceedings Series, Pennington, NJ (1993).
28. Durand, G. Picard, and J.Vedel, *J. Electroanal. Chem.*, **127**, 169 (1981).
29. M. Frank and J. Winnick, *J. Electroanal. Chem*., **238**, 163 (1987).
30. K. Scott, T. Fannon, and J. Winnick, *J. Electrochem. Soc*., **135**, 573 (1988).
31. M. Dojcinovic, M. Susic, and S. Mentus, *J. Mol. Catal*., **11**, 275 (1981).
32. F. Doering and D. Berkel, *J. Catal*., **103,** 126 (1987).
33. F.J. Doering, H.K. Yuen, P.A. Berger, and M.L. Unland, *J. Catal*., **104**, 186 (1987).
34. G.H. Tandy, *J. Appl. Chem*., **6,** 68 (1956).
35. H.F. Topsøe and A. Nielsen, *Trans. Dan. Acad. Techn. Sci*., **1**, 18 (1947).
36. M. Comtat, G. Loubet, and J. Mahenc, *J. Electroanal. Chem*., **40**, 167 (1972).
37. Durand, G. Picard, and J. Vedel, *J. Electroanal. Chem*., **70**, 55 (1976).
38. N.H. Hansen, R. Fehrmann, and N.J. Bjerrum, Inorg. Chem., 21, 744 (1982).
39. R.W. Berg, F. Borup, N.J. Bjerrum, in *Molten Salt Forum*, Switzerland, Trans, Trans Tech Publications, Vol. **1-2**, pp. 69-86 (1993-1994).
40. I.A. Plamback, in *Fused Salt Systems. Encyclopedia of Electrochemistry of the Elements*, A.J. Bard, Editor, p.440, Dekker, Now York and Basel (1976).
41. Rahmel, *Chem. Ing. Tech*., **41,** 169 (1969).
42. B.W. Burrows and G.J. Hills, *Electrochim. Acta*, **15**, 445 (1970).

43. F.G. Salzano and L. Newman, *J. Electrochem. Soc*., **119**, 1273 (1972).
44. L.G. Boxall and K.E.Johnson, *J.Electrochem. Soc*., **118**, 885 (1971).
45. R. Fehrmann, M. Gaune-Escard, and N.J. Bjerrum, *Inorg. Chem*., **25**, 1132 (1987).
46. G. Hatem, R. Fehrmann, M. Gaune-Escard, and N.J. Bjerrum, *J. Phys. Chem*., **91**, 195 (1987).
47. G.E. Folkmann, G. Hatem, R. Fehrmann, M. Gane-Escard, and N.J. Bjerrum, *Inorg. Chem*., **30**, 4057 (1991).
48. D. Karydis, S. Boghosian, R. Fehrmann, and K.M. Eriksen, *J. Catal*., **145**, 312 (1994).
49. F.A. Cotton and G. Wilkinson, *Advanced Inorganic Chemistry*, John Wiley & Sons, New York (1988).
50. H.A. Andreasen, N.J. Bjerrum, and C.E. Foverskov, *Rev. Sci. Instrum*., **48**, 1340 (1977).
51. R.S. Nicholson and I. Shain, *Anal. Chem*., **36**, 706 (1964).
52. R.N. Adams, *Electrochemistry at Solid Electrodes*, p. 126, Marcel Dekker, New York (1969).
53. B. Zachau-Christensen, K. West, and T. Jacobsen, *Mater. Res. Bull*., **20**, 485 (1985).
54. M. Chemla, Commissariat á l'Énergie Atomoque, *Brevet D'Invention, France* 1950, N 1216418.
55. Ben Hadid, G. Picard, and J. Vedel, *J. Electroanal. Chem*., **74**, 157 (1976).
56. M. Skyllas-Kazakos and F. Grossmith, *J. Electrochem. Soc*., **134**, 2950 (1987).
57. H. Kaneko, K. Nozaki, Y. Wada, T. Aoki, A. Negishi, and M. Kamimoto, *Electrochim. Acta*, **36**, 1191 (1991).
58. R. Fehrmann, B. Krebs, G.N. Papatheodorou, R.W. Berg, and N.J. Bjerrum, *Inorg. Chem.*, **25**, 1571 (1986).
59. M.P.Glazyrin, V.N. Krasil'nikov, and A.A. Ivakin, *Zurn. Neorg. Khim. (Russ. J. Inorg. Chem.),* **27**, 3073 (1982).
60. H.C. Mishra and M.C. Symons, *J. Chem. Soc*., 4411 (1962).
61. R.G. Gillespie, R. Kapoor, and E.A. Robinson, *Can. J. Chem*., **44**, 1203 (1966).
62. R.C. Paul, J.K. Puri, and K.S. Malhotra, *J. Inorg. Nucl. Chem*., **33**, 4191 (1971).
63. H.A. Videla and A.J. Arvia, *Electrochim. Acta*, **10**, 21 (1965).
64. A.J. Arvia, A.J. Calandra, and H.A. Videla, *Electrochim. Acta*, **10**, 33 (1965).
65. D. Gilroy, *Electrochim. Acta*, **17,** 1771 (1972).

66. S.E. Rogers and A.R. Ubbelode, *Trans. Faraday Soc*., **46**, 1051 (1950).
67. K.M. Eriksen, R. Fehrmann, G. Hatem, M. Gaune-Escard, O. Lapina, and V.M. Mastikhin, in *Proceedings of 9th International Symposium on Molten Salts*, C.S. Hassey, D.S. Newman, G. Mamantov, and Y. Ito, Editors, PV **94-13**, p. 124, The Electrochemical Society Proceedings Series, Pennington, NJ (1994).
68. S.H. White and U.M. Twardoch, *J. Electrochem. Soc*., **134**, 1080 (1987).
69. B.J. Meehan and S.A. Tariq, *Aust. J. Chem*., **32**, 1385 (1979).
70. H. Kozlowska, B. Conway, and W. Sharp, *J. Electroanal. Chem*., **43**, 9 (1973).
71. D. Dutta and D. Landolt, *J. Electrochem.Soc.*, **119**, 1320 (1972).
72. A.R. Glueck and C.N. Kenney, *Chem.Eng.Sci*., **23**, 1257 (1968)
73. G.K. Boreskov, G.M. Polyakova, A.A. Ivanov, and V.M. Mastikhin, *Dokl.Akad.Nauk*, **210,** 626 (1973).
74. G.K. Boreskov, V.A. Dzisko, D.V. Tarasova, and G.P. Balaganskaya, *Kinet.Katal*., **11**, 181 (1970).
75. V.M. Mastikhin, G.M. Polyakova, Y. Zyulkovskii, and G.K. Boreskov, *Kinet.Kat*., **11**, 1463 (1070).
76. G.M. Polyakova, G.K. Boreskov, A.A. Ivanov, L.P. Davydova, and G.A. Marochkina, *Kinet.Kat*., **12**, 666 (1971).
77. J. Villadsen, and H. Livbjerg, *Catal. Rev. Sci. Eng*., **21**, 73 (1980).
78. H. Jensen-Holm, *Ph.D. Thesis, Technical University of Denmark*, Lyngby (1978).
79. G.K. Boreskov, A.A. Ivanov, B.S. Balzhinimaev, and L.M. Karnatovskaya, *React.Kinet.Catal.Lett*., **14**, 25 (1980).
80. B.S. Balzhinimaev, V.E. Ponomarev, G.K. Boreskov, and A.A. Ivanov, *React.Kinet.Catal.Lett*., **25**, 219 (1984).
81. V.N. Krasil'nikov, M.P. Glazyrin, A.P. Palkin, L.A. Perlyaeva, and A.A. Ivakin, *Russ.J.Inorg.Chem*., **32**, 425 (1987).
82. K. Nielsen, R. Fehrmann, and K. Eriksen, *Inorg.Chem*., **32**, 4825 (1993).
83. V.M. Mastikhin, O.B. Lapina, L.Y. Simonova, and B.S. Balzhinimaev, *Rasplavy (Melts, Russ.)*, **2**, 21 (1990).
84. K.M. Eriksen, D.A. Karydis, S. Boghosian, and R. Fehrmann, *J.Catal*., **155**, 32 (1995).
85. *Instrumental Methods in Electrochemistry, Southampton Electrochemistry Group*, p.p. 178-227, 380, Ellis Horwood Ltd., New York (1990).
86. G. Hatem, M. Gaune-Escard, R. Fehrmann, K.M. Eriksen, *1998 Molten Salts XI*, Pennington, N.J.: The Electrochemical Society, Inc., 483-490.

87. M. Stoukides, *Ind. Engin. Chem. Res*., **27**, 1745 (1988).
88. P.G. Gellings, H.S.A. Koopmans, and A.J. Burggraaf, *Appl. Catal*., **39**, 1 (1988).
89. Yu.S. Chekryshkin, P.S. Dukhanin, A.P. Khaimenov, and A.A. Fyodorov, in *Molten Salt Chemistry and Technology 1998*, H. Wendt, Editor, Trans. Tech. Publications Ltd., Uetikon-Zuerich (1998).
90. C. Pliangos, C. Raptis, Th. Badas, D. Tsiplakides, and C.G. Vayenas, *Electrochim.Acta*, **46**, 331 (2000).
91. C. Pliangos, C. Raptis, Th. Badas, D. Tsiplakides, and C.G. Vayenas, *Solid State Ionics*, **136-137**, 767 (2000).
92. R.M. Lambert, A. Palermo, F.J. Williams, and M.S. Tikhov, *Solid State Ionics*, **136-137**, 677 (2000).
93. I.V. Yentekakis, M. Konsolakis, R.M. Lambert, A. Palermo, and M. Tikhov, *Solid State Ionics*, **136-137**, 783 (2000).
94. N. Macleod, J. Isaak, and R.M. Lambert, *J. Catal*., **198**, 128 (2001).
95. F.J. Williams, A. Palermo, M.S. Tikhov, and R.M. Lambert, *J. Phys. Chem. B*, **105**, 1381 (2001).
96. J. Fóti, O. Lavanchi, and C. Comminelis, *J. Appl. Electrochem*., **30**, 1223 (2000).
97. L. Ploese, M. Salazar, B. Gurau, and E.S. Smotkin, *Solid State Ionics*, **136-137**, 713 (2000).
98. S. Kim and G.L. Haller, *Solid State Ionics*, **136-137**, 693 (2000).
99. I.M. Petrushina, V.A. Bandur, N.J.Bjerrum, F. Cappeln, L. Qingfeng, *J.Electrochem.Soc*., **149**, D143, 2002.
100. I. M. Petrushina, V. A. Bandur, F. Cappeln, N. J. Bjerrum, R. Z. Sørensen, R. H. Refshauge, and Qingfeng Li, *J.Electrochem.Soc*., **150**, D87, 2003.
101. I.M. Petrushina, L.N. Cleemann, R. Refshauge, N.J. Bjerrum, V.A. Bandur, *J.Electrochem.Soc*., **154,** E84, 2007.
102. I.M. Petrushina, N.J. Bjerrum, V.A. Bandur, L.N. Cleemann, *Topics in Catalysis*, **44**, p.427, 2007.
103. L. Qingfeng, X. Gang, H.A.Hjuller, and N.J. Bjerrum, *J. Electrochem. Soc*. **143**, 3114 (1994).
104. L. Qingfeng, X. Gang, H.A. Hjuller, and N.J. Bjerrum, *J. Appl. Electrochem*., **31**, 773 (2001), and references cited therein.
105. Y. Amenomiya, V.J. Birss, M.Goledzinowski, J. Galuszka, and A.R. Sanger, *J. Catal. Rev. – Sci. Eng.*, **32(3)**, 163 (1990).

106. L. Guczi, R.A. Van Santen, and K.V. Sharma, *J. Catal. Rev. – Sci. Eng*., **38(2)**, 249 (1996).

107. I. K. Weissermel and H. J. Arpe, *Industrial Organic Chemistry*, 2nd ed., Verlag chemie, Weinheim (1993).

108. I. Vedrenne, J. Saint-Just, A. Ben Hadid, and G. M. Come, *Catal. Today*, **6**, 381(1990).

109. C. Liu, R. Mallinson, and L. Lobban, *J. Catal*., **179**, 326 (1998).

110. L. W. Niedrach, *J. Electrochem. Soc*., **113**, 645 (1966).

111. S. Seimanides and M. Stoukides, *J. Electrochem. Soc*., **113**, 1535 (1986).

112. S.K. Zecevic, J.S. Wazinright, M.H. Litt, S. Lj. Gojkovic, and R.F. Savinell, *J. Electrochem. Soc.*, **144**, 2973 (1997).

113. R. I. Masel, *Catal. Rev. Sci. Eng.*, **28** (2&3), 335 (1986).

114. R. Burch and A. Ramli, *Appl. Catal., B*, **15**, 49 (1998).

115. R. Burch and A. Ramli, *Appl. Catal., B*, **15**, 63 (1998).

116. R. Mariscal, S. Rojas, A. Gómez-Cortés, G. Díaz, R. Pérez, and J. L. G. Fierro, *Catal. Today*, **75**, 385 (2002).

117. I. V. Yentekakis, R. M. Lambert, M. Konsolakis, and V. Kiousis, *Appl. Catal., B,* **18**, 293 (1998).

118. M. Machida, E. Shono, M. Kimura, and S. Yamauchi, *Catal. Commun*., **4**, 631 (2003).

119. M. Nagaro, T. Yoshii, T. Hibino, M. Sano, and A. Tomita, *Electrochem. Solid-State Let*t., **9**, J1 (2006).

120. R. He, Q. Li, G. Xiao, and N. J. Bjerrum, *J. Membr. Sci*., **226**, 169 (2003).

121. Q. Li, H.A. Hjuller, and N.J. Bjerrum, *Electrochim. Acta*, **45**, 4219 (2000).

122. Y. Jiang, I. V. Yentekakis, and C. G. Vayenas, *Science*, **264**, 1563 (1994).

123. M. Stoukides, *Catal. Rev. - Sci. Eng*., **42**, 1 (2000).

124. N. Lapeña-Rey and P. H. Middleton, Appl. Catal., A, 240, 207 (2003).

125. T. Tagawa, K. Kuroyanagi, S. Goto, S. Assabumrungrat, and P. Praserthdam, *Chem. Eng. J*., **93**, 3 (2003).

126. S. Seimanides and M. Stoukides, *J. Electrochem. Soc*., **133**, 1535 (1986).

127. G.P. van der Laan and A.A.C.M. Beenackers, *Catal. Rev. Sci. Eng*., **41**, 255 (1999).

128. T.M. Gür and R.A. Huggins, *Solid State Ionics*, **5**, 563 (1981).

129. T.M. Gür and R.A. Huggins, *Science*, **219**, 967 (1983).

130. F.G. Williams and R.M. Lambert, *Catal. Lett*., **70(2)**, 9 (2000).

131. A.V. Nikiforov, A.L. Tomas-Garcia, I.M. Petrushina, E. Christensen, N.J. Bjerrum, *Int. J. Hydr. Energy*, **36**, 5797 (2011).
132. J.Polonsky, I.M.Petrushina, E.Christensen, K.Bouzek, C.B. Prag, J.E.T. Andersen, N.J. Bjerrum, *Int. J. Hydr. Energy*, **37**, 2173 (2012).
133. A.V. Nikiforov, I.M. Petrushina, E. Christensen, N.V. Alexeev, A.V. Samokhin, N.J. Bjerrum, *Int. J. Hydr. Energy*, **37**, 18591, (2012).
134. S. Meyer, A.V. Nikiforov, I.M. Petrushina, K. Köhler, E. Christensen, J.O. Jensen, N.J. Bjerrum, *Int. J. Hydr. Energy*, **40**, 2905 (2015).
135. 135. Marshall, B. Børresen, G. Hagen, M. Tsypkin, R. Tunold, *Energy*, **32**, 431 (2007).
136. Y. Zhang, H. Zhang, Y. Ma, J. Cheng, H. Zhong, S. Song, et al., *J. Power Sources*, **195**, 142 (2009).
137. P. Millet, R. Ngameni, S. Grigoriev, *Int. J. Hydr. Energy*, **34**, 5043 (2009).
138. S. Grigoriev, P. Millet, S. Volobuev, V. Fateev, *Int. J. Hydr. Energy*, **34**, 4968 (2009).
139. Q. Li, J.O.Jensen, R.F. Savinell, N.J. Bjerrum, *Progress in Polymer Science*, **34**, 449 (2009).
140. J.O. Jensen, Q. Li, C. Pan, A.P. Vestbø, K. Mortensen, N.H. Petersen et al., *Int. J. Hydr. Energy*, **32**, 1567 (2007).
141. S. Song, H. Zhang, X. Ma, Z. Shao, R.T. Baker, B. Yi, *Int. J. Hydr. Energy*, **32**, 1567 (2007).
142. H. Beer, *Patent NL 6606302 A.* 1966.
143. H. Beer, *US Patent 3,632,498*. 1972.
144. H. Beer, *US Patent 3,711,385*. 1973.
145. S. Grigoriev, P. Millet, S. Korobtsev, V. Porembovskiy, M. Pepic, C. Etievant et al., *Int. J. Hydr. Energy*, **34**, 5986, (2009).
146. A. Nikiforov, I. Petrushina, E. Christensen, A. Tomas-Garcia, N. Bjerrum, *Int. J. Hydr. Energy*, **36**, 111 (2011).
147. *International patent application, 03.01.2008, WO 2008/002150 A1*, PCT/NO2007/00235.03.01.2008.
148. M. Pourbaix, *Atlas d'equilibres electrochimiques*. Paris: Gauthier-Villars; 1963.
149. T. Loucka, *J. Appl. Electrochem*., **7**, 211 (1977).
150. R. Kötz, H. Neff, S. Stucki, *J. Electrochem. Soc*., **131**, 72 (1984).
151. J. Gatineau, K. Yanagita, C. Dussarrat, Microel. Eng., 83, 2248 (2006).
152. R. Kötz, S. Stucki, *Electrocim. Acta*, **31**, 1311 (1986).

153. F.I. Mattos-Costa, P. de Lima-Neto, S.A.S. Machado, L.A. Avaka, *Electrochim. Acta*, **44**, 1515 (1998).

154. P. Millet, N. Mbmba, S. Groriev, V. Fateev, A. Aukauloo, C. Etievant, *Int. J. Hydr. Energy*, **35**, (2010).

155. A.T. Marshall, S. Sunde, M. Tsypkin, R. Tunold, *Int. J. Hydr. Energy*, **32**, 2320 (2007).

156. A. Marshall, B. Børresen, G. Hagen, M. Tsypkin, R. Tunold, *Electrochim. Acta*, **51**, 3161 (2006).

157. J. Cheng, H. Zhang, H. Ma, H. Zhong, Y, Zou, *Int. J. Hydr. Energy*, **34**, 6609 (2009).

158. L.M. Roen, C.H. Paik, T.D. Jarvic, *Electrochem. Solid State. Lett*., **7**, A19 (2004).

159. E. Antolini, E. Gonzalez, *Solid State Ionics*, **180**, 746 (2009).

160. S. Trasatti, *Electrochim. Acta*, **36**, 225 (1991).

161. L. Ouattara, T. Diaco, I. Duo, M. Panizza, G. Foti, C. Comminellis, *J. Electrochem. Soc.*, **150**, D41 (2003).

162. P.V. Kumar, G.S. Gupta, *Steel Research*, **73**, 31 (2002).

163. D.W. Richerson. *Modern ceramic engineering*. 3d ed. Taylor & Francis Group, LLC; 2006.

164. R. Divakar, S.G. Seshadri, M. Srinivasan, *J. Amer. Cer. Soc*., **72**,780 (1989).

165. T. Honji, Y. Mori, K. Hishinuma, K. Kurita, *J. Electrochem. Soc*., **135**, 917 (1988).

166. C.V. Rao, S.K. Singh, V. Viswanathan, *Indian J. Chem. Sec.A-Inorganic Bioinorganic Physical & Analytical Chem*., **47**, 1617 (2008).

167. L. Ma, S. Sui, Y Zhai, *J. Power Sources*, **177**, 470 (2008).

168. R. Adams, R.L. Shrinner, *J. Amer. Chem. Soc*., **45**, 2171 (1923).

169. A. Robin, J.L. Rosa, *Intern. J. Refr. Metals and Hard Mat*., **18**, 13 (2000).

170. A.L. Patterson, *Phys. Rev*., **56**, 978 (1939).

171. A. Marshall, B. Børresen, G. Hagen, M. Tsypkin, R. Tunold, *Mater. Chem. And Phys.*, **94**, 226 (2005).

172. A. Celzard, J.F. Mareche, F. Payot, G. Furdin, *Carbon*, **40**, 2801 (2002).

173. W. Martienssen, H. Warlimont, ed. *Springer handbook of condenced matter and materials data*. Berlin: Springer; 2005.

174. T.J. Schmidt, H.A. Gasteiger, G.D. Stab, P.M. Urban, D.M. Kolb, R.J. Behm, *J. Electrochem. Soc.*, **145**, 2354 (1998).

175. K. Hakket, S. Verhoef, R.A. Catler, D.K. Shetty, *J. Amer. Cer. Soc*., **92**, 2404 (2009).
176. Y. He, Y. Zhu, N. Wu, *J. Solid State Chem*., **177**, 3868 (2004).
177. A.T. Marshall, R.G. Havercamp, *Electrochim. Acta*, **55**, 1978 (2010).
178. Y.E. Roginskaya, T.V. Varlamova, M.D. Golstein, I.D. Belova, B.S. Galyamov, R.R. Shifrina et al., *Mater. Chem. Phys*., **30**, 101 (1991).
179. C. Comminelis, G.P. Vercesi, *J. Appl. Electrochem*. **21**, 335 (1991).
180. J.O'M. Bockris, *J. Chem. Phys*., **24**, 817 (1956).
181. Y. Matsumoto, E. Sato, *Mater. Chem. Phys*., **14**, 397 (1986).
182. L.M. Da Silva, J.F.C. Boods, L.A. De Faria, *Electrocim. Acta*, **46**, 1369, (2001).
183. D.V. Esposito, S.T. Hant, A.L. Stottlemyer, K.D. Dobson, B.E. McCandless, R.W. Birkmire, et al., *Angew. Chem. Int. Ed*., (2010).
184. Y. Shao, J. Liu, Y. Wang, Y. Lin, *J. Mater. Chem*., **19**, 547 (2010).
185. R.B. Levy, M. Boudart, *Science*, **181**, 547 (1973).
186. M.E. Björketun, A.S. Bondarenko, B.L. Abrams, I. Chokendorff, J. Rossmeisl, *Phys. Chem. Chem. Phys*., **12**, 10536 (2010).
187. J. Greeley, T.F. Jaramillo, J. Bonde, I.B. Corkendorff, J.K. Nørskov, *Nature Mater*., **5**, 909 (2006).
188. A. Anastasopoulos, J. Bake, B.E. Hayden, *J. Phys. Chem.: Part C*, **115**, 19226 (2011).
189. V. Nikolova, I. Nikolov, T. Vitanov, L. Yotova, *J. Power Sources*, **12**, 1 (1984).
190. M. Shao, B. Merzougui, K. Shoemaker, L. Stolar, L. Protsailo, Z.J. Mellinger, et al., *J. Power Sources*, **196**, 7426 (2011).
191. *Russian Federation patent # 2311225*; 2007.
192. Z.Z. Fang, X. Wang, T. Ryu, K.S. Hwang, H. Sohn, *Int. J. Refr. & Hard Metals*, **27**. 288 (2009).
193. T. Ryu, H. Sohn, K.S. Hwang, Z.Z. Fang, *Int. J. Refr. & Hard Metals*, **27**, 149 (2009).
194. T. Ryu, H.Y. Sohn, K.S. Hwang, Z.Z. Fang, *J.Amer. Cer. Soc*., **92**, 655 (2009).
195. T. Ryu, H.Y. Sohn, K.S. Hwang, Z.Z. Fang, *J. Mater. Sci*., **43**, 5185 (2008).
196. T. Ryu, H. Sohn, K.S. Hwang, Z.Z. Fang, *J. Alloys and Comp*., **481**, 274 (2009).
197. C. Brady, E. Rees, G. Burstein, *J. Power Sources*, **179**, 17 (2008).
198. N. Armaroli, V. Balzani, *Angew. Chem., Int. Ed*., **46**, 52 (2007).
199. N. Armaroli, V. Balzani, *ChemSusChem*, **4**, 21 (2011).

200. H. A. Gasteiger, S. S. Kocha, B. Sompalli, F. T. Wagner, *Appl. Catal., B*, **56**, 9 (2005).
201. H. A. Gasteiger, J. Garche, in *Handbook of Heterogeneous Catalysis*, 2nd ed.(Eds.: G. Ertl, H. Knözinger, F. Schüth, J. Weitkamp), Wiley-VCH, Weinheim, 2008, pp. 3081-3121.
202. H. A. Gasteiger, N. M. Marković, *Science*, **324**, 48 (2009).
203. W. Wei, G. Jinlong, *Front. Chem. Sci. Eng*., **5**, 2 (2011).
204. F. Schüth, *Chem. Ing. Tech*., **83**, 1984 (2011).
205. R. Schlögl, *Angew. Chem., Int. Ed*., **42**, 2004 (2003).
206. A. Klerke, C. H. Christensen, J. K. Nørskov, T. Vegge, *J. Mater. Chem*., **18**, 2304 (2008).
207. F. Schüth, R. Palkovits, R. Schlögl, D. S. Su, *Energy Environ. Sci*., **5**, 6278 (2012).
208. J. K. Nørskov, T. Bligaard, A. Logadottir, J. R. Kitchin, J. G. Chen, S. Pandelov, U. Stimming, *J. Electrochem. Soc*., **152**, J23 (2005).
209. J. Greeley, T. F. Jaramillo, J. Bonde, I. Chorkendorff, J. K. Nørskov, *Nat.Mater*., **5**, 909 (2006).
210. J. Rossmeisl, Z. W. Qu, H. Zhu, G. J. Kroes, J. K. Nørskov, *J. Electroanal.Chem*., **607**, 83 (2007).
211. I. C. Man, H.-Y. Su, F. Calle-Vallejo, H. A. Hansen, J. I. Martínez, N. G. Inoglu, J. Kitchin, T. F. Jaramillo, J. K. Nørskov, J. Rossmeisl, *ChemCatChem*, **3**, 1159 (2011).
212. M. E. Bjorketun, A. S. Bondarenko, B. L. Abrams, I. Chorkendorff, J. Rossmeisl, *Phys. Chem. Chem. Phys*., **12**, 10536 (2010).
213. H. Dau, C. Limberg, T. Reier, M. Risch, S. Roggan, P. Strasser, *ChemCatChem*, **2**, 724 (2010).
214. W.-F. Chen, J. T. Muckerman, E. Fujita, *Chem. Commun*., **49**, 8896 (2013).
215. G. Bianchi, F. Mazza, S. Trasatti, *Z. Phys. Chem*., **226**, 40 (1964).
216. J. D. Voorhies, *J. Electrochem. Soc.*, **119**, 219 (1972).
217. A. M. Human, H. E. Exner, *Mater. Sci. Eng. A*, 209, 180 (1996).
218. K. M. Andersson, L. Bergström, *Int. J. Refract. Met. Hard Mater*., **18**, 121 (2000).
219. B. Bozzini, G. P. De Gaudenzi, A. Fanigliulo, C. Mele, *Mater. Corros*., **54**, 295 (2003).

220. M. C. Weidman, D. V. Esposito, I. J. Hsu, J. G. Chen, *J. Electrochem. Soc*., **157**, F179 (2010).
221. P. R. Patil, S. H. Pawar, P. S. Patil, *Solid State Ionics*, **136–137**, 505 (2000).
222. E. C. Weigert, A. L. Stottlemyer, M. B. Zellner, J. G. Chen, *J. Phys. Chem. C*, **111**, 14617 (2007).
223. F. Harnisch, U. Schröder, M. Quaas, F. Scholz, *Appl. Catal., B*, **87**, 63 (2009).
224. F. Harnisch, G. Sievers, U. Schröder, *Appl. Catal., B*, **89**, 455 (2009).
225. T. G. Kelly, J. G. Chen, *Chem. Soc. Rev*., **41**, 8021 (2012).
226. T. G. Kelly, S. T. Hunt, D. V. Esposito, J. G. Chen, *Int. J. Hydrogen Energy*, **38**, 5638 (2013).
227. D. V. Esposito, J. G. Chen, *Energy Environ. Sci.*, **4**, 3900 (2011).
228. D. V. Esposito, S. T. Hunt, Y. C. Kimmel, J. G. Chen, *J. Am. Chem. Soc*., **134**, 3025 (2012).
229. Y. C. Kimmel, D. V. Esposito, R. W. Birkmire, J. G. Chen, *Int. J. Hydrogen Energy*, **37**, 3019 (2012).
230. C. Ma, J. Sheng, N. Brandon, C. Zhang, G. Li, *Int. J. Hydrogen Energy*, **32**, 2824 (2007).
231. Y. Liu, W. E. Mustain, *Int. J. Hydrogen Energy*, **37**, 8929 (2012).
232. S. Wirth, F. Harnisch, M. Weinmann, U. Schröder, *Appl. Catal., B*, **126**, 225 (2012).
233. A. T. Garcia-Esparza, D. Cha, Y. Ou, J. Kubota, K. Domen, K. Takanabe, *ChemSusChem*, **6**, 168 (2013).
234. G. Bronoel, E. Museux, G. Leclercq, L. Leclercq, N. Tassin, *Electrochim. Acta*, **36**, 1543 (1991).
235. H. Vrubel, X. Hu, *Angew. Chem., Int. Ed*., **51**, 12703 (2012).
236. M. D. Scanlon, X. Bian, H. Vrubel, V. Amstutz, K. Schenk, X. Hu, B. Liu, H. H. Girault, *Phys. Chem. Chem. Phys*., **15**, 2847 (2013).
237. E. C. Weigert, J. South, S. A. Rykov, J. G. Chen, *Catal. Today*, **99**, 285 (2005).
238. W. F. Chen, C. H. Wang, K. Sasaki, N. Marinkovic, W. Xu, J. T. Muckerman, Y. Zhu, R. R. Adzic, *Energy Environ. Sci*., **6**, 943 (2013).
239. A. Ursua, L. M. Gandia, P. Sanchis, *Proc. IEEE*, **100**, 410 (2012).
240. K.-D. Kreuer, *Chem. Mater*., **8**, 610 (1996).
241. T. Norby, *Solid State Ionics*, **125**, 1 (1999).
242. O. Paschos, J. Kunze, U. Stimming, F. Maglia, *J. Phys.: Condens. Matter*, **23**, 234110 (2011).

243. A. Goñi-Urtiaga, D. Presvytes, K. Scott, *Int. J. Hydrogen Energy*, **37**, 3358 (2012).
244. D. A. Boysen, T. Uda, C. R. I. Chisholm, S. M. Haile, *Science*, **303**, 68 (2004).
245. S. M. Haile, C. R. I. Chisholm, K. Sasaki, D. A. Boysen, T. Uda, *Faraday Discuss.*, **134**, 17 (2007).
246. A. Hindhede Jensen, Q. Li, E. Christensen, N. J. Bjerrum, *J. Electrochem. Soc*., **161**, F72 (2014).
247. A. L. Tomás García, Q. F. Li, J. O. Jensen, N. J. Bjerrum, *Int. J. Electrochem. Sci.*, **9**, 1016 (2014).
248. A. V. Nikiforov, I. M. Petrushina, J. O. Jensen, N. J. Bjerrum, *Adv. Mater. Res*., **699**, 596 (2013).
249. S. T. Oyama, in *Handbook of Heterogeneous Catalysis*, 2nd ed. (Eds.: G. Ertl, H. Knözinger, F. Schüth, J. Weitkamp), Wiley-VCH, Weinheim, 2008, pp. 342-356.
250. N. Gaston, S. Hendy, *Catal. Today*, **146**, 223 (2009).
251. M. Michman, L. Appelbaum, J. Gun, A.D. Modestov, O. Lev, *Organometallics*, 33, 4729 (2014).
252. C. Costentin, J.-M. Savéant, *ChemElectroChem*, **1**, 1226 (2014).
253. Electrochemistry as a Tool for Study, Development and Promotion of Catalytic Reactions. *Lecture (by invitation) in the Department of Chemistry, Technical University of Munich, 15 December, 2014*.
254. I.M.Petrushina, K. Wonsyld, L.N.Cleemann, N.J. Bjerrum, *Proceedings. 2nd International Conference on the Electrochemical Promotion of Catalysis (EPOCAP)*, Oleron Island, France (29 September – 3 October, 2008), 183 (2009).
255. S.D. Ebbesen, S.H. Jensen, A. Hauch, M.B. Mogensen, *Chem. Rev*., 2014.
256. K. Xie, Y. Zhang, G. Meng, J.T.S. Irvine, *J. Mater. Chem*., **21**, 195 (2011).

11. LIST OF ABBREVIATIONS

BET	Brunauer, Emmett and Teller technique for measurement of surface area based on physical adsorption of nitrogen.
CV	Cyclic voltammetry.
DSA	Dimentionally stable anode.
DTA	Differentiale thermal analysis.
EDL	Electric double layer.
EDLE	Electric double layer promotion effect.
EDX	Energy-dispersive X-ray spectrometer.
EEPP	Promotion effect cause by electrochemically produced catalyst promoters.
EMF	Electromotive force.
EP	Electrochemical promotion.
FTS	Fischer-Tropsch synthesis.
GDL	Gas diffusion layer.
HER	Hydrogen evolution reaction.
ICP-MS	Inductively coupled plasma mass spectrometry.
NEMCA	Non-faradaic electrochemical modification of catalytic activity.
OCM	Oxidative coupling of methane.
OCP	Open circuit potential.
OCV	Open circuit voltage.
OER	Oxigen evolution reaction.
PBI	Polybenzimidazole.
PEM	Proton exchange membrane.
PEMWE	Proton exchange membrane water electrolyzer.
PTFE	Polytetrafluoroethylene (Teflon).
QMS	Quadrupole mass analyzer.
RHE	Reversible hydrogen electrode.
r.p.m.	Rotations per minute.

SCE	Calomel reference electrode.
SEM	Scanning electrone microscope.
SHE	Standard hydrogen electrode.
SOEC	Solid oxide electrochemical cell.
TEM	Transmission electrone microscopy.
TG	Thermogravimetry.
TFMSA	Trifluoromethanesulfonic acid.
SSA	Specific surface area.
XRD	X-ray diffraction.
YSZ	Yttria-stabilized zirconia.

12. LIST OF SYMBOLS

A	Surface area of electrode, cm^2.
A_a	Constant in the Arhenius rquation for anodic reaction.
A_c	Constant in the Arhenius rquation for cathodic reaction.
$C_O(0,t)$	Surface comcentration of oxidized particles, *mol/L*.
$C_R(0,t)$	Surface comcentration of oxidized particles, *mol/L*.
D	Diffusion coefficient, cm^2s^{-1}.
E	Potential, *V (mV).*
E°	Standard equilibrium potential, *V (mV).*
E_p	Peak potential, *V (mV).*
$E_{p/2}$	Half-peak potential, *V (mV).*
F	Faraday's constant, 96480 C/mol.
ΔG_a^a	Gibb's activation free energy for anodic reaction, *kJ/mol*.
ΔG_a^c	Gibb's activation free energy for anodic reaction, *kJ/mol*.
ΔG^{0a}	Gibb's standard activation free energy for electrochemical reaction, *kJ/mol*.
I	Current, *A (mA).*
i	Current density, A/cm^2 (mA/cm^2).
I_p	Peak current, *A (mA).*
i_p	Peak current density, A/cm^2 (mA/cm^2).
I_0	Exchange current, *A (mA).*
i_0	Exchange current density, A/cm^2 (mA/cm^2).
k_f	Rate constant of forward reaction, *cm/s*.
k_b	

k_a	Rate constant of backward reaction, *cm/s*.
k_c	Rate constant of anodic reaction, *cm/s*.
	Rate constant of cathodic reaction, *cm/s*.
k^0	Standart rate constant, *cm/s*.
k_s	Specific rate constant, *cm/s*.
K	Shape factor from the Scherrer equation.
n	Number of electrons participating in electrochemical reaction.
n_α	Number of electrons participating in the rate-determing step of the charge transfer of electrochemical reaction.
OCV	Open-curcuit voltage
R	Gas constant, $J\ mol^{-1}K^{-1}$.
r_0	Rate of catalytic reaction under polarization, $mol\ s^{-1}cm^{-}.^{2}$
r	Rate of catalytic reaction without polarization, $mol\ s^{-1}cm^{-}.^{2}$
T	Absolut temperature, *K*.
V_E	Potential scan rate, *V/s (mV/s).*
V_{WR}	Votage between electrodes in the electrochemical cell used in the study on electrochemical promotion
z_i	Charge of *i* ions.

13. GREEK SYMBOLS

α	Transfer coefficient.
$\bar{\mu}_i$	Electrochemical potential of *i* species, *kJ/mol*.
μ_i	Chemical potential of *i* species, *kJ/mol*.
ϕ	Electric (inner) potential of a phase, *V(mV).*
η	Polarization (overpotential), *V(mV)*.
Λ	Enhansment factor.
ρ	Enhansment ratio.
$\Delta\Phi$	Work function.
ξ	Coefficient from the Metcalfe equation (p.20).
$\Delta\Psi$	Outer potential, *V(mV)*.
$\Delta\chi$	Surface potential, *V(mV)*.
λ	X-ray wavelength, A.
β	Peak width, radian.
θ	Bragg angle of the peak.
τ	Average crystal size from Scherrer equation (p.114), *nm*.

DTU Energy is a department of the Technical University of Denmark. The department was created in 2012, bringing together outstanding research groups from Risø DTU National Laboratory for Sustainable Energy and DTU Chemistry
Our research span from fundamental investigations to component manufacture with a focus on industrial collaboration and industrially relevant processes.
We have 230 staff members.